Performance of Reinforced Concrete Flat Slabs Exposed to Fire

By

Guoqiang (Grant) Wang

Supervised by

Professor Andrew H. Buchanan

Associate Supervisors

Associate Professor Peter J. Moss

Dr. Rajesh Dhakal

Fire Engineering Research Report 06/2

2006

A thesis submitted in partial fulfilment of the requirements for the degree of Master of Engineering in Fire Engineering

Department of Civil Engineering
University of Canterbury
Private Bag 4800
Christchurch, New Zealand

For a full list of reports please visit http://www.civil.canterbury.ac.nz/fire/fe_resrch_reps.shtml

ABSTRACT

A number of researchers have focused on the performance of reinforced concrete slabs exposed to fire. These studies have shown that the membrane forces and the redistribution of bending moments in the slabs considerably affected the behaviour of the slabs in fire conditions. Consequently, the fire resistance of the slabs can be enhanced if tensile membrane behaviour is mobilised. However, the behaviour of reinforced concrete slabs in fire conditions is not clearly known.

This thesis uses a non-linear finite element program, SAFIR, developed at the University of Liege, Belgium, to model reinforced concrete flat slabs and one-way slabs at elevated temperatures. The slabs were modelled as 3-D shell elements in the numerical structural models.

The research analyses nine-bay flat slabs exposed to an ISO 834 Standard fire beneath with and without a decay phase. The location of the fire is varied from beneath all the bays to beneath the middle strip bays and the middle bay of the flat slabs. The study also considers the surrounding thermal conditions of the flat slabs. In addition, the research also analyses one-way slabs exposed to an ISO 834 Standard fire with and without a decay phase; the restraint conditions on the supports are varied. Furthermore, the effect of the widths of one-way slabs on the distributions of membrane forces and bending moments is investigated.

It was found that the location of the fire under flat slabs and the arrangement of reinforcing bars in flat slabs significantly affect the distribution of bending moments and membrane forces in flat slabs. It was also found that the worst scenario of fire exposure could be when the flat slabs are exposed to fire with a decay phase or after the fire was exhausted or extinguished. The fire resistance of flat slabs is significantly increased if tensile membrane action can be mobilised. However, the distribution of membrane forces in the slabs is non-linear.

ACKNOWLEDGEMENTS

The researcher would like to thank the following people. Without their advice, encouragement and support, this thesis would not be completed.

- My supervisors, Professor Andrew H. Buchanan, Associate Professor Peter J. Moss, and Dr. Rajesh Dhakal of the University of Canterbury for their inspiration, guidance and enthusiasm.
- Professor Jean-Marc Franssen of the University of Liege, Belgium, for his invaluable advice with the SAFIR program.
- Dr. Linus C. S. Lim for his intelligent research in reinforced concrete slabs using SAFIR.
- Greg Armfield of the Academic Skills Centre at the University of Canterbury for his advice in English language.
- Dr. Charley Fleischmann and Michael Spearpoint for their excellent arrangement and management of research and courses in ME (fire).
- The Department of Civil Engineering at the University of Canterbury for its excellent research facilities.
- My friend Dr. Ping Dong for his introducing the major of ME (fire).
- Hang Xu for her patience and support during the research.
- Last but foremost, to my parents and parents-in-law, for their unwavering support in spirit and livelihood.

TABLE OF CONTENTS

LIST OF FIGURES

LIST OF TABLES

GLOSSARY OF TERMS

A	Cross sectional area of heated floor	m^2
b	Square root of the thermal inertia of compartment linings	$Ws^{0.5}/m^2K$
C	Compressive force in concrete	kN
C	Constant for a given concrete type	
C	Bending moment coefficient	
c_c	Concrete clear cover of reinforcing bars	m (mm)
c_p	Specific heat of steel	J/kg^oC
c_p	Specific heat of concrete	J/kgK
D	External diameter	M
dT/dt	Temperature reduction rate	^oC/hour
E	Modulus of elasticity of concrete	kP_a
$E_{c,o}$	Elastic modulus of concrete	Gpa
EI	Flexural stiffness of the structural member	$kN\text{-}m^2$
$E_{s,o}$	Elastic modulus of reinforcing bars	Gpa
f'_c	Compressive strength of concrete	Mpa
f'_t	Tensile strength of concrete	Mpa
$f_c(T)$	Characteristic compressive strength of concrete at temperature of T	MP_a
F_v	Ventilation factor	
$f_{y,o}$	Yield strength of reinforcing bars	Mpa
G	Dead load	kN/m^2
h	Thickness (or depth) of the slab	m (mm)
k_c	Coefficient of reduction of the characteristic compressive strength of concrete	
k_s	Coefficient of cold-worked steels at elevated temperatures	
L	Span length of slab	M
L_h	Heated length of reinforced concrete slab-and-joist specimens	M
L_s	Original length of steel	M
L_x	X-direction span of slab	M
L_x	Length (or span) of the slab	M
L_{xn}	Clear span of the slab	M
L_y	Width of the slab	M

M	Bending moment in the slab	kN-m
M_{cold}	Design bending moment in cold conditions	kN-m
M_f	Bending moment capacity in fire conditions	kN-m
M_{fire}	Design bending moment in fire conditions	kN-m
M_T	Bending moment capacity due to axial force	kN-m
n	Exponent	
Q	Live load	kN/m^2
R	Fire endurance	Minutes
R'_{cold}	Negative load capacity at cold conditions	
r_{bow}	Bowing radius of the slab	M
R_{cold}	Positive load capacity at cold conditions	
R_{fire}	Positive load capacity in fire conditions	
r_{load}	Load ratio at fire condition	
S	Tensile force in steel	kN
T	Axial restraint force or thermal thrust	kN
T	Temperature	^oC
t	Time	Minutes
t	Slab thickness	Inches
T_0	Ambient temperature	^oC
t_h	Time	Hours
w	uniformly distributed load on slab	kN/m^2
w	Uniformly distributed load applied on the slab	kN/m^2
x	Distance from the support to the section being calculated	M
z_o	Distance between the position of the axial restraint force and the centroidal axis of the slab at the supports	M

Δ	Midspan vertical deflection	M
Δ_0	Vertical deflection at Point-O using the exclusive connection model	M
Δ_1	Vertical deflection at Point-O using the inclusive connection model	M
Δ_{edge}	Vertical deflection at the edge of the slab	M
ΔL	Expand length in slab (expand length in steel)	M
ΔL	Permitted expansion of reinforced concrete slab-and-joist specimens	M
Δ_{mid}	Vertical deflection at the centre of the slab	M
α_p	Percentage difference of the vertical deflections	%
ε_c	Coefficient of thermal strain of concrete	
$\varepsilon_{th,\,s}$	Thermal expansion of steel	
λ_a	Thermal conductivity of steel	W/m^{o}C
λ_c	Thermal conductivity of concrete	W/mK
μ	Poisson's ratio of the concrete	
Θ	Bowing angle of the slab	Degree
θ_c	Temperature	^{o}C

1. INTRODUCTION

1.1. Performance of Reinforced Concrete Flat Slabs in Fire

Reinforced concrete slabs are widely used in buildings as floor systems. The flat slab is an important type of reinforced concrete floor system. Since the first flat slab was built by C.A.P. Turner in 1906 (Sozen et al., 1980), some design methods for flat slabs have been developed and ACI (1992) has introduced two methods to design flat slabs at ambient conditions. For research purpose, several numerical methods based on finite element theories have been developed to analyse the behaviour of flat slabs at ambient conditions. Enochsson and Dufvenberg (2001) analysed the behaviour of flat slabs at ambient conditions using the finite element method and found that modelling parameters significantly affected the analysis results.

The design of reinforced concrete slabs for fire resistance is usually based on prescriptive generic ratings that specify the minimum slab dimensions and concrete covers to reinforcing bars. These fire resistance classifications are generally conservative and they are based on standard fire tests using furnaces which are seldom representative of actual construction practices. Gustaferro et al. (1980) calculated the structural fire endurance of an interior bay of a flat plate floor system based on restraint only and found that the fire endurance for the flat plate exceeded three hours, which was greater than the requirement of the building codes in which all interior bays should have structural fire endurances of least two hours. If redistribution of applied moments was included in the analysis, it would provide additional fire endurance. Exterior bays, which are restrained by spandrel beams (edge beams) and columns, have considerable fire endurance. Restraint to thermal expansion increases the structural fire endurance of continuous structures even further.

In recent years, real fires and full scale fire tests in multi-storey steel framed buildings in the UK have shown that steel framed buildings with concrete floor slabs have higher levels of fire resistance than would be expected from traditional considerations of fire resistance of steel and concrete structures (Bailey et al, 1999).

Some experimental tests and theoretical analyses have shown that fire resistance of slabs can be increased if they are continuous or axially restrained by the surrounding structure

(Buchanan, 2001). Previous research on the slabs at ambient conditions have been conducted by Wood (1961), Sawczuk et al. (1965), Taylor (1965) and Hayes (1968). They have found that the membrane action affected the load capacity of the slabs. During 1995 and 1996, six localised fire tests were conducted on the full-scale, eight storey, steel-framed building at the Building Research Establishment's Cardington Laboratory. No structural failure was observed during the tests, although the displacements were very large (Bailey et al, 1999). An ambient temperature test to simulate fire behaviour showed that a two-way composite slab could carry loads greater than predicted by the yield line design theory (Bailey et al., 2000).

Three reinforced concrete two-way slabs were tested with exposure to the ISO 834 standard fire by Lim (2003). The slabs supported the loads for three hours of fire exposure without collapse despite suffering significant deflections and loss of flexural strength. The membrane action of one-way and two-way concrete floor systems exposed to the fire has been studied by Lim (2003) using SAFIR, a non-linear finite element program. The analyses showed that Pin-Pin supported slabs have excellent fire resistance if the axial restraint stiffness is high and if the position of the thrust acting at the supports is positioned well below the centroidal axis of the slabs. The analyses also showed that tensile membrane action can be maintained to provide fire resistance of two-way slabs.

All the experimental tests and theoretical analyses of reinforced concrete slabs are based on the assumptions that the surrounding structure has sufficient strength and stiffness. Full-scale fire tests at Cardington showed that steel beams, as the supports of concrete slabs, suffered huge deflections and deformations (Figure 1-1). The unprotected reinforced concrete floor slabs on steel decking did not collapse after a compartment burnout, despite very high measured steel temperatures and considerable deformations (Bailey et al, 1999). There are no relative reports about the behaviour of reinforced concrete flat slabs in fire exposure when the surroundings of the slabs have considerable deformations.

Figure 1-1 Large deflections of the composite slabs following the fire tests at the Cardington steel building (Newman et al., 2000)

1.2. Impetus of the Research

The impetus of this research is to investigate two aspects that influence the design of reinforced concrete slabs in fire: membrane action and redistribution of bending moments.

1.2.1. Membrane action in slabs

The membrane action in slabs can be clarified to tensile membrane action and compressive membrane action when the slabs are subjected to fire.

The tensile membrane action has been known by structural engineers for 40 years. Park (1964) developed a theory to determine the load carrying capacity at large deflections by considering the tensile membrane action. Recently, Park et al. (2000) found that significant tensile membrane action in slabs can occur only if the movement of the edges of slabs is restrained when the slabs are at ambient temperatures. The tensile membrane action of slabs is not fully understood, especially at elevated temperatures. However, based on the tests, a design method for determining the ultimate load carrying capacity of two-way slabs has been developed by considering the effects of tensile membrane enhancement at elevated temperatures (Bailey et al., 2000a, 2000b; Bailey, 2001). The tensile membrane action in slabs is sensitive to the duration of fire exposure, the restraint of the edges of slabs, and the arrangement of reinforcing bars in slabs.

The compressive membrane action has been found in experimental fire tests of slabs exposed to fire (Selvaggio et al., 1963; Issen et al., 1970). These tests have shown that the compressive membrane action can increase the fire resistance of reinforced concrete slabs and a simple hand calculated method for determining the fire resistance of slabs by considering the effects of compressive membrane action has been developed. This method is the only available simple hand method. Several researchers (Anderberg et al., 1982; Harmathy, 1993; Lim, 2003) found that the compressive membrane action is sensitive not only to the duration of fire exposure, the location of the restraint on the edges of slabs and the arrangement of reinforcing bars in slabs, but also to the ratio of the span to the thickness of slabs.

1.2.2. Redistribution of bending moments in slabs

Redistribution of bending moments can occur when plastic hinges develop in slabs. The redistribution of bending moments can give significant advantages in the fire design of continuous structural members (Buchanan, 2001). When the redistribution of bending moments occurs, the cold top reinforcing bars have to resist the larger applied moments, while the hot bottom reinforcing bars resist smaller applied moments due to the reduced yield strength of the bars at elevated temperatures. A 2-D analysis method for uniformly loaded, fire-exposed exterior and interior spans of continuous members considering the redistribution of bending moments at failure has been developed by Gustafson et al. (1980). 3-D analyses for reinforced concrete floor systems in fire exposure can be performed using special purpose computer programs, such us SAFIR. The design of reinforced concrete floor systems exposed to fire is more complicated and difficult than the design of structural members because lateral deformations and resulting P-Δ effects must be considered in the design of the floor systems.

1.3. Objectives of the Research

The objectives of this thesis are:

1. To verify the behaviour of one-way reinforced concrete slabs under fire exposure using 3-D shell element models in SAFIR.
2. To investigate the membrane action and the redistribution of bending moments in reinforced concrete flat slabs at ambient temperatures and under an ISO 834 Standard fire with or without a decay phase using 3-D shell element models in SAFIR.
3. To provide recommendations for the design of reinforced concrete flat slabs in the accidental action of fires.

1.4. Organization of the Thesis

The thesis includes eight chapters. Chapter 1 (this chapter) briefly introduces the research project and outlines the objectives and scopes of the research. Chapter 2 reviews previous works that are relevant to reinforced concrete slabs under fire exposure. The thermal and mechanical properties of steel and concrete in fire conditions are also detailed in Chapter 2. The capabilities of the SAFIR program are described in Chapter 3.

Chapter 4 investigates the thermal behaviour of reinforced concrete slabs under ISO 834 Standard fire exposure and introduces the thermal models which are used in Chapter 5, Chapter 6, and Chapter 7 for the analyses of the structures or structural members in fire conditions.

Chapter 5 verifies the behaviour of one-way slabs under fire exposure using 3-D shell element models in SAFIR. The 3-D analysis of one-bay flat slabs at ambient conditions and in fire conditions is carried out in Chapter 6. Chapter 6 also examines the modelling technique for the buildings with flat slab floor systems using SAFIR. Chapter 7 investigates the behaviour of flat slabs in fire conditions by considering the effect of the position of fire in the building with a nine-bay flat slab floor system. Finally, Chapter 8 gives the conclusions and recommendations from this research.

2. LITERATURE REVIEW: REINFORCED CONCRETE SLABS IN FIRE

This chapter focuses attention on the literature which is relevant to reinforced concrete slabs in fires. This literature review covers the design methods for reinforced concrete slabs, the incidence of fires in reinforced concrete buildings, and the properties of concrete and steel at elevated temperatures. The relevant literature to the thermal behaviour of concrete slabs will be briefly summarized in Chapter 4.

2.1. Introduction of Reinforced Concrete Floor Systems

There are many forms of reinforced concrete slab floors since they have been introduced in buildings. Reinforced concrete floor systems can be classified in many ways, but the common classification of the slabs is by their structural actions. The slabs are categorised into three types: one-way spanning slabs, two-way spanning slabs, and flat slabs (or flat plates). Many factors affect the choice of the type of slabs for a particular floor system, such us the economy of construction, design loads, required spans, serviceability requirements, and strength requirements (Park et al., 2000).

The general definition of the one-way slab is that the slab spans in one direction between beams or walls, as shown in Figure 2-1 (a) to (c). The two-way slab is the slab supported on beams or walls on all sides of each panel, as shown in Figure 2-1 (d). When the aspect ratio (i.e. the longer supported length against the shorter supported length) is less than 2, the slab is treated as a two-way slab in normal conditions (Figure 2-1 (d)). The examples of flat slabs that are supported directly on columns are shown in Figure 2-1 (e) to (h). Flat slabs may have drop panels ((Figure 2-1 (f)) or drop panels with capitals (Figure 2-1 (g)) that allow the slabs to be thinner than those without drop panels and capitals. Flat slabs without drop panels and capitals or with capitals hidden in columns are called flat plates (Figure 2-1 (e)). The slab shown in Figure 2-1 (h) is called a waffle slab where a set of crossing joists with small spacing relative to the span support a thin top slab. The design method for either flat slabs or two-way slabs can be used in the design of waffle slabs (Park et al., 2000).

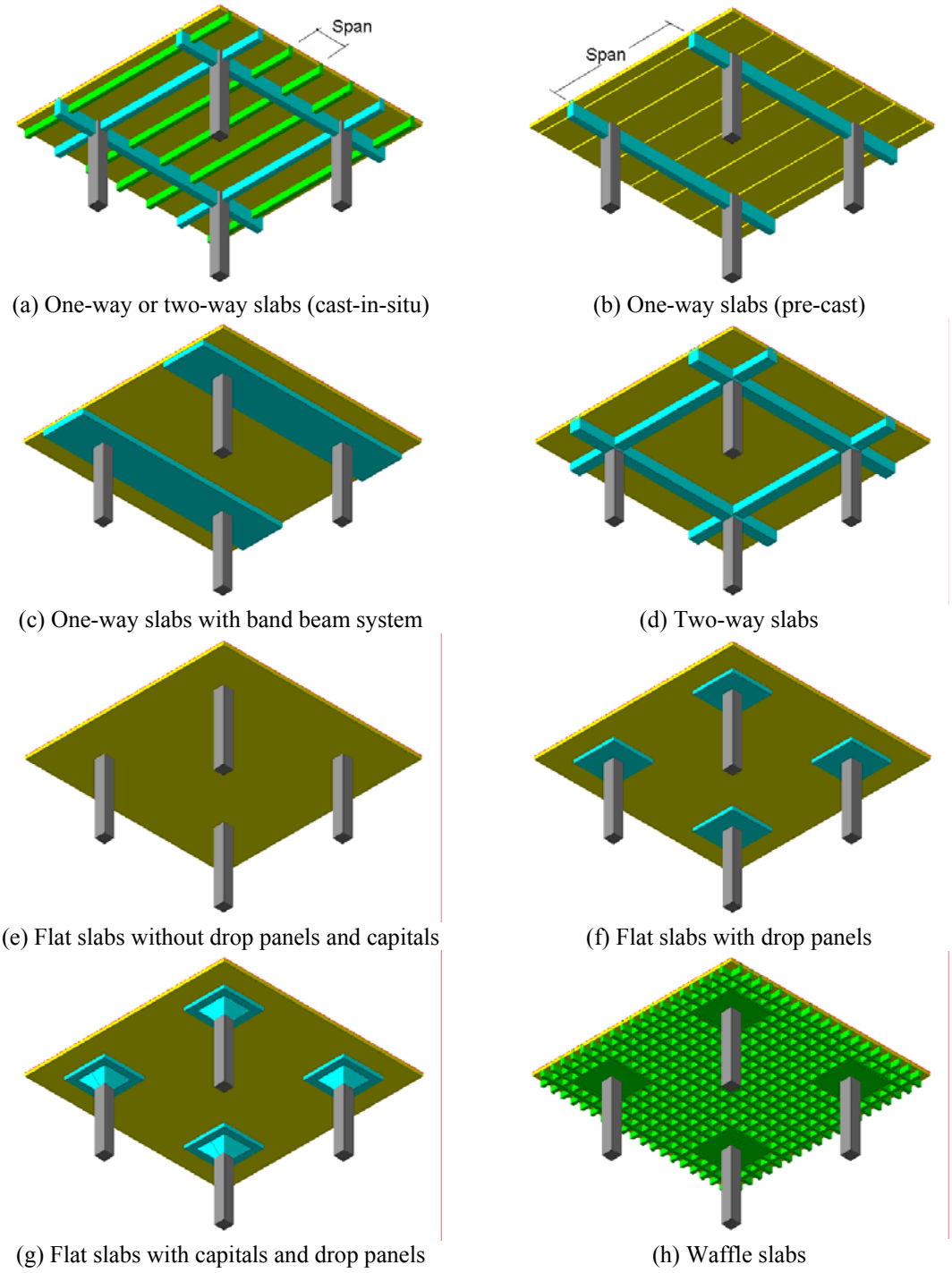

(a) One-way or two-way slabs (cast-in-situ)

(b) One-way slabs (pre-cast)

(c) One-way slabs with band beam system

(d) Two-way slabs

(e) Flat slabs without drop panels and capitals

(f) Flat slabs with drop panels

(g) Flat slabs with capitals and drop panels

(h) Waffle slabs

Figure 2-1 Classification of reinforced concrete floor systems

The analysis of the behaviour of two-way reinforced concrete slabs exposed to fire using 3-D shell elements models in SAFIR, a computer program that will be detailed in Chapter 3 of this thesis, has been performed by Lim (2003). The analysis of the behaviour of one-way slabs (in Chapter 5) and flat slabs (in Chapter 6 and Chapter 7) exposed to fire using 3-D shell element models will be carried out in this research.

2.2. The Fire Design of Reinforced Concrete Slabs

Choosing the design methods for reinforced concrete slabs exposed to fire depends on the support conditions of the slabs. Building codes generally give recommendations for the slab design in fire exposure and rational design methods are summarised by Gustaferro et al. (1980), Harmathy (1993), Purkiss (1996), Buchanan (2001) and Fleischmann et al. (2002).

2.2.1. Code requirement of the fire design of slabs

A general requirement of fire resistance ratings for the fire resistances of slabs is specified in most national building codes. Wade (1991) has summarized the generic fire resistance ratings for reinforced concrete beams, slabs and columns. Those fire resistance ratings for reinforced concrete slabs are listed in Table 2-1, where the requirements for minimum dimensions and minimum covers for fire resistance ratings from 0.5 hour to 4 hours are detailed.

Table 2-1 Fire resistance ratings of reinforced concrete slabs (data from Wade (1991))

Fire-resistance Rating	0.5 hour	1.0 hour	1.5 hours	2.0 hours	3.0 hours	4.0 hours	Notes
	Thickness /Cover	Thickness /Cover	Thickness /Cover	Thickness /Cover	Thickness /Cover	Thickness /Cover	
Document, standard or code							
MP9:1989 (NZ)	60/15	80/20	100/20	120/20	150/23	175/25	1
BS8110:1085 (UK)	75/15	95/20	110/25	125/35	150/45	170/55	2
BRE:1998 (UK)	75/15	95/20	110/25	125/35	150/45	175/55	3
FIP/CEB:1975 (EUR)	60/10	80/20	100/30	120/40	150/55	175/65	4
CEB:1987 (EUR)	60/10	80/25	100/35	120/45	150/60	175/70	5
UBC:1988 (USA)	-/-	89/19	-/-	127/25	157/25	-/32	6
AS 3600:1988 (AUS)	60/15	80/20	100/25	120/30	150/45	170/55	7

Notes:

1. Simply supported
2. Dense aggregate, plain soffit, simply supported
3. Dense aggregate, plain soffit, simply supported, effective cover
4. Dense aggregate, one-way span, simply supported, critical temperature=550^{o}C
5. Dense aggregate, one-way span, simply supported, critical temperature=550^{o}C, cover to steel axis
6. Siliceous aggregate
7. One-way simply supported

The unit of thickness and cover is millimetre.

In New Zealand, the Design of Concrete Structures NZS 3101 (SNZ, 1995) states that reinforced concrete slabs should fulfil three criteria required by the New Zealand Building Code (BIA, 1992) to satisfy the fire resistance. The three criteria are stability, integrity, and

insulation. To meet the stability criterion, the slab must have a minimum concrete cover to the reinforcing steel, which is specified in the code. To meet the integrity criterion, the slab must have an ability to prevent the passage of flames through the slab, which is determined by a fire resistance rating for integrity in the code. To meet the insulation criterion, the slab must have an effective thickness and the aggregate type of concrete should be considered.

In Europe, the European Standard is widely accepted by European countries. Eurocode 2 (EC2, 2002) has similar fire resistance criteria to those given in the New Zealand Building Code (BIA, 1992). To determine the fire resistance of slabs, the support conditions of slabs must be considered. The fire resistance of simply supported solid slabs, continuous solid slabs, flat slabs, and ribbed slabs is detailed in the code. For example, the requirement for flat slabs is stated in Eurocode 2 (EC2, 2002) as:

"1. The following rules apply to flat slabs where the moment redistribution according to Section 2 of EN 1992-1-1, does not exceed 15%. Otherwise axis distances should be taken as for one-way slab (Column 3 in Table 5.8) and the minimum thickness from Table 5.9.
2. For fire rating of REI 90 and above, at least 20% of the total top reinforcement in each direction over intermediate supports, required by EN 1992-1-1, should be continuous over the full span. This reinforcement should be placed in the column strip.
3. Minimum slab-thicknesses should not be reduced (e.g. by taking floor finishes into account).
4. The axis distance $\boldsymbol{a}$ *denotes the axis distance of the reinforcement in the lower layer."*

ASTM E119 (ASTM, 1999), Standard Test Methods for Fire Tests of Building Construction and Materials, gives the fire resistance ratings for various types of floor systems. The fire resistance ratings are also relative to restrained support conditions. In ASTM E119, the restrained system is defined to be a system in which the expansion of the heated member is resisted by external forces. ASTM E119 also states that the adequate restraint can be present in interior bays and exterior bays of framed buildings when:

"The space between the ends of precast units and the vertical faces of the supports, or between the ends of solid or hollow-core slab units does not exceed 0.25 percent of the length for normal weight concrete members or 0.1 percent of the length for structural lightweight concrete members."

2.2.2. Simply support unrestrained one-way slabs

Figure 2-2 (a) shows an unrestrained one-way slab with the span of L_x exposed to a fire beneath. A uniformly distributed load, w, is applied to the slab, which is supported on two rollers so there are no longitudinal restraining forces on the slab. The applied moment and nominal moment are shown in Figure 2-2 (b) where R_{cold} and R'_{cold} are the load capacity of the slab in normal (cold) conditions and R_{fire} is the load capacity of the slab in fire conditions. For the strength domain design of slabs in fire conditions, R_{fire} must be greater than the maximum applied service load moment ($M_{fire} = wL_x^2 / 8$) at midspan.

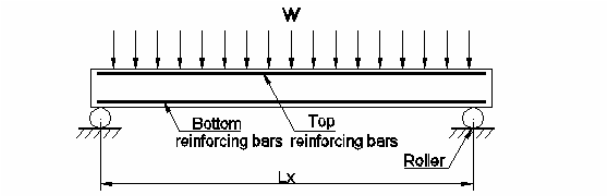

(a) A simply supported one-way slab

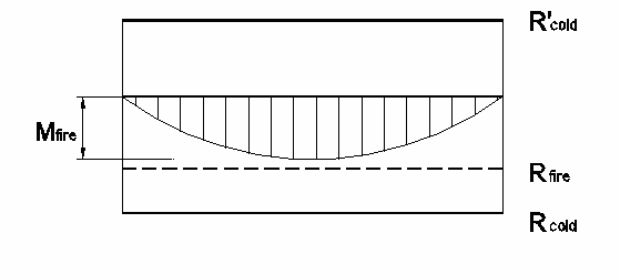

(b) Design bending moment and load capacity diagram

Figure 2-2 Design bending moment and load capacity diagram for a simply supported one-way slab

Normally, for a simply supported unrestrained one-way slab, the top of the slab remains at ambient temperature conditions even after 120 minutes of fire exposure. Therefore, only the strength reduction of reinforcing bars on the bottom of the slab needs to be considered.

The fire endurance of simply supported, unrestrained one-way slabs depends upon applied loads, the temperature-strength characteristics of reinforcing bars, and the concrete cover to the reinforcing steel. Because of the lack of benefit of continuity and restraint to thermal expansion, there are no advantages in making analyses for the fire endurance of simply supported, unrestrained slabs (Gustaferro et al., 1980).

2.2.3. Continuous unrestrained one-way slabs

Figure 2-3 (a) shows an interior span of a continuous unrestrained one-way slab supported on rollers, so there are no longitudinal restraining forces on the slab exposed to a fire beneath. The design bending moments and load capacities of the slab are shown in Figure 2-3 (b) where dashed lines are for the slab in fire conditions.

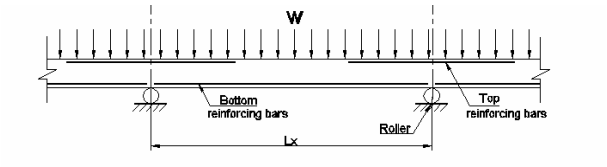

(a) An interior span of the one-way slab

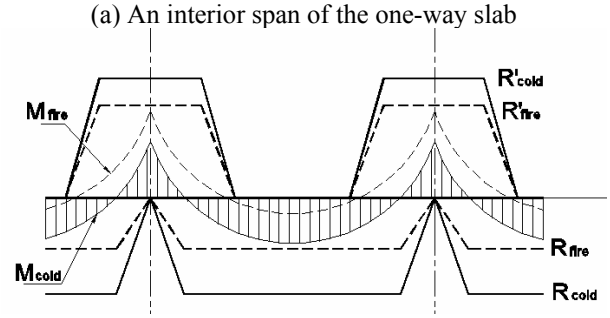

(b) Design bending moment and load capacity of the slab in normal and fire conditions (dashed lines are in fire conditions)

Figure 2-3 Redistribution of bending moments in the interior span of the continuous unrestrained one-way slab

When the temperature increases in the slab, the top reinforcing bars effectively remain cool after the bottom bars get hot. The hot bottom bars resist smaller applied positive moments because of the reduction of their yield strength under fire exposure. Therefore, the relative cool top bars have to resist the larger applied negative moments. Changing the distribution of applied bending moments is called the redistribution of bending moments. Figure 2-3 (b) shows that the large portion of the interior span is subjected to the negative moment when the slab is exposed to fire because the redistribution of bending moments occurs in the slab.

Using structural engineering principles, the reduced load capacity of the slab can be related to redistributed applied bending moments at failure. If the available load capacity of the slab is equal to or greater than the redistributed applied bending moments (R_{fire} *or* $R'_{fire} \geq M_{fire}$), the fire endurance of the slab is adequate.

Because of the presence of the redistribution of bending moments in reinforced continuous slabs under fire exposure, it is evident that continuous slabs have much more fire endurance

than simply supported unrestrained slabs when they have the same cross-sectional dimensions, material properties, and are subjected to the same applied load.

2.2.4. Simply supported and restrained one-way slabs

Figure 2-3 (a) shows a simply supported, restrained one-way slab exposed to a fire underneath. The applied bending moments and load capacity of the slab in normal and fire conditions are shown in Figure 2-34 (b) where dashed lines are those for the slab in fire conditions.

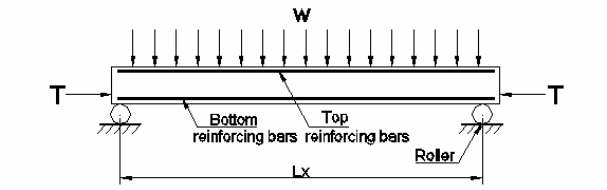

(a) A simply supported restrained one-way slab exposed to a fire beneath

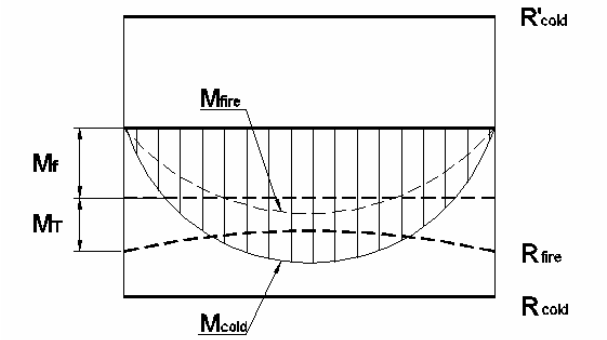

(b) Design bending moments and load capacity of the slab in normal and fire conditions (dashed lines are in fire conditions)

Figure 2-4 Effect of axial restraint forces on bending moments

Figure 2-4 (b) shows that the total load capacity, R_{fire}, includes two parts: the elevated temperature bending moment capacity, M_f, and the moment due to axial restraint forces, M_T.

Based on the derivation derived from Harmathy (1993), at the stage of imminent collapse, the equilibrium between acting and resisting moments at the midspan is:

$$R_{fire} = \frac{wL_x^2}{8} - T(z_0 - \Delta) \qquad \textbf{Equation 2-1}$$

where R_{fire} is the positive flexural capacity of the slab at elevated temperature (kNm/m), w is the uniformly distributed load applied on the slab (kN/m), L_x is the clear span of the slab (m), T is the axial restraint force (kN), z_o is the distance between the position of the axial restraint force and the centroidal axis of the slab at the supports (m), and Δ is the vertical deflection in the midspan (m), as shown in Figure 2-5.

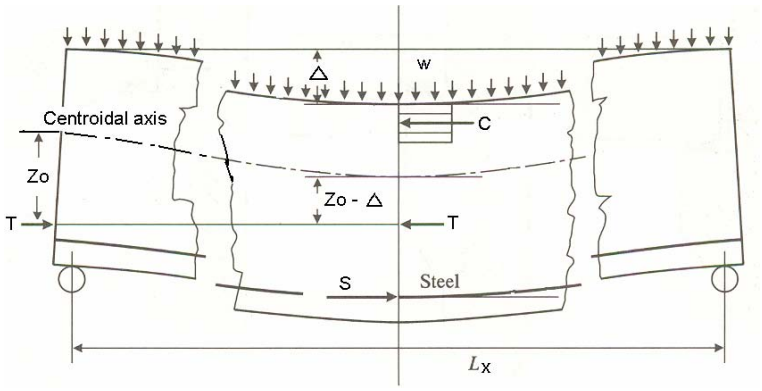

Figure 2-5 Free body diagram of the restrained simply support slab

The equilibrium of forces can be expressed as:

$$C = T + S \qquad \textbf{Equation 2-2}$$

where C is the compressive force in concrete (kN) and S is the tensile force in steel (kN), as shown in Figure 2-5.

A step-by-step method has been developed by Gustaferro et al. (1989) to take into account the beneficial effect of axial restraint forces. This semi-empirical method based on numerous tests at Portland Cement Association (PCA) furnace is the only one available simple hand calculating method.

The beneficial effect of compressive axial restraint on fire resistance depends on the location of the line of axial restraint forces. Lim (2003) found that compressive axial restraint was beneficial to slabs if the line of axial restraint forces was located well below the centroidal axis, but if the line of axial restraint forces was located close to the centroidal axis, the compressive axial restraint was not beneficial to the fire resistance of slabs. Experimental fire tests have shown that the line of axial restraint forces acts near the bottom in common support conditions for cast-in-place concrete slabs and the actual location of the line of axial restraint forces changes throughout the fire tests depending on the shape of slabs, the type of concrete, the amount of reinforcement, the stiffness of restraining frames, and the amount of permitted expansion (Gustaferro et al., 1980).

After significant periods of fire exposure, large deflections can occur in a slab. The slab will collapse because of the rapidly increase of deflections when there are no axial tensile restraint forces at the supports. When the supports of the slab have sufficient anchorage and tensile

capacity to resist the tensile restraint forces, which are produced by catenary action in the large deflections of slabs, the slab can not collapse after considerable periods of fire exposure. When the elevated temperature bending moment capacity, M_f, drops to zero, the slab deforms into a catenary and all of the moments are resisted by the moments due to axial restraint forces, M_T. The tensile force at the end supports, T, can be expressed as Equation 2-3 if the slab deforms into a catenary.

$$T = \frac{wL_x^2}{8} \cdot \frac{1}{\Delta} \qquad \textbf{Equation 2-3}$$

2.2.5. Numerical computer programs

Special computer programs should be used in the analysis of the behaviour of reinforced concrete slabs under any types of fire exposure with complicated support conditions. A number of computer programs have been developed in different parts of the world.

Olenick and Carpenter (2003) have summarised the computer models for the response of building structural elements to fire exposure. Table 2-2 lists the fire endurance models emphasising the simulation of concrete structural members.

Table 2-2 Fire endurance models emphasising the simulation of concrete structural members

Model	Country	Identifying Reference	Description
CEFICOSS	BELGIUM	(132)	Fire resistance model
CMPST	FRANCE	(127)	Mechanical resistance of sections at elevated temperature
COMPSL	CANADA	(87)	Temperatures of multilayer slabs during exposure to fires
FIRES-T3	US	(88)	Finite element heat transfer for 1-, 2- or 3-D conduction
HSLAB	SWEDEN	(89)	Transient temperature development in a heated slab composed of one or several materials
SAFIR	BELGIUM	(93)	Thermal and mechanical analysis of structures exposed to fire
SISMEF	FRANCE	(127)	Mechanical behaviour of steel and concrete composite structures exposed to fire
STA	UK	(126)	Transient conduction in heated solid objects
TASEF	SWEDEN	(96)	Finite element method for temperature analysis of structures exposed to fire
TCSLBM	CANADA	(97)	Two dimensional temperature distributions for fire-exposed concrete slab/beam assemblies
THELMA	UK	(98)	Finite-element code for thermal analysis of building components in fire
TRB	NEW ZEALAND	(99)	Fire resistance of concrete slabs and floor systems
These models have been identified by the authors, but no references or survey information was provided: ABAQUS (US), ALGOR (US), ANSYS (US), COSMOS/M (US), FASBUS, LUSAS (UK), NASTRAN (US), TAS (US), VULCAN (UK), and WALL2D (CANADA).			
Sources of data: Olenick and Carpenter (2003)			

Fire endurance models simulate the response of building structural members to fire exposure. Structural members are divided into small elements, the thermal heat transfer and mechanical behaviour of the elements are analysed using the equations, and then the time of structural failure is determined.

The interfaces of the programs listed in Table 2-2 are not as user-friendly as typical commercial building design programs. Graphical user-interfaces have been developed for some programs, such as SAFIR which will be used to analyse the behaviour of reinforced concrete slabs in this research.

2.3. Flat Slabs under Fire Exposure

2.3.1. Flat slabs at ambient conditions

The first flat slab was built by C.A.P Turner in 1906, but before the finite element methods were introduced for the analysis of flat slabs, there were no accurate analysis methods for flat slabs, especially before the 1910s, when the results of the various design methods varied by up to 400 percent (Sozen et al., 1980).

Based on the experimental tests and the analysis for the distribution of moments using elastic theories, ACI (1992) has introduced two design methods that can be used to design flat slabs: a direct design method and an equivalent frame method.

The direct design method is only used for a slab system with three or more continuous spans in each direction. This method includes three fundamental steps: the first step is the determination of the total factored static moment or design moment, the second step is the distribution of the total factored static moment for the negative and positive regions, and the final step is the distribution of the negative and positive factored moments to the columns and middle strips and to the beams.

The equivalent frame method, which has fewer limitations than the direct design method, can be used to calculate a more general slab system. The equivalent frame comprises three parts: horizontal slab strips, columns or other vertical supporting members, and the elements of the structure that provide moments transferred between horizontal and vertical members.

Most codes allow flat slabs to be designed using any method if it satisfy the general principles stated in the code, described by Park et al. (2000), who also illustrated that there are compressive and tensile membrane action in slabs under normal temperature conditions, which were not considered in the design of reinforced concrete slabs; if the membrane forces in slabs are considered, the ultimate loads of concrete slab systems may be significantly increased.

The ultimate load of flat slabs at ambient conditions can be determined by yield-line theory (Park et al., 2000). Yield-line theory is an upper bound approach initiated by Ingerslev and greatly extended and advanced by Johansen (Park et al., 2000). The ultimate load is

determined using the principle of virtual work or equations of equilibrium. The moments at the plastic hinge lines are the ultimate moments of resistance of the sections. Yield-line theory is applicable to slabs with uniformly distributed reinforcement. The Yield-line theory is also possible to be used to analyse slabs with non-uniformly distributed reinforcement; however, there are some extra problems, and the processes have not been generalized to the extent that they have been for the slabs with uniformly distributed reinforcement. Yield-line theory assumes a flexural collapse mode; this means, the slab should have sufficient shear strength to prevent a shear failure.

2.3.2. Fire endurance of flat slabs based on restraint to thermal expansion

Gustaferro et al. (1980) introduced a method to determine the fire endurance of floor systems based on restraint to thermal expansion. Expansive forces, or thermal thrusts, are developed in floor systems when a fire occurs beneath an interior bay of a multi-bay reinforced concrete floor system. The thermal thrusts in the heated floor tend to push against the surrounding unheated part of the slab. The forces are great enough to exceed the compressive strength of concrete if the stress relaxation in the concrete at high temperatures is not considered.

A more convenient analysis method for determining the structural fire endurance of interior bays of floor systems is the thick-walled cylinder analysis method based on restraint to thermal expansion. Figure 2-6 shows the fire beneath the shaded bay of a portion of a multi-bay concrete floor system.

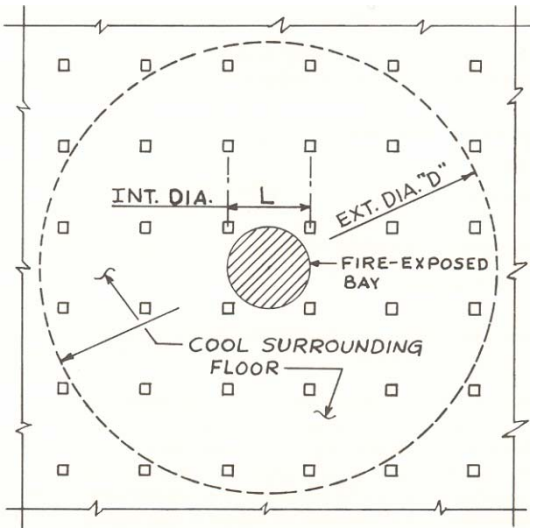

Figure 2-6 Thick-walled cylinder analysis (Gustaferro et al., 1980)

The shaded bay shown in Figure 2-6 is restrained by the surrounding part of the floor with thermal thrust, T, and it must displace the surrounding slab interface a total of ΔL (m) which was the expanded length over the span length, L (m). The expansion can be calculated uisng Equation 2-4 when the floor is treated as a slice of a thick-walled cylinder with an internal diameter L and external diameter D (m). The material of the cylinder is assumed to behave elastically.

$$\Delta L = \frac{TL}{AE}\left(\frac{D^2 + L^2}{D^2 - L^2} + \mu\right) \qquad \textbf{Equation 2-4}$$

where A is the cross sectional area of the heated floor (m^2), E is the modulus of elasticity of concrete (kP_a), μ is the Poisson's ratio of concrete, and T is the thermal thrust (kN).

The example calculation of an interior bay of a flat plate floor system given by Gustaferro et al. (1980) has shown that the fire endurance of the slab with a thickness of 200mm, a minimum concrete cover of 20mm, and the bay sizes of $6m \times 6m$ exceeds 3 hours.

2.4. Analysis of Two-Way Slabs Using 3-D Shell Element Models in SAFIR

Lim (2003) has analysed a two-way slab with 4.16m length, 3.16m width, and 0.1m thickness using the SAFIR 3-D shell element model. The slab carried a constant uniformly distributed load of 5.4kN/m^2 and was exposed to an ISO 834 Standard fire for up to four hours. Some factors that may have affected the results of the simulation were investigated. The behaviour of the slab modelled using the SAFIR model was compared with an experimental test of the slab with the same characteristics.

The findings of the analysis of two-way slabs by Lim (2003) are briefly listed below.

- The effect of the number of shell elements

The number of elements used in the SAFIR models only affected the behaviour of slabs at the stages approaching failure. The slabs with the coarser grid had the higher failure time at larger deflections. A recommendation was given that for prediction of the failure of slabs accurately, the finer grid would be used.

- The effect of concrete tensile strengths

The results of the analysis of slabs were sensitive to concrete tensile strengths when the amount of reinforcing bars in the slabs was small. Zero concrete tensile strength could be used in the analyses of the behaviour of the slabs in existing structures.

- Membrane forces in slabs

The membrane forces in two-way slabs were the tensile forces at the midspan region surrounded by a compression ring at the outer edges. The magnitudes of the membrane forces decreased from the ignition to the exhaust of the fire. Two-way slabs had good behaviour in fire conditions due to the tensile membrane action in the slabs.

- Comparison of SAFIR modellings and the experimental fire tests

The comparison of the experimental fire tests and SAFIR analyses showed that the models with and without the outer edges agreed with the experimental results when the concrete tensile strength was taken as 1.5MP_a.

Lim (2003) also found that the corner restraint of slabs and beam-column connections were very important in the behaviour of slabs in fire exposure. It was recommended that beam-column connections would be designed to resist high tension forces.

2.5. Incidents of Fire in Multi-Storey Buildings

There have been several incidents of fire in multi-storey concrete buildings, although, in general, concrete structures have a reputation for good behaviour in fire. Beitel et al. (2002) have reviewed the historical information on fire incidences in multi-story buildings which resulted in structural collapse. Lim (2003) has mentioned four severe fire incidents in multi-story buildings that related to concrete floor systems.

2.5.1. Incidents of fire in multi-storey concrete buildings

A total of 22 cases of fire related collapse in multi-story buildings from 1970 to 2002 were surveyed by Beitel et al. (2002) and seven of those fire-induced collapse events of concrete buildings are summarised in Table 2-3.

Table 2-3 Summary of concrete multi-story building fires with collapse (the data originally from Beitel et al. (2002))

Building Name	Location	Number of Floors and Occupancy	Date, Approximate Time of Collapse	References
Apartment block	St. Petersburg Russia	19 Residential	June 3, 2002. Starting at 1 hour fire duration	1
Jackson Street Apartment	Hamilton, Ontario Canada	21 Residential	February 8, 2002	2
Pentagon	Washington, DC USA	5 Office	Sept. 11, 2001 30 minutes after jet impact	3
Textile Factory	Alexandria Egypt	6 Commercial	July 21, 2000 After 9 hours of fire	4
CESP, Sede 2	Sao Paulo Brazil	21 Office	May 21, 1987 After 2 hour fire	5
Katrantzos Sport Department store	Athens Greece	8 Commercial	Dec. 19, 1980	6
Military Personnel Record Centre	Overland, MO USA	6 Office	July 12, 1973	7

References (Beitel et al., 2002)

1. "Russian Apartment Block Collapses", BBC News Online: World:Europe, June 3, 2002.
2. Stepan, Cheryl, "I Thought the Worst was Over; Firefighers Buried for 30 Minutes", *The Hamilton Spectator*, Feb, 9, 2002, pg. A-03.
3. FEMA 403, "World Trade Center Building Performance Study: Data Collection, Preliminary Observations, and Recommendations," FEMA, Washington, DC, May 2002.
4. "Egyptian Prime Minister Visits Site of Factory Collapse", *Reuters News*, July 22, 2000.
5. Berto, Antonio Fernando and Tomina, Jose Carlos, "Lessons From the Fire in the CESP Administration Headquarters" IPT Building Technologies, Sao Paulo, Brazil, 1988.
6. Papaioannou, Kyriakos, "The Conflagration of Two Large Department Stores in the Centre of Athens," *Fire and Materials*, **Vol. 10**, John Wiley and Sons, Ltd.,1986, pg 171-177.
7. Sharry, John A., Culver, Charles, Crist, Robert, and Hillelson, Jeffrey, "Military Personnel Records Center Fire," *NFPA Fire Journal,* Quincy, MA, May 1974.

Apartment block in St. Petersburg

The building was a nine-storey concrete apartment block. After one hour's fire exposure, the building totally collapsed (Figure 2-7). There was only one casualty and about 400 other residents successfully evacuated the burning building before the collapse. The ignition of the fire was due to the ongoing reconstruction work at the site that had accidentally ruptured a gas line.

Figure 2-7 Collapse of the burning apartment block in St. Petersburg, Russia (Beitel et al., 2002)

Jackson Street Apartment

The building was a 21-storey apartment building. The fire caused partial collapse of a floor and ceiling assembly. Several firefighters were injured and no fatalities were reported.

Pentagon

The Pentagon building, a famous building in Washington, USA, is a 5-storey cast-in-place reinforced concrete building. There were some partial structural collapses in the building due to the ensuing fires approximately 30 minutes after the impact of a jet (Figure 2-8).

Figure 2-8 The Pentagon collapse from the September 11, 2001 attack (Beitel et al., 2002)

Textile Factory in Egypt

The building was a six-storey reinforced concrete building used as a textile factory. The fire was ignited in a storage room at the ground floor. Because of non-functioning of fire extinguishers, the fire quickly spread to other parts of the building before firefighters arrived. After approximately nine hours' burning, the fire was under control and subsiding, but the building suddenly collapsed and 27 people were killed.

CESP, Sede 2

The CESP Building 2 was a 21-storey office building where the headquarters of the Sao Paulo Power Company (CESP) was located. The building was constructed of reinforced concrete framings with ribbed slab floors. Automatic fire detectors and manual fire alarms were equipped, but there was no automatic sprinkler system in the building. The fire started on the fifth floor in the adjacent building (CESP Building 1) which was connected by six footbridges with CESP Building 2. The fire quickly spread from Building 1 to Building 2 and the fire in Building 2 caused the collapse of the structural core area throughout the full building height (Figure 2-9) after approximately two hour's burning. The thermal expansion of the horizontal concrete T-beams in the fire was the main reason for the collapse.

Figure 2-9 CESP Building 2 core collapse in Sao Paulo, Brazil (Beitel et al., 2002)

Katrantzos Sport Department store

The building was an eight-storey reinforced concrete building that was used as a sport department store. The suspected arson fire started at the seventh floor and quickly spread throughout the building because of the lack of vertical or horizontal compartmentalization and

the absence of automatic sprinkler systems. The major part of the building from the fifth to eighth floor collapsed, which was caused by the restraint of differential thermal expansion in the structure (Figure 2-10).

Figure 2-10 Katrantzos Department building in Athens after the 1980 fire (Beitel et al., 2002)

Military Personnel Record Centre

The building was a six-story office building constructed of reinforced concrete. The fire started on the sixth floor and was fully extinguished after 4 days due to the high fuel load on the sixth floor. A partial roof collapse began after approximately 12 hours of fire exposure and later the collapse and damage were due to the large horizontal expansion of the concrete roof slab. Almost 600mm lateral roof displacements occurred in one corner. Figure 2-11 shows the damage of concrete columns due to the thermal expansion of the roof slab.

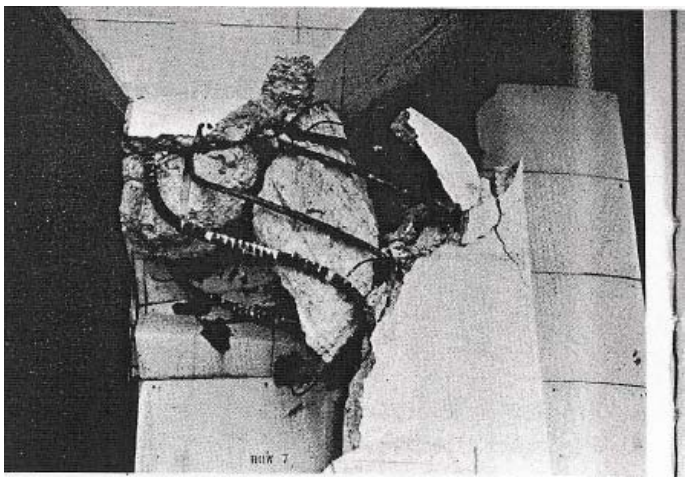

Figure 2-11 Large lateral deformations and failure of columns at sixth floor of Military Personnel Records Centre (Beitel et al., 2002)

2.5.2. Incidents of fire in multi-storey buildings emphasizing the behaviour of slabs in fire

Several incidents of fire in multi-storey buildings, which emphasize the behaviour of slabs in fire conditions, surveyed by Lim (2003) are summarised in Table 2-4.

Table 2-4 Summery of multi-story building fires with emphasis of the behaviour of slabs in fire conditions

Building Name	Location	Number of Floors and Occupancy	Date	References
One Meridian Plaza	Philadelphia, PA USA	38 Office	1991	Routley et al. (1991)
Broadgate	London U.K.	14 Office	1990	Newman et al. (2000)
Kimberley-Clark building		4 Paper manufacture	1978	Vecchio et all (1990)
Kellogg Factory	Manchester U.K.	5 Factory	1967	Cembureau and FIP (1979)

Source of data: Lim (2003)

One Meridian Plaza

The building is a 38 storey office building. The floor system is a composite steel-concrete floor system with a two-hour fire rating. The fire started on the twenty-second storey. Figure 2-12 shows that after 19 hours' fire exposure the beams and floor systems suffered very large deflections. The floor system did not collapse because of the benefits of the high level redundancy on the fire resistance of steel frame structures.

Figure 2-12 Large vertical deflections of the steel beams and floor system after the fire in the One Meridian Plaza (Reproduced from Lim (2003))

Broadgate

The building is a 14-storey office building. The floor system is a composite floor slab supported by composite trusses and beams. The fire temperatures reached in excess of 1000^{o}C

and the composite floor suffered deflections as large as 0.6m. In a range of places, the reinforcement in slabs had failed, but the structure did not collapse, as the applied loads were redistributed to the stronger and cooler parts of the structure.

Kimberley-Clark building (data originally from Vecchio et al. (1990))

The building, which was used for paper manufacturing, is a four-storey concrete building. The floor system is a reinforced concrete flat slab system with six bays in each direction. The thickness of the flat slabs is 200mm. The third floor of the building collapsed down to the basement level and then a major fire occurred in the lower stories of the structure. It is worth to be mentioning that Vecchio et al. (1990) have analysed the structure in fire conditions using a 2-D model in TEMPEST, a computer program that can perform geometric and material non-linearity and material degradation at elevated temperatures and membrane forces in slabs. They found that compressive membrane forces in the slabs contributed to the increased load carrying capacity of the slabs. They also found that the slabs would collapse only if considerable elongation was present in the slabs. If the elongation was resisted by the surrounding structure, there would be high forces in the slabs (Equation 2-4).

Kellogg Factory

The building is a five storey reinforced concrete factory. The floors above the fire room deformed as two-way slabs which were supported on concrete beams with very large vertical deflections after eight hour's burning before the fire was controlled. The slab did not collapse due to the proper anchorage of the reinforcing bars in slabs to the surrounding structures, as shown in Figure 2-13 (a) and Figure 2-13 (b).

(a) The view of the floor above the fire

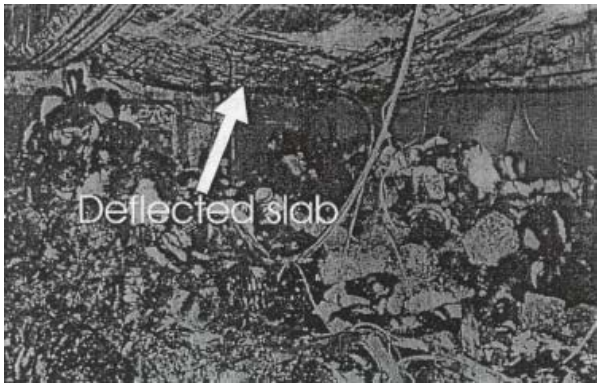

(b) The view of the floor over the fire

Figure 2-13 The Kellogg Factory fire in Manchester, UK (reproduced from Lim (2003))

2.6. Steel Thermal Properties

2.6.1. Thermal conductivity (λ_a)

The thermal conductivity is defined as the ratio of heat flux to the temperature gradient and is used to measure the ability of a material to conduct heat.

EC3 (1995) gives the following equations for the thermal conductivity of steel, λ_a:

$For \ \ 20°C \le T < 800°C$

$$\lambda_a = 54 - 3.33 \times 10^{-2} T \ \ (\text{W/m}^{\circ}\text{C}) \qquad \textbf{Equation 2-5}$$

$For \ \ 800°C \le T < 1200°C$

$$\lambda_a = 27.3 \qquad (\text{W/m}^{\circ}\text{C}) \qquad \textbf{Equation 2-6}$$

Based on these equations, a curve of the thermal conductivity of steel against the temperature is plotted in Figure 2-14. The graph shows the thermal conductivity of steel varies according to temperatures. The value for the thermal conductivity of steel linearly declines from 53.3W/m°C at 20°C to 27.3W/m°C at 800°C and then remains a constant of 27.3W/m°C until 1200°C.

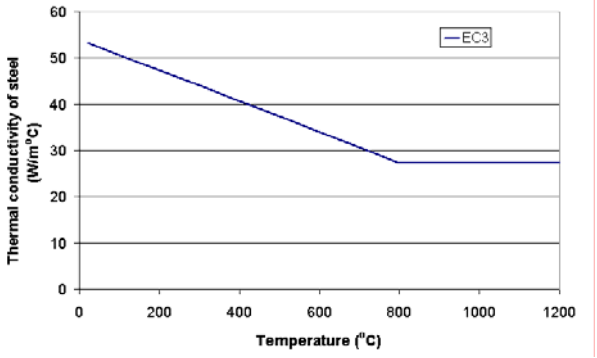

Figure 2-14 Thermal conductivity of steel against temperatures according to EC3 (1995)

The typical values of the thermal conductivity of steel are shown in Figure 2-15 (Pettersson et al., 1976; Malhotra, 1982). The graph shows that the thermal conductivity of steel nonlinearly declines from 20°C to 800°C, depending on the amount of alloying elements in the steel and the heat treatment to the steel.

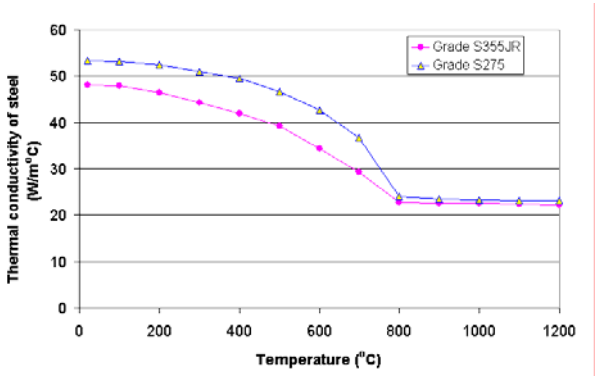

Figure 2-15 Variation of the thermal conductivity of steel against temperatures (Pettersson et al., 1976; Malhotra, 1982)

2.6.2. Specific heat (c_p)

The specific heat of a material is defined as the amount of required heat per unit mass to change the temperature of the material by one degree.

EC3 (1995) gives the following equations for the specific heat of steel, c_p, which hold up to 1200°C.

$For\ 20°C \le T < 600°C$

$$c_p = 425 + 7.73\times10^{-1}T - 1.69\times10^{-3}T^2 + 2.22\times10^{-6}T^3 \ (\text{J/kg°C}) \qquad \textbf{Equation 2-7}$$

$For\ 600°C \le T < 735°C$

$$c_p = 666 + 13002/(738 - T) \qquad (\text{J/kg°C}) \qquad \textbf{Equation 2-8}$$

$For\ 735°C \le T < 900°C$

$$c_p = 545 + 17820/(T - 731) \qquad (\text{J/kg°C}) \qquad \textbf{Equation 2-9}$$

$For\ 900°C \le T < 1200°C$

$$c_p = 650 \qquad (\text{J/kg°C}) \qquad \textbf{Equation 2-10}$$

These equations can be represented as the curves shown in Figure 2-16. For convenient use, a constant of 600J/kg°C is taken as a typical value for c_p.

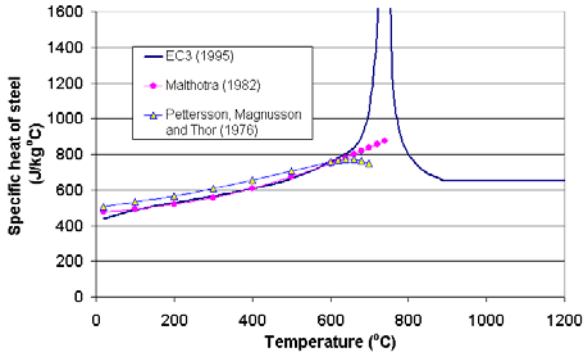

Figure 2-16 Variation of the specific heat of steel against temperatures according to EC3 (1995), Malhotra (1982) and Pettersson et al. (1976)

Malhotra (1982) gives an equation of the specific heat of steel that is expressed as:

$For\ 20°C \le T < 750°C$

$$c_p = 475 + 9.56\times10^{-2}T + 6.01\times10^{-4}T^2 \ \text{(J/kg°C)} \qquad \textbf{Equation 2-11}$$

Malhotra's equation holds up to 750°C at which the specific heat of steel is discontinuous in the EC3's equations. Malhotra's equation is also plotted in Figure 2-16 with the test data from Pettersson et al. (1976).

2.6.3. Thermal expansion

According to EC3 (1995), free thermal expansion of structural and reinforcing steel may be taken according to the following equations. However, the value of the thermal expansion depends on carbon contents in the steel and the heat treatment to the steel.

$For\ 20°C \le T < 750°C$

$$\Delta L / L_s = -2.416\times10^{-4} + 1.2\times10^{-5}T + 0.4\times10^{-8}T^2 \qquad \textbf{Equation 2-12}$$

$For\ 750°C \le T < 860°C$

$$\Delta L / L_s = 11\times10^{-3} \qquad \textbf{Equation 2-13}$$

$For\ 860°C \le T$

$$\Delta L / L_s = -6.2\times10^{-4} + 2.0\times10^{-5}T \qquad \textbf{Equation 2-14}$$

Anderberg (1983) gives an equation (Equation 2-15) for the thermal expansion of steel, which is slightly different from the equations given by EC3 in the range of temperatures from ambient temperatures to 750°C.

$$\varepsilon_{th,s} = -3.0\times10^{-4} + 1.2\times10^{-5}T + 0.4\times10^{-8}T^2 \qquad \textbf{Equation 2-15}$$

Note that Anderberg uses $\varepsilon_{th,\,s}$ as the symbol for the thermal strain of steel rather than $\Delta L/L_s$.

Both equations of the thermal expansion of steel are plotted in Figure 2-17. These curves show that the Anderberg's equation gives zero thermal strain at 25°C while the EC3's equations give zero thermal strain at 20°C.

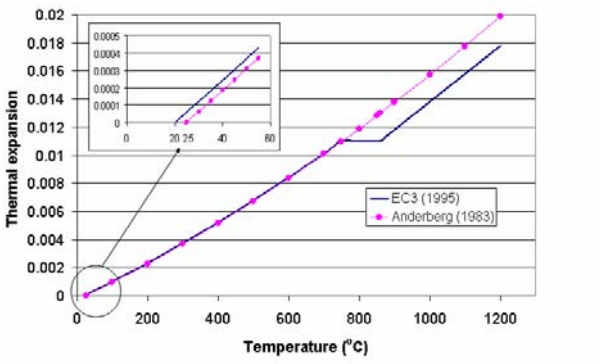

Figure 2-17 The thermal expansion of steel $\Delta L/L_s$ according to EC3 (1995) and Anderberg (1983)

2.7. Steel Mechanical Properties

2.7.1. Ultimate and yield strengths

The ultimate and yield strengths of reinforcing steel have been well-defined in many building codes, but the reduction of the ultimate and yield strengths of steel with temperatures are difficult to define because the yield point disappears at elevated temperatures (Buchanan, 2001). Figure 2-18 (a) shows the reduction of the ultimate and yield strengths of hot-rolled steel and Figure 2-18 (b) shows the reduction of the ultimate and yield strengths of cold-worked steel. In these graphs, the vertically hatched and horizontally hatched areas represent ultimate strength values and yield strength values, respectively. Curve a is the curve recommended by the Institution of Structural Engineers (cited from Harmathy (1993)) for both ultimate strength and yield strengths and curve b is the Brokenbrough-Johnston curve (cited from Harmathy (1993)) for yield strengths that has been adopted by some fire safety design guides (Harmathy, 1993). Comparing these graphs, it is apparent that the reduction of ultimate and yield strengths with the elevated temperatures is more pronounced for cold-worked steel than for hot-rolled steel.

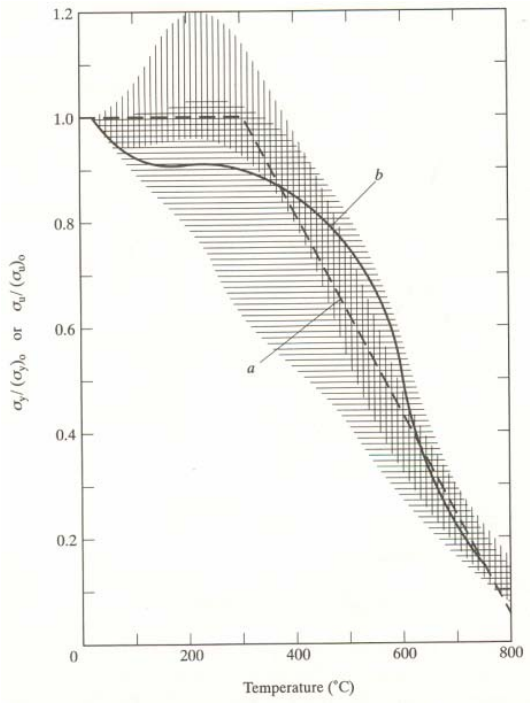

(a) Ultimate and yield strengths of hot-rolled steel

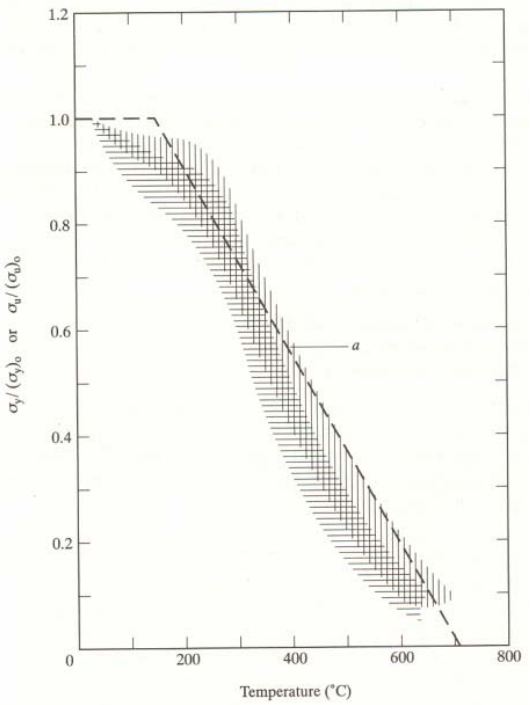

(b) Ultimate and yield strengths of cold-worked steel

In the graphs, σ_y and σ_u stand for yield and ultimate strengths at elevated temperatures, whilst $(\sigma_y)_o$ and $(\sigma_u)_o$ stand for yield and ultimate strengths at a ambient temperature.

Figure 2-18 Ultimate and yield strengths of steel (Harmathy, 1993)

Based on EC2 (2002), the variation of the proportional limit and yield strength of hot-rolled steel and cold-worked steel is shown in Figure 2-19 and Figure 2-20, respectively. For compression reinforcement in compressive zones of beams and slabs, EC2 (2002) gives the strength reduction at 0.2% proof strain for Class N reinforcement, as shown in Figure 2-21, which also applies for tension reinforcement where the strains are less than 2%.

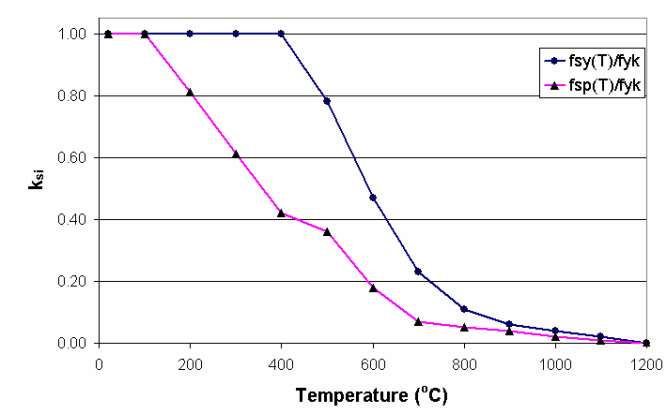

Figure 2-19 Coefficient k_s of hot-rolled steel at elevated temperatures according to EC2 (2002)

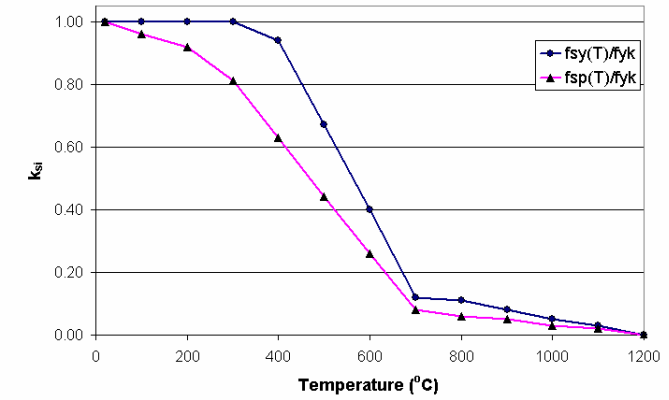

Figure 2-20 Coefficient k_s of cold-worked steels at elevated temperatures according to EC2 (2002)

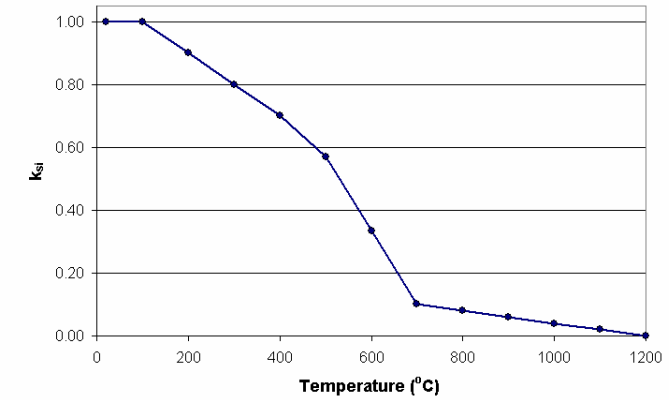

Figure 2-21 Coefficient k_s of compression reinforcement and tension reinforcement for strains less then 2% according to EC2 (2002)

2.7.2. Modulus of elasticity

The modulus of elasticity for low-carbon and medium-carbon steel and low-alloy steel is about 210×10^3 MPa at 20°C and decreases with the rise of temperatures. The rates of the reduction of modulus vary for various types of steel. Figure 2-22 shows the reduction of modulus of elasticity with temperatures for various types of steel. The graph shows that the modulus of elasticity of reinforcing steel decreases faster than the modulus of other types of steel.

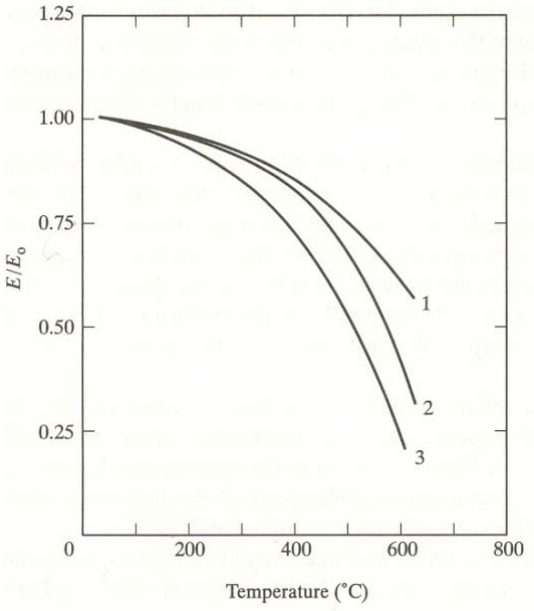

Figure 2-22 Variation of modulus of elasticity of steel with temperatures (Harmathy, 1993)
curves: 1, structural steel; 2, pre-stressing steel; 3, reinforcing steel

2.7.3. Deformation of steel at elevated temperatures

The deformation of steel at elevated temperatures is represented by the total strain, which includes three parts: thermal strain, creep strain, and stress-related strain.

Thermal strain

The thermal strain of steel, also called the thermal expansion of steel, has been discussed in Section 2.6.3.

Creep strain

The creep strain is very small in structural steel at normal temperatures, but it is very significant at temperatures over 500°C. Kirby and Preston (1988) have found that the creep strain highly depends on the temperature and stress level of steel. Figure 2-23 shows the creep

strain of steel tested in tension. In the graph, the creep strain curve becomes almost vertical when steel with a particular stress reaches a particular temperature.

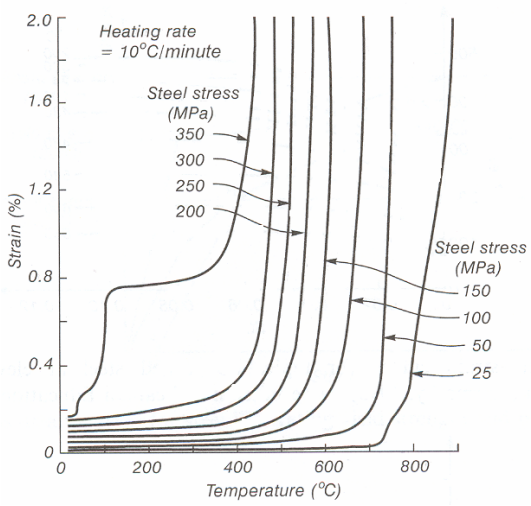

Figure 2-23 The creep strain of steel tested in tension (Kirby and Preston, 1988)

Stress-related strain

The stress-related strain curves for structural steel at elevated temperatures can be obtained directly from steady-state tests or derived from the results of transient tests. The typical stress-strain curves for hot rolled steel at elevated temperatures are shown in Figure 2-24. The graph illustrates that the ultimate strengths of steel increase in the 180°C to 370°C interval; whereas, the yield strengths steadily decline when the temperature rises.

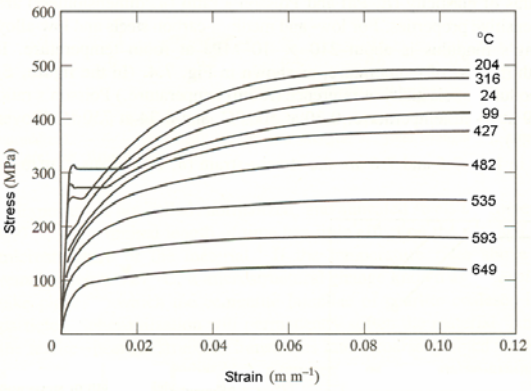

Figure 2-24 Stress-strain curves at various temperatures for structural steel (Harmathy, 1993)

EC-2 (2002) gives a formula to describe the relationship of stress-strain. At a given temperature, the stress-strain curve can be drawn using three parameters: the slope of the linear elastic range, E_s, the proportional limit, σ_{spr}, and the maximum stress level, f_y. The EC-2 stress-strain relationships have been developed to allow for the effect of creep in the steel at elevated temperatures. These relationships are intended for use in finite element computer programs which do not explicitly include time-dependent material properties, such as creep.

2.8. Concrete Thermal Properties

2.8.1. Thermal conductivity (λ_c)

EC2 (2002) gives an upper limit equation and a lower limit equation to describe the thermal conductivity of normal weight concrete, λ_c. The thermal conductivity of normal weight concrete may be determined using these equations. The equation of the upper limit thermal conductivity for normal weight concrete is expressed as:

$$For\ 20°C \le \theta_c \le 1200°C$$

$$\lambda_c = 2 - 0.2451(\theta_c/100) + 0.0107(\theta_c/100)^2 \quad \text{W/mK} \qquad \textbf{Equation 2-16}$$

The equation of the lower limit thermal conductivity for normal weight concrete is represented as:

$$For\ 20°C \le \theta_c \le 1200°C$$

$$\lambda_c = 1.36 - 0.136(\theta_c/100) + 0.0057(\theta_c/100)^2 \quad \text{W/mK} \qquad \textbf{Equation 2-17}$$

The variation of the upper and lower limit thermal conductivity against temperatures is shown in Figure 2-25.

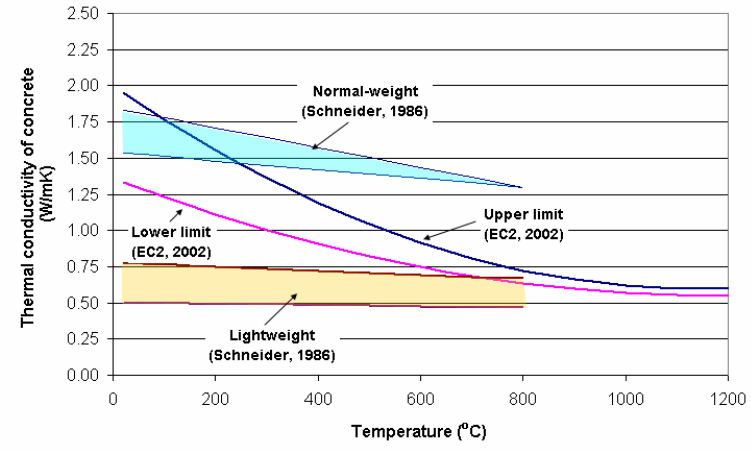

Figure 2-25 Variation of the thermal conductivity of concrete against temperatures according to EC2 (2002) and Schneider (1985)

The thermal conductivity for various concrete is also shown in Figure 2-25 (Schneider, 1985). It is found that the thermal conductivity for normal-weight aggregate concrete falls into a band and for lightweight concrete lies in between two lines with significant lower values.

2.8.2. Specific heat (c_p)

The specific heat of concrete, c_p, is significantly affected by moisture contents, but it is not very sensitive to either aggregate types or mix proportions (Schneider, 1985).

EC2 (2002) gives the equations of the specific heat for dry concrete as following:

$For\ 20°C \le \theta \le 100°C$

$$c_p = 900 \quad \text{J/kgK} \qquad \textbf{Equation 2-18}$$

$For\ 100°C < \theta \le 200°C$

$$c_p = 900 + (\theta - 100) \quad \text{J/kgK} \qquad \textbf{Equation 2-19}$$

$For\ 200°C < \theta \le 400°C$

$$c_p = 1000 + (\theta - 200)/2 \quad \text{J/kgK} \qquad \textbf{Equation 2-20}$$

$For\ 400°C < \theta \le 1200°C$

$$c_p = 1100 \quad \text{J/kgK} \qquad \textbf{Equation 2-21}$$

2.8.3. Thermal expansion

The thermal expansion, which is the same in all directions, is caused by temperature changes. The thermal expansion is typically non-uniform throughout the structures due to temperature non-uniformity and the stresses that arise in the structures (Bažant et al. 1996).

Hardened cement paste

When the hardened cement paste is heated up to about 150°C, the maximum expansion is reached. Between 150 and 300°C there is no further expansion in the paste, while between 300 and 800°C the paste shrinks and at 800°C the shrinkage of the paste is between 1.6 and 2.2 percent (Bažant et al. 1996) mainly because of the loss of moisture from the hardened cement paste.

Thermal expansion of aggregate

Generally, there are 65% to 80% aggregates in concrete, so the aggregates have a significant effect on the thermal expansion of concrete exposed to elevated temperatures (Bažant et al., 1996). Bažant et al. (1996) reported that Griffiths (1936) found that the thermal expansion of concrete is mainly affected by the percentage weight of silica in the rock. Quartzite and sandstone, which have high contents of silica, have high coefficients of thermal expansion, ranging from $9\times10^{-6}\ °C^{-1}$ to $10\times10^{-6}\ °C^{-1}$, while limestone, which has little or no silica, has the lowest coefficient, on average about $5.5\times10^{-6}\ °C^{-1}$.

Thermal expansion of concrete

The relationship between the thermal expansion and elevated temperatures up to 1200°C is linear, as shown in Figure 2-26. The graph shows that the thermal expansion of concrete made with different aggregates is significantly affected by the type of aggregates. At 600°C, the thermal expansion of sandstone aggregate concrete is about twice that of concrete made with expanded slag aggregates. At temperatures greater than 600 and 800°C, most concrete stop expanding and begin to shrink in some cases because of the shrinkage of hardened cement pastes and the dryness and decomposition of calcium silicate hydrates in the cement paste (Lim, 2003).

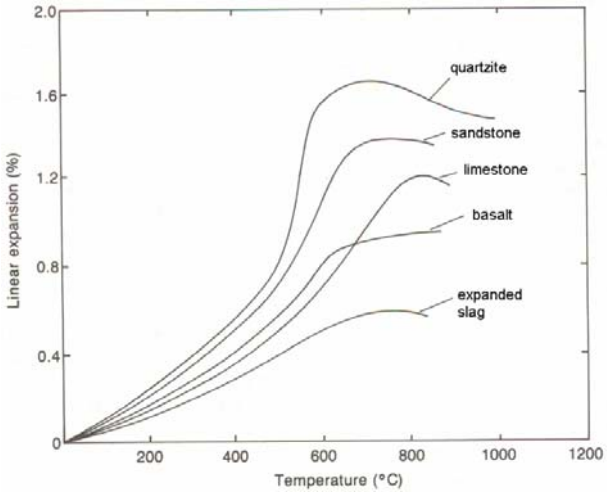

Figure 2-26 The linear thermal expansion of concrete made with various conventional aggregates, as a function of temperatures (reproduced from Bažant et al. (1996))

The coefficient of the thermal strain of concrete in EC2 (2002) is determined from the following with reference to the length of concrete specimens at 20°C:

Concrete with siliceous aggregates:

$For\ 20°C \le T \le 700°C$

$$\varepsilon_c = -1.8\times10^{-4} + 9\times10^{-6}T + 2.3\times10^{-11}T^3 \qquad \textbf{Equation 2-22}$$

$For\ 700°C < T \le 1200°C$

$$\varepsilon_c = 14\times10^{-3} \qquad \textbf{Equation 2-23}$$

Concrete with calcareous aggregates:

$For\ 20°C \le T \le 805°C$

$$\varepsilon_c = -1.2\times10^{-4} + 6\times10^{-6}T + 1.4\times10^{-11}T^3 \qquad \textbf{Equation 2-24}$$

$For\ 700°C < T \le 1200°C$

$$\varepsilon_c = 12\times10^{-3} \qquad \textbf{Equation 2-25}$$

The variation of the thermal elongation of concrete against temperatures is illustrated in Figure 2-27.

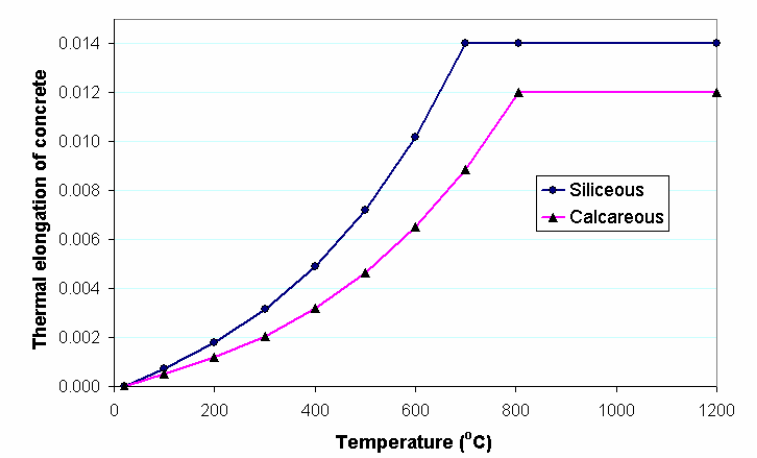

Figure 2-27 Thermal elongation of siliceous and calcareous aggregate concrete according to EC2 (2002)

2.9. Concrete Mechanical Properties

2.9.1. Compressive strength

The compressive strengths of concrete at elevated temperatures are related to aggregates and stress levels (Schneider, 1985). The strength ratio of calcareous aggregate concrete under various stress conditions is shown in Figure 2-28, while the effect of aggregate types on compression strengths is shown in Figure 2-29. These graphs show that the compressive strengths of concrete decline when the temperature rises.

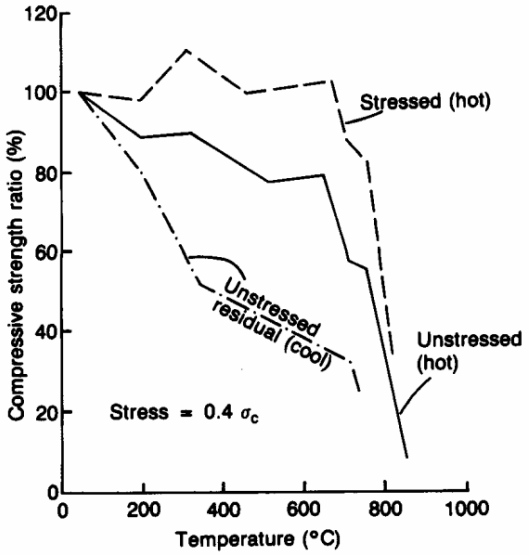

Unstressed: *the unloaded specimen was heated to the required temperature and then loaded to failure while hot.*
Stressed: *the specimen was loaded in compression and then heated to required temperature. The load was then increased until failure occurred.*
Unstressed residual: *the unloaded specimen was heated to the required to the required temperature and then allowed to cool slowly to room temperature. After seven days the specimen was loaded to failure in compression.*

Figure 2-28 Strength ratio of calcareous aggregate concrete under various conditions, as a function of temperatures (Bažant et al., 1996)

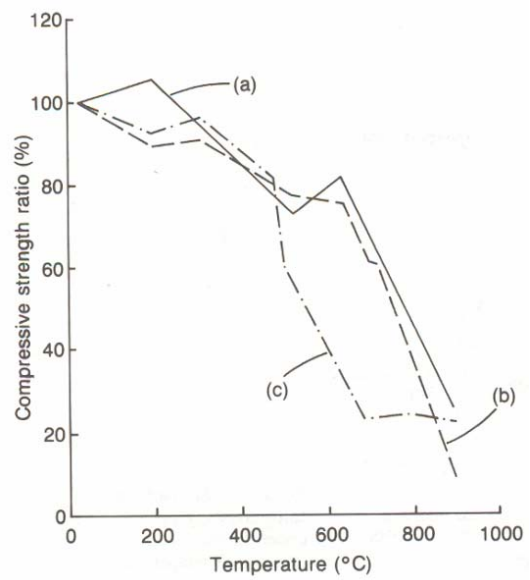

(a) *expanded shale aggregate light weight concrete (1:4.8:0.78)*
(b) *calcareous aggregate concrete (1:8.0:0.55)*
(c) *siliceous aggregate concrete (1:7.8:0.51)*

Figure 2-29 Effect of aggregate types on compression strengths of specimens stress-free during heating and loaded while hot as a function of temperatures (Bažant et al., 1996)

EC2 (2002) gives a coefficient, k_c, to express the reduction of characteristic compressive strengths of concrete. The coefficient, k_c, is expressed as:

$$k_c(T) = f_c(T) / f_c(20°C)$$ **Equation 2-26**

The curve for the coefficient of the reduction of characteristic compressive strengths of concrete in EC2 (2002) is shown in Figure 2-30.

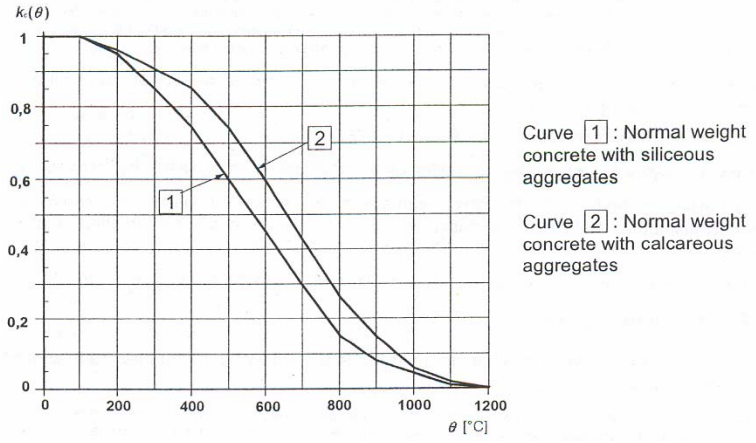

Figure 2-30 Coefficient k_c allowing for decrease of characteristic strengths of concrete (EC2, 2002)

2.9.2. Modulus of elasticity

Figure 2-31 shows the reduction of modulus of elasticity for various types of aggregates with elevated temperatures. The main reason for the reduction of modulus of elasticity is the breakage of bonds in the microstructure of cement pastes when the temperature rises, whilst the increase of rapid short-time creep also contributes the reduction of modulus of elasticity. The elastic modulus of siliceous aggregate concrete significantly falls at temperatures above 900°C.

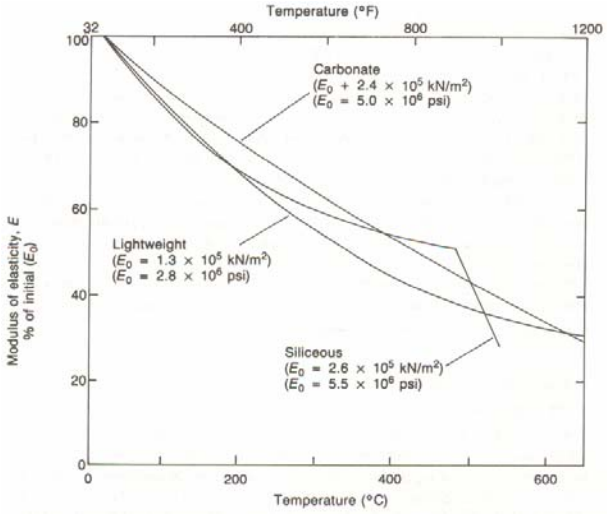

Figure 2-31 Reduction of modulus of elasticity for various types of aggregates with elevated temperatures (Bažant et al., 1996)

Generally, concrete which contains more compatible and chemically stable aggregates such as limestone has a lower reduction of the elastic modulus of concrete.

2.9.3. Deformation of concrete at elevated temperatures

The deformation of concrete at elevated temperatures usually includes four components: the thermal strain, the stress-related strain, the creep strain, and the transient strain (Buchanan, 2002). The total deformation in different concrete at elevated temperatures is shown in Figure 2-32.

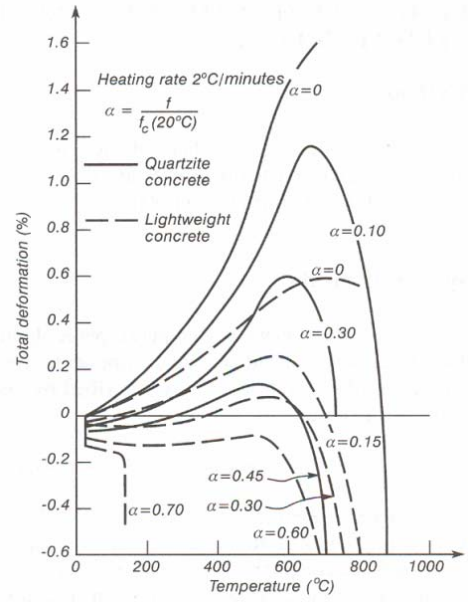

Figure 2-32 Total deformation in different concrete at elevated temperatures (reproduced from Buchanan (2002), original from Schneider (1988))

Thermal strain

The thermal strain of concrete, also called thermal expansion, has been discussed in Section 2.8.3.

Stress-related strain

The stress-related strain is a function of the applied stress and the temperature of concrete. Based on the experimental tests, Purkiss (1996) gives the stress-strain curves of concrete at elevated temperatures, as shown in Figure 2-33.

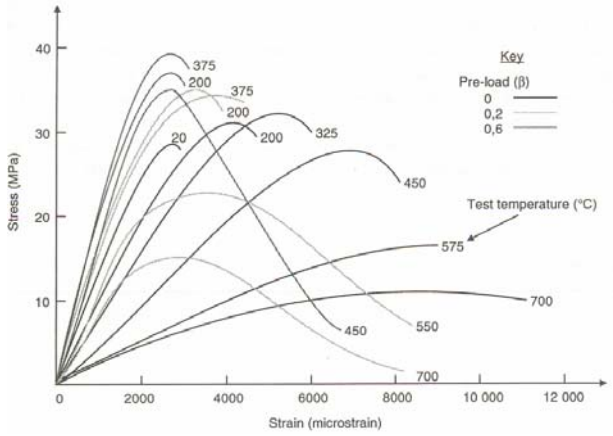

Figure 2-33 Stress-strain curves for concrete with pre-loads at elevated temperatures (Purkiss, 1996))

EC2 (2002) gives a mathematical model for the stress-strain relationship of concrete under compression at elevated temperatures, as shown in Figure 2-34.

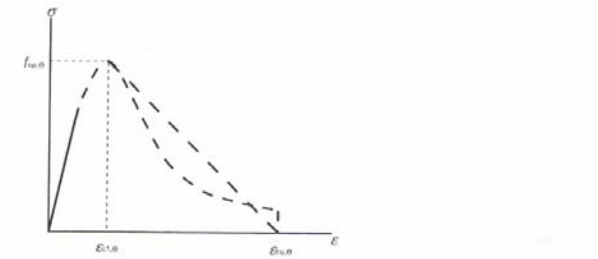

Range	Stress $\sigma(\theta)$
$\varepsilon \le \varepsilon_{c1,\theta}$	$\frac{3\varepsilon f_{c,\theta}}{\varepsilon_{c1,\theta}\left(2+\left(\frac{\varepsilon}{\varepsilon_{c1,\theta}}\right)^3\right)}$
$\varepsilon_{c1(\theta)} < \varepsilon \le \varepsilon_{cu,\theta}$	For numerical purposes a descending branch should be adopted. Linear or non-linear models are permitted.

Figure 2-34 Mathematical model for the stress-strain relationship of concrete under compression at elevated temperatures (EC2, 2002)

As for steel, the EC-2 stress-strain relationships have been modified to indirectly allow for the effect of creep in the concrete.

Creep strain

The creep strain is a function of the applied stress, temperature and time. The value of the creep strain of concrete at elevated temperatures is significantly greater than in the normal room temperature (Purkiss, 1996). Figure 2-35 (a) and Figure 2-35 (b) show the typical creep data for concrete carrying 22.5% load and 45% load, respectively.

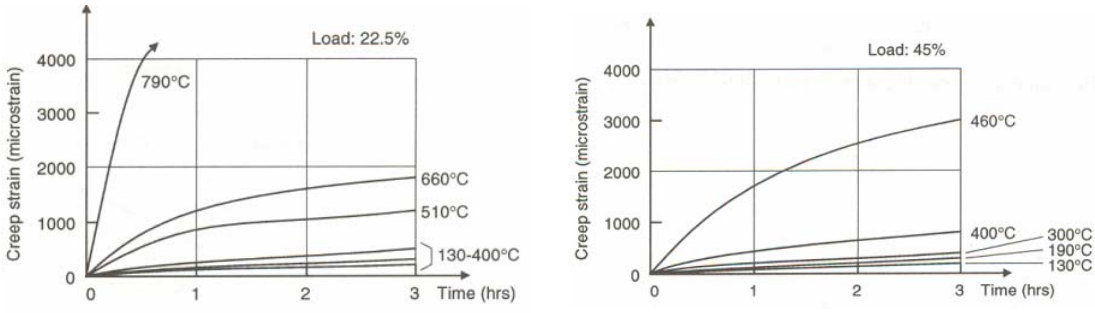

(a) Load: 22.5% (b) Load: 45%

Figure 2-35 Isothermal creep data for concrete at elevated temperatures (Anderberg and Thelandersson, 1976, reproduced from Purkiss (1996))

Transient strain

The transient strain, which does not exist for steel, is a function of the applied stress and temperature. Anderberg and Thelandersson (1976) found that the transient strain is unmeasurable and is only present on the first heating of concrete. The transient strain can be determined by extracting the thermal strain, the stress-related strain, and the creep strain from the total strain of concrete.

2.10. Summary

This chapter has summarized a large amount of literatures on the performance of concrete and concrete structures in fire conditions.

Reinforced concrete floor system can be classified in one-way slabs, two-way slabs and flat slabs. The fire design of reinforced concrete slabs in most national design codes is based on the fire resistance ratings. Performance based fire design can be carried out for one-way slabs with simple support conditions, while for the fire design of slabs by considering the beneficial effect of axial restraint forces, only one semi-empirical method based on numerous tests is available in hand calculation. Professional computer programs must be used in the analysis of the behaviour of concrete slabs under any types of fire exposure with complex supporting conditions. A number of computer programs for the analysis of structures in fire conditions have been developed in different parts of the world.

Two design methods can be used for the design of flat slabs at ambient temperature conditions: direct design method and equivalent frame method, while Yield-line theory can be used to predict the ultimate loads on flat slabs. Fire endurance of flat slabs can be determined using the method based on restraint to thermal expansion. The analysis of two-way slabs in fire conditions using 3-D shell element models have been carried out and it is found that membrane forces in the slabs significantly affect the fire behaviour of the slabs.

Concrete structures have a reputation for good behaviour in fires, although, there have been several incidents of fires in multi-storey concrete buildings. Eleven cases of fire-related collapse or damage in buildings are mentioned in this chapter.

The thermal and mechanical properties of steel and concrete at elevated temperatures are the main factors affected the design of reinforced concrete slabs in fire conditions. The thermal properties of steel and concrete include thermal conductivity, specific heat and thermal expansion, whilst the mechanical properties of steel and concrete include compressive strength, modulus of elasticity and deformation at elevated temperatures.

3. ANALYSIS METHODS USING THE SAFIR FINITE ELEMENT SOFTWARE

In this chapter a computer program, SAFIR, which is used for the analysis of flat slabs in this research, will be described briefly. SAFIR is a non-linear finite element program for analysing steel and composite structures exposed to fire. SAFIR has been developed by J.M. Franssen at the University of Liege, Belgium since 1980s.

3.1. Introduction of SAFIR

Based on the *User's Manual for SAFIR 2001* (Franssen et al., 2002a), some characteristics of SAFIR are described. Further information related to the program can be found elsewhere (Franssen et al., 2002b).

3.1.1. Capabilities of SAFIR

Three types of calculations, named thermal, torsional, and structural analysis, can be performed by SAFIR. Geometrical non-linearity due to large displacements and material non-linearity in the thermal and mechanical properties can be accounted for by its structural analysis. SAFIR can perform structural analysis at ambient temperatures, although it was developed for performing structural analysis under fire conditions (Franssen et al., 2002a).

3.1.2. Common features in all analyses

The common features in all computations include optimization of the matrix, which can be performed by using internal re-numbering of the system equations, master-slave relations, which can impose two different nodes with the same temperature or the same displacement, graphic pre-processing capabilities, which are performed by *SAFIRwizard*, and post-processing capabilities, which are carried out by *DIAMOND2002 XP*.

3.1.3. Sign conventions

The Cartesian system of coordinates is used for Global Axes when defining a structure using SAFIR. There are two coordinate axial systems in SAFIR, the Global and Local axes system. For the 2-D analysis, the axes are tagged as G1 and G2, while the local axes are tagged L1 and L2 (where the label of G is derived from Global and the label L is derived from Local). Based on the 'right-hand rule', applied moments and rotations are positive in the counter-clockwise direction; applied forces and the displacements are positive in the direction of G1

and G2 (Figure 3-1). For 3-D analysis, the axes are tagged as G1, G2 and G3 and the local axes are tagged L1, L2 and L3. The movement G1, G2 and G3 is dextrorse; applied forces and moments, displacements and rotations are all positive in the G1, G2 and G3 directions. For convenient use, the axes tags of G1, G2, and G3 are preferred to the axes tags of x, y, and z, respectively.

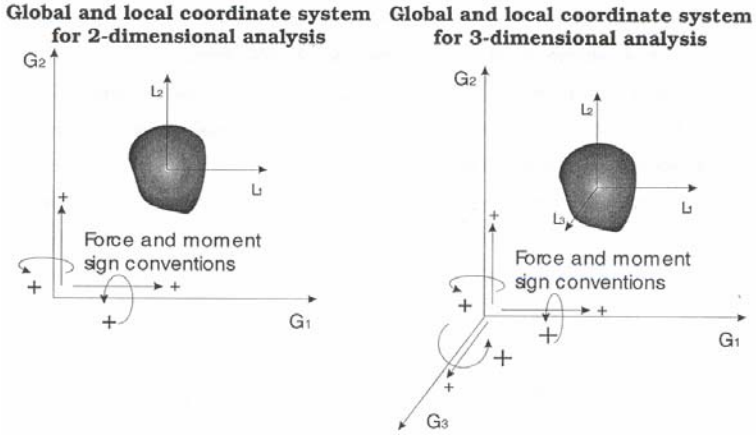

Figure 3-1 Positive sign conventions used in SAFIR (Lim, 2003)

The stresses and the axial forces that are obtained as a summation of all the stresses are positive in tension. In the beam elements, the moments, which are obtained as the summation of $y_i\sigma_i$ (y_i are measured on the local axis), are positive when the fibres in tension have a positive local coordinate.

3.2. Thermal Analysis

The thermal analysis needs to be carried out before the structural analysis of fire exposed structures. The structures are discretised to structure members (beams, columns, slabs or trusses), which can be modelled as 2-D solid elements for the 2-D sections and 3-D solid elements for the 3-D elements in SAFIR.

2-D solid elements and 3-D solid elements can be analysed with the thermal analysis function of the program. The results of thermal calculations can be visually analysed using *Diamond2002 XP*. The output of 2-D thermal calculations can be utilised to perform two- or three-dimensional structural analysis, while the output of 3-D thermal calculations can not. A *.TEM* file is created for beam elements or *.TSH* file for shell elements.

3.3. Torsional Analysis

The torsional analysis can be performed on all cross-section shapes, which are discretised to 2-D solid elements in SAFIR. The results of the torsional analysis are stored in a file with the extension of *.TEM*. The torsional stiffness can be added to beam elements via the result files of the thermal analysis for the same cross-section. The materials of the 2-D solid elements are considered to be in the elastic stage at ambient temperatures. Therefore, the obtained torsional stiffness should be adjusted in order to take into account an increase of temperatures during the fire. The torsional stiffness remains a constant value throughout the simulation of mechanical behaviours. For the structure with 3-D beam elements, the torsional analysis must be performed.

3.4. Structural Analysis

The structural analysis in fire conditions is performed after thermal analysis (for 2-D and 3-D structural analysis) and torsional analysis (for 3-D structural analysis with beam elements). Truss and beam elements are available for 2-D and 3-D structural analysis; in addition, shell elements are available for discretising the floor system of structures in 3-D structural analysis. Large displacements, thermal strain effects and temperature dependant nonlinear materials are considered in truss, beam and shell elements. Due to using the arc length technique in SAFIR, the local failure of a structural member does not lead to imperilling the complete structure.

For analysis of reinforced concrete flat slabs in this thesis, beam and shell elements will be used. Therefore, in this section the SAFIR beam and shell elements will be introduced with more details.

3.4.1. SAFIR beam elements

There are a number of assumptions for the beam elements in the SAFIR program:

1. The Bernoulli Hypothesis is considered.
2. Shear energy of the plane sections in the finite elements is ignored.
3. Plastifications are only considered in the longitudinal direction of beam elements; this means uniaxial constitutive models are used in the beam elements.
4. Non-uniform torsion is accounted for.

The geometrical location of 2-D beam elements needs three nodes to describe it. Figure 3-2 shows that N1 and N2 represent the end nodes of a beam element in space and N3, which is

between the two end nodes, supports the non-linear component of longitudinal displacements. N1 and N2 have three degrees of freedom consisting of two displacements and one rotation in 2-D beam elements.

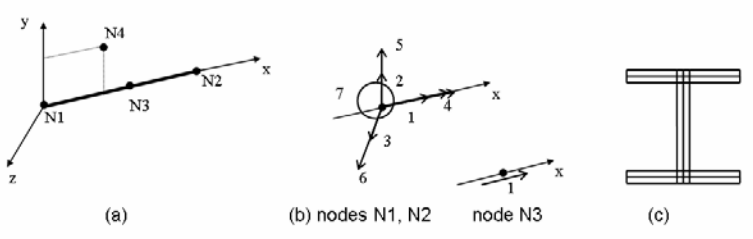

Figure 3-2 Beam elements (a) Local axes (b) Degrees of freedom at nodes (c) The cross section (Franssen et al, 2002b)

The additional node, N4, is required for 3-D beam elements to define the position of the local y-axis of beam elements. N1 and N2 have seven degrees of freedom, three displacements, three rotations and a warping degree of freedom (Figure 3-2). The integration along the length of beams is performed with Gauss integration and two or three integration points are used.

The properties of the cross-section of beam elements are defined by thermal analysis and are stored in a file with the extension name of *.TEM*. The cross-section of beam elements is discretised to 2-D solid elements in the thermal analysis for the same cross-section. These solid elements are also referred to as 'fibres' in the beam cross-section. Each fibre can have its own material; the area of the fibre can be modified manually using text-editors. This function is commonly used to justify the cross-area of reinforcing bars in the cross-section of reinforced concrete beams and columns.

The beam elements are connected each other by joint points. The joint points of beam elements can be modified by changing the value of NODELINE in the file, which is the input file of thermal analysis for the cross-section of beam elements. The beam elements with different joint points are treated as different kinds of beam elements (Figure 3-3).

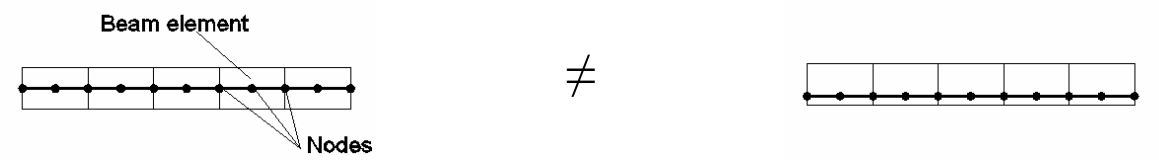

Figure 3-3 Beam elements with different position of joint points

3.4.2. SAFIR shell elements

There are several assumptions for the shell elements in the SAFIR program:

1. The shear strain energy in the finite elements is neglected and the shear strain at the Gauss points is set to zero.
2. The out-of-plane displacements and rotations are parabolic along each side.
3. The rotations along the edges vary linearly.
4. The shell element has a cubic membrane displacement field.
5. The cross-section of reinforcing bars is not subtracted from the plane section of shell elements; steel and concrete are simultaneously present at the location of reinforcing bars.
6. Only axial direction actions are resisted by the reinforcing bars; the reinforcing bars cannot directly resist shear forces.

Geometrically defining shell elements in SAFIR program is by a four-node quadrilateral element with constant thickness, h (Figure 3-4). In Figure 3-4 four corner nodes are denoted as 1, 2, 3, and 4, while the middle points of the edges of shell elements are denoted as a, b, c, and d; the centre of the local system of coordinates is the intersection point of line a-c and line b-d. The direction of the z axis is perpendicular to the a-c and b-d plane.

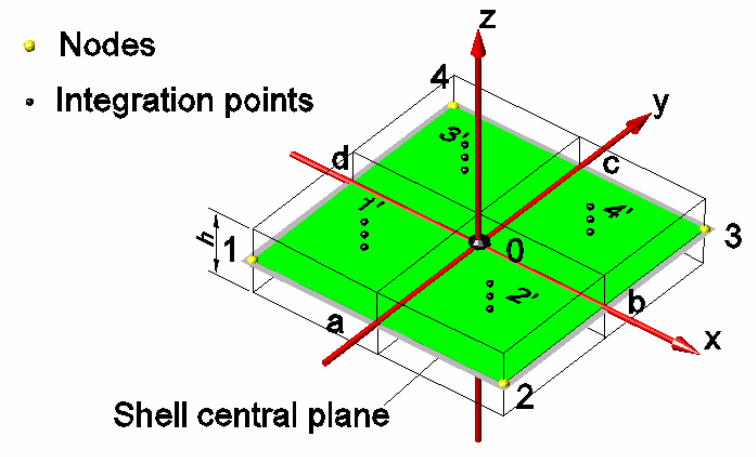

Figure 3-4 Geometry of the shell element

Four Gauss integration points on the surface of shell elements are denoted as 1', 2', 3', and 4' in Figure 3-4. Along the thickness, h, of shell elements, there are also Gauss integration points which range from 2 to 10, defined by users.

The reinforcing bars in shell elements are modelled as a thin sheet of steel, which is called the smeared model. The horizontal position of the reinforcing layers in shell elements is parallel to the local x-y plane, while the vertical position is defined by its local vertical coordinate; the orientation of reinforcing bars relatives to the local x axis. The information of reinforcing bars is defined in the file with the extension of *.TSH*, in which multiple layers of reinforcing bars can be accepted.

The shell elements are connected each other by joint points. The joint points of shell elements can be modified by changing Local y-coordinates in the file, which is the input file of the thermal analysis for the cross-section of shell elements. The shell elements with different joint points are treated as different kinds of shell elements (Figure 3-5).

Figure 3-5 Shell elements with different position of joint points

3.4.3. Output of the structural analysis

For every time step when convergence is reached, the following data are calculated and can be written in the output file, which has an extension file name *.OUT*:

1. The displacements of the structure at each node
2. Temperatures in the fibres of beam elements
3. The values of balance forces
4. Internal forces and tangent moduli in beam elements
5. Stresses, strains, bending moments and membrane forces in shell elements.

3.5. Analysis Procedure Using SAFIR

The analysis procedure using the SAFIR finite element program is shown in Figure 3-6. At thermal analysis steps, the files with the expansion *.IN* can be created using *SafirWizard* for the normal cross-section of structural members.

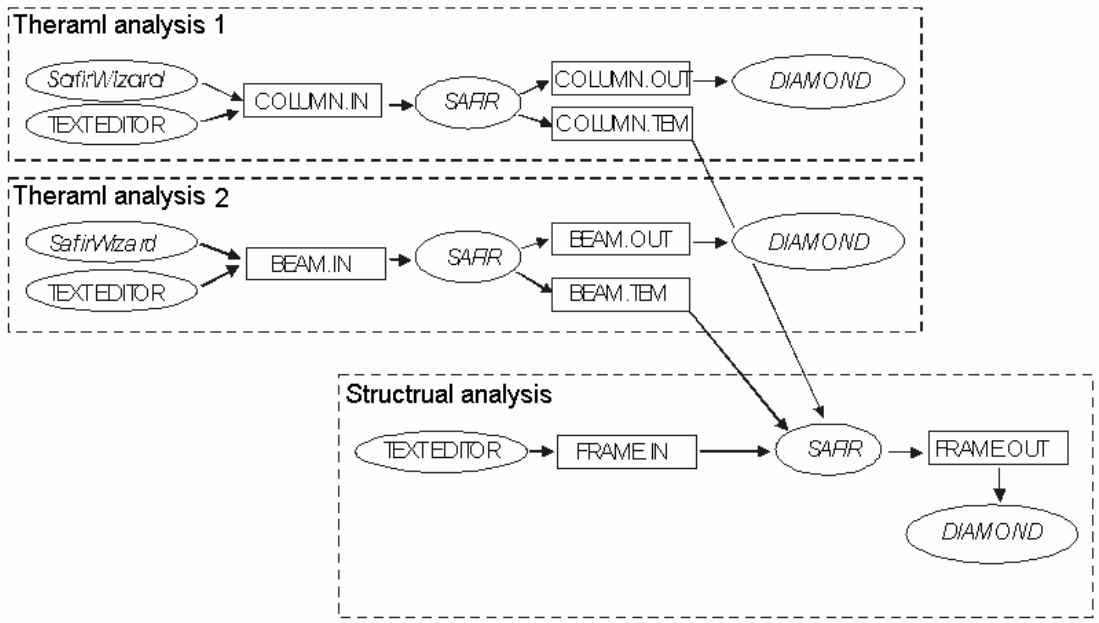

Figure 3-6 The files and steps of analysis procedure in SAFIR (Franssen et al., 2002a)

A visualization analysis procedure using SAFIR, the finite element software is shown on the next page in Figure 3-7. The structure is discretized to structural members, which are described as elements (solid, beam, and shell elements) in SAFIR. 2-D solid elements are used in the thermal and torsion analysis. 3-D shell and beam elements are used in the structural analysis. The input data can be edited using any kind of text editors. The outputs of the thermal and torsion analysis are stored in two files. Both can be edited using any kind of text editors; one file has the extension name *.OUT* and the other has the extension name *.TEM* (or *.TSH* for shell elements). The files of thermal analysis, which are modified using the results of torsion analysis, are used in structural analysis. The output of structural analysis is stored in a file with the extension name *.OUT*. All the *.OUT* files can be graphically represented by *DIAMOND2002 XP* except the *.OUT* files for torsion analysis.

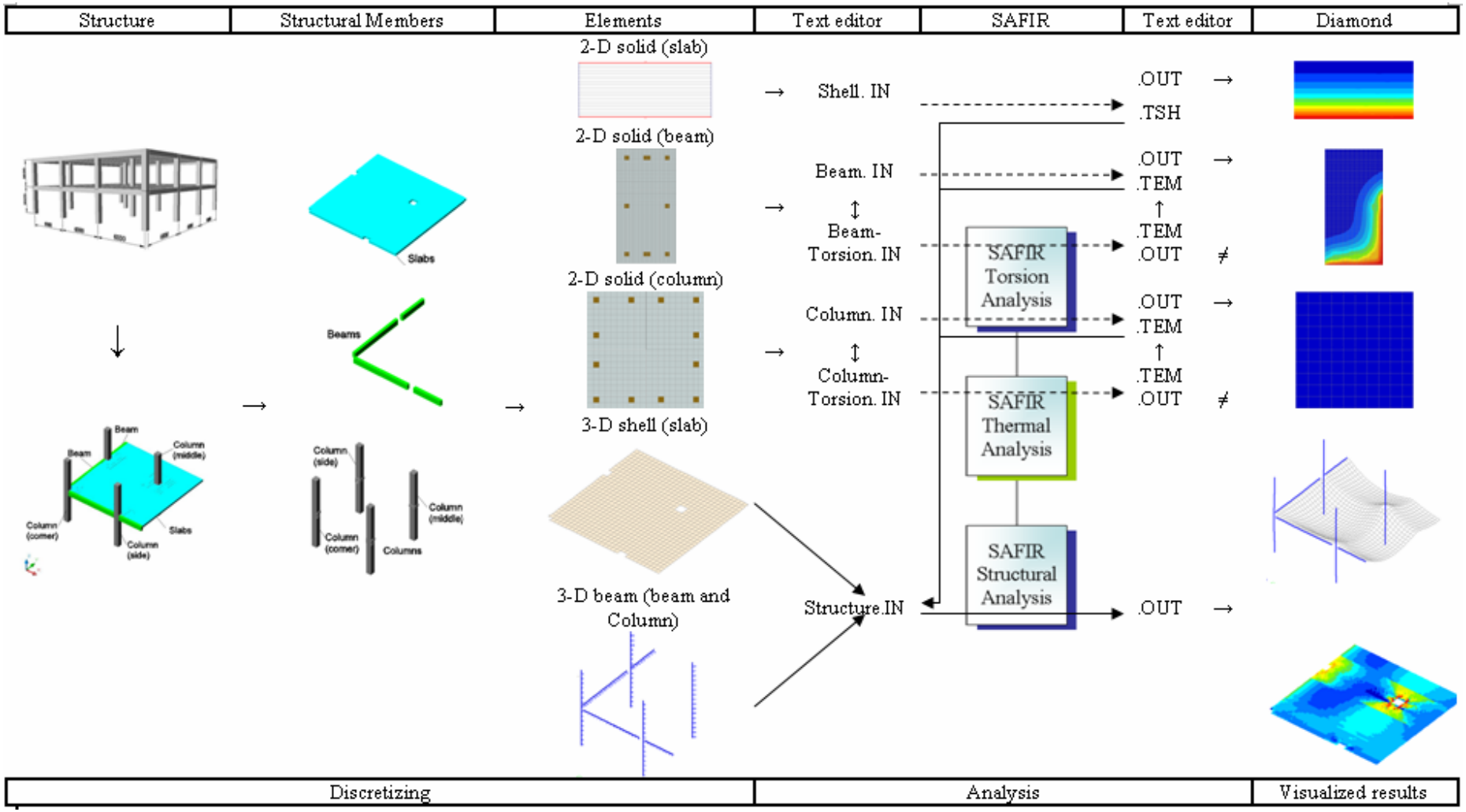

Figure 3-7 An example of analysis procedure using SAFIR

4. THERMAL ANALYSIS OF REINFORCED CONCRETE SLABS

The thermal behaviour of reinforced concrete slabs under ISO 834 Standard fires exposure is investigated in this chapter of the thesis. The purpose of this chapter is to verify the function of thermal analysis in SAFIR and carry out the thermal analysis for the structural members which will be used in structural analysis of reinforced concrete slabs in Chapter 5, Chapter 6, and Chapter 7. The effect of the boundary thermal conditions of slabs and the presence of reinforcing bars in slabs on the thermal analysis is discussed. Determining the fire endurance of slabs using SAFIR is also performed in this section.

4.1. Introduction

The design fire curve that has been used in this thesis is the ISO 834 Standard fire curve (ISO, 1975). Two fire scenarios are considered; one is that the duration of fire exposure reaches four hours and not exceeds the end point of fire tests; the other one is that the duration of fire exposure is persistent for up to one hour followed by a decay phase of the fire.

4.1.1. Fire test standard

Fire-resistance testing began in Germany in the 1880s. Nowadays, some countries have their standards for the fire-resistance testing (Harmathy, 1993), such as:

- AS 1530.4 Part 4 in Australia
- NBN 713020 in Belgium
- CAN 4-S101 in Canada
- DS 105 in Denmark
- DIN 4102 Part 4 in Germany
- BS 476:Parts 20, 21, 22, and 23 in the United Kingdom
- ASTM E119 in the United States

For the purpose of fire-resistance testing, standard fires have been developed in many countries. The standard fire curve that can be used to analyse the behaviour of structures exposed to fires is expressed as a temperature-time curve. The standard fire curves of fire-test furnaces in some countries are shown in Figure 4-1 (Lie, 1972)

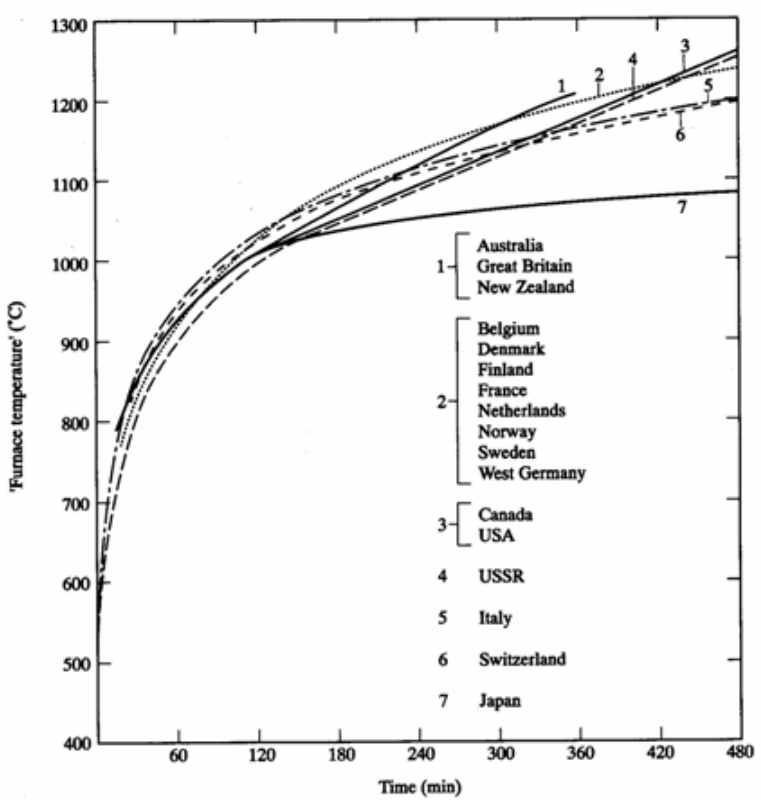

Figure 4-1 Temperature-time curves in various national fire-resistance test standards (Lie, 1972)

The standard temperature-time curves from ASTM E119 (ASTM, 1999) and ISO 834 are similar, however, they can be described by different equations (Equation 4-1 and Equation 4-2).

The ISO 834 Standard fire curve (ISO, 1975) is defined as:

$$T = 345\log_{10}(8t + 1) + T_0 \qquad \textbf{Equation 4-1}$$

where T is the fire temperature (^{o}C), T_0 is the ambient temperature (^{o}C), and t is the time (minutes).

Initially, the ASTM E119 fire curve is defined by a number of discrete points. An equation given by Lie (1995) approximately describes the ASTM E119 fire curve and is defined as:

$$T = 750[1 - e^{-3.79553/\sqrt{t_h}}] + 170.41\sqrt{t_h} + T_0 \qquad \textbf{Equation 4-2}$$

where T is the fire temperature (^{o}C), t_h is the time (hours), and T_0 is the ambient temperature (^{o}C).

For the fire tests of building components, the duration of fire tests is defined as when the end points are reached. The end point criteria defined in ASTM E119 include stability (structural), integrity (flame passage), and insulation (heat transmission). Gustaferro et al. (1980) summarized a number of the fire tests for concrete floor systems and found that the fire endurance was determined by heat transmission rather than by the structural end point. The heat transmission end point defined in ISO 834 is that an average temperature of the unexposed surface of floors is 140°C or a maximum temperature of 180°C. The similar heat transmission end point is also defined in ASTM E119, as that the temperature of the unexposed surface of floors (roofs, or walls) is not rise an average temperature of 121°C (250°F) or a maximum temperature of 163°C (325°F) at any point. If the ambient temperature is 20°C, the heat transmission end point defined in these standards will be the same.

Because the ISO 834 fire-resistance test standard contains the entire essential features of similar standards and is expected to gain acceptance by all countries (Harmathy, 1993), the ISO 834 Standard fire will be used in this thesis to model the fire scenarios. The heat transmission end point in ISO 834 is also considered in performing the thermal analysis of concrete slabs.

4.1.2. The ISO 834 Standard fire with a decay phase

The ISO 834 Standard fire is a non-linear rapid growth fire and there is no decay phase in it. The full process of fire development includes four phases, as shown in Figure 4-2 (Buchanan, 2001). The graph shows that the decay phase is an important part of the full process of fires.

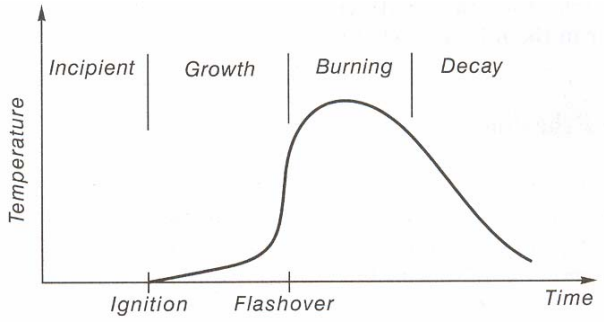

Figure 4-2 Temperature-time curve for the full process of fire development (Buchanan, 2001)

The ISO 834 Standard fire with a decay phase added is defined as the decay phase occurred at 60 minutes after the initial growth phase of fires in this research of the thesis. The decay phase is simply considered to be a linear reduction of fire temperatures. The rate of temperature reduction is originally given by Feasey et al. (2002), as:

$$\frac{dT}{dt} = \left(\frac{dT}{dt}\right)_{ref} \sqrt{\frac{F_v / 0.04}{b / 1900}}$$ **Equation 4-3**

where dT/dt is the temperature reduction rate (°C/hour), $(dT/dt)_{ref}$ is the reference decay rate (°C/hour), F_v is the ventilation factor, and b is the square root of the thermal inertia of compartment linings ($Ws^{0.5}/m^2K$).

Lim (2003) gave the decay rate to be 500°C/hour by assuming the ventilation factor F_v of 0.04, square root b of 1900 $Ws^{0.5}/m^2K$ (concrete compartment linings), and reference decay rate $(dT/dt)_{ref}$ of 500°C/hour for 60 minutes' fire exposure. This decay rate will be used in this thesis for the fire scenario of the ISO 834 Standard fire with a decay phase.

The temperature-time curves of the ISO 834 Standard fire with or without a decay phase are shown in Figure 4-3. The fire temperature reached 945°C at 60 minutes. At 170 minutes, the temperature of the fire with a decay phase declined to the ambient temperature (20°C), while the temperature of the fire without a decay phase increased to 1102°C at 170 minutes and 1153°C at 240 minutes.

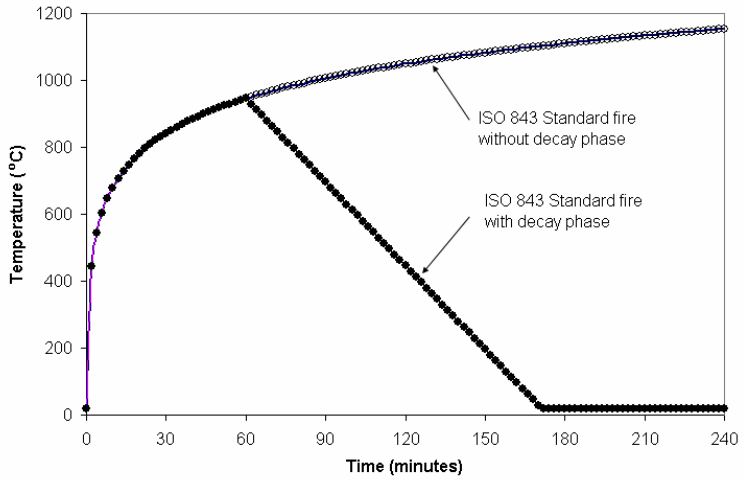

Figure 4-3 ISO 834 Standard fire curves with or without a decay phase

4.1.3. Heat transmission in concrete slabs

Based on the fire tests of concrete slabs, it is found that the slab thickness and the type of concrete aggregate are the main factors affected the temperature rise on the unexposed surface of slabs, as shown in Figure 4-4 (Gustaferro et al., 1980).

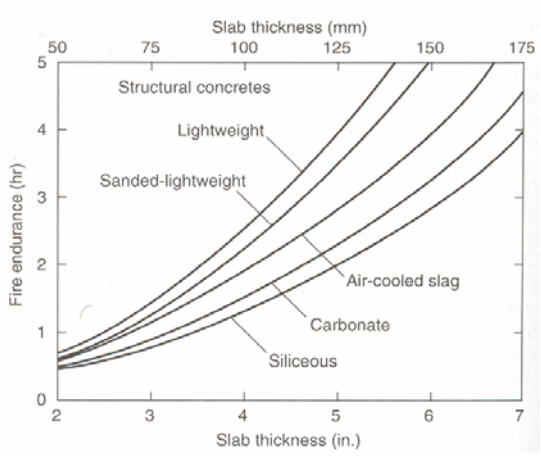

Figure 4-4 Fire endurance of concrete slabs – effects of thickness and type of concrete aggregate – based on heat transmission (Gustaferro et al., 1980)

The curves in Figure 4-4 can be approximately expressed as:

$$R = Ct^n$$ **Equation 4-4**

where R is the fire endurance in minutes, C is a constant for a given concrete type (values range from 6 to 11), t is the slab thickness in inches, and n is an exponent (values range from 1.65 to 2.0).

Floor slabs are often constructed as the concrete base slabs with overlays or undercoatings of either insulating materials or other types of concrete (Fleischmann and Buchanan, 2002). These types of composite assemblies of floors are called multi-course floors. Fire endurance of terrazzo floors based on heat transmission is shown in Figure 4-5 (Abrams and Gustaferro, 1969). It shows that the concrete base slab with a sand cushion had the largest fire endurance due to the effect of thermal isolation of the sand cushion.

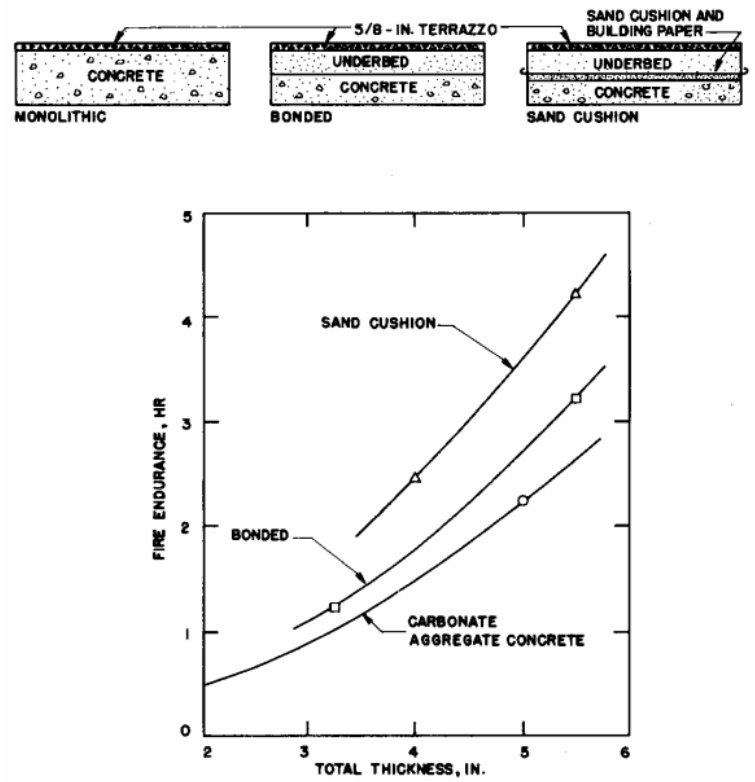

Figure 4-5 Fire endurance of terrazzo floors – base on heat transmission (Abrams and Gustaferro, 1969)

Some other factors affecting the heat transmission in concrete slabs, such as unit weight, air contents, and maximum aggregate size were investigated by Gustaferro et al. (1980), who also found that the average temperature of reinforcing bars approximately equals to the temperature of the concrete at the level of the centre of the bars when the slabs are exposed to fires from below.

4.2. The thermal Analysis of Concrete Slabs

SAFIR, a finite element computer program, is used to analyse the thermal behaviour of reinforced concrete slabs. The thermal analysis of the cross-sections of slabs is performed before the structural analysis to determine the distribution of temperatures through the across-sections. Single course concrete slabs with a thickness of 0.2m exposed to an ISO 834 Standard fire with or without a decay phase are investigated.

4.2.1. Thermal model of the slabs in SAFIR

A typical thermal model in SAFIR is shown in Figure 4-6 (a) which shows that the cross-section of the slab with a thickness of 0.2m is discretized into 20 four-node quadrilateral solid elements. The typical distribution of temperatures in the cross-section of the slab exposed to an ISO 834 Standard fire is shown in Figure 4-6 (b).

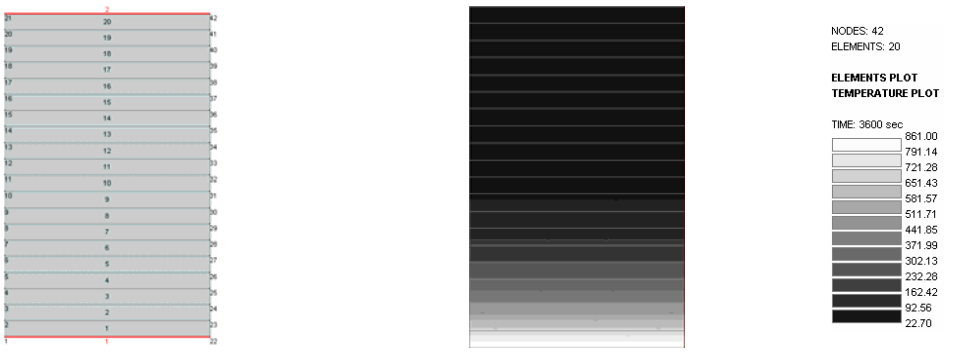

(a) The thermal model of the slab (b) Distribution of temperatures in the slab

Figure 4-6 The thermal model of a cross-section and the distribution of temperatures in the slab

Assuming that the distribution of temperatures is not affected by reinforcing bars in slabs, the reinforcing bars are not included in the thermal analysis and the temperature of reinforcing bars equals the temperature of the concrete at the same level of slabs.

During the thermal analysis, the concrete of slabs are taken as SILCONCEC2 (siliceous aggregate concrete for EC2) and the reinforcing bars are taken as STEELEC2 (hot rolled steel in EC2); both are embedded in the computer program, SAFIR (Franssen et al., 2002a). There are four factors for concrete that users need to determine (the values in the parentheses are used for the thermal analysis of cross-sections for structural members in this thesis):

- Moisture content (92 kg/m^3)
- Convection coefficient on hot surfaces (25 W/m^{2}K)
- Convection coefficient on cold surfaces (9 W/m^{2}K)
- Relative emissivity (0.56)

4.2.2. The effect of varying the thickness of slabs

It is evident to find that the numbers and the sizes of solid elements in SAFIR slightly affect the thermal analysis of concrete slabs when the numbers of the elements through the depth of slabs are not less than 20 (slabs with normal thicknesses between 0.10m and 0.20m). The effect of varying the thermal models for thermal analysis of slabs in SAFIR is not detailed in this thesis.

The analysis of heat transmission of concrete slabs with the thickness range from 0.06m to 0.2m is carried out using SAFIR. The ISO 834 Standard fire is beneath the slabs and the temperature above the slabs is assumed to be 20^{o}C. The curves of the relationship between the thickness of slabs and the time when the temperatures of the unexposed surface of slabs (the top surface) reached 140^{o}C are plotted in Figure 4-7 (the SAFIR curve with or without a decay phase of the fire). The curve plotted using Equation 4-4 with the constant C of 8.5 and the exponent n of 1.7 is also illustrated in Figure 4-7 (the Equation 4-4 curve).

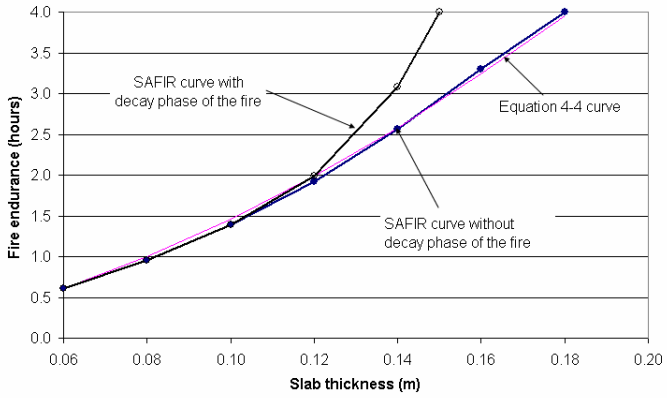

Figure 4-7 Effect of fire endurance by varying the thickness of slabs

Figure 4-7 shows that the results of thermal analysis using SAFIR perfectly matched the results obtained from Equation 4-4, which is based on the fire tests. The temperature on the top surface of 0.2m thickness slabs was 106^{o}C after four hours' fire exposure. After 1.4 hours' fire exposure, the temperature on the top surface of 0.1m thickness slabs was greater than 140^{o}C and the end point based on heat transmission was reached. Considering the slabs exposed to an ISO 834 Standard fire for 60 minutes and followed by a decay phase, if the thickness of slabs was greater than 0.16m, the end point based on heat transmission was never reached. The fire endurance of the slabs with the thickness range from 0.12m to 0.16m exposed to the fire with a decay phase was longer than those slabs exposed to the fire without a decay phase.

The distribution of temperatures through the depth of the 0.2m thickness slab exposed to an ISO 834 Standard fire without a decay phase is shown in Figure 4-8. It shows that the temperature at 0.03m above the bottom of the slab increased from 20°C at 1 minute to 700°C at 180 minutes and continuously increased to 775°C at 240 minutes when the simulation was stopped.

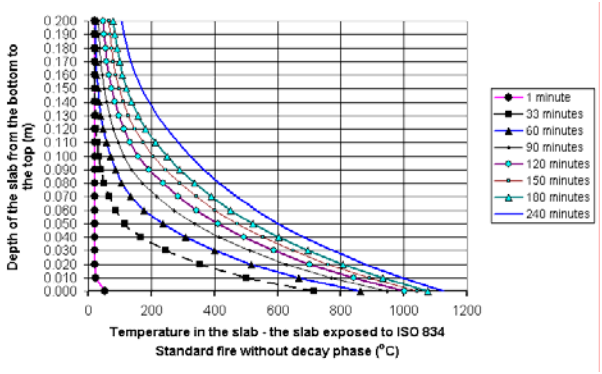

Figure 4-8 Distribution of temperatures in the slab exposed to an ISO 834 Standard fire without a decay phase

Figure 4-9 shows the distribution of temperatures of the slab with a thickness of 0.2m exposed to an ISO 834 Standard fire with a decay phase. The graph shows that the temperature at 0.03m above the bottom of the slab increased from 20°C at 1 minute to 450°C at 90 minutes and then declined to 160°C at 240 minutes when the simulation was stopped; the maximum temperature of 456°C was reached at 84 minutes. When the temperatures on the bottom region of the slab significantly declined in the decay phase of the fire, the temperatures on the top region of the slab still increased slightly due to a wave of heat moving through the slab.

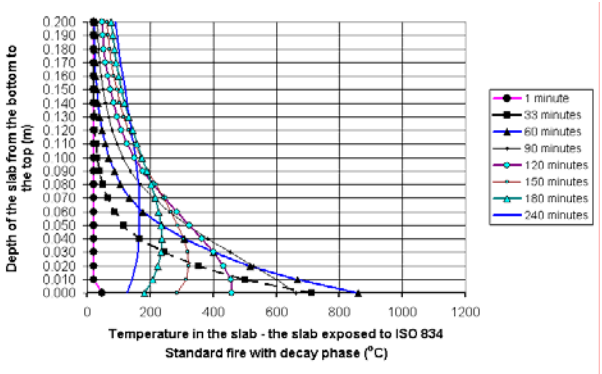

Figure 4-9 Distribution of temperatures in the slabs exposed to an ISO 834 Standard fire with a decay phase

4.2.3. The effect of the boundary thermal conditions of slabs

In this thesis, four kinds of edge thermal conditions of the 0.2m thickness slabs are investigated, as shown in Figure 4-10 (a) to (d). The dark colour region in the graphs represents the location of fires. The distinct line in Figure 4-10 (b) to (d) is defined as the vertical boundary line of fires.

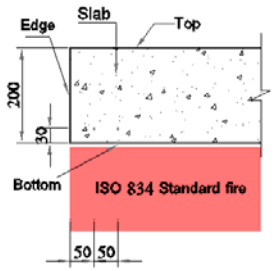

(a) Fire beneath slabs (slabs with free edges)

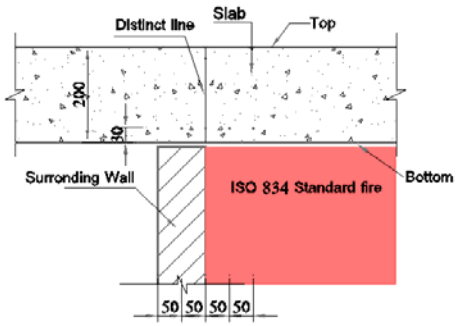

(b) Fire beneath slabs within the fire room

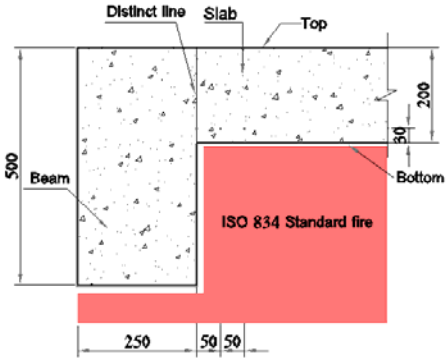

(c) Fire beneath slabs and beams and the inside surface of beams

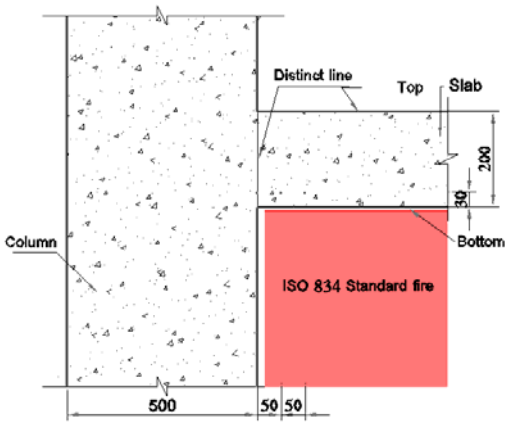

(d) Fire beneath slabs at the connection of columns and slabs

Figure 4-10 Boundary thermal conditions of slabs

Figure 4-10 (a) shows that the fire is beneath slabs which have free edges and the temperatures above the top surface and beyond the free edge of slabs remain a constant of 20^{o}C. The temperatures at 30mm above the bottom of slabs against the time are shown in Figure 4-11 (a). It shows that temperatures in slabs were not affected by the boundary condition when the distance from the free edge of slabs was greater than 0.1m. Only the region of 0.1m from the free edge was affected in this case, so the thermal model in the edge region of slabs was simplified the same as in the middle region of slabs (Figure 4-11 (b) and Figure 4-11 (c)).

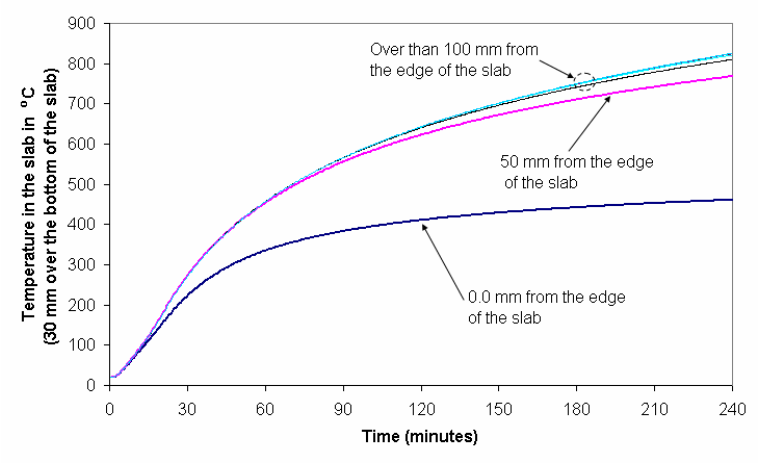

(a) Temperatures in slabs against the time

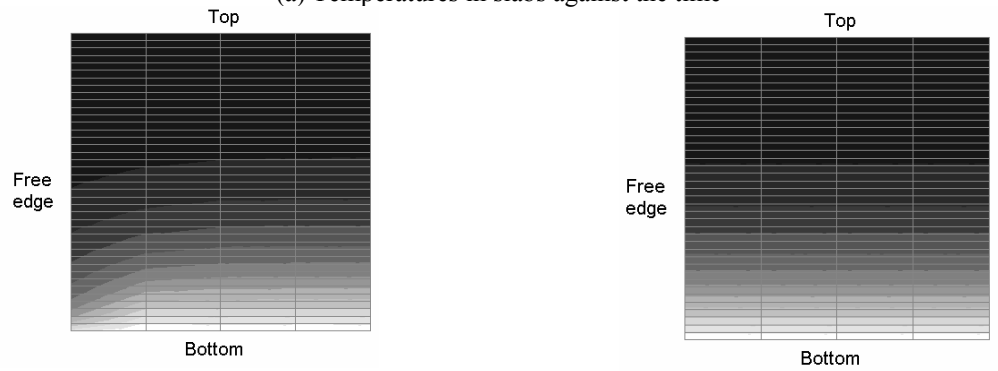

(b) Before the simplification of the thermal model (b) After the simplification of the thermal model

Figure 4-11 Temperatures in slabs (The fire beneath the bottom of slabs with free edges)

Figure 4-10 (b) shows that the fire is beneath slabs within the fire room. The fire is blocked by the vertical surrounding walls with a thickness of 0.1m. The temperatures above the top surface of slabs, within the walls, and beneath the slabs in adjacent rooms remain a constant of 20^{o}C. The temperatures at 30mm above the bottom of slabs against the time are shown in Figure 4-12 (a). In this case, the distinct line is at the inside surface of the walls in the fire room. The temperatures at the region beyond 50mm from the distinct line to the adjacent rooms were less than 200^{o}C at 240 minutes, whilst the temperatures at the distinct line reached 500^{o}C at 240 minutes, but beyond 100mm from the distinct line the temperatures were not affected by the boundary condition. Thus, the thermal model of slabs, in this case, was simplified as that the temperatures within 50mm from the distinct line to the adjacent rooms was the same as the temperatures in the middle regions of slabs in the fire room and beyond 50mm from the distinct line toward the adjacent rooms the temperatures of slabs remained an ambient temperature of 20^{o}C, as shown in Figure 4-12 (b) and Figure 4-12 (c).

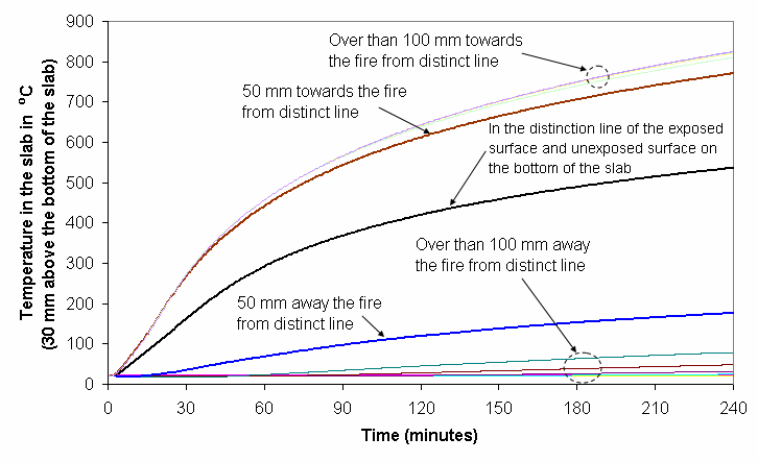

(a) Temperatures in slabs against the time

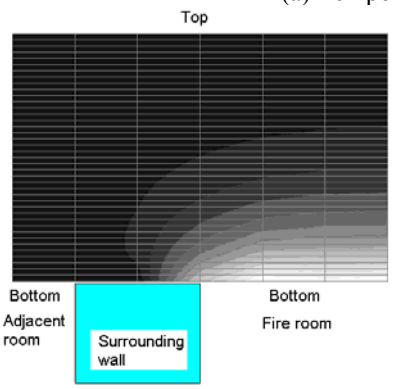

(b) Before the simplification of the thermal model

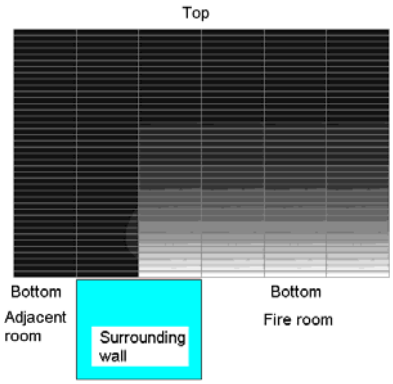

(b) After the simplification of the thermal model

Figure 4-12 Temperatures in slabs (The fire beneath the bottom of slabs within the fire room)

Figure 4-10 (c) shows that the fire is beneath slabs and beams and the inside surface of beams. The temperatures over the top of slabs and beams and beyond the outside surface of beams remain an ambient temperature of 20°C. The beam elements for beams and the shell elements for slabs could be any side of the distinct line, as shown in Figure 4-10 (c). On the left side of the distinct line in the graph the structural members were defined as the beam elements in SAFIR, whilst on the right side of the distinct line the structural members were defined as shell elements. The temperatures at 30mm above the bottom of slabs against time are shown in Figure 4-13 (a). It shows that the temperatures at 240 minutes reached 600°C at the distinct line and 750°C at 100mm from the distinct line in slabs, whilst the temperatures of slabs in the middle region of slabs in the fire room reached 775°C, as mentioned in Section 4.2.2 and shown earlier in Figure 4-8. In this case, the thermal model of slabs was simplified the same as in the middle region of slabs in the fire room (Figure 4-13 (b) and Figure 4-13 (c)).

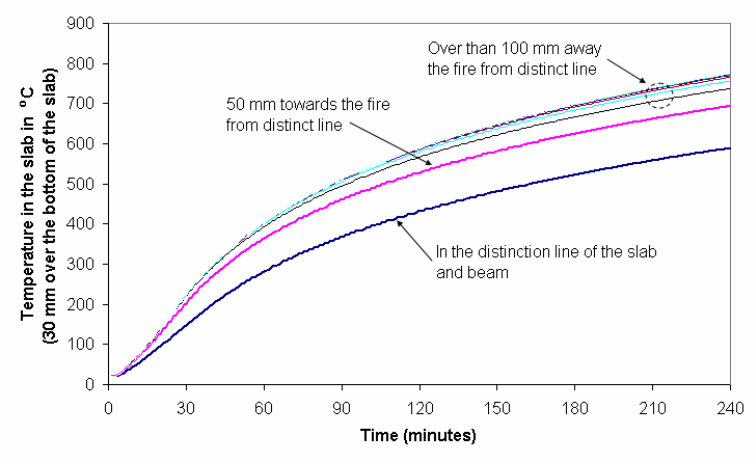

(a) Temperatures in slabs against the time

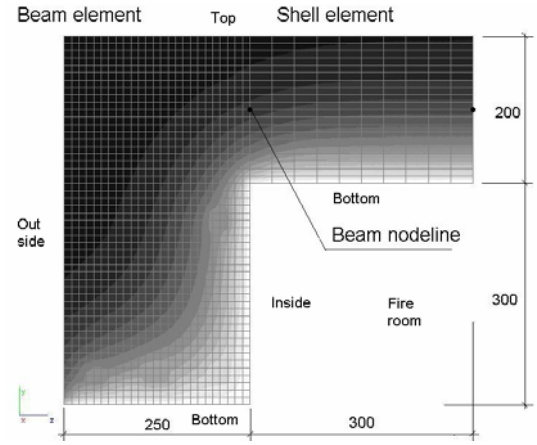

(b) Before the simplification of the thermal model

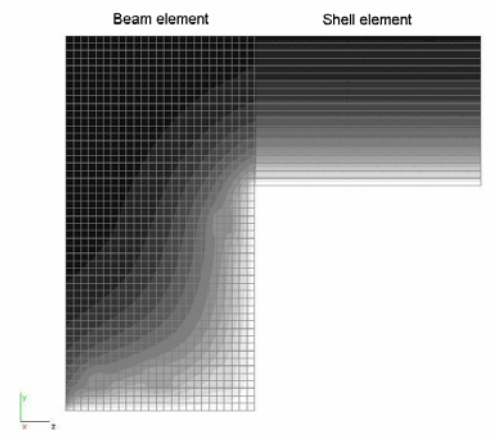

(b) After the simplification of the thermal model

Figure 4-13 Temperatures in slabs (The fire beneath slabs and beams and the inside surface of beams)

Figure 4-10 (d) shows that the fire is beneath slabs at the connection of columns and slabs. Reinforced concrete columns are more difficult to take account of in fire conditions. Because the research of this thesis focuses attention on the analysis of floor systems, in the further analysis, the columns are assumed to be thermally protected against the rise of the temperatures in the columns, so the temperatures in the columns remain at an ambient temperature of 20^{o}C throughout the simulation of structures at ambient and fire conditions. The temperatures in slabs at the connection are assumed to be the same as in the middle region of slabs, as shown in Figure 4-14.

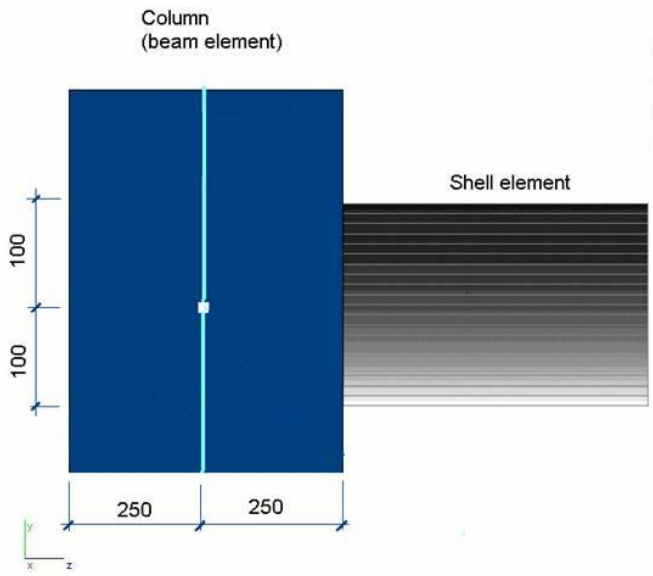

Figure 4-14 Temperatures in slabs (The fire beneath slabs at the connection of columns and slabs)

The analysis of the thermal boundary conditions of slabs in this section indicates that the effect of the thermal boundary conditions of slabs exposed to fires is within 200mm around the distinct line of the fires or within 100mm from the free edge of slabs. The simplified SAFIR thermal models will be used in the simulation of structures at ambient and fire conditions.

4.2.4. The effect of reinforcing bars in slabs

In the thermal models of shell elements, the effect of the reinforcing bars is not considered. This section of the thesis investigates the effect of the reinforcing bars in slabs on the distribution of temperatures of the slabs. 2-D solid elements in SAFIR are used in the thermal models of slabs.

Figure 4-15 (a) shows a 2-D thermal model of slabs with the presence of reinforcing bars in it. A 0.2m thick slab is discretized into 170 2-D solid elements arranged in 17 columns and 20 rows in SAFIR. Each reinforcing bar in the slab is modelled as a 10mm square solid element. The centroid of the reinforcing bars on the bottom is at 30mm above the bottom of the slab, while on the top the centroid is at 30mm below the top of the slab. The spacing of the bars is 125mm. The temperature of reinforcing bars is taken as the average temperature of the four nodes of the solid element. The concrete temperature at 30mm above the bottom of the slab is taken as in the middle point between the two reinforcing bars.

Figure 4-15 (b) shows a 2-D thermal model of slabs that does not consider the effect of reinforcing bars in slabs. A 0.2m thick slab is discretized into 20 2-D solid elements arranged in one column and 20 rows in SAFIR. The temperature of the reinforcing bars on the bottom in the slab is taken the same as the concrete temperature at 30mm above the bottom of the slab, whilst the temperature of the reinforcing bars on the top is taken the same as the concrete temperature at 30mm below the top of the slab.

After 60 minutes' fire exposure, the distribution of temperatures in the slab with the presence of reinforcing bars is shown in Figure 4-15 (c). It shows that the temperatures in the reinforcing bars were slightly lower than the temperatures in the concrete below the centroid of the bars and slightly higher than the temperatures in the concrete above the centroid of the bars. Figure 4-15 (d) shows that the distribution of temperatures in the slab without reinforcing bars was horizontally constant.

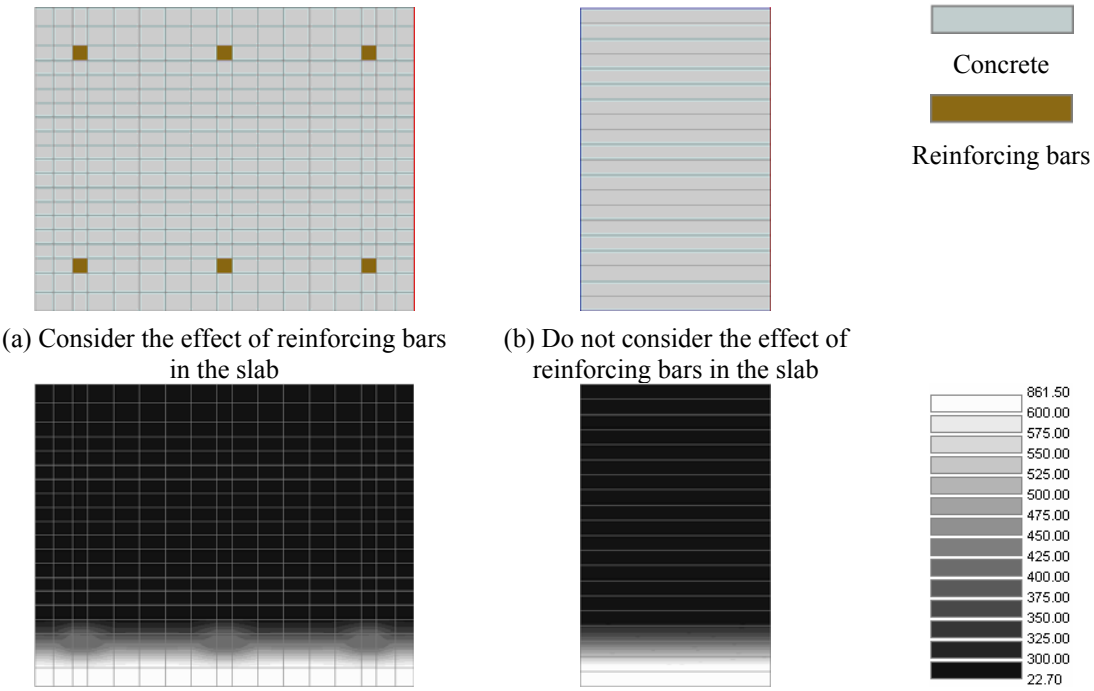

(a) Consider the effect of reinforcing bars in the slab

(b) Do not consider the effect of reinforcing bars in the slab

(c) Distribution of temperatures after 60 minutes' fire exposure (the slab with reinforcing bars)

(d) Distribution of temperatures after 60 minutes' fire exposure (the slab without reinforcing bars)

Figure 4-15 The distribution of temperatures in the slab with or without reinforcing bars in it

Figure 4-16 shows the comparison among the temperatures of the reinforcing bars, the concrete with the reinforcing bars, and the concrete without the reinforcing bars at 30mm above the bottom of the slab. Figure 4-16 (a) shows the temperature of the slab exposed to an ISO Standard fire without a decay phase and Figure 4-16 (b) shows the temperature of the slab exposed to an ISO Standard fire with a decay phase. These graphs show that the three

temperature-time curves were very close. Therefore, the presence of reinforcing bars in thermal models does not excessively affect the distribution of temperatures in slabs.

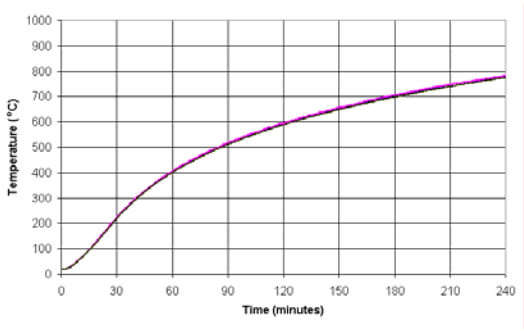

(a) The slab exposed to an ISO 834 Standard fire without a decay phase

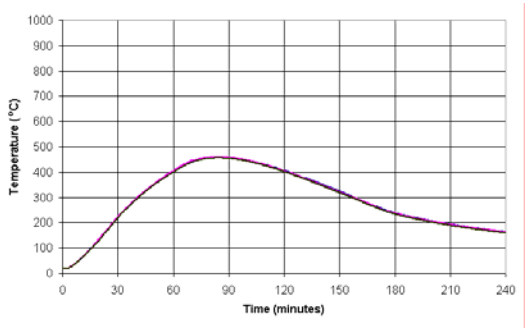

(a) The slab exposed to an ISO 834 Standard fire with a decay phase

Figure 4-16 The comparison among the temperatures of the reinforcing bars, the concrete with or without the reinforcing bars at 30mm above the bottom of the slab

Based on the data in Figure 4-16, the temperatures at 30mm above the bottom of the slab are detailed in Table 4-1. It shows that the maximum difference of temperatures was less than 8°C.

Table 4-1 The comparison among temperatures of the reinforcing bars and the concrete with and without reinforcing bars at 30mm above the bottom of the slab

Temperature (°C)		Reinforcing bars	The concrete with the reinforcing bars	The concrete without the reinforcing bars
The fire without a decay phase	60 minutes	403	407	402
	120 minutes	593	595	588
	180 minutes	702	705	697
	240 minutes	779	782	775
The fire with a decay phase	60 minutes	403	407	402
	120 minutes	406	405	402
	180 minutes	239	238	234
	240 minutes	164	163	160

4.3. Conclusions

- The prediction of fire endurance of slabs using SAFIR is accurate compared with experimental data. Fire endurance of four hours can be reached in 0.2m thick slabs.
- The effect of the boundary thermal conditions of slabs is within a small region that is not greater than 0.2m around vertical fire boundaries (the thickness of slabs is 0.2m). The simplified thermal models of slabs can be used in structural analysis in SAFIR.
- The temperatures of the bottom reinforcing bars are slightly affected in the simplified thermal models. The assumption of absence of reinforcing bars in the thermal models of slabs does not significantly affect the distribution of temperatures in slabs.

5. ANALYSIS OF ONE-WAY SLABS UNDER FIRE EXPOSURE

In order to develop an understanding of the fundamental behaviour of slabs under fire exposure with varying surrounding restraint conditions, this chapter investigates one-way slabs with free edges under fire exposure from beneath. The purpose of the analysis is to investigate the effects of the surrounding restraints of one-way slabs on the distribution of membrane forces and bending moments in one-way slabs. 3-D shell elements in SAFIR are used to model the slabs. The displacements, the distribution of bending moments and the membrane forces in one-way slabs are tackled by varying the surrounding restraint conditions. The effect of Y-direction bowing action on one-way slabs is also discussed. A short comparison between using 2-D beam elements and 3-D shell elements in SAFIR to model one-way slabs is present in Section 5.4. The effect of the ratio of the width to the span on the behaviour of one-way slabs is carried out in Section 5.5.

5.1. Introduction

5.1.1. The thermal expansion and bowing of concrete elements

When concrete members are heated uniformly on all the sides, a cubic solid concrete block will expand in three directions, but a concrete beam will mainly expand along the longitudinal axis, whilst a concrete slab will mainly expand in two directions in the horizontal plane and a concrete wall will expand in two directions in the vertical plane, if the effect of restraints on the surroundings of concrete members is not considered (Figure 5-1). It is evident that the modelling parameters significantly affect the modelling results when finite element methods are used. For modelling a cubic solid concrete block, as shown in Figure 5-1 (a), the 3-D solid element model in SAFIR are a suitable model to be used. However, the analysis of large displacements can not be performed in solid elements. For modelling a concrete beam, as shown in Figure 5-1 (b), the proper model can be the 2-D or 3-D beam element model in SAFIR, depending on the assumptions for simplified structures. For modelling a slab or a wall, as shown in Figure 5-1 (c) and Figure 5-1 (d), the more precise model should be the 3-D shell element model in SAFIR. However, slabs and walls which perform as one-way structural members can be modelling as 2-D beam elements in SAFIR by ignoring the two-way action in slabs or walls (Lim, 2003).

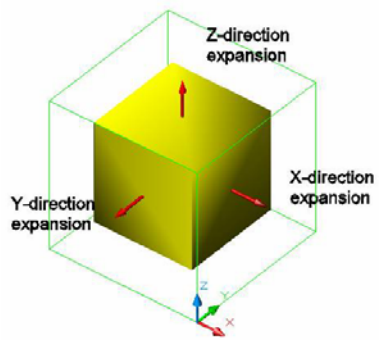

(a) Expansion of cubic solids in three directions

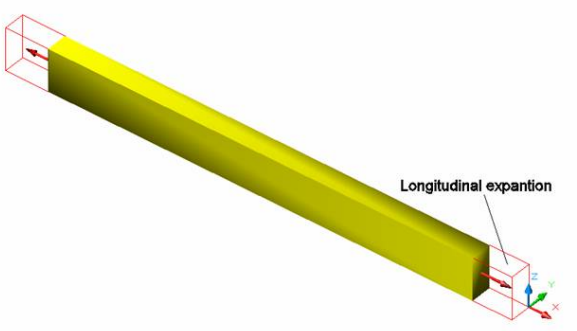

(b) Expansion of beams along the longitudinal axis

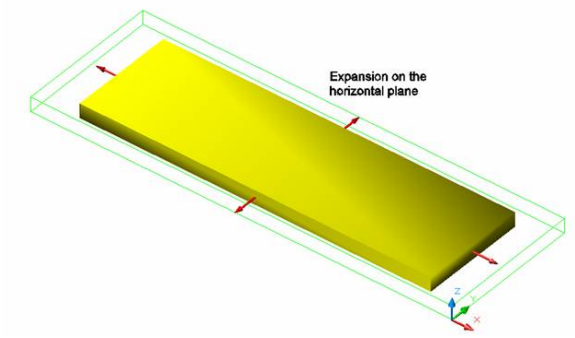

(c) Expansion of slabs in the horizontal plane

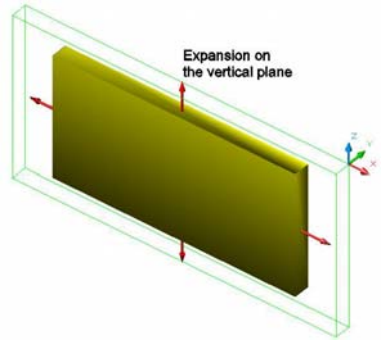

(d) Expansion of walls in the vertical plane

Figure 5-1 Expansion of concrete elements under heating

If restraints apply on the boundaries of concrete members, expansive forces, or thermal thrusts, are developed under heating. The calculating of the magnitude of thermal thrusts under fire conditions is not simple because of stress relaxation in concrete at high temperatures and the response of the unheated portion of structures (Gustaferro et al., 1980). Figure 5-2 shows a summary of data on the maximum thermal thrust forces developed during the fire tests of reinforced concrete slab-and-joist specimens. The specimen was permitted to expand and the amount of permitted expansion was expressed as percentage of its heated length, $\Delta L/L_h$ (ΔL is the permitted expansion and L_h is the heated length). The heated length is defined as the length of the specimen in the direction of thermal thrust forces when the specimen was exposed to fires during the tests (Gustaferro et al., 1980).

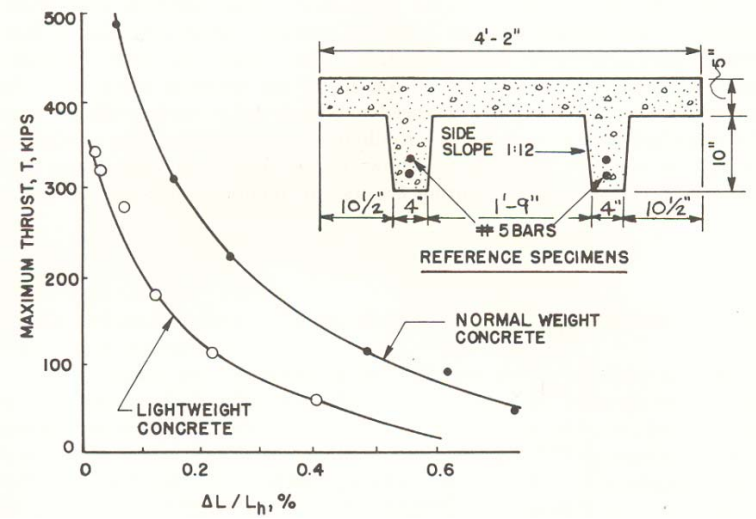

Figure 5-2 Maximum restraining forces measured during the tests of reinforced concrete slab-and-joist specimens (Reproduced from Gustaferro et al. 1980)

If concrete members are heated from beneath, the temperature gradient in the members will produce the bowing action on the members. Figure 5-3 (a) shows that a concrete beam heated beneath will bow down in one direction, while a concrete slab will bow down in two directions (Figure 5-3 (b)), if the restraints on the concrete members are absent.

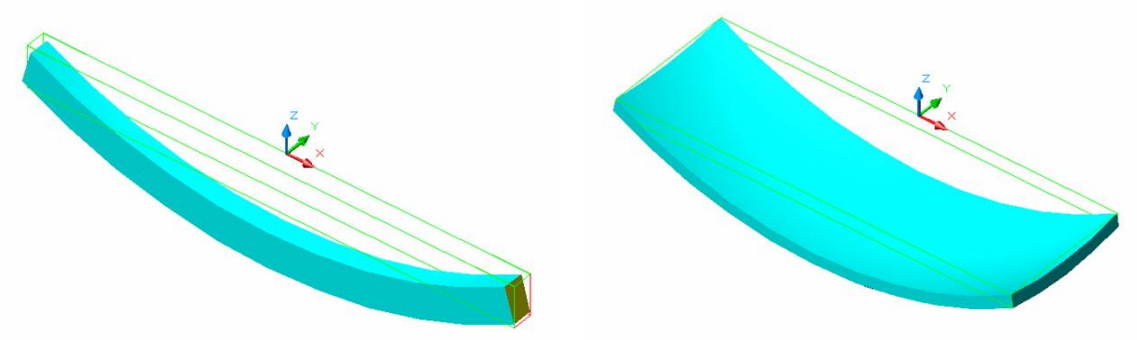

(a) Beams bow down in one direction (b) Slabs bow down in two directions

Figure 5-3 Bowings of beams and slabs under heating beneath

The thermal stress is a 3-direction stress in concrete members. The main action of the thermal stress in concrete members depends on the ratio of dimensions of the members and the surrounding restraints upon the members. If horizontal or vertical restraints are applied to concrete slabs by considering the bowing action on the two directions, the calculation of axial forces, bending moments, and deflections of slabs is more complicated. Therefore, the 3-D analysis method using professional computer programs to analyse the behaviour of slabs are a suitable method.

5.1.2. Review of 2-D analysis for one-way slabs under fire exposure

At ambient conditions, for design purposes, a one-way reinforced concrete slab is assumed to act as a series of parallel strips of the slab over the supports. The analysis results are precise enough to be used in engineering projects because the two-way action is very small in one-way slabs at ambient conditions. In fire conditions, thermal bowing in two directions significantly affects the behaviour of the slabs which performed as one-way slabs at ambient conditions. The effect of thermal bowing action on the behaviour of one-way slabs will be discussed later in this chapter.

Ignoring the two-way action of slabs, Lim (2003) investigated the membrane action in one-way concrete flat slabs under ISO 834 Standard fire exposure. In his research, a one-way slab was modelled as 2-D beam elements l by considering the different positions of the line of the thrust in slabs. The modelling procedure for a one-way slab using 2-D beam elements in SAFIR with axial restraints on the supports is shown in Figure 5-4. A reinforced concrete slab with 5.0m spans and 1.0m widths (Figure 5-4 (a)) was discretized into eight strips with widths of 0.125m. Each strip had identical behaviours for bending moments, axial forces, and deflections in 2-D analysis, so choosing any strip would not make any difference to the results of modellings using SAFIR (Figure 5-4 (b) and (c)). The SAFIR model of a strip of the one-way slab with 20 beam elements is shown in Figure 5-4 (d).

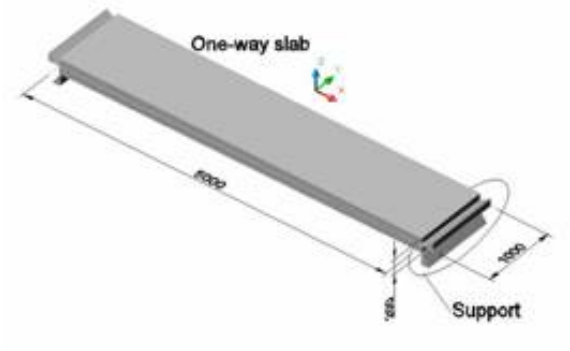

(a) A one-way slab (width: 1.0m; span: 5.0m.)

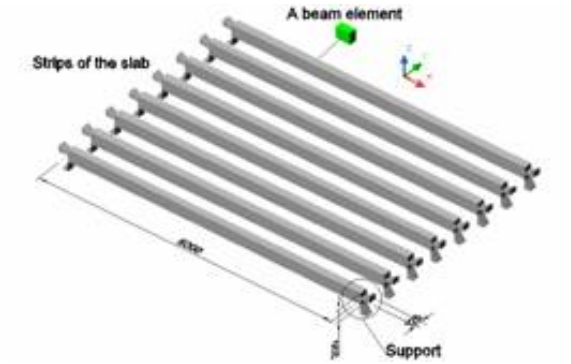

(b) The slab was discretized to 8 strips

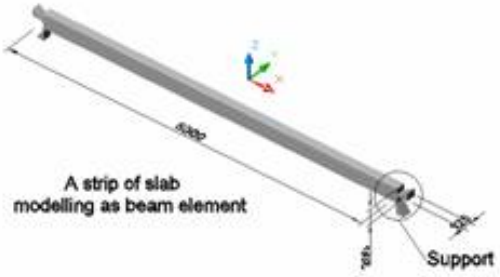

(c) A strip of the slab is modelled

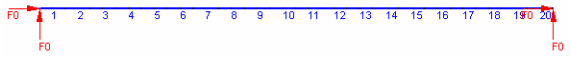

(d) The 2-D beam element model in SAFIR (20 beam elements)

Figure 5-4 Procedure of the modelling of the one-way slab in SAFIR

Using the 2-D beam element model in SAFIR, Lim (2003) found that Pin-Pin supported slabs with full horizontal restraints were sensitive to the position of the line of the thrust and the compressive axial restraint was not beneficial to the fire resistance of the slabs if the line of the thrust was located close to the centroid axis. The results of the vertical deflections and axial forces at the midspan of the slabs that plotted by Lim (2003) are shown in Figure 5-5 (a) and Figure 5-5 (b), respectively.

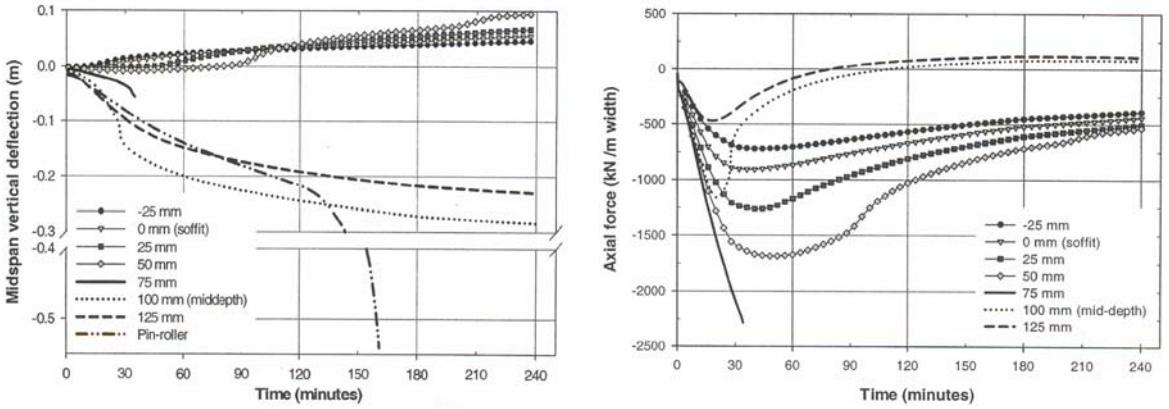

(a) Vertical deflections at midspan of the slabs (b) Axial forces in the slabs

Figure 5-5 Analysis of pin-pin supported one-way slabs using 2-D beam elements in SAFIR (Lim, 2003)

Figure 5-5 shows if the position of the line of the thrust is lower than 50mm from middepth of the slabs (the depth of the slabs is 200mm), the deflections of the slabs in the midspan move upward and the axial forces in the slabs are compression forces.

5.2. The 3-D SAFIR Model of One-Way Slabs

Figure 5-6 shows a typical reinforced concrete one-way slab which is modelled using 3-D shell elements in SAFIR. The thickness of the slab is 0.2m and the span of the slab is 5.0m, whilst the width of the slab is 1.0m. The width of slabs will range from 0.5m to 2.0m for analysing the effect of varying the width of slabs in Section 5.5.

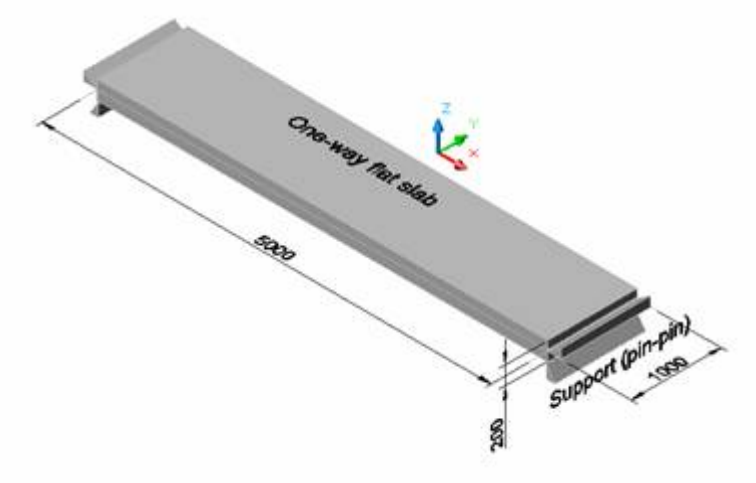

Figure 5-6 A typical reinforced concrete one-way slab

5.2.1. Properties of the slab

The properties and parameters of the one-way slab that was taken as the same as in the 2-D analysis mentioned earlier in Section 5.1.2 are summarised in Table 5-1.

Table 5-1 Properties and parameters of the one-way slab

Slab geometry		
Length	L_x	5.00 m
Width	L_y	1.00 m
Thickness	h	0.20 m
Concrete properties		
Compressive strength	f'_c	30.0 MPa
Tensile strength	f'_t	0.00 MPa
Elastic modulus	$E_{c,o}$	18.0 GPa
Concrete model		Siliceous aggregate (EC2, 1995)
Concrete clear cover	c_c	30 mm
Reinforcing bars' properties		
Yield strength	$f_{y,o}$	430 MPa
Elastic modulus	$E_{s,o}$	210 GPa
Steel model		Hot-rolled steel (EC2, 1995)

5.2.2. Applied loads on the slab

The applied uniformly distributed loads on the one-way slab are listed in Table 5-2. The fire load of 6.9kN/m^2 is the input load in SAFIR when the slab is exposed to fires.

Table 5-2 Applied loads on the one-way slab

Loads		
Self weight + Superimposed dead load	G	5.3 kN/m^2
Live load	Q	4.0 kN/m^2
Ultimate load (1.2G + 1.6Q)		12.8 kN/m^2
Fire load (1.0G + 0.4Q)		6.9 kN/m^2
Fire Exposure		ISO 834 standard fire (4 hour duration) with or without a decay phase
Initial temperature		20.0 ^{o}C

5.2.3. Reinforcement of the slab

In the X-direction the reinforcing bars (longitudinal reinforcing bars) on the top and bottom of the slab are 8Φ12 (8 is the number of the reinforcing bars and 12 (mm) is the diameter of the bars) with the spacing of 0.125m arranged in the cross-section of the slab. The clear cover for the top and bottom bars is 30mm. In the Y-direction the reinforcing bars on the bottom of the slab are 33Φ8 with the spacing of 0.15m as distribution or temperature reinforcing bars; the position of the bars is just over the X-direction reinforcing bars on the bottom. The reinforcing bars on the top of the slab in the Y-direction are 25Φ8 with spacing of 0.2m and the position of the bars is just beneath the X-direction reinforcing bars on the top.

5.2.4. The SAFIR thermal model

The ISO 834 Standard fire is beneath the slab. The duration of the fire is up to 240 minutes for general. The thermal properties of reinforced concrete slabs with a thickness of 0.2m were detailed earlier in Chapter 4 of this thesis. All the shell elements have the same temperature history in the modelling.

5.2.5. The SAFIR structural model

The slab shown earlier in Figure 5-6 is simplified to a quarter of the slab, as shown in Figure 5-7 (a), because the structure and the fire exposure are symmetrical in the X-direction and the Y-direction. A typical SAFIR structural model for one-way slabs which has 80 shell elements is shown in Figure 5-7 (b). The squared areas with width (or length) of 0.125m in the graph

indicate the shell elements. The boundary support and restraint conditions of the slab are varied in the analyses.

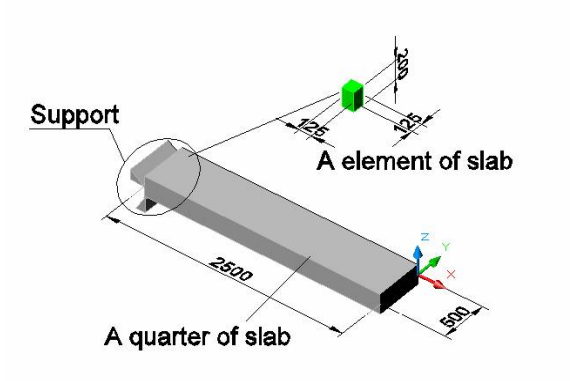

(a) A quarter of the slab is modelled in SAFIR

(b) The typical SAFIR model for one-way slabs with 80 shell elements (A quarter of the slab)

Figure 5-7 The SAFIR structural model for one-way slabs

Two edges of the slab that are perpendicular to the span direction are Pin-Pin connected with the supports and the other two edges parallel to the span direction are free edges. The vertical position of the line of the thrust is on the centroid axis of the slab (the middepth of the slab). Three types of supports shown in Figure 5-8 are used in the modelling of one-way slabs. Figure 5-8 (a) shows the Pin-Pin supports with X-, Y-, and Z-direction restraints that means there are no X-, Y-, and Z-direction displacements at the supports; Figure 5-8 (b) shows the Pin-Pin supports with X- and Z-direction restraints that indicates the slab can freely move in the Y-direction; Figure 5-8 (c) illustrates the free to rotate with Z-direction restraint only, so the slab can freely move in the two directions: the X-direction and the Y-direction.

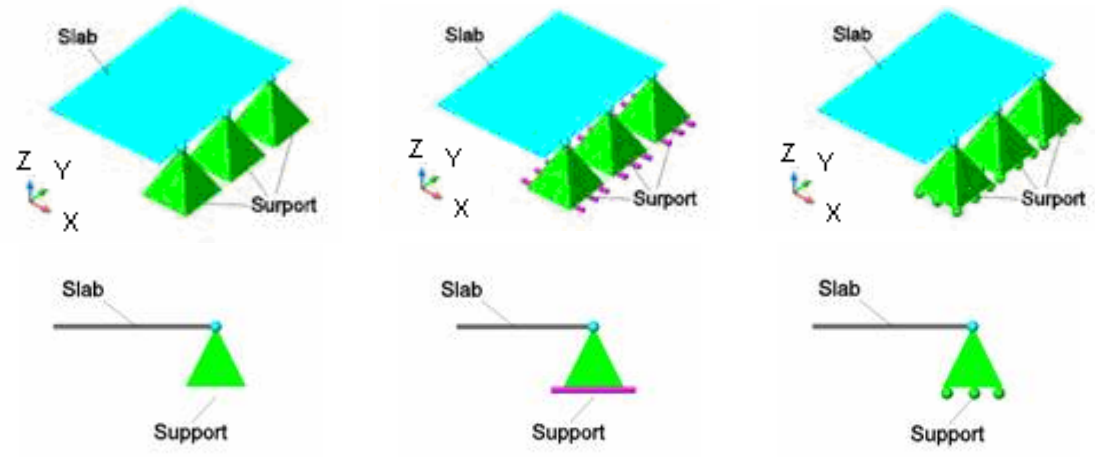

(a) Pin-Pin supports with X-, Y-, and Z-direction restraints

(b) Pin-Pin supports with X- and Z-direction restraints

(c) Free to rotate with Z-direction restraint

Figure 5-8 Types of supports on the two edges perpendicular to the span direction of the slab

5.2.6. Assumptions

The assumptions of using shell elements in SAFIR were detailed earlier in Chapter 3 of this thesis. In addition, some assumptions are also made during the analysis of one-way slabs.

- The fire exposure beneath the slab is uniform.
- Shear failure of the slab is not considered in the analysis.
- The out-of-plane flexural stiffness of the slab is infinite.

5.2.7. Conventional signs for one-way slabs

Conventional signs of one-way slabs, which will be used in the following discussion in this chapter, are shown in Figure 5-9, in which the small squares (0.125m X 0.125m) indicate the shell elements. Two strips are defined along the X-direction of the coordinate system: Strip-A and Strip-B, while four sections are defined along the Y-direction: Section-1, Section-2, Section-3, and Section-4. Strip-A and Strip-B are called Central strip and Edge strip respectively when discussing the effect of varying the width of slabs in Section 5.5.

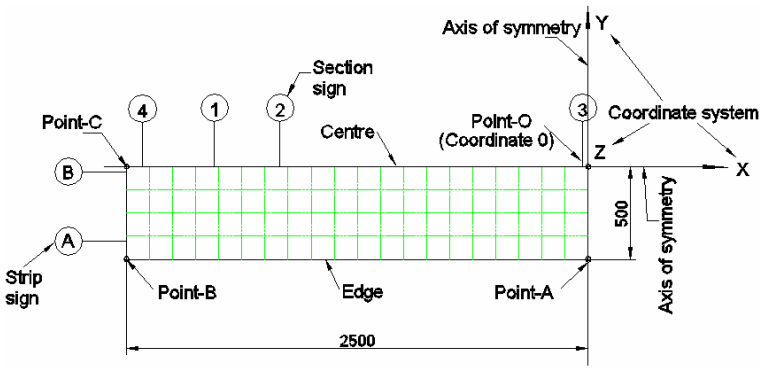

Figure 5-9 Conventional signs of one-way slabs

Four points shown in Figure 5-9 are defined as the four corners of a quarter of slabs: Point-O, Point-A, Point-B, and Point-C. X-coordinate and Y-coordinate of the four points are listed in Table 5-3. Point-O is also the original point of the coordinate system. The Pin-Pin supports of slabs are along the line from Point-B to Point-C and the midspan of slabs is along the line from Point-A to Point-O. The free edge of slabs is along the line from Point-B to Point-A, while the centre of slabs is along the line from Point-C to Point-O.

Table 5-3 X-coordinate and Y-coordinate of the points (units: m)

Point	Point-O	Point-A	Point-B	Point-C
Coordinate (X,Y)	(0, 0)	(0, -0.5)	(-2.5, -0.5)	(-2.5, 0)

5.3. The Slab in Fire Conditions with Vertical Restraints at Supports

This section discusses the behaviour of one-way slabs with full restraints in the Z-direction and free to rotate at supports (simply supported one-way slabs without restraints in horizontal directions), as shown in Figure 5-10 (a). The boundary conditions of the supports in the SAFIR structural model are shown in Figure 5-10 (b).

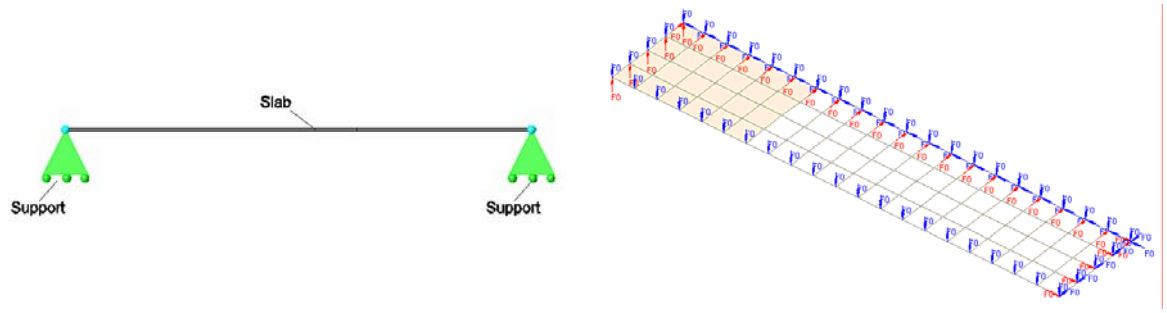

(a) Simplified diagram of one-way slabs with Z-direction restraints (5m span one-way slab)

(b) The SAFIR structural model with support boundary conditions (a quarter of the slab)

Figure 5-10 The SAFIR structural model of Pin-Pin supports with Z-direction restraints

5.3.1. The slab at ambient conditions

At ambient conditions, the vertical deflections of the slab increased in direct ratio to the applied load until the collapse of the slab, as shown in Figure 5-11. The slab collapsed under the uniformly distributed load of 17.3kN/m^2 when the vertical displacement at Point-O reached 0.078m. There were no membrane forces in the slab at ambient conditions due to the support and restraint conditions of the slab. The initial vertical deflection under the fire exposure at Point-O was 0.03m when the applied uniformly distributed load on the slab was 6.9kN/m^2.

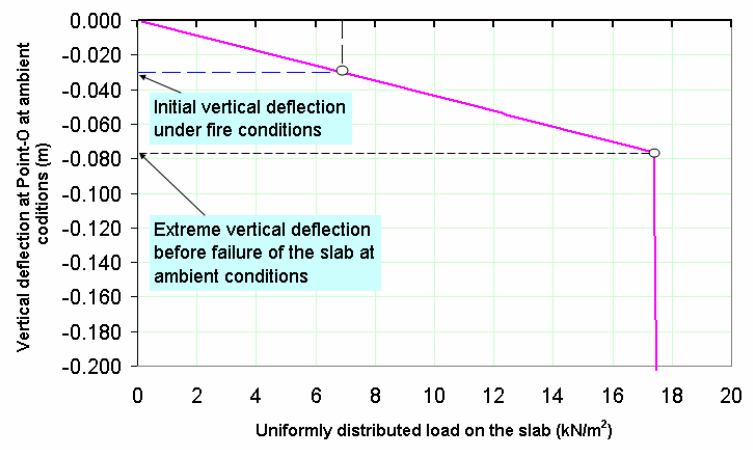

Figure 5-11 Vertical deflections of the slab at Point-O at ambient conditions (with Z-direction restraints)

5.3.2. Displacements of the slab in fire conditions

Vertical deflections (Z-direction)

Figure 5-12 shows the vertical deflections of the slab at Point-O under an ISO 834 Standard fire. The graph shows that the vertical deflection reached 0.3m at 120 minutes and then dramatically increased to 0.6m at 129 minutes when the slab collapsed because the slab became an unstable structure with a plastic hinge in the midspan of the slab.

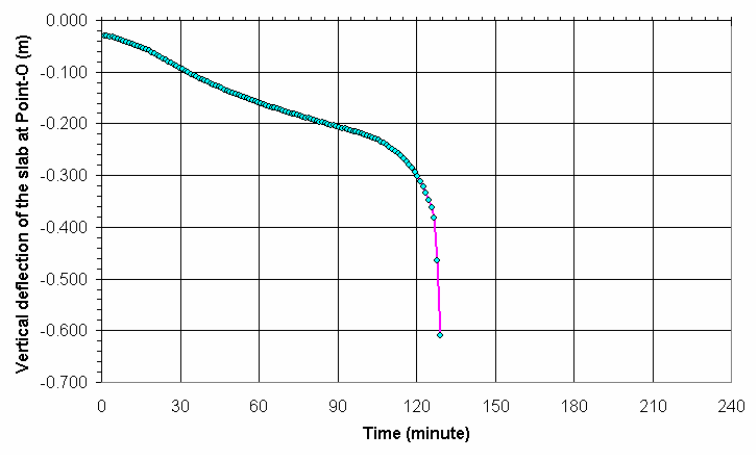

Figure 5-12 Vertical deflections of the slab at point-O (the midspan of the slab)

The distributions of the vertical deflections of the slab at 1 minute and 60 minutes are shown in Figure 5-13 (a) and Figure 5-13 (b), respectively. The graphs show that the vertical deflections in the centre of the slab were greater than at the edge even for one minute's fire exposure.

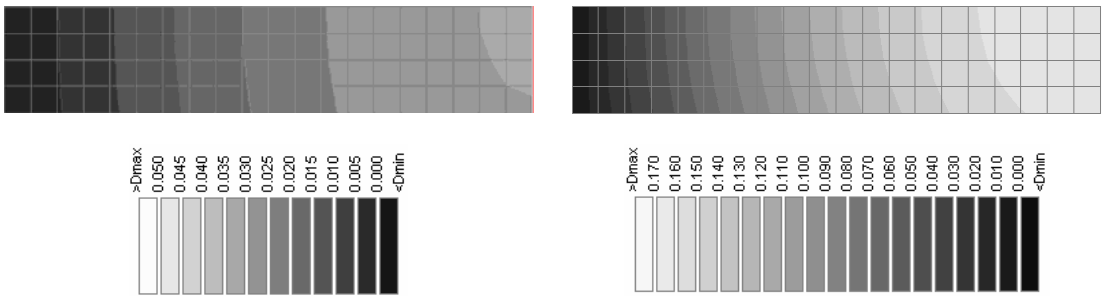

(a) Distribution of vertical deflections of the slab at 1 minute

(b)) Distribution of vertical deflections of the slab at 60 minutes

Figure 5-13 Distributions of vertical deflections of the slab (with Z-direction restraint)

Figure 5-14 (a), (b), and (c) show the distributions of the vertical deflections of the slab along Section-1, -2, and -3, respectively. For numerically comparing the bowing action in the Y-direction, two concepts: ***bowing angle*** and ***bowing radius*** are introduced in this thesis.

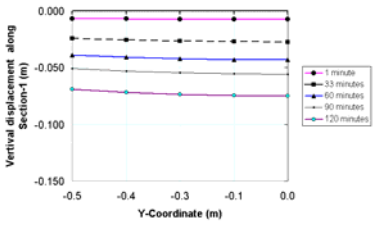

(a) Distribution of vertical deflections of the slab along Section-1

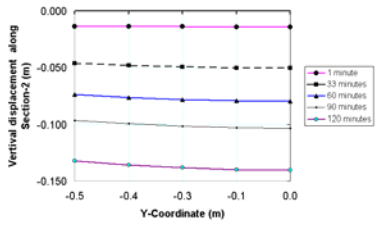

(b) Distribution of vertical deflections of the slab along Section-2

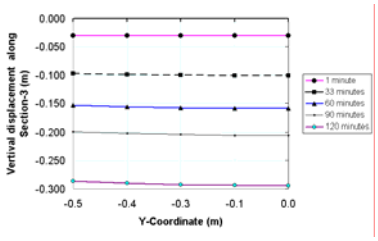

(c) Distribution of vertical deflections of the slab along Section-3

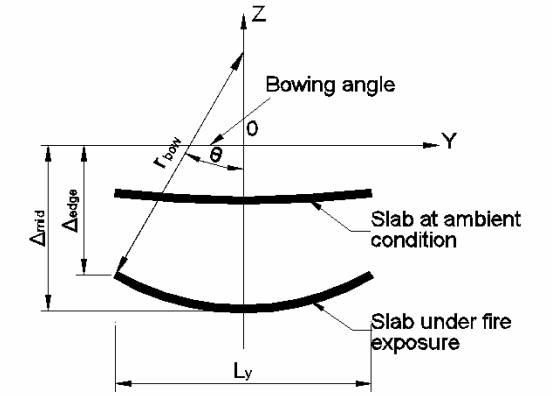

(d) Definition of the bowing angle Θ and bowing radius r_{bow} of the slab

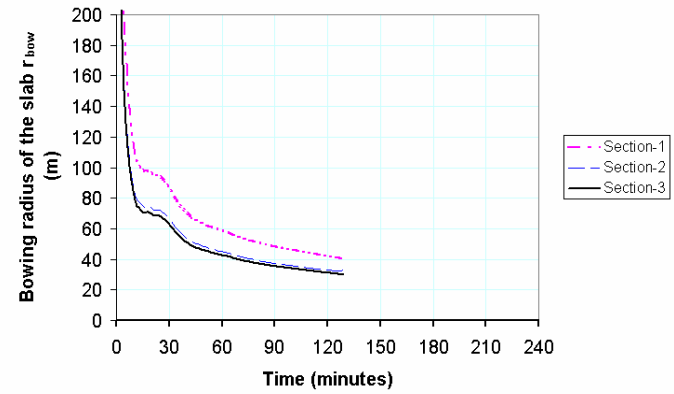

(e) Y-direction bowing radius at Section-1, -2, and -3

Figure 5-14 Analysis of the vertical displacement of the slab at Section-1, -2, and -3

The bowing angle of sections in the slab, as shown in Figure 5-14 (d), is defined as:

$$\theta = 2 \times \tan^{-1}\left(\frac{\Delta_{edge} - \Delta_{mid}}{0.5 \times L_y}\right) \qquad \textbf{Equation 5-1}$$

where Θ is the bowing angle of the slab (degree), Δ_{edge} is the vertical deflection at the edge of the slab in sections (m), Δ_{mid} is the vertical deflection at the centre of the slab in sections (m), and L_y is the width of the slab (m). Therefore, the bowing radius, r_{bow} (m), can be expressed as:

$$r_{bow} = \frac{0.5 L_y}{\sin(\theta)} \qquad \textbf{Equation 5-2}$$

The Y-direction bowing radius in Section-1, Section-2, and Section-3 against time of the fire exposure is shown in Figure 5-14 (e). It shows that the Y-direction bowing radius in Section-2 was slightly larger than in Section-3 but less than in Section-1 because Section-1 was close to

the supports of the slab. The bowing angle at the supports was zero throughout the simulation. The effect of Z-direction restraints at the supports on the Y-direction bowing vanished at 1.0m away from the supports. The bowing radius in the midspan of the slab dramatically dropped to 70m at 15 minutes and then slowly declined to 58m at 33 minutes. After that it smoothly declined to 30m at 129 minutes when the simulation was stopped due to the collapse of the slab. The concepts of the bowing angle and bowing radius reflect the deviation of the vertical deflections along the sections of the slab and will be used later to discuss the effect of Y-direction bowing action on the slab.

Horizontal displacements (X-direction)

Figure 5-15 (a) shows the distribution of the X-direction displacements of the slab at the supports (from Point-B to Point-C). The graph shows that the displacement was almost a constant value along the supports. A slight deference of the X-direction displacements was present in the region close to Point-B. The X-direction displacement at Point-C against time is shown in Figure 5-15 (b). At the initial stage of the fire, the slab moved towards the supports and at 33 minutes the maximum movement of 0.0014m was reached (the initial X-direction displacement was 0.0002m), and then the direction of the movement was changed to towards the midspan of the slab. The X-direction displacement constantly increased from -0.0012m at 33 minutes to 0.0016m at 100 minutes, after that the displacement rapidly increased to 0.008m at 120 minutes. The slab collapsed at 129 minutes when the X-displacement was dramatically increased to 0.058m. At Point-C, the ratio of the X-direction displacement over a half length of the span of the slab was 0.048% (0.0012/2.5) at 33 minutes, whilst the ratio was 0.32% (0.008/2.5) at 120 minutes. The orientation of X-direction displacements can be used to predict the trend of the development of the membrane forces in the slab when the supports of the slab in the X-direction were restrained. When the trend of movement of the slab is towards the supports, the compressive membrane forces can develop in the slab which was fully restrained in the X-direction.

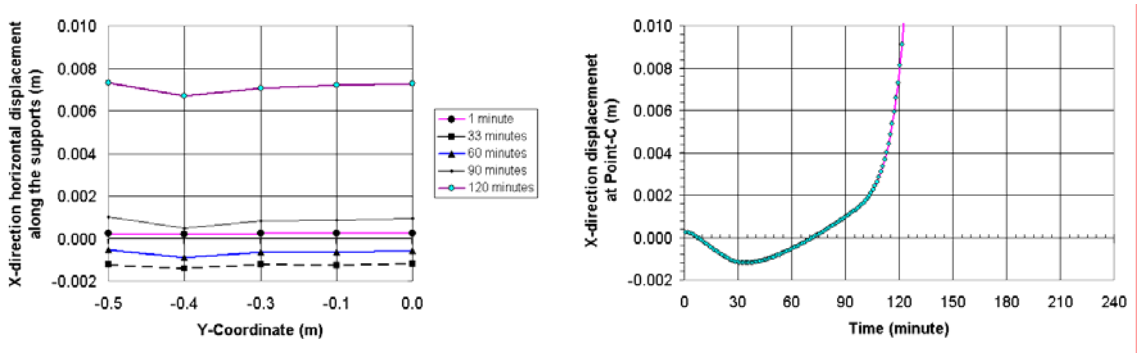

(a) Distribution of X-direction displacements of the slab at the supports (Point-B to Point-C)

(b) X-direction displacements of the slab at Point-C against the time

Figure 5-15 X-direction displacements of the slab at the supports

Horizontal displacements (Y-direction)

The Y-direction displacements of the slab along the free edge (from Point-B to Point-A) are shown in Figure 5-16 (a). The graph shows that the Y-direction displacement at Point-B was greater than at Point-A. The Y-direction displacements remained a constant value along Point-A to 1.5m away from Point-A (un-shaded region in Figure 5-16 (a)). The maximum difference between the Y-direction displacement at Point-A and Point-B was less than 0.001m throughout the simulation, as shown in Figure 5-16 (b). At Point-A, the Y-direction displacement was 0.0022m at 120 minutes and the ratio of the Y-direction displacement over a half width of the slab was 0.44% (0.0022/0.5), which was greater than the ration of the X-direction displacement over a half span (0.32%) at Point-C.

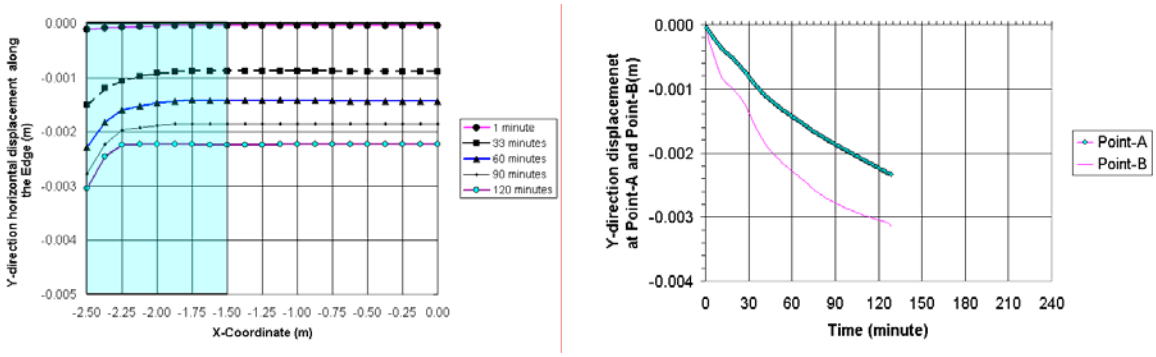

(a) Y-direction displacement along the free edge

(b) Y-direction displacement at Point-A and Point-B against time

Figure 5-16 Y-direction displacements along the free edge (from Point-B to Point-A)

5.3.3. Bending moments of the slab in fire conditions

X-direction bending moments

X-direction bending moments along Strip-A and Strip-B are shown in Figure 5-17 (a) and Figure 5-17 (b), respectively. The graphs show that the significant difference of the curvatures of bending moments was present in the shaded regions within these graphs. The bending moments remained almost constant along Strip-A or Strip-B after 33 minutes. At 0.5m away from the supports, the bending moment was almost zero in Strip-A after 33 minutes, while the bending moment was roughly -16kN-m/m in Strip-B after 33 minutes. The support conditions of the slab affected the distribution of the bending moments in the region close to the supports and did not affect the distribution of the bending moments in the region close to the midspan of the slab.

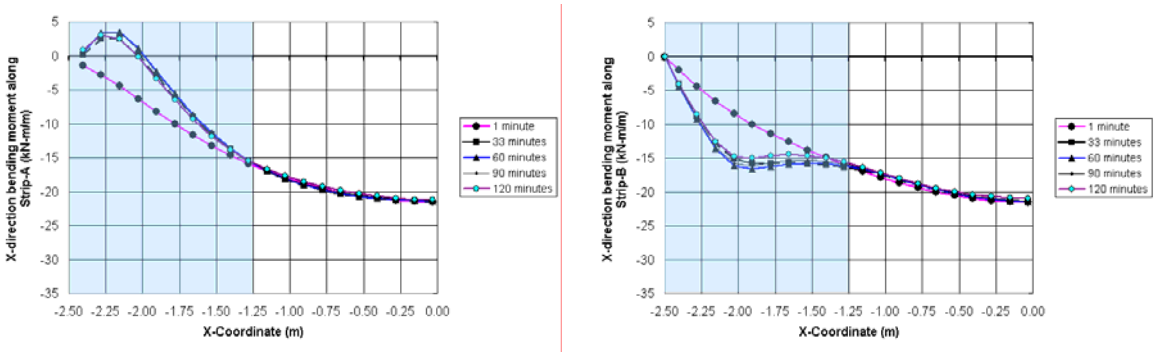

(a) X-direction bending moments along Strip-A (b) X-direction bending moments along Strip-B

Figure 5-17 X-direction bending moments along Strip-A and Strip-B

Figure 5-18 shows the distributions of X-direction bending moments along Section-1, Section-2, and Section-3. The distribution of bending moments along Section-1 was much more irregular than along Section-2 from 33 minutes to 120 minutes. The bending moments remained a constant value of -21kN-m/m along Section-3 throughout the simulation.

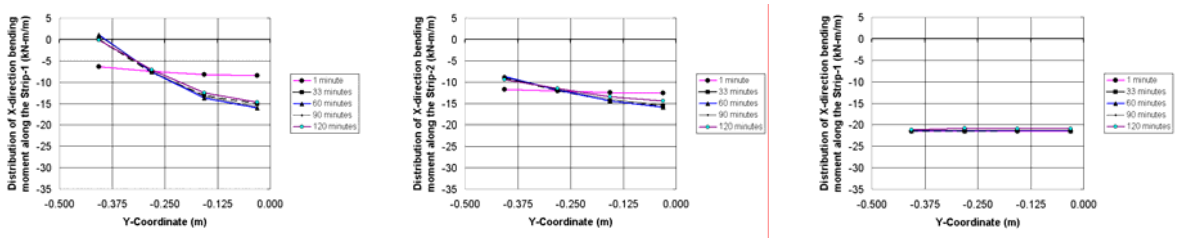

(a) Distribution of X-direction bending moments along Section-1 (b) Distribution of X-direction bending moments along Section-2 (c) Distribution of X-direction bending moments along Section-3

Figure 5-18 Distributions of X-direction bending moments along Section-1, Section-2, and Section-3

The distributions of X-direction bending moments in the slab at 1 minute and 60 minutes are shown in Figure 5-19 (a) and Figure 5-19 (b), respectively. In the region close to the supports, the distribution of bending moments was more variable at 60 minutes than at 1 minute because of the effect of Y-direction bowing action on the slab.

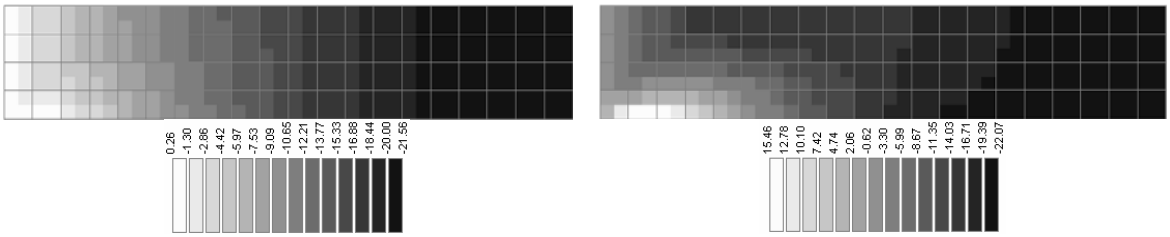

(a) Distribution of X-direction bending moments at 1 minute (kN-m/m)

(b) Distribution of X-direction bending moments at 60 minutes (kN-m/m)

Figure 5-19 Distributions of X-direction bending moments in the slab

Figure 5-20 (a) and Figure 5-20 (b) show the X-direction bending moments against the time in Section-1 and Section-2, respectively. The line between the lines of the bending moments at Strip-A and Strip-B was the average value of the bending moments in these sections. The bending moments at Strip-A and Strip-B in Section-1 at 1 minute were almost the same as the average bending moment of -7.5kN-m/m, but at 60 minutes the bending moments became a positive value of 1kNm/m at Strip-A and a negative value of -16kNm/m at Strip-B, as shown in Figure 5-20 (a). At 60 minutes, the difference of the bending moments in Section-1 was 17kN-m/m, while it was only 9kN-m/m in Section-2, as shown in Figure 5-20 (b).

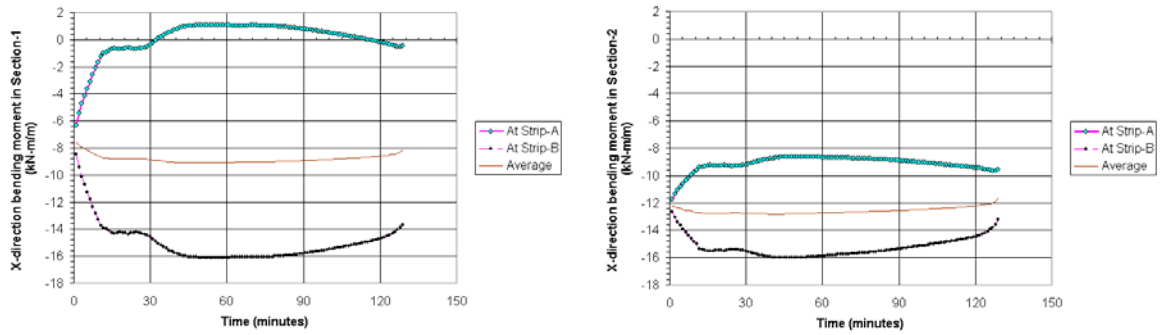

(a) X-direction bending moments against the time in Section-1

(b) X-direction bending moments against the time in Section-2

Figure 5-20 X-direction bending moments against the time in Section-1 and Section-2

Total X-direction bending moments in the sections (the total value is in 0.5m width of the slab) are shown in Figure 5-21. It shows that the total bending moments in the sections almost remained constant from 15 minutes to 120 minutes. However, the distribution of bending moments was variable along Section-1 and Section-2.

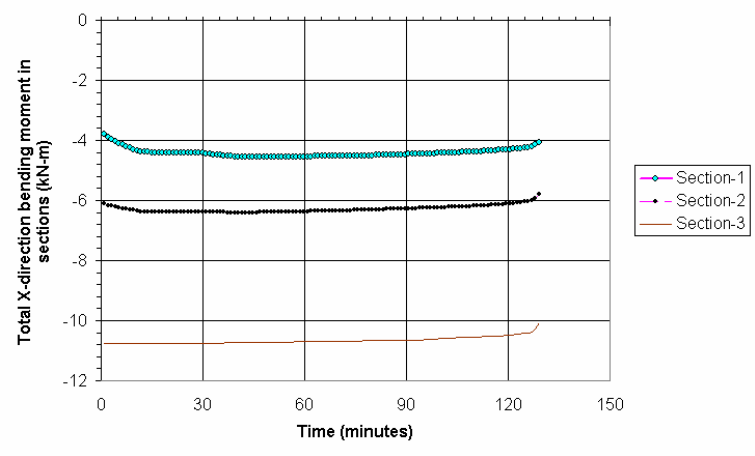

Figure 5-21 Total X-direction bending moments in sections (in 0.5m width)

According to the equilibrium of bending moments, the bending moments of simply supported one-way slabs at ambient conditions can be calculated using Equation 5-3.

$$M = \frac{w \cdot (L_x - x) \cdot x \cdot L_y}{2} \qquad \textbf{Equation 5-3}$$

where M is the bending moment in the slab at x away from the supports (kN-m), w is the uniformly distributed load applied on the slab (kN/m^2), L_x is the span of the slab (m), L_y is the width of the slab (m), and x is the distance from the supports to the section being calculated (m).

The total bending moments in the sections that were calculated using Equation 5-3 (L_x=5m, L_y=0.5m, w=6.9kN/m^2) are listed in Table 5-4. Comparing with the modelling value of the bending moments, as shown earlier in Figure 5-21, it is evident that the calculated value and modelling value of the total bending moments were more variable in Section-1 and Section-2, but completely the same in Section-3 because the Y-direction bowing action significantly affected the distribution of bending moments in Section-1 and Section-2. Therefore, Equation 5-3 only can precisely predict the X-direction bending moments close to the midspan of the slab when the slab was exposed to fires.

Table 5-4 Bending moments of the simply support one-way slab at ambient conditions

Section	Section-1	Section-2	Section-3
x (m)	0.5	0.75	2.5
M (Equation 5-3) (kN-m)	3.88	5.50	10.78
M (Figure 5-21) (kN-m)	4.40	6.20	10.70

Y-direction bending moments

Figure 5-22 (a) and Figure 5-22 (b) show the distributions of Y-direction bending moments in the slab at 1 minute and 60 minutes, respectively. The Y-direction bending moments were mainly present in the region of 0.5m from the supports; beyond this region the Y-direction bending moments were almost zero. At 60 minutes the maximum Y-direction bending moment was 10.55kN-m/m (Figure 5-22 (b)), which was only a half of the maximum X-direction bending moment of 21.4kN-m/m in the midspan.

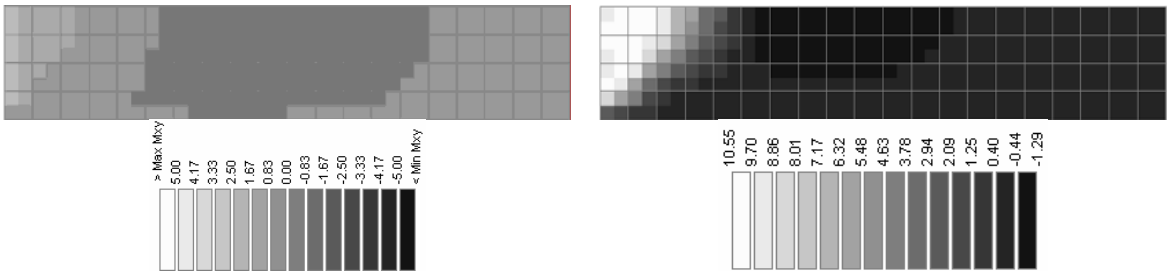

(a) Distribution of Y-direction bending moments at 1 minute (kN-m/m)

(b) Distribution of Y-direction bending moments at 60 minutes (kN-m/m)

Figure 5-22 Distributions of Y-direction bending moments at 1 minute and 60 minutes

Figure 5-23 shows Y-direction bending moments along Section-1 and Section-2. The maximum value of the Y-direction bending moment along Section-1 was less than 4.0kNm/m (Figure 5-23 (a)), whilst it was just over -1.0kN-m/m along Section-2 (Figure 5-23 (b)).

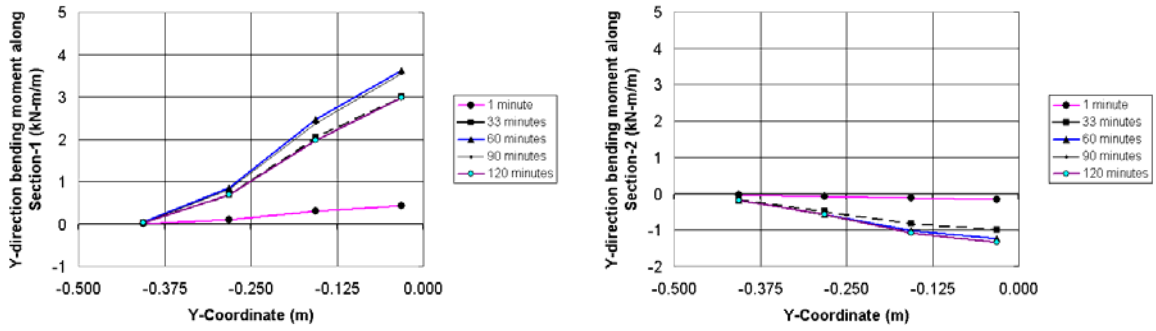

(a) Y-direction bending moments along Section-1

(b) Y-direction bending moments along Section-2

Figure 5-23 Distributions of Y-direction bending moments along Section-1 and Section-2

5.3.4. Membrane forces of the slab in fire conditions

According to the equilibrium of horizontal forces along the X-direction and Y-direction, in any cross-section of Pin-Pin supported slabs without X-direction and Y-direction restraints the total membrane forces should be zero. It is evident that the membrane forces in one-way slabs were self-balanced horizontal forces in sections under fire exposure, as shown in Figure 5-24. However, the membrane forces at ambient conditions were zero. Figure 5-24 shows that the maximum compressive membrane force was close to the free edge of the slab. Therefore, the details of reinforcement in the edge region of reinforced concrete one-way slabs should be carefully designed when the slab was exposed to fires.

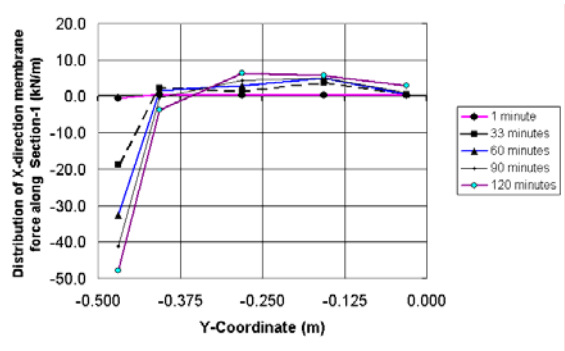

(a) Distribution of membrane forces along Section-1

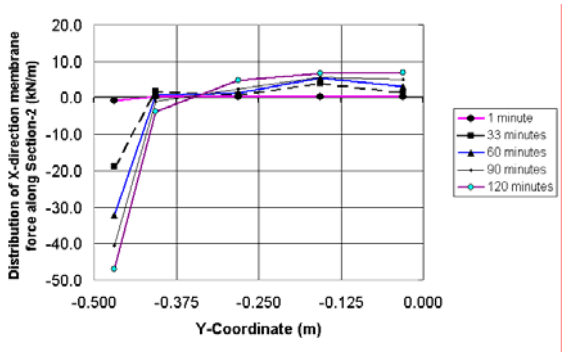

(b) Distribution of membrane forces along Section-2

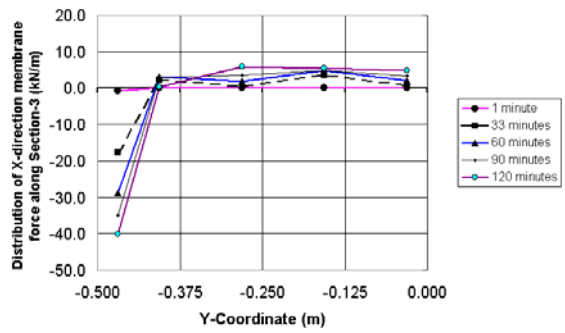

(c) Distribution of membrane forces in Section-3

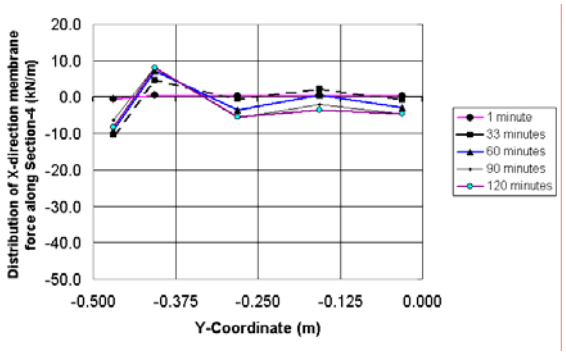

(d) Distribution of membrane forces in Section-4

Figure 5-24 Distributions of membrane forces in Section-1, Section-2, Section-3, and Section-4

5.3.5. Conclusions

The analysis of one-way slabs with full restraints in the Z-direction at the supports when the slabs were exposed to an ISO 834 Standard fire has shown that:

- The slab collapses at 129 minutes when the slab is exposed to the fire from beneath.
- The Y-direction bowing action, the bending moments, and the displacements of the slab are significantly affected by Z-direction restraints within 0.5m from the supports.
- The bending moments are non-linearly distributed along the cross-section in the region close to the supports, while they are linearly distributed along the cross-section in the region close to the midspan; the bending moments in the midspan can be predicted using the principles of structural mechanics.
- X-direction membrane forces are present in the cross-section of the slab as self-balanced forces along the cross-section.

5.4. The Slab in Fire Conditions with X-Direction and Z-Direction Restraints

This section presents the behaviour of Pin-Pin supported slabs with full restraints in the X-direction and Z-direction, as shown in Figure 5-25 (a). The boundary conditions of the supports in the SAFIR structural model are shown in Figure 5-25 (b).

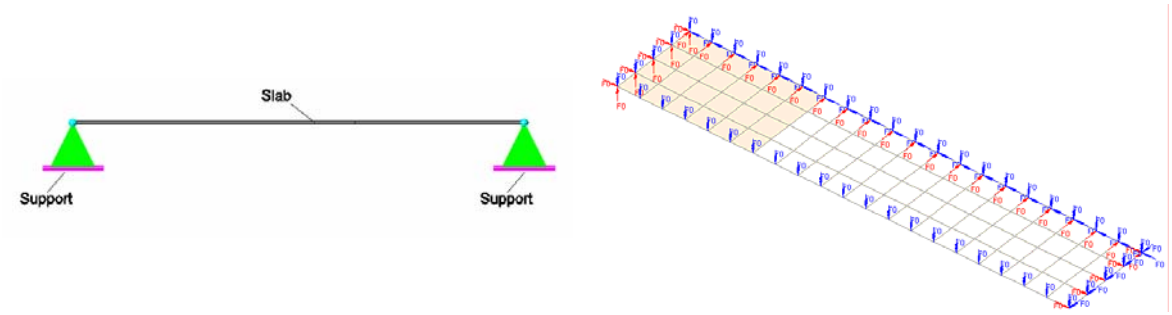

(a) Simplified diagram of Pin-Pin supported slabs with full restraints in the X-direction and Z-direction (5m span one-way slab)

(b) The SAFIR model with support boundary conditions (a quarter of the slab)

Figure 5-25 The SAFIR structural model of Pin-Pin supported slabs with X-direction and Z-direction restraints

5.4.1. The slab at ambient conditions

The vertical deflections at Point-O of the slab at ambient conditions are shown in Figure 5-26. It shows that the vertical deflection increased in direct ratio to the uniformly distributed load on the slab until the load reached 17kN/m^2. When the load exceeded 17kN/m^2, which coordinated with the extreme load on the slab with Z-direction restraint only, the vertical deflection non-linearly increased against the load on the slab until the collapse of the slab. At ambient conditions the slab collapsed with the maximum vertical deflection of 0.164m when the uniformly distributed load on the slab reached the significant value of 27.6kN/m^2. The extreme load on the slab with X-direction restraints was greater than the extreme load on the slab without X-direction restraints because of the development of the membrane forces in the slab at ambient temperatures. The initial vertical deflection under fire exposure at Point-O was 0.029m (the uniformly distributed load on the slab was 6.9kN/m^2).

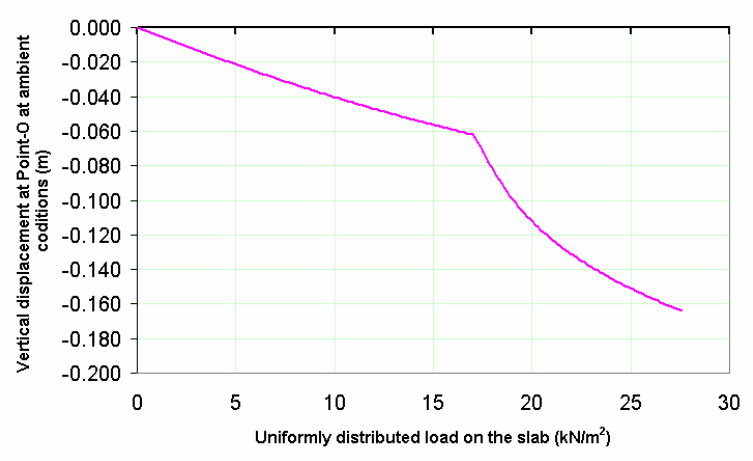

Figure 5-26 Vertical deflections at Point-O of the slab at ambient conditions (Pin-Pin supports with X-direction restraints)

The initial membrane forces in the slab under fire exposure were sensitive to the position of the line of X-direction axial restraints at the supports. Figure 5-27 shows the membrane forces in Strip-B and the vertical deflections at Point-O of the slab at ambient conditions by varying the position of the line of X-direction axial restraints. The graph shows when the position of the line of the axial restraints was on the centre or the bottom of the cross-section of the slab, the membrane forces were positive values if the uniformly distributed loads on the slab were greater than 6.9kN/m^2. The initial membrane force in Strip-B of the slab under fire exposure was a tensile force of 30kN/m (the position of the line of the axial restraint was on the centre of the cross-section of the slab at the support and the applied load on the slab was 6.9kN/m^2).

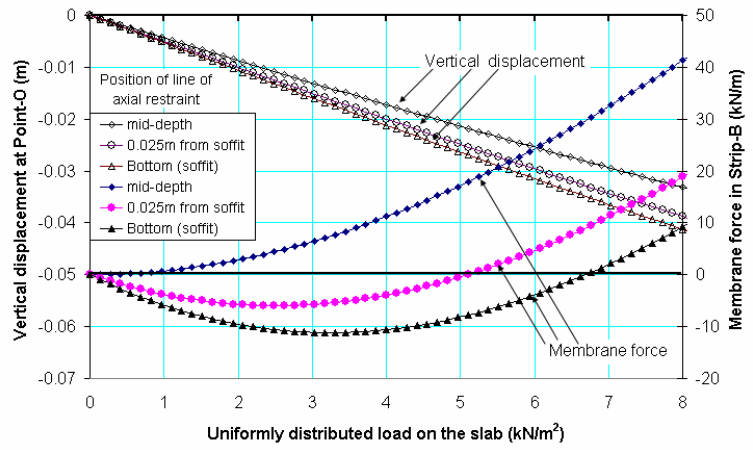

Figure 5-27 Vertical deflections and membrane forces in the midspan of the slab at ambient conditions

The development of thrusts (or compressive membrane forces) in slabs depends not only on the position of the line of axial restraints but also on the ratio of the span to the thickness of slabs. It is evident that if the ratio of the span to the thickness of slabs is small (i.e. less than 14), the behaviour of the slabs with horizontal restraints is mainly affected by the beam-action and the thrust on the supports is significant; if the ratio of the span to the thickness of slabs is large (i.e. greater than 18), the behaviour of the slabs is mainly affected by the plane-action and the thrust on the supports is small and when the applied load on slab increases, tensile axial forces will develop in the slabs.

5.4.2. Displacements of the slab in fire conditions

Vertical deflections (Z-direction)

Figure 5-28 shows the vertical deflections at Point-O of the slab when the slab was exposed to an ISO 834 Standard fire. The graph shows that the vertical deflection dramatically increased from the initial deflection of 0.029m to 0.166m at 60 minutes, and then constantly increased to 0.265m at 180 minutes; after that it slightly increased to 0.283m at the end of the simulation. There is a crinkle on the vertical deflection curve at 180 minutes that indicated the slab deformed to a catenary hanging on the supports. The slab did not collapse at the end of the simulation due to the development of the tensile membrane forces in the slab.

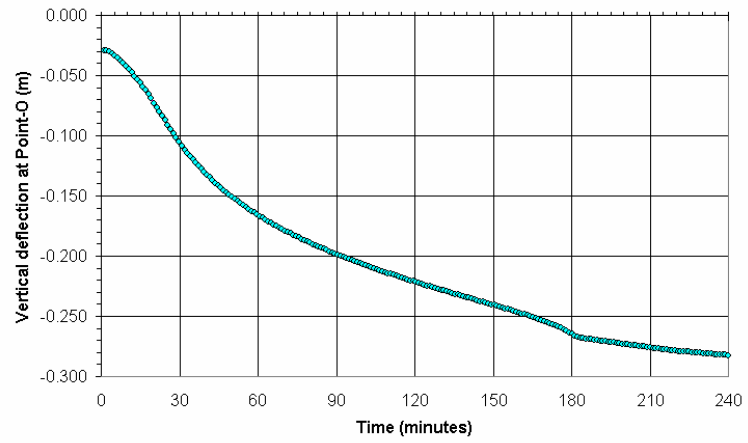

Figure 5-28 Vertical deflections at Point-O of the slab

(Pin-Pin supports with X-direction restraints)

The distributions of vertical deflections of the slab at 1 minute and 60 minutes are shown in Figure 5-29 (a) and Figure 5-29 (b), respectively. Compared with Figure 5-13, it is found that

the distributions of vertical deflections between the slabs with or without X-direction restraints had similar patterns but slightly different magnitudes.

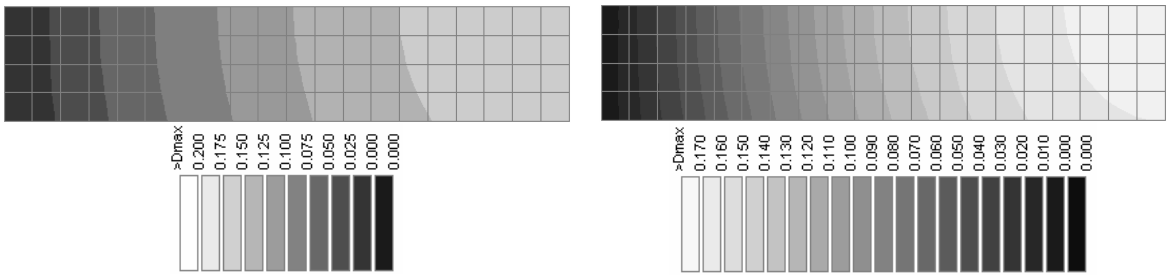

(a) At 1 minute (b) At 60 minutes

Figure 5-29 Distributions of vertical deflections of the slab exposed to an ISO 834 Standard fire (Pin-Pin supports with X-direction restraints)

Figure 5-30 (a) shows the Y-direction bowing radius at Section-1, Section-2, and Section-3 of the slab which was fully restrained in the X-direction. The bowing radius in Section-2 was slightly larger than in Section-3 at the initial stage of the fire. Before 120 minutes, the tendency of the reduced bowing radius in the slab with X-direction restraints was the same as the tendency in the slab without X-direction restraints in Section-3, as shown in Figure 5-30 (b). In the duration from 33 minutes to 120 minutes, the difference of the bowing radius between the slabs with and without X-direction restraints was less than 4% in Section-3. The bowing radius of the slab with X-direction restraints was less than the bowing radius of the slab without X-direction restraints because of the effect of X-direction restraints at the supports on the slab. The bowing radius in the slab with X-direction restraints decreased to 27m at 240 minutes. The X-direction restraints greatly affected the bowing of the slab at the initial stage of the fire (before 33 minutes in this case), but slightly affected the bowing of the slab at the post stage of the fire.

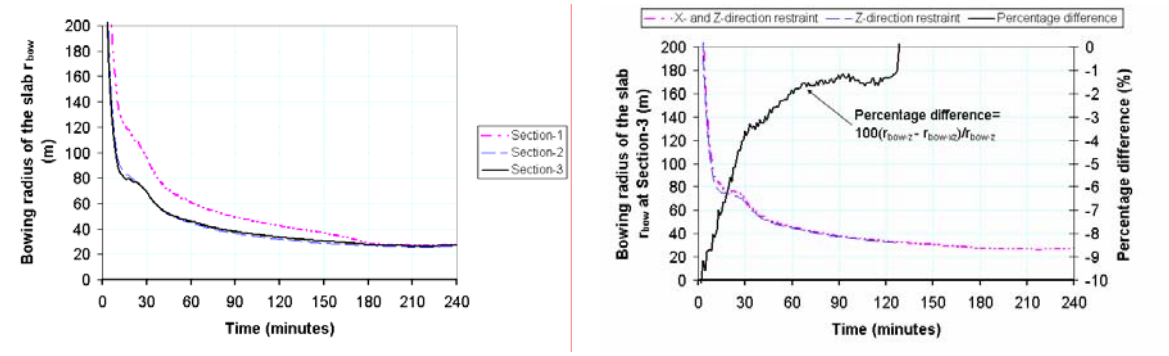

(a) Y-direction bowing radius at Section-1, -2 and -3 (b) Comparison of bowing radius between with and without X-direction restraints at Section-3

Figure 5-30 Y-direction bowing radius of the slab

Horizontal displacements (Y-direction)

The Y-direction displacements along the free edge of the slab are shown in Figure 5-31 (a). It shows that the Y-direction displacements remained constant along Point-A to 1.5m from Point-A (un-shaded region in Figure 5-31 (a)). The Y-direction displacement at Point-B was greater than at Point-A, as shown in Figure 5-31 (b). At Point-A, the Y-direction displacement almost linearly increased from 1 minute to 240 minutes. At Point-B, the maximum Y-direction displacement of 0.0037m was reached at 150 minutes, and then slightly declined to 0.0036m at 180 minutes; after that, it steadily increased to 0.0037m at the end of the simulation. The development of the Y-direction displacements along the edge of the slab indicates that the behaviour of the slab significantly changed after 180 minutes when the slab deformed to a catenary.

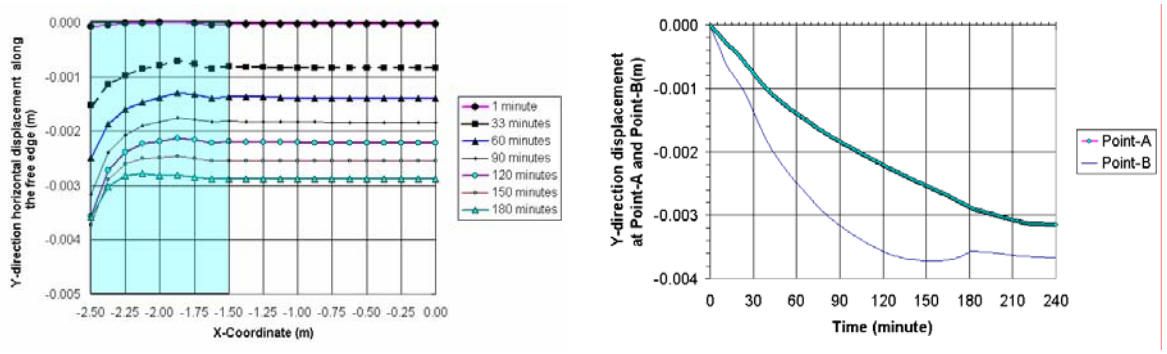

(a) Y-direction displacement along the free edge

(b) Y-direction displacement at Point-A and Point-B against time

Figure 5-31 Y-direction displacement along the free edge (Point-B to Point-A)

Horizontal displacements (X-direction)

The X-direction displacements of the slab at the supports were zero because of full restraints on the X-direction at the supports. The support conditions of the slab significantly affect the behaviour of the slab under fire exposure. So, the further studies of one-way slabs in fire conditions using 3-D shell elements in SAFIR by considering the stiffness of the supports in the X-direction are recommended.

5.4.3. Bending moments of the slab in fire conditions

X-direction bending moments

X-direction bending moments along Strip-A and Strip-B are shown in Figure 5-32 (a) and Figure 5-32 (b), respectively. In the shaded region of these graphs, the curvatures of bending moments were significantly dissimilar. At 120 minutes the maximum bending moment was a negative value of -11kNm/m at 0.5m from the supports in Strip-B, but it was a positive value of 2kNm/m at 0.5m from the supports in Strip-A because of the effect of Y-direction bowing action.

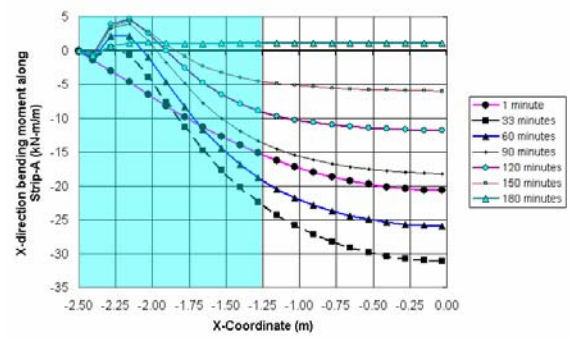

(a) X-direction bending moments along Strip-A

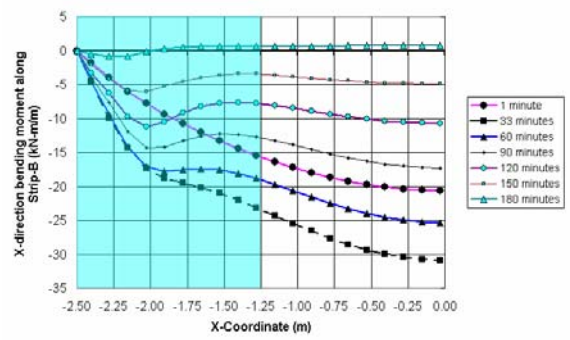

(b) X-direction bending moments along Strip-B

Figure 5-32 X-direction bending moments along Strip-A and Strip-B

(Pin-Pin supports with X-direction restraints)

The distributions of X-direction bending moments in the slab at 1 minute and 60 minutes are shown in Figure 5-33 (a) and Figure 5-33 (b), respectively. Compared with Figure 5-19, it is found that the distributions of bending moments were similar between the slabs with and without X-direction restraints in the region close to the supports.

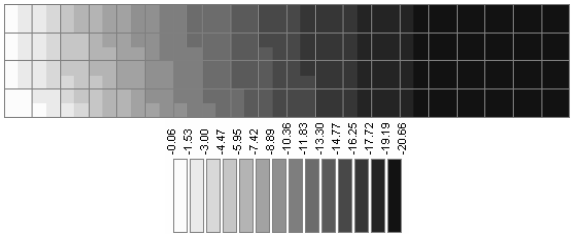

(a) Distribution of X-direction bending moments at 1 minutes (kN-m/m)

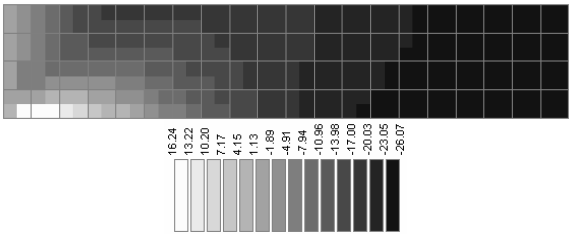

(b) Distribution of X-direction bending moments at 60 minutes (kN-m/m)

Figure 5-33 Distributions of X-direction bending moments of the slab

(Pin-Pin supports with X-direction restraint)

Figure 5-34 shows the distributions of X-direction bending moments along Section-1, Section-2, and Section-3. The graph shows that the closer to the support, the more non-linear the distribution of X-direction bending moments in sections was.

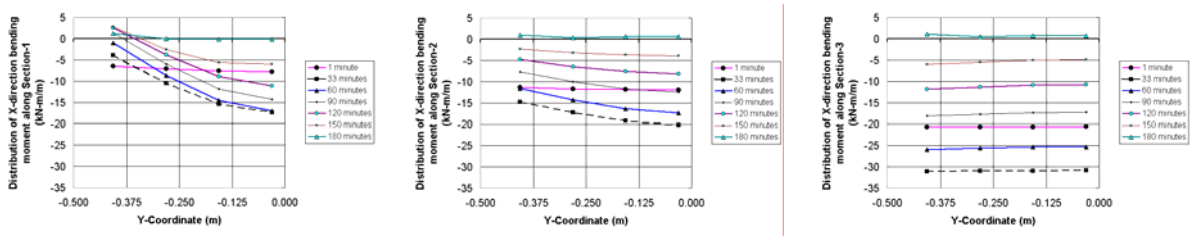

(a) Distribution of X-direction bending moments along Section-1

(a) Distribution of X-direction bending moments along Section-2

(a) Distribution of X-direction bending moments along Section-3

Figure 5-34 Distributions of X-direction bending moments along the Section-1, Section-2, and Section-3 (Pin-Pin supports with X-direction restraints)

Figure 5-35 (a) shows the X-direction bending moments against the time in Section-1, which was 0.5m away from the supports. The graph shows that the maximum average bending moment of -12.0kNm/m was reached at 33 minutes; meanwhile, the bending moment was -17kN-m/m at Strip-B (close to the centre) and was -4kN-m/m at Strip-A (close to the edge). At 33 minutes the difference of the bending moments between at Strip-A and at Strip-B in Section-1 was 13.0kN-m/m, while the difference was only 5.0kN-m/m in Section-2, as shown in Figure 5-35 (b). The distribution of bending moments along the cross-sections of the slab was more non-linear in the slab closer to the supports.

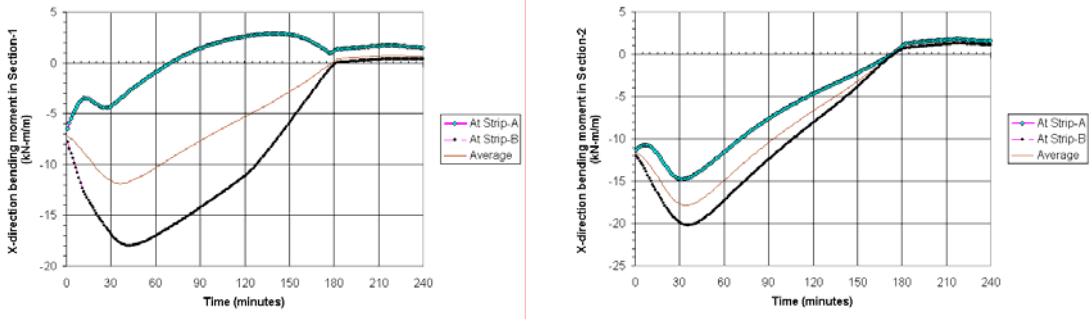

(a) X-direction bending moments against the time in Section-1

(b) X-direction bending moments against the time in Section-2

Figure 5-35 X-direction bending moments against the time in Section-1 and Section-2 (Pin-Pin supports with X-direction restraint)

Figure 5-36 shows X-direction bending moments against the time in Section-3. The graph shows that the bending moments at Strip-A were slightly greater than at Strip-B in Section-3,

as the bending moments almost linearly distributed along Section-3. The bending moment increased from -20.0kN-m/m at 1 minute to the maximum value of -31.0kNm/m at 33 minutes, and then linearly declined to zero at 175 minutes. After that, it slightly increased to 2.0kN m/m at 180 minutes and remained constant until the end of the simulation. The slab did not collapse at the end of the simulation, but was showing a large vertical deflection and deformed to a catenary after 180 minutes.

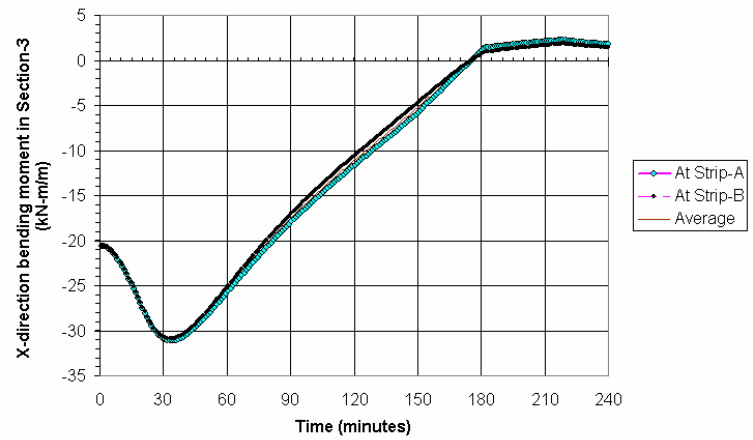

Figure 5-36 X-direction bending moments against the time in Section-3

(Pin-Pin supports with X-direction restraints)

The redistribution of X-direction bending moments of the slab was present in the slab under the fire exposure due to the effect of X-direction axial restraints, which improved the ability to prevent the collapse and enhanced the fire endurance of the slab.

Y-direction bending moments

Figure 5-37 shows the distributions of Y-direction bending moments at 1 minute and 60 minutes. The patterns of the distributions of Y-direction bending moments in Figure 5-37 were almost the same as the patterns shown earlier in Figure 5-22, so the X-direction restraints on the supports did not affect the distribution of Y-direction bending moments.

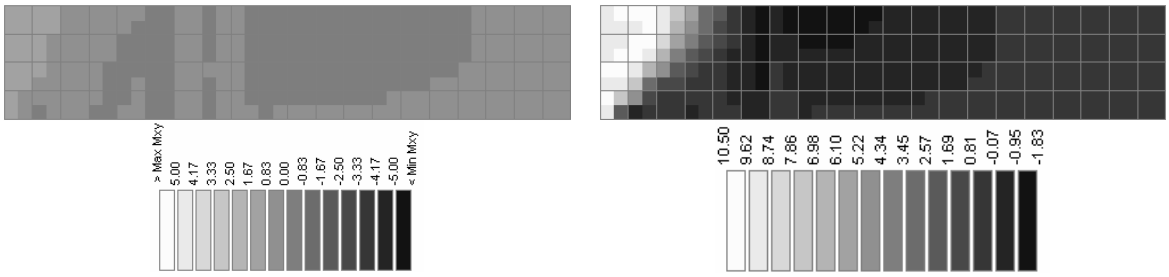

(a) Distribution of Y-direction bending moments at 1 minute (kN-m/m)

(b) Distribution of Y-direction bending moments at 60 minutes (kN-m/m)

Figure 5-37 Distributions of Y-direction bending moments at 1 minute and 60 minutes (Pin-Pin supports with X-direction restraints)

The numerical diagrams of Figure 5-38 (a) and Figure 5-38 (b) show the Y-direction bending moments along Section-1 and Section-2, respectively. The Y-direction bending moments in Section-1 were greater than in Section-2, but they all had small values compared with the X-direction bending moments in the midspan of the slab. The graphs also show that the redistribution of bending moments was present in the Y-direction.

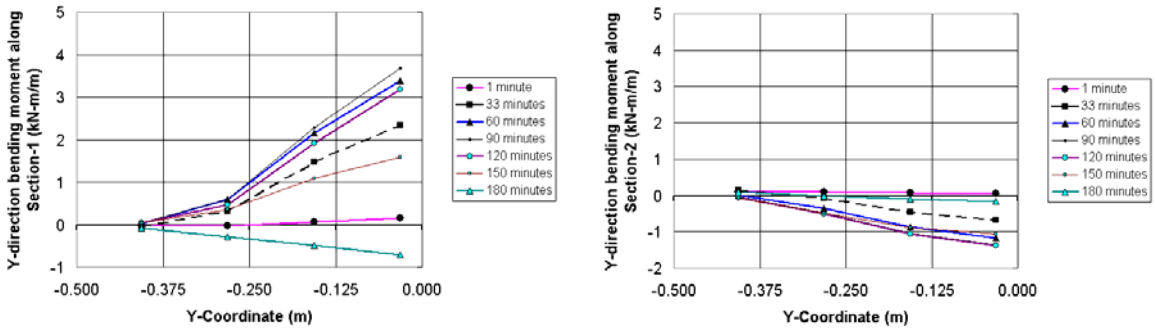

(a) Y-direction bending moments along Section-1

(b) Y-direction bending moments along Section-2

Figure 5-38 Y-direction bending moments along Section-1 and Section-2 (Pin-Pin supports with X-direction restraints)

5.4.4. Membrane forces of the slab in fire conditions

The distributions of X-direction membrane forces along Section-1, Section-2, Section-3, and Section-4 are shown in Figure 5-39. The graphs show that the X-direction membrane forces were non-linearly distributed along these sections due to the effect of the Y-direction bowing action in the slab.

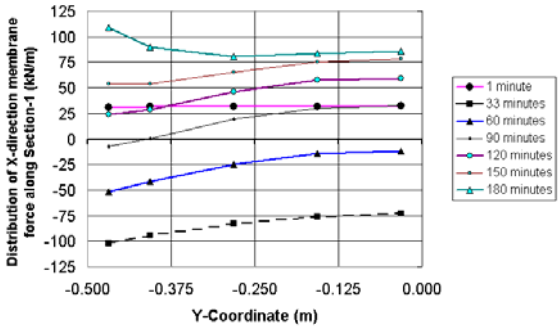

(a) Distribution of X-direction membrane forces along Section-1

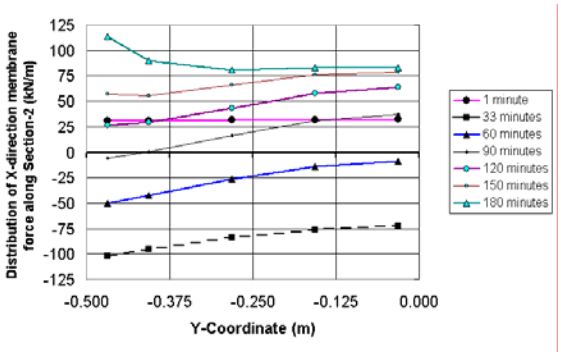

(b) Distribution of X-direction membrane forces along Section-2

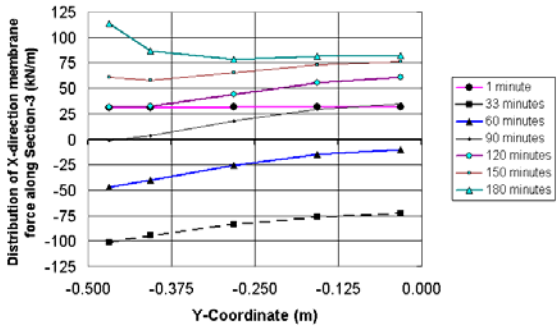

(c) Distribution of X-direction membrane forces along Section-3

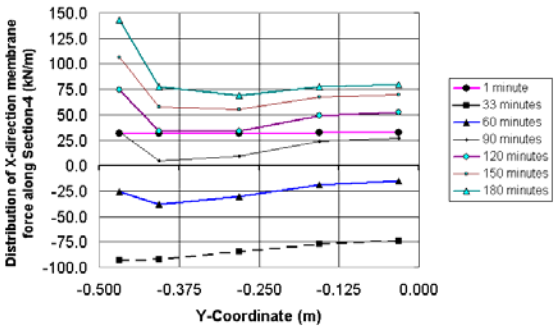

(d) Distribution of X-direction membrane forces along Section-4

Figure 5-39 Distributions of membrane forces along Section-1, Section-2, Section-3, and Section-4 (Pin-Pin supports with X-direction restraints)

The membrane forces along Strip-A and Strip-B in the sections are shown in Figure 5-40 (a) and Figure 5-40 (b), respectively. The graphs show that the membrane forces remained constant along Strip-A and Strip-B. The compressive membrane force in Strip-A dramatically increased to -100kN/m at 29 minutes, and then declined to zero at 90 minutes; after that, the tensile membrane forces developed in Strip-A and at 180 minutes the maximum tensile membrane force of 90kN/m was reached. A tensile membrane force plateau was formed in the duration from 180 minutes to the end of the simulation. In Strip-B the compressive membrane force dramatically increased to -80kN/m at 29 minutes, which was less than the membrane

force in Strip-A. The compressive membrane force declined to zero at 65 minutes in Strip-B, and then the tensile membrane forces developed and at 180 minutes the peak value of 80kN/m was reached; after that, a tensile membrane force plateau was formed until 240 minutes. At 180 minutes the temperatures of the bottom reinforcing bars in the slab exceeded 700°C (the temperatures in the slabs were detailed earlier in Chapter 4), at which the yield strength of the hot-rolled steel dramatically declined to almost zero, but the temperatures of the top reinforcing bars remained less than 180°C, at which the yield strength of the hot-rolled steel remained the same as at ambient temperatures, so the tensile membrane forces were mainly present in the top reinforcing bars. The top reinforcing bars must be thermally protected by concrete; otherwise, the top reinforcing bars will be directly exposed to fires and the slab would collapse before 180 minutes. It is evident that to prevent the collapse of the slab, the slab must have an adequate amount of top reinforcing bars, which must be effectively anchored in the supports.

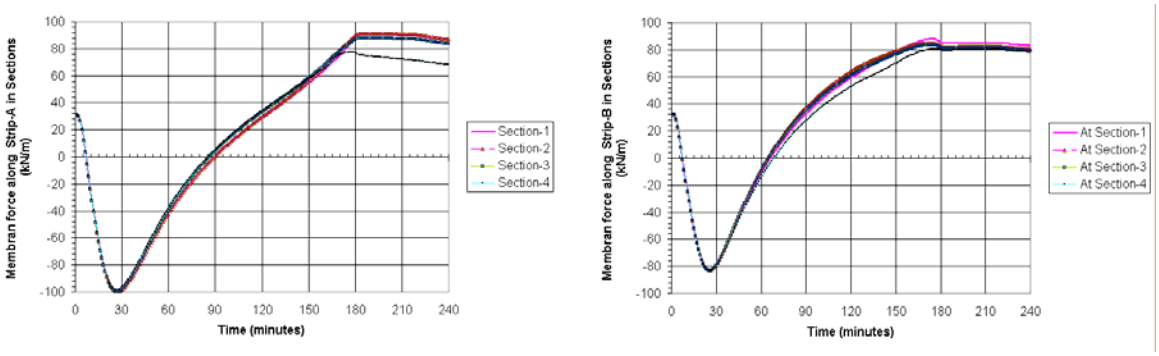

(a) Membrane forces along Strip-A in the sections (b) Membrane forces along Strip-B in the sections

Figure 5-40 Membrane forces along Strip-A and Strip-B in the sections (Pin-Pin supports with X-direction restraints)

Figure 5-41 shows X-direction membrane forces along Section-3. The graph shows that when the average value of the membrane forces was zero at 74 minutes, a compressive membrane force of -17kN/m was present in Strip-A and a tensile membrane force of 14kN/m was present in Strip-B. The development of the tensile membrane forces in the slab close to the free edge occurs later than in the slab close to the centre; this phenomenon is called the ***tensile membrane force lag*** in this thesis. The concept of the tensile membrane force lag will be used in the discussion of the membrane forces in slabs.

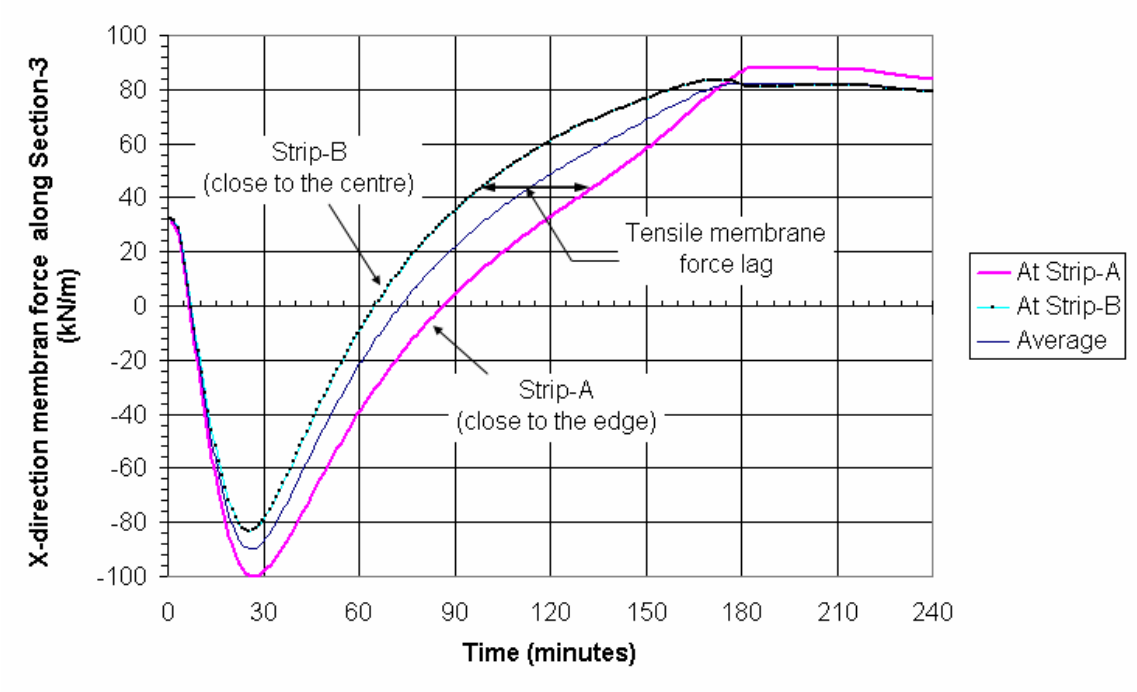

Figure 5-41 X-direction membrane forces along Section-3 in the slab

(Pin-Pin support with X-direction restraints)

5.4.5. The effect of Y-direction restraints of the slab in fire conditions

The behaviour of Pin-Pin supported slabs with full restraints in the X-direction, Y-direction and Z-direction are discussed briefly in this section of the chapter. The purpose of this section is to investigate the effects of Y-direction restraints at the supports on the behaviour of the slab exposed to an ISO 834 Standard fire. The simplified diagram of the slab is shown in Figure 5-42 (a) and the SAFIR structural model with the boundary conditions of the supports is shown in Figure 5-42 (b).

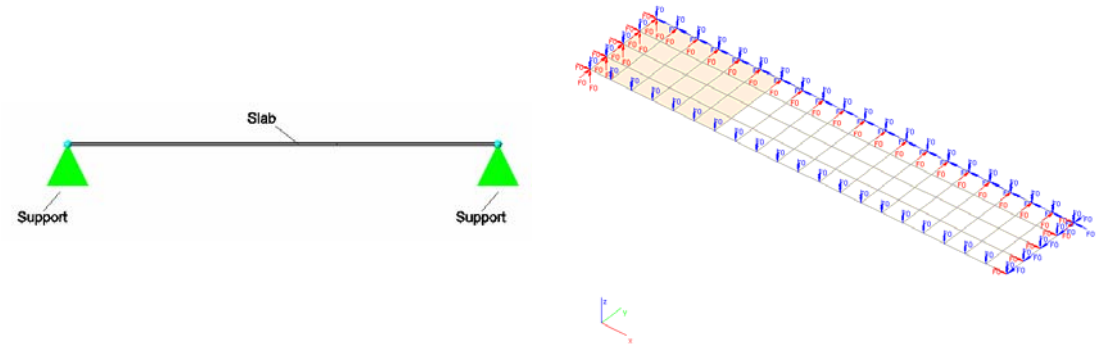

(a) Simplified diagram with fully restraints in the X-, Y-, and Z-direction (5m span one way slab)

(b) The SAFIR model with support boundary conditions (a quarter of the slab)

Figure 5-42 The SAFIR structural model of Pin-Pin supports with X-direction, Y-direction, and Z-direction restraints

It is evident that the Y-direction restraints did not obviously affect the X-direction bending moments, the X-direction membrane forces, the distribution of Y-direction bending moments, the bowing action in the Y-direction, and the vertical deflections of the slab, but significantly affected the Y-direction displacements and Y-direction membrane forces of the slab in the region from the supports to 0.5m away from the supports (the shaded region in Figure 5-43).

Figure 5-43 shows the Y-direction displacements along the free edge of the slab when the supports were restrained in the X-direction and Y-direction. Compared with Figure 5-31, it is found that the un-shaded region in Figure 5-43 was the same as in Figure 5-31.

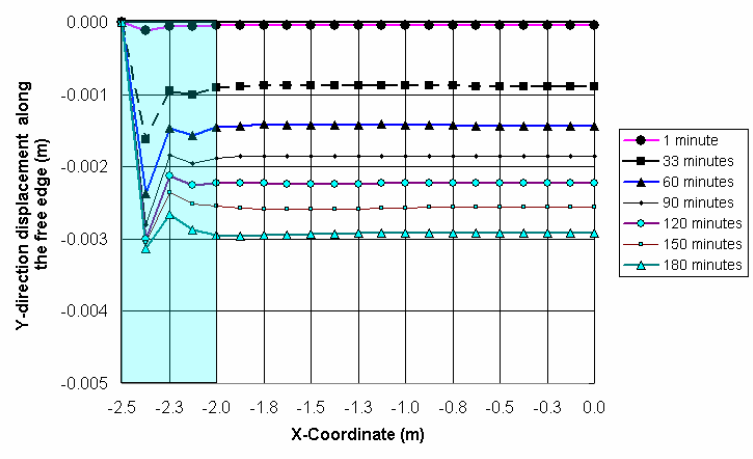

Figure 5-43 Y-direction displacements along the free edge of the slab

(Pin-Pin supports with X-direction and Y-direction restraints)

Figure 5-44 shows a comparison of Y-direction membrane forces in Section-4 between the slabs with and without the Y-direction restraints. Figure 5-44 (b) shows that there were no compressive membrane forces in the edge of the slab when the supports of the slab were not restrained in the Y-direction; whilst, Figure 5-44 (a) shows that the compressive membrane forces were present in the edge of the slab when the supports of the slab were restrained in the Y-direction.

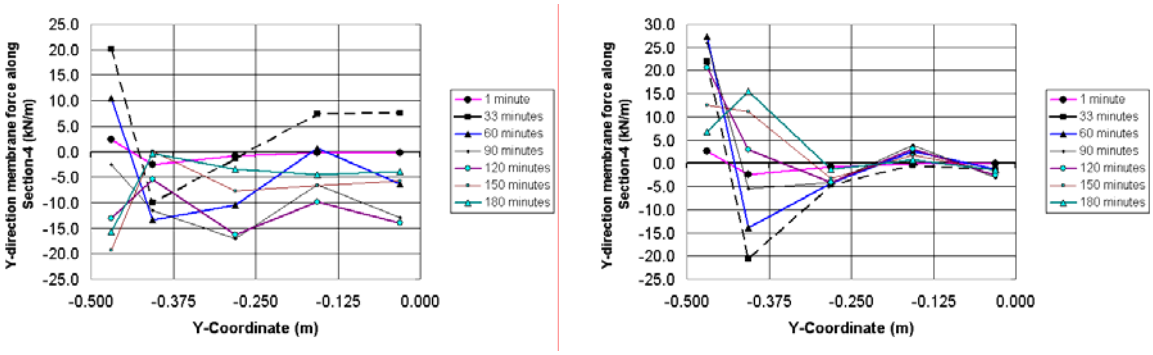

(a) Y-direction membrane forces in Section-4 with Y-direction restraint

(b) Y-direction membrane forces in Section-4 without Y-direction restraint

Figure 5-44 Comparison of Y-direction membrane forces in Section-4 of the slab with and without Y-direction restraints

5.4.6. Comparison of using 3-D and 2-D models in the analysis of one-way slabs

This section of the chapter presents a short comparison of using 3-D shell elements and 2-D beam elements in the analysis of one-way slabs exposed to an ISO 834 Standard fire. The slab was restrained in the X-direction on the supports. The 3-D shell element model was detailed earlier in this chapter, while the 2-D beam element model was detailed by Lim (2003). Two aspects of the behaviours of one-way slabs are compared in this section: vertical deflections and membrane forces in the slab.

Vertical deflections of the slab in fire conditions

Figure 5-45 shows a comparison of the vertical deflections at the midspan of the slab under fire exposure between using the 2-D beam element model and the 3-D shell element model. The graph shows that the magnitude and trend of the vertical deflections after 180 minutes, when the slab deformed to a catenary, were completely the same using both models, but they were different in the duration from 1 minute to 180 minutes because the development of the compressive membrane forces in the slab was different in magnitudes between using these two models. The vertical deflection was 0.029m at the initial time (1 minute) of the fire using the 3-D model, while it was 0.010m at 1 minute using the 2-D model. The trend of development of vertical deflections in the initial stage (1 minute to 30 minutes) was completely different between using these two models. The vertical deflection increased to 0.11m at 30 minutes using the 3-D model, while it dramatically dropped to 0.15m at 30 minutes using the 2-D model because the development of the compressive membrane forces in the slab using the 2-D model accelerated the development of the vertical deflections at the midspan of the slab. The trend of development of vertical deflections in the duration of 30 minutes to 180 minutes was similar when using the two different models.

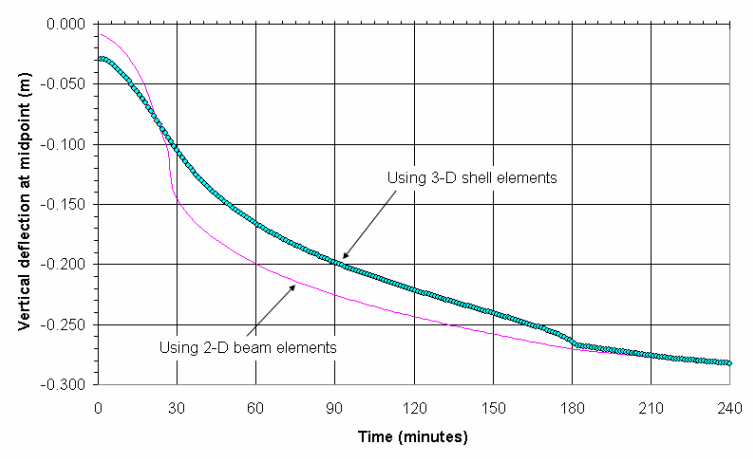

Figure 5-45 Comparison of vertical deflections at midspan of the slab

Membrane forces of the slab in fire conditions

Figure 5-46 shows a comparison between membrane forces using the 3-D shell element model and axial forces using the 2-D beam element model at the midspan of the slab under fire exposure. The graph shows that the magnitude and trend of the membrane forces (or the axial forces) after 180 minutes when the slab was deformed to a catenary were completely the same using both models, but they were different in the duration from 1 minute to 180 minutes. One reason for the differentials between the membrane forces using the two models was that the Y-direction bowing action was considered in 3-D shell element models and the other reason was that the vertical deflections at the initial time were *underestimated* using 2-D models or *overestimated* using 3-D models due to the differentials in the assumptions in the two kinds of finite element models. Therefore, the membrane forces at the initial time of the simulation were completely different. The membrane force was a tensile force of 30kN/m using the 3-D model, while it was a compressive force of 200kN/m using the 2-D model. At 18 minutes the compressive force using the 2-D model dramatically increased to 1100kN/m, while it slightly increased to 85kN/m using the 3-D model. After 180 minutes the tensile membrane force remained a constant value of 85kN/m until the end of the simulation using both models.

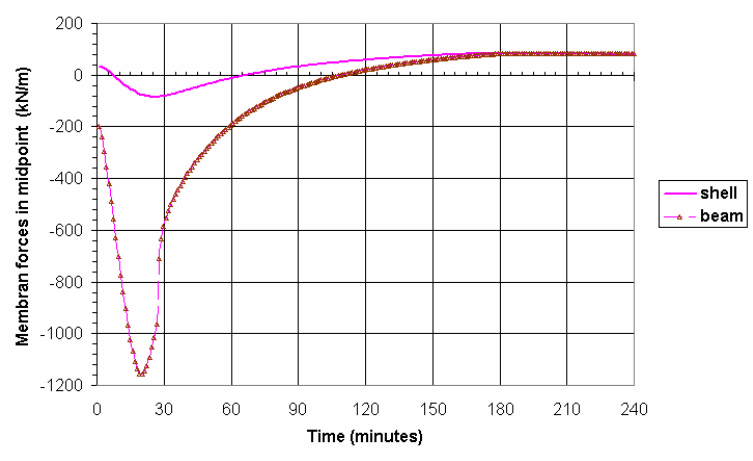

Figure 5-46 Comparison of membrane forces in the midspan of the slab

To sum up, both models can precisely predict the failure of the slab. However, the development of the vertical deflections and membrane forces (or axial forces) is completely different using these two different kinds of structural models in SAFIR.

5.4.7. Conclusions

The analyses of Pin-Pin supported one-way slabs with full X-direction and Z-direction restraints at the supports using 3-D shell elements in SAFIR when the slabs exposed to an ISO 834 Standard fire have shown that:

- Both the 2-D beam element model and the 3-D shell element model can precisely predict the failure of the slab, but the process of the development of vertical deflections and membrane forces is completely different.
- Y-direction restraints at the supports do not obviously affect the behaviour of the slab in the X-direction.
- The Y-direction bowing of the slab is slightly reduced by the X-direction restraints at the supports in the initial stage of the fire (1 minute to 33 minutes).
- The bending moments are non-linearly distributed along the cross-section close to the supports.
- The tensile membrane force lag is present in the slab.
- The top reinforcing bars are the key in preventing the collapse of the slab.

5.5. The Effect of Varying the Widths of the Slabs in Fire Conditions

This section investigates the one-way slabs with X-direction and Z-direction restraints exposed to an ISO 834 Standard fire by varying the widths of the slabs. The purpose of this section is to analyse how the Y-direction bowing action affects the behaviour of the slabs by varying the widths of the slabs. The widths of the slabs range from 0.5m to 2.0m (0.5m, 0.75m, 1.0m, 1.5m and 2.0m).

5.5.1. Vertical deflections of the slabs in fire conditions

The vertical deflections at the midpoint of the slabs (Point-O) against the time are illustrated in Figure 5-47(a). It shows that the vertical deflections of the wider slabs were larger than the vertical deflections of the narrower slabs at Point-O. The percentage difference of the vertical deflections between the slabs is plotted in Figure 5-47 (b). It shows that in the duration of 33 minutes to 150 minutes the percentage difference of the vertical deflections almost remained constant. In this period the vertical deflection of the 1.0m width slab was 3.2% less than that of the 2.0m width slab and 0.8% larger than that of the 0.5m width slab.

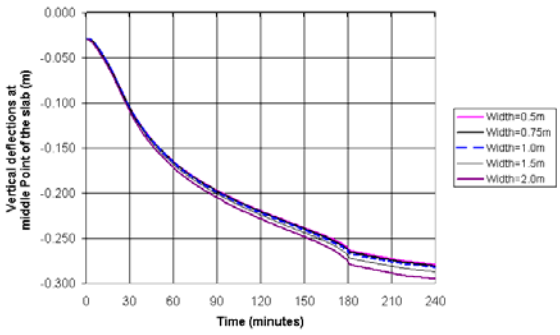

(a) Vertical deflections at middle point of the slabs

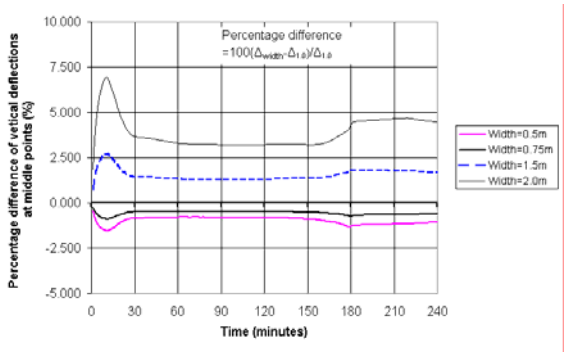

(b) Percentage differences of the vertical deflections of the slabs

Figure 5-47 Comparison of vertical deflections at midpoint

(Pin-Pin supports with X-direction restraints)

The bowing radius of the slabs against the time is shown in Figure 5-48 (a). It shows that the bowing radius was the same for the slabs with different widths in the tendency, but was different in the magnitude, especially when the widths of the slabs were greater than 1.0m. The percentage difference of the bowing radius between the slabs against the time is shown in Figure 5-48 (b). It shows that when the width of the slab was less than 1.0m, the bowing

radius almost remained constant throughout the simulation. When the width of the slab was 2.0m, the bowing radius at 30 minutes was 7.5% less than when the width of the slab was 1.0m, but at 150 minutes it was 2.5% greater than when the width of the slab was 1.0m. This indicates that the width of the slab significantly affected the Y-direction bowing if the width of the slab was greater then 1.0m. The slab with a wider width tended to reduce the bowing in the midspan when the slab was exposed to an ISO Standard fire, so the bowing action was significant within the slabs with the wider widths.

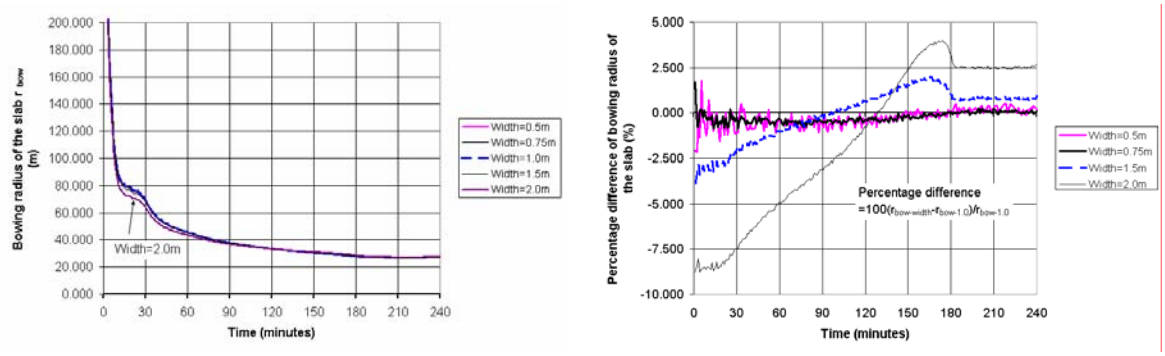

(a) Bowing radius of the slabs (b) Percentage difference of the bowing radius

Figure 5-48 Comparison of bowing radius in Section-3

(Pin-Pin supports with X-direction restraints)

5.5.2. Bending moments of the slabs in fire conditions

X-direction bending moments

Figure 5-49 shows the curvatures of the X-direction bending moments along Strip-A and Strip-B at 1 minute to 120 minutes when the slabs were exposed to an ISO 834 Standard fire beneath. These graphs gave a concept of how the X-direction bending moments were affected by varying the widths of the slabs. At the initial stage (at 1 minute), the bending moments of the slabs were almost not affected by varying the widths of the slabs, as shown in Figure 5-49 (a) and Figure 5-49 (b). At this stage, the bending moments constantly distributed along the cross-section at the middle span. After the initial stage (after 33 minutes) the curvatures of the bending moments were variable in the slabs, as shown in Figure 5-49 (c) to Figure 5-49 (g). The wider the width of slabs, the more variable the bending moments in slabs were.

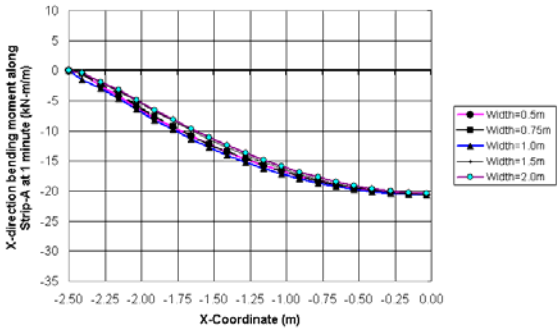

(a) Along Strip-A at 1 minute

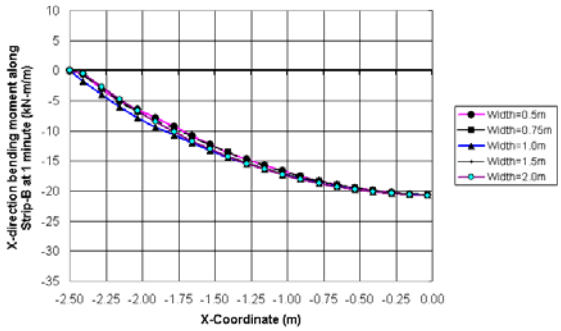

(b) Along Strip-B at 1 minute

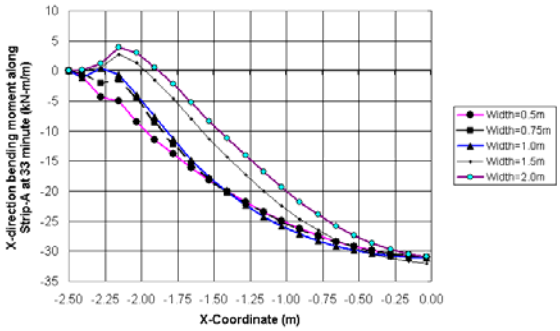

(c) Along Strip-A at 33 minutes

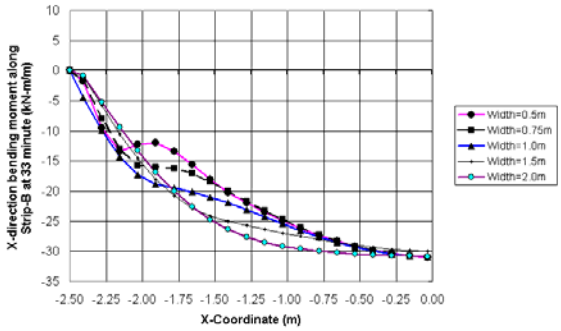

(d) Along Strip-B at 33 minutes

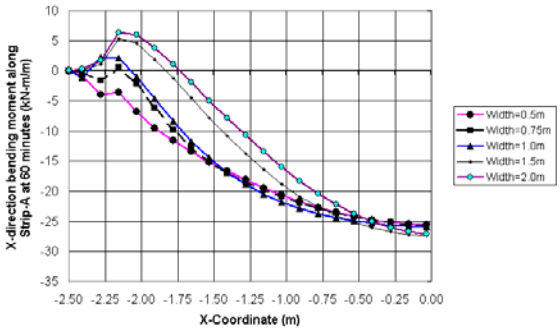

(e) Along Strip-A at 60 minutes

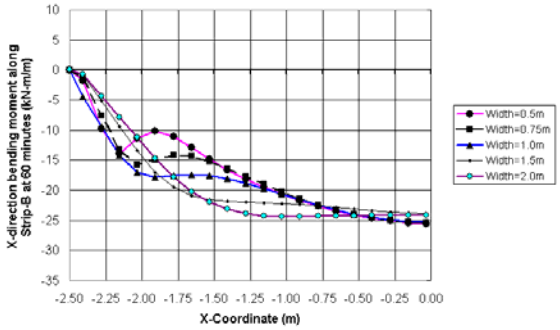

(f) Along Strip-B at 60 minutes

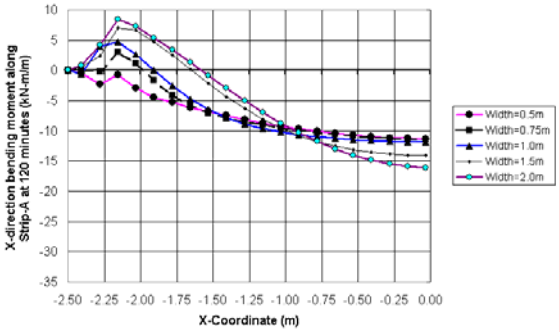

(g) Along Strip-A at 120 minutes

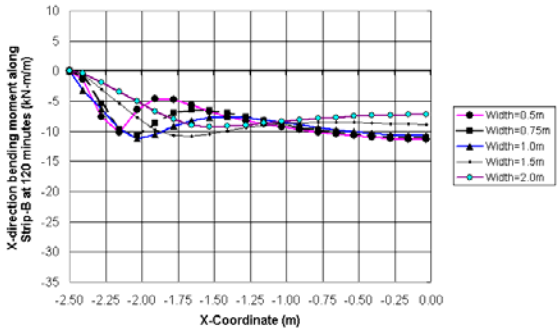

(g) Along Strip-B at 120 minutes

Figure 5-49 Bending moments in Strip-A and Strip-B of the slabs at different times

(Pin-Pin supports with X-direction restraints)

Figure 5-50 shows the X-direction bending moments in the midspan of the slabs in Strip-A and Strip-B. The graphs show that when the duration of the fire was greater than 60 minutes the larger X-direction bending moments were in the wider slabs in Strip-A (the edge strip of

slabs) while in Strip-B the smaller X-direction bending moments were present in the narrower slabs. The distribution of X-direction bending moments along the cross-section of the slab was more irregular in the wider slabs due to the effect of the Y-direction bowing action.

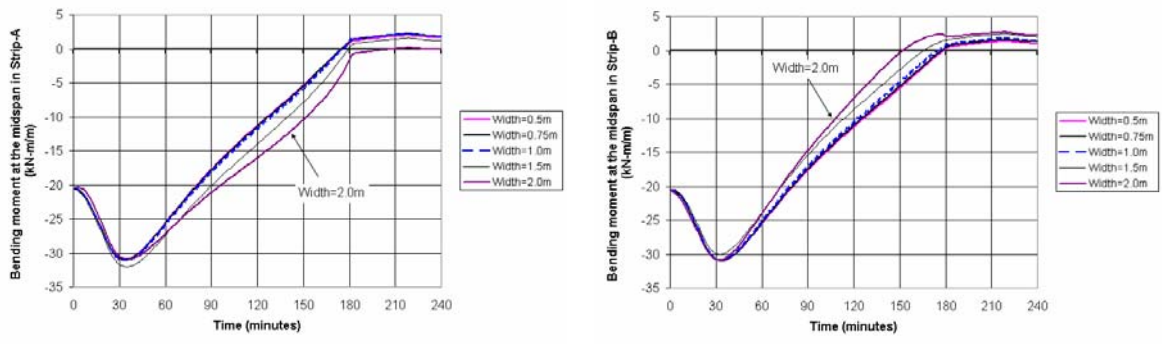

(a) Bending moment in the midspan in Strip-A (b) Bending moment in the midspan in Strip-B

Figure 5-50 X-direction bending moments in Section-3 of the slabs

(Pin-Pin supports with X-direction restraints)

Y-direction bending moments

The distributions of Y-direction bending moments in the slabs with widths of 1.0m, 1.5m, and 3.0m are shown in Figure 5-51. It shows that the Y-direction bending moments were present within the region of a half-width of the slabs from the supports. The maximum Y-direction bending moment was less than 12kN-m/m in all the cases; this value was significantly less than the maximum X-direction bending moment in the midspan of the slabs. The Y-direction bending moments were positive, so tensile strengths were in the top reinforcing bars of the slabs.

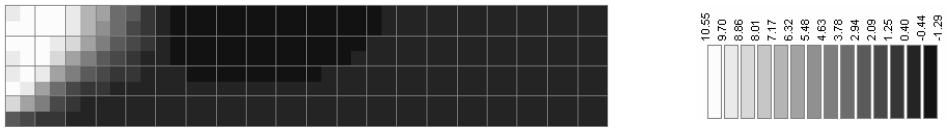

(a) Distribution of Y-direction bending moments at 60 minutes (Width=1.0m)

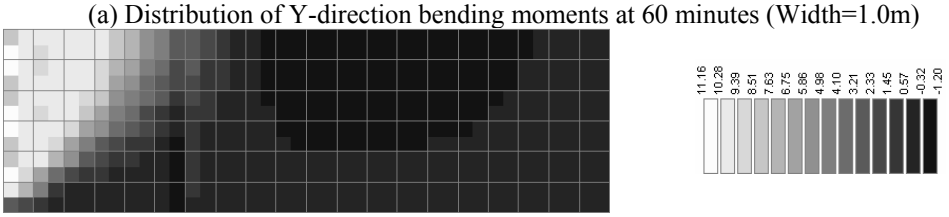

(b) Distribution of Y-direction bending moments at 60 minutes (Width=1.5m)

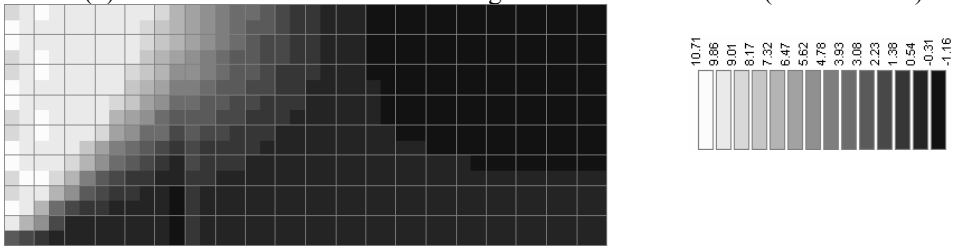

(c) Distribution of Y-direction bending moments at 60 minutes (Width=2.0m)

Figure 5-51 Distributions of Y-direction bending moments of the slabs at 60 minutes

(Pin-Pin supports with X-direction restraints)

5.5.3. Membrane forces of the slabs in fire conditions

Figure 5-52 (a) and Figure 5-52 (b) show the membrane forces at the midspan in Strip-A and Strip-B by varying the widths of the slabs, respectively. The graphs show that the membrane forces were much more changeable along the cross-section of the slabs with the wider widths. The membrane forces in the 2.0m width slab changed to tensile forces at 45 minutes in Strip-B, while in Strip-A they changed to tensile forces at 165 minutes; the development of the tensile membrane forces in Strip-A were later than in Strip-B for 120 minutes. The tensile membrane force lag in the slabs with wider widths was longer than in the slabs with narrower widths because of the effect of the Y-direction bowing action in slabs. At 180 minutes the slabs deformed to catenaries in all the cases because the yield strength of the reinforcing bars on the bottom of the slabs dramatically dropped to nearly zero.

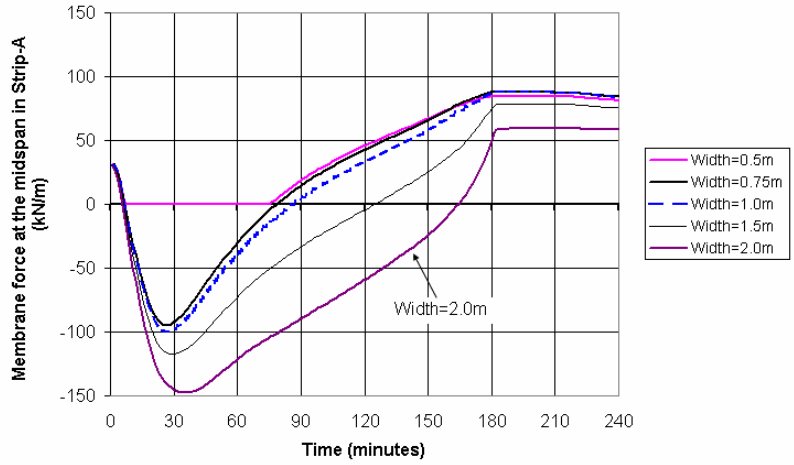

(a) Membrane forces at the midspan in Strip-A

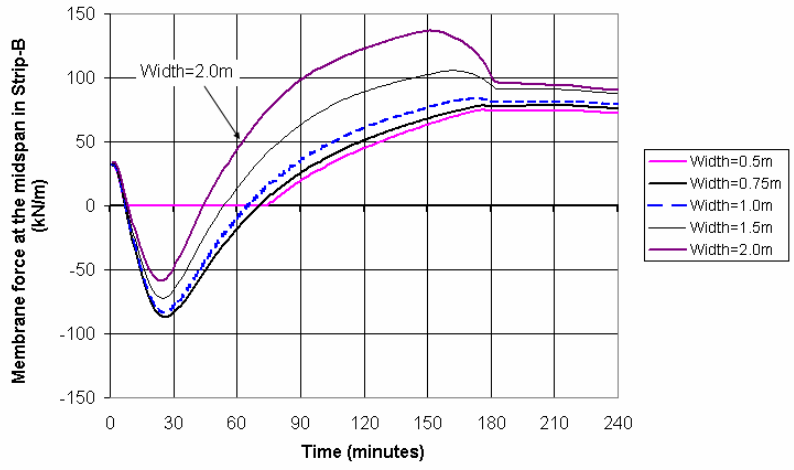

(b) Membrane forces at the midspan in Strip-B

Figure 5-52 Membrane forces at the midspan in Strip-A and Strip-B of the slabs (Pin-Pin supports with X-direction restraints)

5.5.4. Conclusions

The analyses of Pin-Pin supported slabs with full X-direction and Z-direction restraints with varying the widths of the slabs exposed to an ISO 834 Standard fire have shown that:

- The wider slab has the larger vertical deflection in the midpoint of slab.
- The tendency of the bowing radius is the same in the slabs with different widths.
- The distribution of bending moments along the cross-section is more non-linear in the wider slab than in the narrower slab.
- The tensile membrane force lag is greater in the wider slab than in the narrower slab.

5.6. The Slab in the Fire with a Decay Phase

The purpose of this section is to investigate the behaviour of one-way slabs under fires with a decay phase. The structural model of one-way slabs is the same as that which was described earlier in Section 5.4. The ISO 834 Standard fire with a decay phase was detailed earlier in Chapter 4 in this thesis.

5.6.1. Displacements of the slab in fire conditions

Vertical deflections (Z-direction)

Figure 5-53 shows the vertical deflections of the slab at Point-O, which was subjected to an ISO 834 Standard fire with a decay phase. The graph shows that the maximum vertical deflection was 0.183m at 85 minutes. At 170 minutes when the fire was exhausted, the vertical deflection declined to 0.125m and when the simulation was stopped, the vertical deflection declined to 0.087m, which was three times the initial deflection at Point-O.

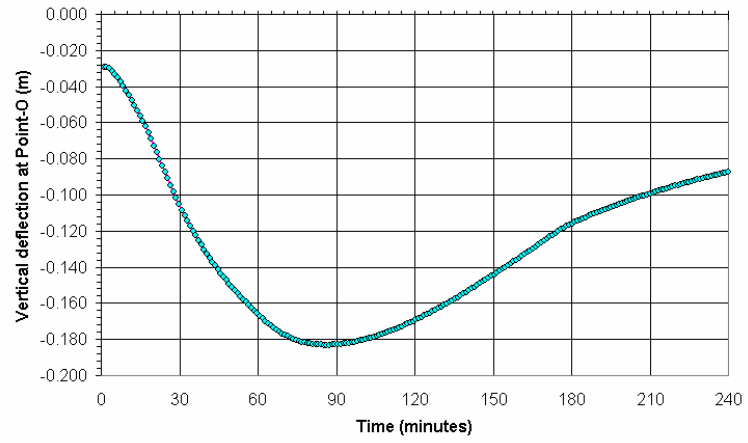

Figure 5-53 Vertical deflections of the slab at Point-O in the fire with a decay phase

Figure 5-54 shows the bowing radius of the slab when it was exposed to the fire with a decay phase. The graph shows that the minimum bowing radius of 40m was reached at 85 minutes in the midspan (Section-3) when the maximum vertical deflection at Point-O was reached. After 85 minutes, the bowing radius in the midspan smoothly increased to 313m at 240 minutes in Section-3, while the bowing radius in Section-1 increased to 480m at the end of the simulation. The changes of the bowing radius indicate that the Y-direction bowing was reduced within and after the decay phase of the fire.

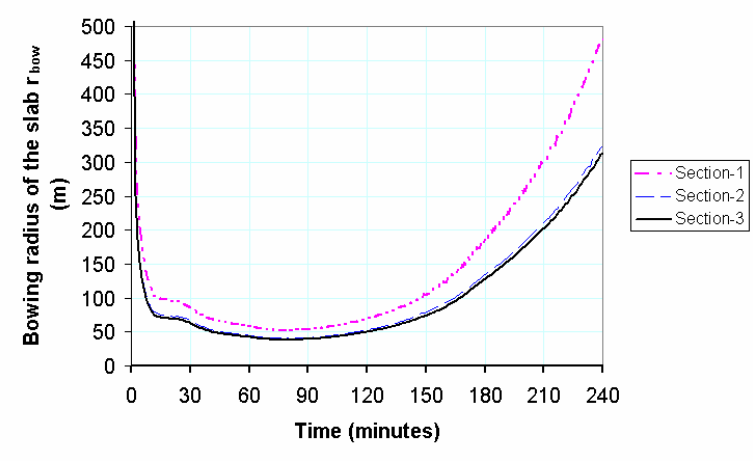

Figure 5-54 Bowing radius of the slab in the fire with a decay phase

Horizontal displacements (Y-direction)

The Y-direction displacements along the free edge of the slab when it was exposed to an ISO 834 Standard fire with a decay phase are shown in Figure 5-55. It shows that at 1 minute the Y-direction displacements were almost zero along the free edge of the slab, while at 90 minutes it increased to 0.0016m at Point-A and at 180 minutes the Y-direction displacement declined to 0.001m. The width of the slab under fire conditions slightly increased due to the increase of Y-direction displacements.

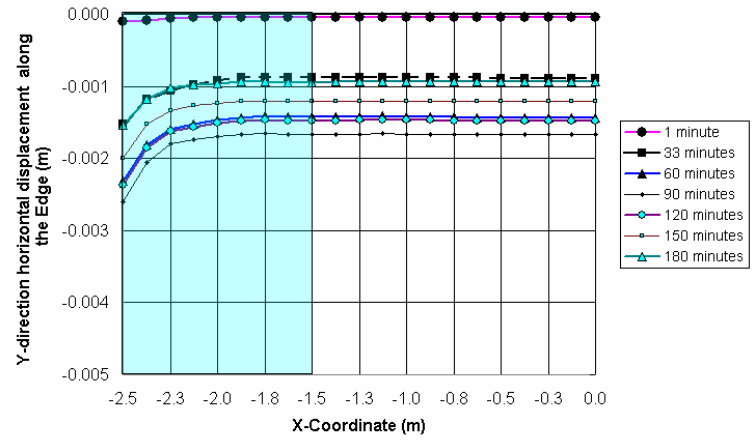

Figure 5-55 Y-direction displacements along the free edge of the slab in the fire with a decay phase

5.6.2. Bending moments of the slab in fire conditions

X-direction bending moments

Figure 5-56 shows the X-direction bending moments along Strip-A and Strip-B in the slab exposed to an ISO 834 Standard fire with a decay phase. At 1 minute, the curvatures of bending moments were the same as the curvatures of bending moments at ambient temperatures; after that, the curvatures significantly changed in the shaded regions in the graphs. When the decay phase of the fire was reached, the bending moments significantly increased in the slab close to the midspan.

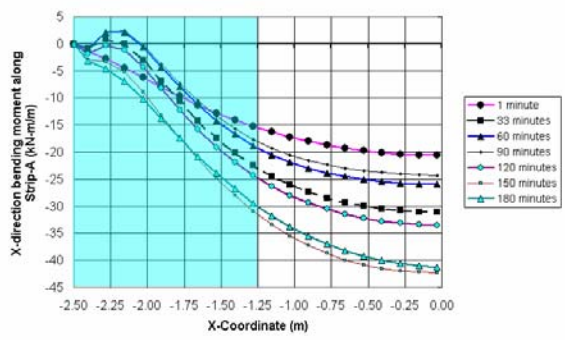

(a) X-direction bending moments along Strip-A

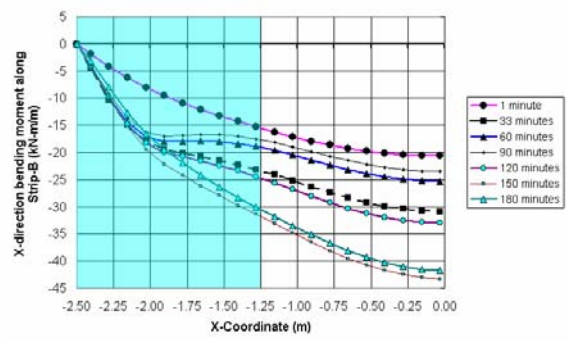

(b) X-direction bending moments along Strip-B

Figure 5-56 X-direction bending moments along Strip-A and Strip-B of the slab in the fire with a decay phase

The X-direction bending moments in the sections, as shown in Figure 5-57, were linearly distributed along Section-3, but non-linearly distributed along Section-1 and Section-2, especially before the decay phase of the fire was reached due to the effect of the Y-direction bowing action. The maximum X-direction bending moment was present in the midspan of the slab.

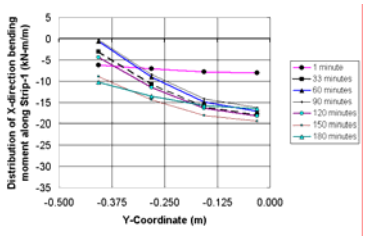

(a) Distribution of X-direction bending moments along Section-1

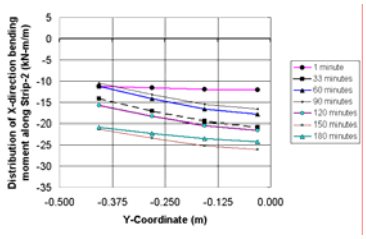

(a) Distribution of X-direction bending moments along Section-2

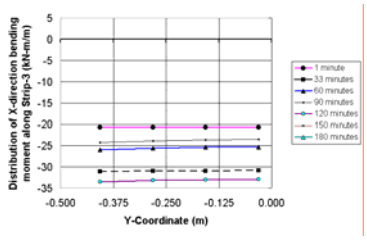

(a) Distribution of X-direction bending moments along Section-3

Figure 5-57 Distribution of X-direction bending moments along the sections of the slab in the fire with a decay phase

Figure 5-58 shows the X-direction bending moments in the midspan of the slab exposed to an ISO 834 Standard fire with a decay phase. The graph shows that the bending moments were

almost linearly distributed along the cross-section in the midspan. The bending moment reached its first peak value of -31kN-m/m at 33 minutes, and then declined to -23kN-m/m at 80 minutes when the vertical displacement almost reached the maximum value. In the duration of 80 minutes to 150 minutes, the bending moment linearly increased from -23kN m/m to -43kN-m/m and at 150 minutes the trend of the development of negative bending moments suddenly changed to decreasing from increasing because the plastic hinges were formed in the slab. After the plastic hinges were present in the slab, the bending moments in the midspan gradually declined until the end of the simulation.

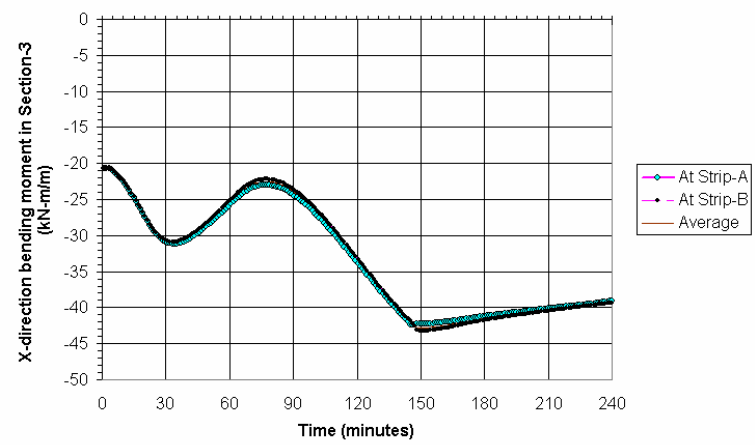

Figure 5-58 X-direction bending moments in the midspan of the slab in the fire with a decay phase

Figure 5-59 shows the X-direction bending moments against the time in Section-1 and Section-2 when the slab was exposed to the fire with a decay phase. Figure 5-59 (a) shows that at 80 minutes the bending moment was almost zero at Strip-A (close to the edge of the slab) and was 16kN-m/m at Strip-B; the difference of the bending moments between at Strip-A and Strip-B was 16kN-m/m in Section-1, whilst the difference was only 6kNm/m in Section-2. The distribution of bending moments was more non-linear along the sections in the region close to the supports.

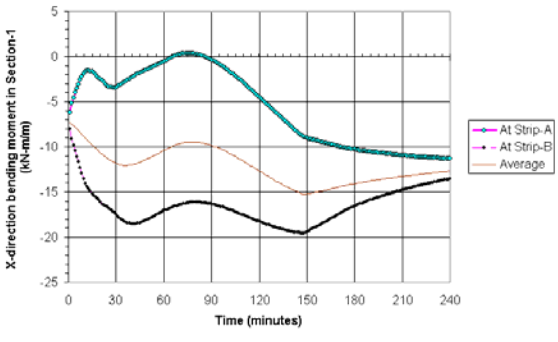

(a) X-direction bending moment against time in Section-1

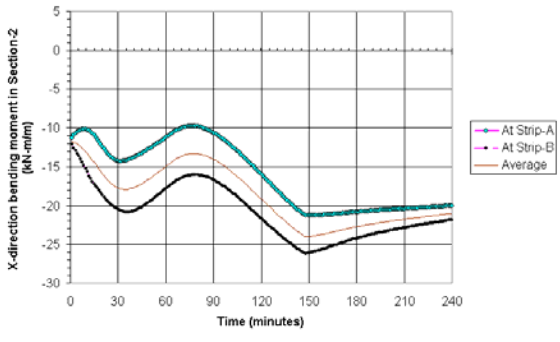

(b) X-direction bending moment against time in Section-2

Figure 5-59 X-direction bending moments against the time in Section-1 and Section-2 of the slab in the fire with a decay phase

Y-direction bending moments

Figure 5-60 shows the Y-direction bending moments along Section-1 and Section-2 when the slab was exposed to the fire with a decay phase. The graphs show that the Y-direction bending moment in Section-1 close to the centre of the slab increased from almost zero to 3.7kN-m/m at 90 minutes and then declined to 1.8kNm/m at 180 minutes. The Y-direction bending moments along Section-2 were negative values, which were less than -1.2kN-m/m throughout the simulation. The magnitude and distribution of Y-direction bending moments were not sufficiently affected by the fire with a decay phase.

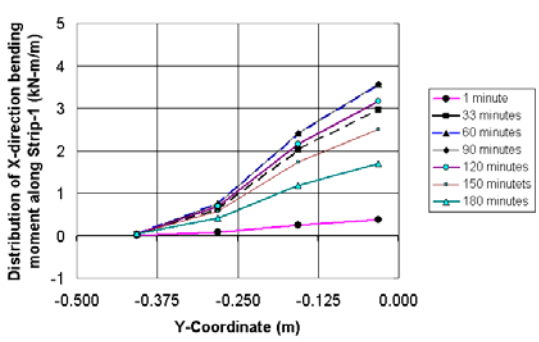

(a) Y-direction bending moment along Section-1

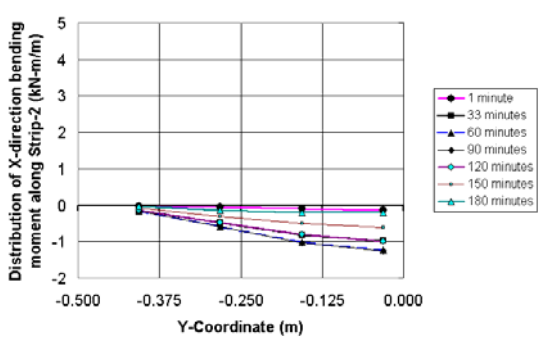

(b) Y-direction bending moment along Section-2

Figure 5-60 Y-direction bending moments along Section -1 and Section-2 of the slab in the fire with a decay phase

5.6.3. Membrane forces of the slab in fire conditions

The distributions of the membrane forces along the sections of the slab are shown in Figure 5-61. The graphs show that the membrane forces in the slab non-linearly distributed along the cross-sections of the slab in fire conditions.

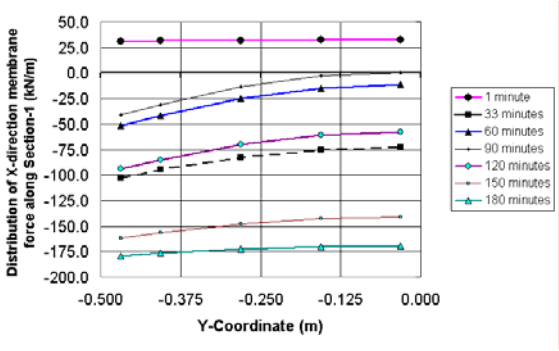

(a) Distribution of X-direction membrane forces along Section-1

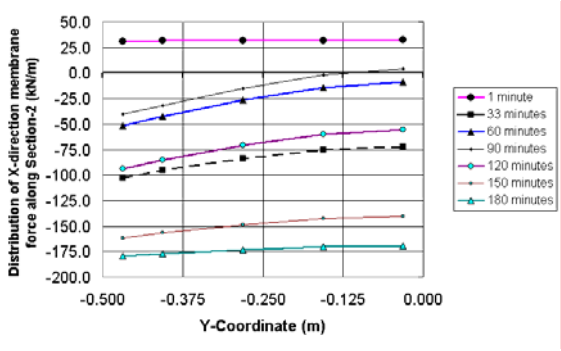

(b) Distribution of X-direction membrane forces along Section-2

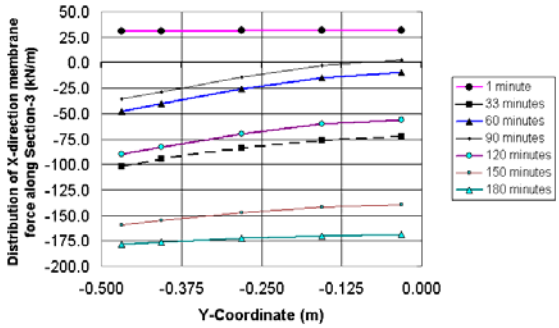

(c) Distribution of X-direction membrane forces along Section-3

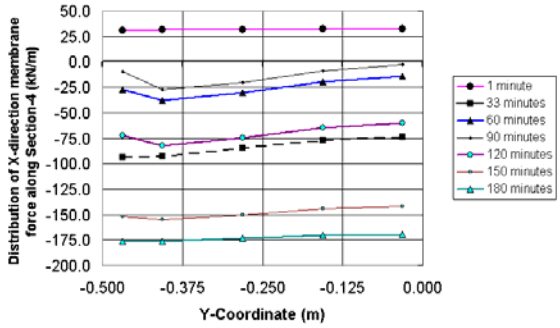

(d) Distribution of X-direction membrane forces along Section-4

Figure 5-61 Distributions of X-direction membrane forces along the sections of the slab in the fire with a decay phase

Figure 5-62 shows the X-direction membrane forces along Strip-B in the sections when the slab was exposed to the fire with a decay phase. The graph shows that the membrane forces remained a constant value at the same time along the strip, but significantly changed throughout the simulation. At the initial stage of the fire the membrane force dropped to a compressive force and at 28 minutes the first peak value of compressive membrane forces of -83kN/m was reached, and then declined to zero at 65 minutes; after that, the tensile membrane force was developed and it reached the peak value of 10kN/m at 78 minutes. At 90 minutes the tensile membrane force declined to zero again. After 90 minutes the compressive membrane force was present in the slab and increased to -145kN/m at 150 minutes. There was a crinkle in the membrane force curve at 150 minutes because the plastic hinges were formed in the slab. When the fire exhausted at 170 minutes, the

compressive membrane force increased to -160kN/m and continuously increased to -202kN/m at the end of the simulation. The maximum membrane force in the slab was present at 240 minutes. At the end of the simulation the second peak value of compressive membrane forces was not reached.

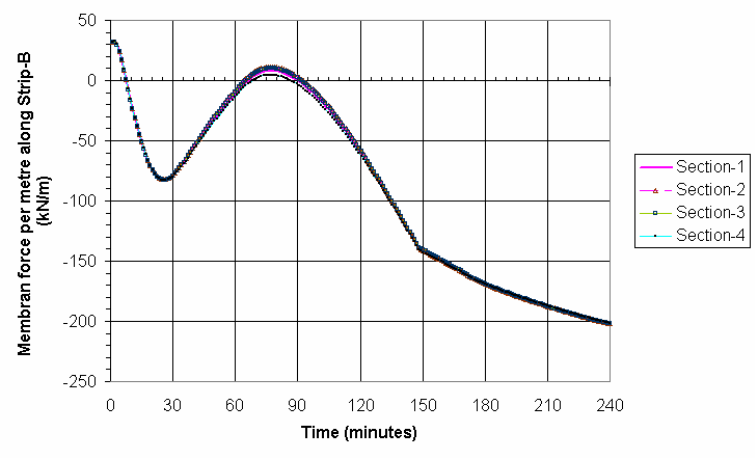

Figure 5-62 Membrane forces along Strap-B in the sections of the slab in the fire with a decay phase

Figure 5-63 shows the membrane forces along the midspan (Section-3) when the slab was exposed to the fire with a decay phase. The graph shows that the tensile membrane force lag was present in the slab close to the edge of the slab. The average membrane forces in Section-3 remained compressive forces throughout the simulation. At 240 minutes the phenomenon of the tensile membrane force lag disappeared due to the declining of the temperatures and reducing of the Y-direction bowing action in the slab.

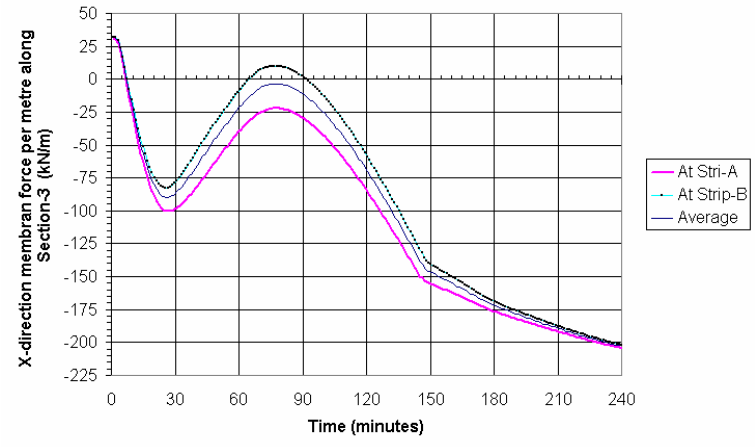

Figure 5-63 Membrane forces along Section-3 of the slab in the fire with a decay phase

Because the effect of the compressive membrane force of -140kN/m combined with the effect of the maximum bending moment of -43kN-m/m in the midspan at 150 minutes, the plastic hinges were formed in the midspan of the slab. The angle of rotations in the X-direction at Point-O against the time is shown in Figure 5-64. It shows that the angle of rotations at Point-O suddenly enlarged at 150 minutes which indicated a hinge was formed at Point-O.

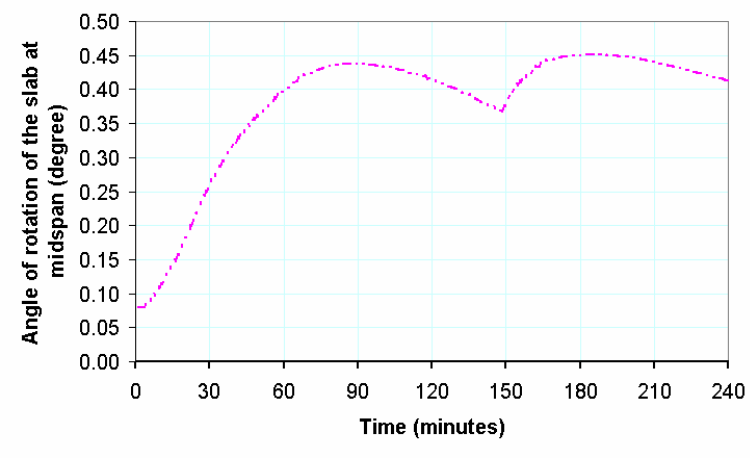

Figure 5-64 The angle of rotations of the slab at Point-O (midspan)

5.6.4. Conclusions

The analysis of Pin-Pin supported slabs with full X-direction and Z-direction restraints at the supports when the slabs were exposed to an ISO 834 Standard fire with a decay phase has shown that:

- The vertical deflection at the middle point (Point-O) declines within and after the decay phase of the fire.
- The bending moments dramatically increase within the decay phase of the fire until the plastic hinges are formed in the slab.
- The compressive membrane forces dramatically increase within and after the decay phase of the fire.
- The plastic hinges are formed in the slab at 150 minutes due to the increase of compressive membrane forces and bending moments in the slab.
- The worst scenario of one-way slabs in fire conditions could be when the slabs are exposed to the fire with a decay phase.

5.7. Conclusions

The main findings of the 3-D analyses of one-way slabs using the SAFIR shell element models are listed below:

- Y-direction bowing actions, bending moments and displacements in the region close to the supports are significantly affected by Z-direction restraints (vertical restraints at the supports).
- The Y-direction restraints at the supports do not obviously affect the behaviour of the slab in the X-direction.
- The bending moments are non-linearly distributed along the cross-sections of the slab in the region close to the supports. The distribution of bending moments along the cross-sections is more non-linear in the wider slab than in the narrower slab.
- The tensile membrane force lag is present in the slab due to the earlier development of the compressive membrane forces in the region close to the edge. The tensile membrane force lag in the edge strip of the slab is greater in the wider slab than in the narrower slab.
- The top reinforcing bars in the slab are the key to preventing the collapse of the slab when it is restrained in the X-direction at the supports.
- The worst scenario of one-way slabs with horizontal restraints at the supports could be when the slabs are exposed to the fire with a decay phase.

6. THE ANALYSIS OF ONE-BAY FLAT SLABS AT AMBIENT AND FIRE CONDITIONS

This chapter covers the analyses of one-bay flat slabs without edge beams at ambient and fire conditions using SAFIR. The purposes of this chapter are to investigate the behaviour of flat slabs without edge beams and to inspect modelling technique using SAFIR. At ambient conditions, the applied uniformly distributed loads on the one-bay flat slab increase from zero to the loads that cause the collapse of the slab. The ultimate load on the slab is determined using SAFIR. In fire conditions, the first floor slab is exposed to an ISO 834 Standard fire with or without a decay phase beneath for 240 minutes (4 hours). The displacements, the distributions of bending moments, and the membrane forces in the slab are investigated. The effect of the connection model of columns, slabs and the edge strip of the slab in SAFIR is discussed.

6.1. Introduction of the Modelled Structure

Figure 6-1 shows a two-level building which will be modelled using SAFIR. The floor system of the building is a reinforced concrete flat slab without edge beams. The slab is supported on four corner columns. The centre-line spans of the building are 6m in two directions; the clear height of each level is 3.6m. The research is focused on the first floor slab and only a quarter of the first floor slab is modelled because of the symmetry of the structure in two directions, the X-direction and Y-direction.

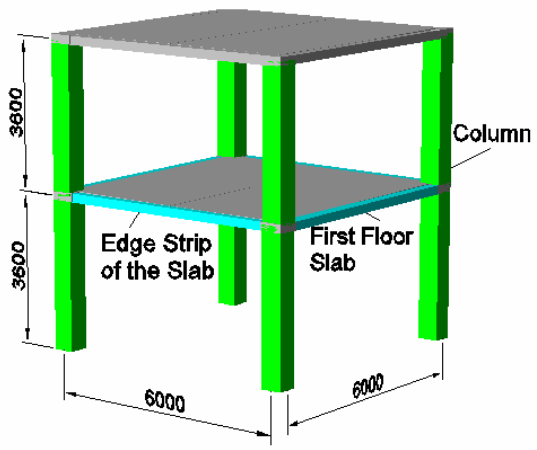

Figure 6-1 Perspective view of the one-bay flat slab in a two-level building

6.1.1. Dimensions and properties of the structure

A plan view of the first floor and a profile of the structure are shown in Figure 6-2 (a) and Figure 6-2 (b), respectively. The graphs show that the structure comprises two kinds of structural members: reinforced concrete flat slabs and corner columns. The spans of the slab are 6.5m in two directions and the thickness of the slab is 0.2m. The cross-section of the columns is 0.5m square. The shaded portion of the slab shown in Figure 6-2 (a) is modelled using SAFIR. Normally, the details of reinforcement at the edge region of the flat slab are different to the other regions; therefore, this region, where the arrangement of reinforcing bars may differ with the other regions of the slab, is defined to be a region of 0.25m width from the edge of the slab, as shown in Figure 6-2.

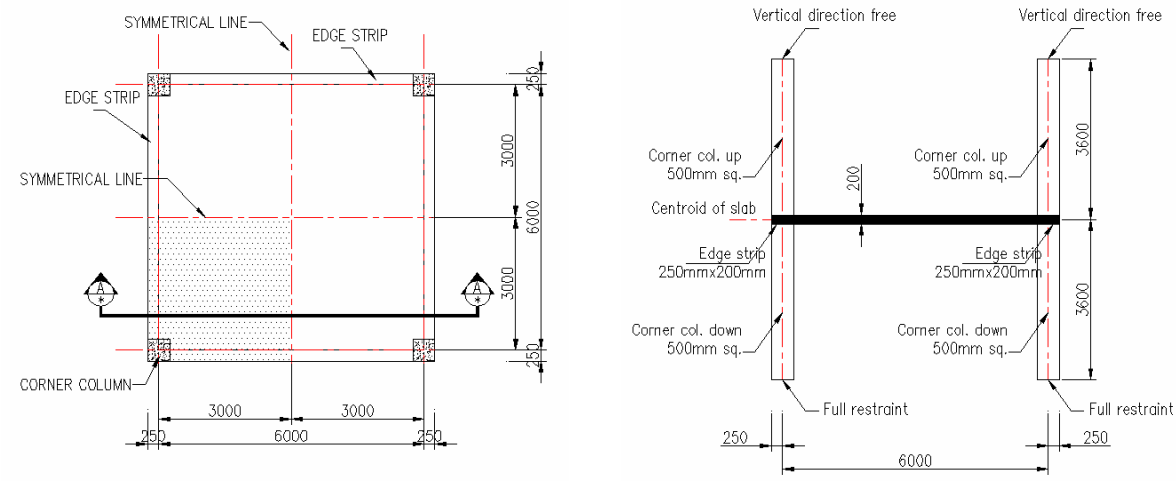

(a) Layout of the first floor of the structure (units: mm)

(b) Profile view of the section A (unites: mm)

Figure 6-2 Layout of the first floor and section view of the structure

The geometries of the flat slab, the cross-section of the columns, the properties of concrete and reinforcing steel are detailed in Table 6-1.

Table 6-1 Properties and parameters of the structure with one-bay flat slabs

Flat Slab geometry		
Centre-line Span (x-direction,)	Lx:	6.0m
Center-line Span (y-direction)	Ly:	6.0m
Depth	h:	0.2m
Aspect ratio	L/h:	30
Section of the column		
Cross-section		0.5m x 0.5m
Length	Lc	3.6 m (the ground and first floor)
Concrete properties (column and slabs)		
Compressive strength (ambient temperature)	f'_c:	36 MPa
Elastic modulus (ambient temperature)	$E_{c,o}$:	18 GPa
Tensile strength	f'_t:	Zero
Concrete model (thermal and mechanical)		Siliceous aggregate (EC2, 1995)
Concrete cover (at fire conditions)	c_c:	30 mm (centroid of reinforcing bars)
Reinforcing Steel properties (column and slabs)		
Yield strength (ambient temperature)	$f_{y,o}$:	565 MPa
Elastic modulus (ambient temperature)	$E_{s,o}$:	210 GPa
Steel model (thermal and mechanical)		Hot-rolled steel (EC2, 1995)

6.1.2. Applied loads on the structure

The uniformly distributed loads on the slab are detailed in Table 6-2, where the live load on the slab is 2.5kN/m^2. The applied load on the slab is 6.3kN/m^2 when the slab is exposed to the fire from beneath. The vertical load applied to the top of the column is 55.79kN either at ambient or fire conditions. The ultimate load on the slab is verified using SAFIR.

Table 6-2 Uniformly distributed loads on the one-bay flat slab

Loads		
Self weight + Superimposed dead load	G	5.3 kN/m^2
Live load	Q	2.5 kN/m^2
Ultimate load (1.2G + 1.6Q)		10.4 kN/m^2
Fire load (1.0G + 0.4Q)		6.3 kN/m^2
Fire Exposure		ISO 834 standard fire (4 hour duration)
Initial temperature		20.0 ^{o}C

6.1.3. Reinforcement of the structure

The reinforcing bars in slabs and columns are shown in Figure 6-3. Because one-bay flat slabs without edge beams are not recommended to be built in most building codes, the arrangement of reinforcing bars in the slab, as shown in Figure 6-3(a) and Figure 6-3(b), is determined according to the arrangement of reinforcing bars for multi-bay flat slabs in ACI 318-89 (Revised 1992) (ACI, 1992). When the distribution of reinforcing bars is determined, the

ultimate load on the slab is verified using SAFIR, because SAFIR can be used to predict the ultimate load on slabs (Lim, 2003). The reinforcing bars on the top level of the slab are shown in Figure 6-3 (a), where the distribution (or temperature) reinforcing bars of Φ8@200 in the two directions are not shown. The reinforcing bars on the bottom level of the slab are shown in Figure 6-3 (b), where only a half length of the reinforcing bars is illustrated. The length of the bottom level reinforcing bars is continuous along the span. The cross-section of the column is a square with a width (or length) of 0.5m, as shown in Figure 6-3 (c). The stirrups of the column are also detailed in the graph; however, they are not modelled using SAFIR. The details of the reinforcing bars in the edge strips of the slab are different from those in the other parts of the slab; the longitudinal reinforcing bars in the edge strips of the slab are surrounded by stirrups (Figure 6-3 (d)), whilst there are no stirrups in the other parts of the slab (Figure 6-3 (e)). Discussion about the shear design of flat slabs is present later in Section 7.1.3 of Chapter 7.

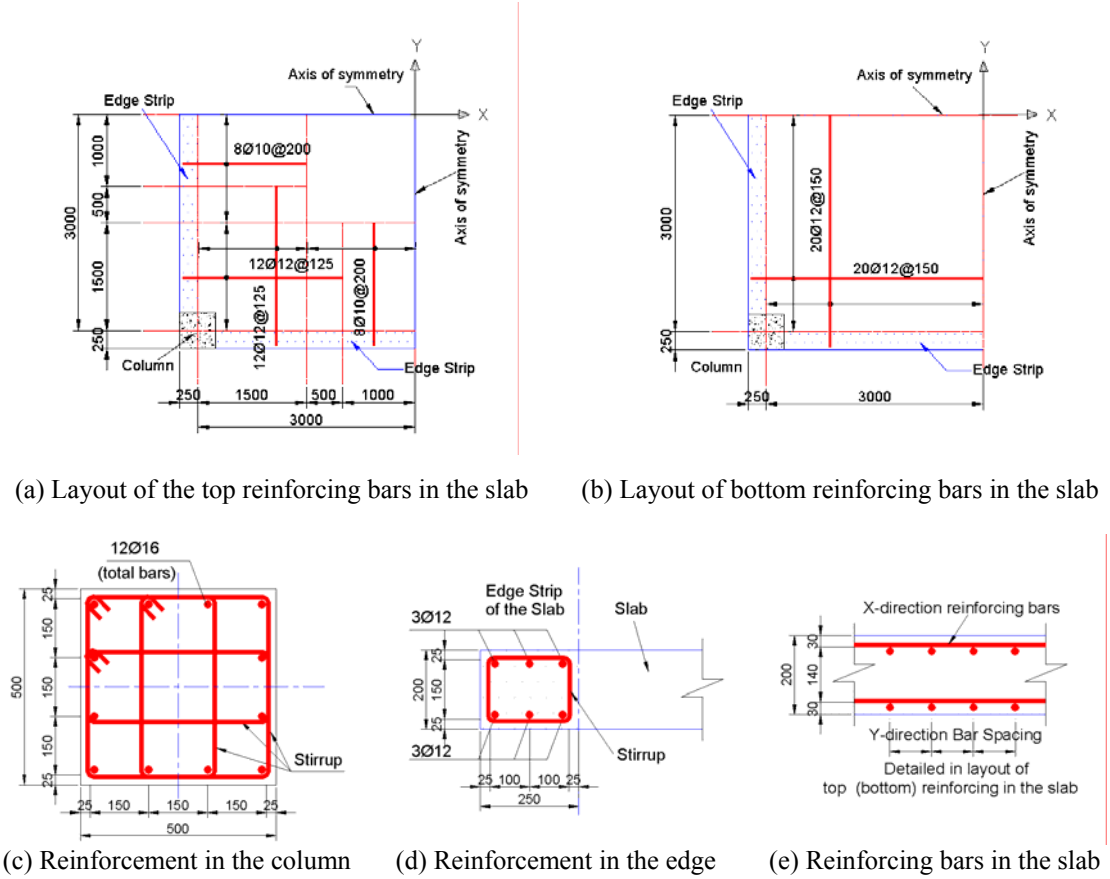

(a) Layout of the top reinforcing bars in the slab

(b) Layout of bottom reinforcing bars in the slab

(c) Reinforcement in the column

(d) Reinforcement in the edge strip of the slab

(e) Reinforcing bars in the slab

Figure 6-3 Reinforcement of slabs and columns

6.2. SAFIR Models of One-Bay Flat Slabs

This section of the chapter details the structural model of one-bay flat slabs in SAFIR. The model is used in the later sections of this chapter to simulate the one-bay flat slab at ambient or fire conditions.

6.2.1. The thermal model

The thermal analysis of slabs was presented earlier in Chapter 4 of this thesis. The thermal model of slabs was shown earlier in Figure 4-6. The effect of the reinforcing bars in slabs was not considered in the thermal model. It was assumed that the temperatures of the reinforcing bars equalled the temperatures of the concrete at the same horizontal levels in slabs. The edge strips of the one-bay flat slab were simplified to be the same as the other parts of the slab. The columns were at ambient temperature conditions throughout the simulation.

The temperature history of the top and bottom reinforcing bars in the slab exposed to an ISO834 Standard fire without a decay phase is shown in Figure 6-4 (a). It shows that the temperatures of the top and bottom reinforcing bars increased throughout the simulation. The temperature history of the top and bottom reinforcing bars in the slab exposed to an ISO834 Standard fire with a decay phase is shown in Figure 6-4 (b). It shows that the temperatures of the top reinforcing bars increased throughout the simulation, while the temperatures of the bottom reinforcing bars rose and dropped in the duration of fire exposure due to the effect of the decay phase of the fire.

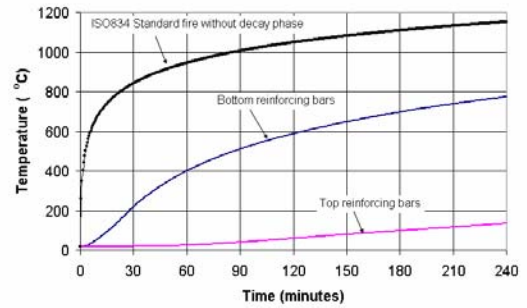

(a) Under ISO834 Standard fire without a decay phase

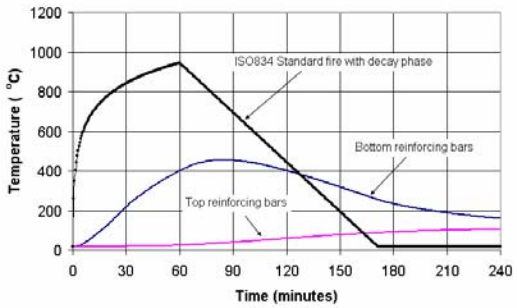

(a) Under ISO834 Standard fire with a decay phase

Figure 6-4 Temperature history in the slab

When the structural analysis at ambient temperature conditions is performed, the thermal analysis of slabs does not need to be carried out.

6.2.2. The SAFIR structure model

The first floor of the structure with four corner columns is analysed, while the roof of the structure is simplified as the vertical loads applied on the top of the columns. Because of the symmetry of the structure in two directions, the structure (Figure 6-5 (a)) is simplified as a quarter of the structure (Figure 6-5 (b)) with applied surrounding support conditions. The column is modelled as 3-D beam elements and the slab is modelled as 3-D shell elements in SAFIR. The edge strips of the slab can be modelled as either 3-D shell elements (Figure 6-5 (c)) or 3-D beam elements (Figure 6-5 (d)). In general, the edge strips of the slab are modelled as 3-D shell elements. The structural model in which the edge strips of the slab are modelled as 3-D beam elements in SAFIR is not detailed in this thesis.

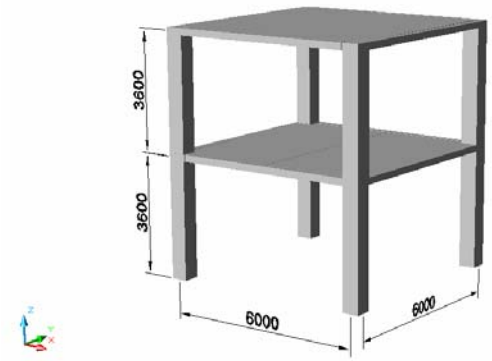

(a) The structure before the simplification

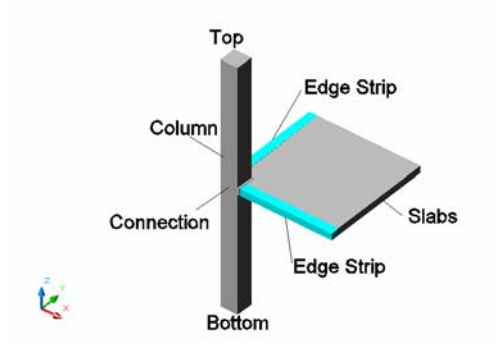

(b) The structure is simplified as a quarter of the structure

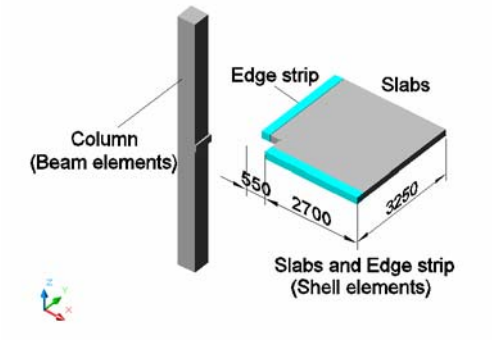

(c) The edge strips are modelled as 3-D shell elements

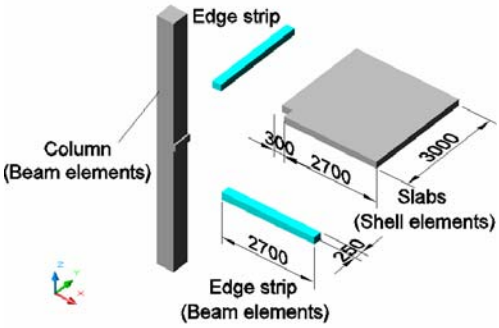

(d) The edge strips are modelled as 3-D beam elements

Figure 6-5 Simplifying and discretising of the structure

The columns are fixed on all the degrees of freedom (three degrees of movement, three degrees of rotations, and one degree of warping) at the end of the bottom level and fixed on the all the degrees of freedom except the vertical displacement at the end of the top level. The signs of the fixings on columns in SAFIR are shown in Figure 6-6. The warping degree of freedom in beam elements can not be displayed.

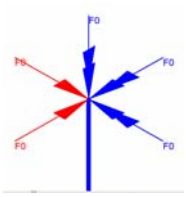

Fixings on the top of columns

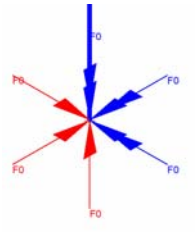

Fixings on the bottom of columns

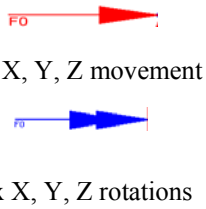

Symbol of fixings

Figure 6-6 Signs of the fixings on columns of the structure in SAFIR

Figure 6-7 shows the modelling of the connection among the column, slabs, and the edge strips of the slab. The modelling of the connection is fulfilled using the function of the master-slave relations of displacements in SAFIR; the displacements at the shell element nodes (node: 40, 52, 62, 63, 64) are assumed to be the same at the beam element node (node: 17). The advantages of this connection model are that the column keeps the same square shape throughout the simulation and the concentration of the internal stress in the slab at the connection can be reduced.

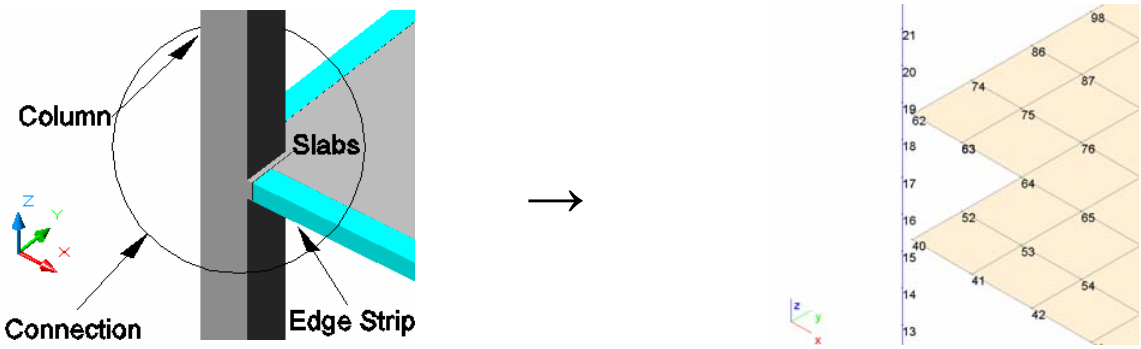

The connection in the real structure

The connection in the SAFIR model

Figure 6-7 Modelling of the connection among the column, slabs and edge strips of the slab

The non-linear analysis of structures in fires is a complicated procedure. There are no perfect computer structural models in the simulation. The results of the simulation of structures are sensitive to the structural models. The rotation of columns at connections may affect the accuracy of the simulation. When the rotation of columns at connections is small and the cross-section of columns is not too large, the results of the modelling using the master-slave relations in connection models are acceptable in the field of engineering. The concept of the effect of the rotation of columns at connections can be expressed as shown in Figure 6-8. The graph shows that the vertical displacements of the slab when considering the effect of rotation

of the column are slightly greater than when the effect is not considered. The discussion of the effect of the rotation of columns on the vertical deflections of the slab at ambient and fire conditions will be presented later in Section 6.3.4 and Section 6.4.4, respectively.

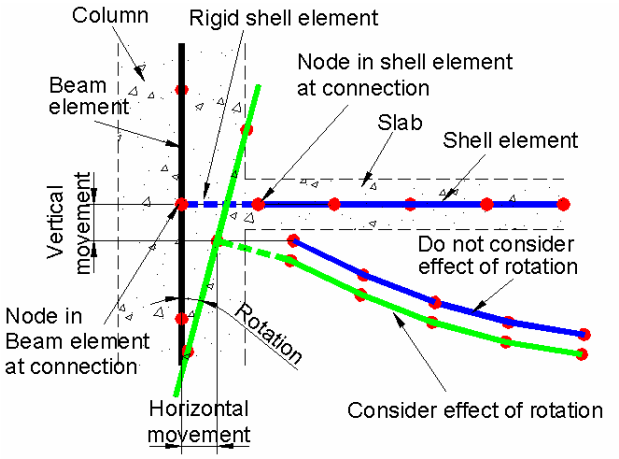

Figure 6-8 Concepts of the effect of the rotation of columns at connections

The SAFIR structural model of the one-way flat slab, which has 117 shell elements and 16 beam elements, is shown in Figure 6-9 (a). The applied surrounding support conditions are also shown in the graph. The cross-section of the column is shown in Figure 6-9 (b), where a quarter of the cross-section of the column is displayed because of the symmetry of the cross-section in two directions. The area of reinforcing bars (dark coloured squares in the Figure 6-9 (b)) can be adjusted in the input file, which has the expansion name of *.TEM* and in which the information about the cross-section of the column is stored. The reinforcing bars in the slab are modelled as a reinforcing sheet in SAFIR (Franssen et al., 2002a). The position of the reinforcing sheet is assumed to be 30 mm below the top of the slab for the top reinforcing bars in the two directions and 30 mm above the bottom of the slab for the bottom reinforcing bars in the two directions (Figure 6-9 (c)).

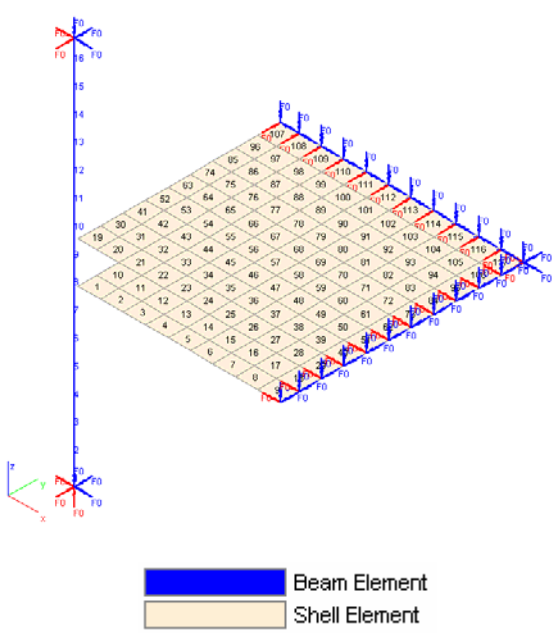

(a) Isometric view of the SAFIR model of the structure

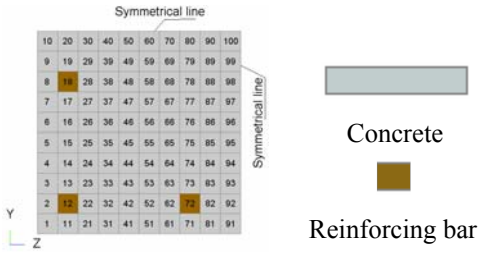

(b) A quarter of the column modelled in SAFIR (the cross-section)

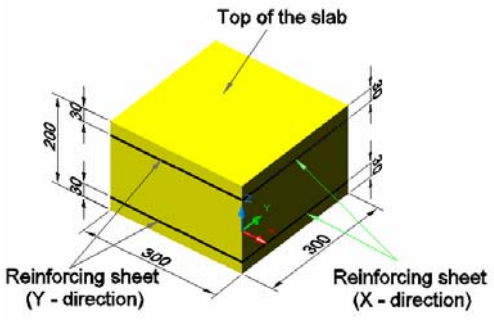

(c) The position of reinforcing bars in the slab

Figure 6-9 The SAFIR structural model of the one-bay flat slab with a column on the corner

6.2.3. Assumptions of the analysis

The assumptions of using shell elements and beam elements in SAFIR were detailed earlier in Chapter 3 of this thesis. In addition, some assumptions are also made during the simulation of one-bay flat slabs.

- The differences of the displacements of the nodes at the connection among the columns, slabs, and the edge strips of the slab are ignored due to the master-slave relations of the displacements of these nodes.
- Both the X-direction and Y-direction of the reinforcing bars on the top or bottom levels are in the same levels in the slab.
- The effect of the stirrups in columns and the edge strips of the slab are ignored.
- The fire exposure beneath the slab is uniform.
- The Shear failure of the slab is not considered in the analysis.
- The out-of-plane flexural stiffness of the slab is infinite.

6.2.4. Conventional signs of the one-bay flat slab

The top view of a quarter of the one-bay flat slab is shown in Figure 6-10. For conveniently describing the behaviour of the slab, four points, three strips and three sections are defined. The Point-B, Point-O and Point-C represent the three corners of the slab, while Point-A is the centroid of the column. Point-O is not only the midpoint of the one-bay flat slab but also the absolute coordinate zero point. Therefore, the coordinates for these points are (0, 0) for Point-O, (-3, -3) for Point-A, (0, -3.25) for Point-B, and (-3.25, 0) for Point-C. The strips, which are along the X-direction, are indicated by letters (i.e. Strip-A, Strip-B and Strip-C). The sections, which are along the Y-direction, are indicated by numbers (i.e. Section-1, Section-2 and Section-3).

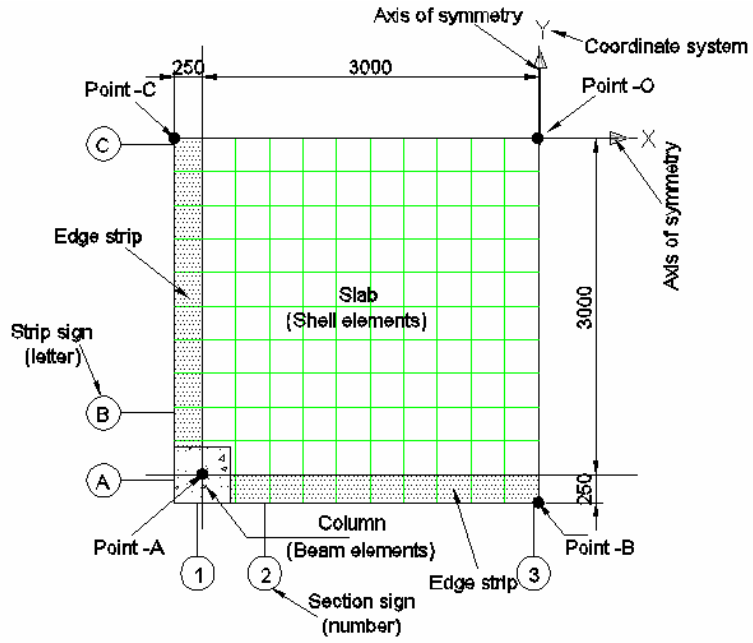

Figure 6-10 Conventional signs of the one-way flat slab

6.3. Behaviour of the One-Bay Flat Slab at Ambient Conditions

This section presents the behaviour of a one-bay flat slab at ambient temperature conditions. The purpose of the analysis is to assess the capability of SAFIR 3-D shell element models in predicting the ultimate load of one-way flat slabs at ambient conditions. The effect of the connection model at ambient conditions is also discussed. The uniformly distributed loads applied on the slab start at zero and increase until failure occurs.

6.3.1. Displacements of the one-bay flat slab

The vertical deflections at Point-O of the slab against the uniformly distributed loads, which ranged from 0.0kN/m^2 to 12.0kN/m^2, are plotted in Figure 6-11. It shows that when the load increased to 6.3kN/m^2, the vertical deflection reached 0.065m and when the load increased to 10.4kN/m^2 the vertical deflection linearly increased to 0.128m. The increase of the vertical deflections was proportional to the increase of the loads when the loads ranged from zero to 10.4kN/m^2. When the load exceeded 10.4kN/m^2, the vertical deflection at Point-O dramatically increased to 0.325 under the load of 10.9kN/m^2. The simulation was stopped when the load exceeded 10.9kN/m^2 because the slab became an unstable structural system and collapsed.

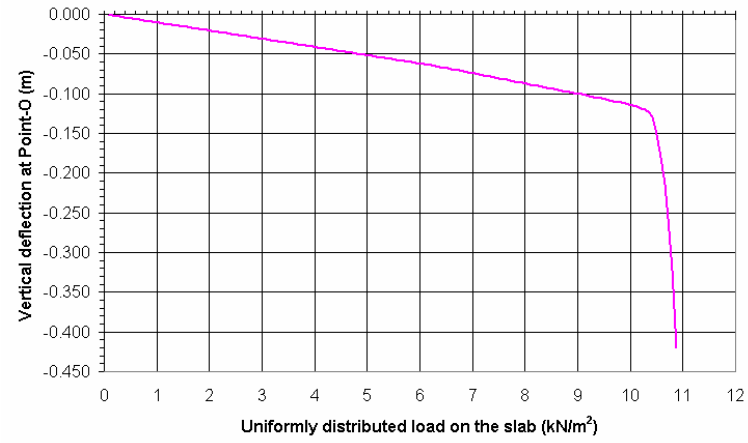

Figure 6-11 Vertical deflections of the slab at Point-O

The distributions of the vertical deflections of the slab at the loads of 6.3kN/m^2 and 10.4kN/m^2 are shown in Figure 6-12. The graphs show that the largest vertical deflection was in the midpoint (Point-O) of the slab.

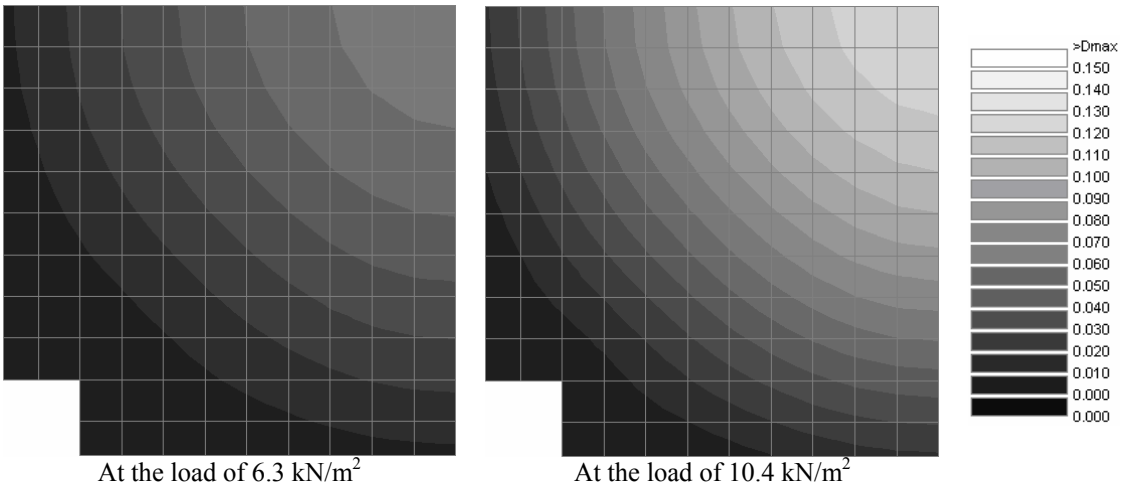

At the load of 6.3 kN/m^2 At the load of 10.4 kN/m^2

Figure 6-12 Distributions of the vertical deflections of the slab at loads of 6.3 and 10.4kN/m^2

Figure 6-13 shows the patterns of the horizontal displacements of the slab at loads of 6.3kN/m^2 and 10.4kN/m^2. The graphs show that the edge of the slab moved towards the central parts of the slab because of the effect of the large vertical deflections of the slab under the increased loads. Using the connection model (the effect of the rotation of columns on the vertical deflections of the slab is not considered), as shown earlier in Figure 6-7, the shape of the column at the corner of the slab remained a square shape throughout the simulation.

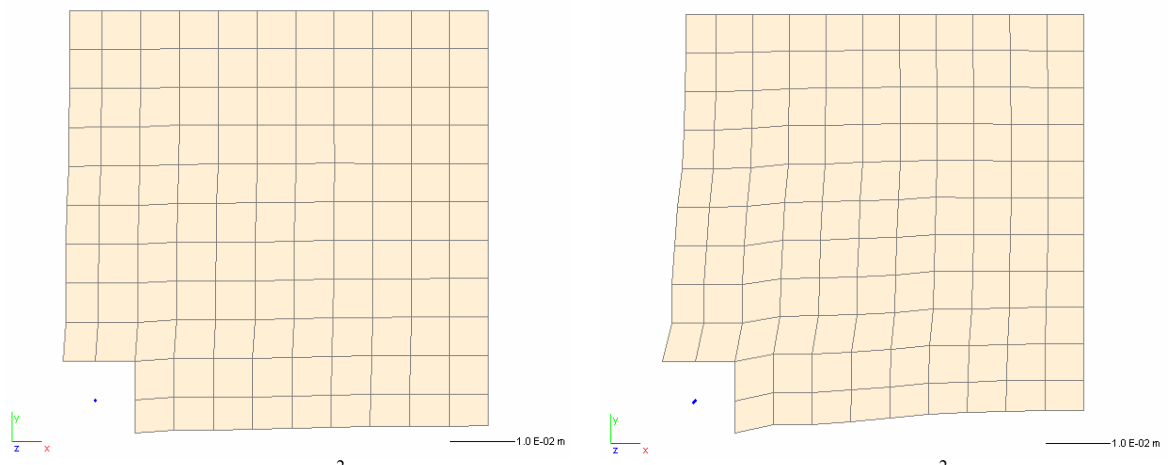

At loads of 6.3kN/m^2 (scale:10) At loads of 10.4kN/m^2 (scale:10)

Figure 6-13 Horizontal displacements of the slab

6.3.2. X-direction bending moments in the slab

Because of the symmetry of the structure to the two-directions, the X-direction and Y-direction, only X-direction bending moments are discussed.

The distribution of X-direction average bending moments and the total bending moments in the slab along Section-3 are shown in Figure 6-14 (a) and Figure 6-14 (b), respectively. The hogging moments are positive and the sagging moments are negative in the graphs. Figure 6-14 (a) shows that the bending moments in the edge strip of the slab were greater than in the middle parts of the slab due to the effect of the magnitude of reinforcing bars in the edge strip of the slab and the effect of the restraints of the columns on the strips of the slab between the columns. The bending moments in the middle parts of the slab almost constantly distributed along Secion-3. Figure 6-14 (b) shows that the total bending moments in Section-3 increased in direct ratio with the applied loads on the slab. When the uniformly distributed load on the slab increased to 10.4kN/m^2, the total bending moment along Section-3 reached -70kN-m.

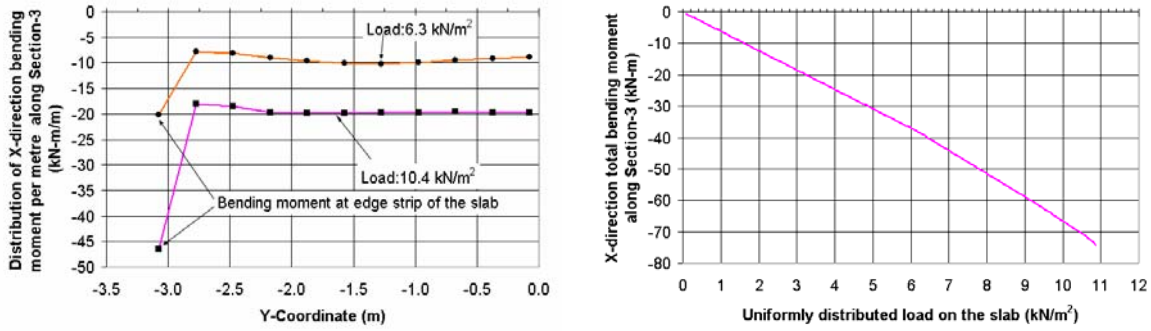

(a) Distribution of X-direction bending moments along Section-3

(b) X-direction total bending moments along Section-3

Figure 6-14 X-direction bending moments along Section-3

The distributions of X-direction bending moments at the loads of 6.3kN/m^2 and 10.4kN/m^2 are shown in Figure 6-15. The graphs show that the hogging moments were in the region close to the column and sagging moments were in the region close to the midspan of the slab.

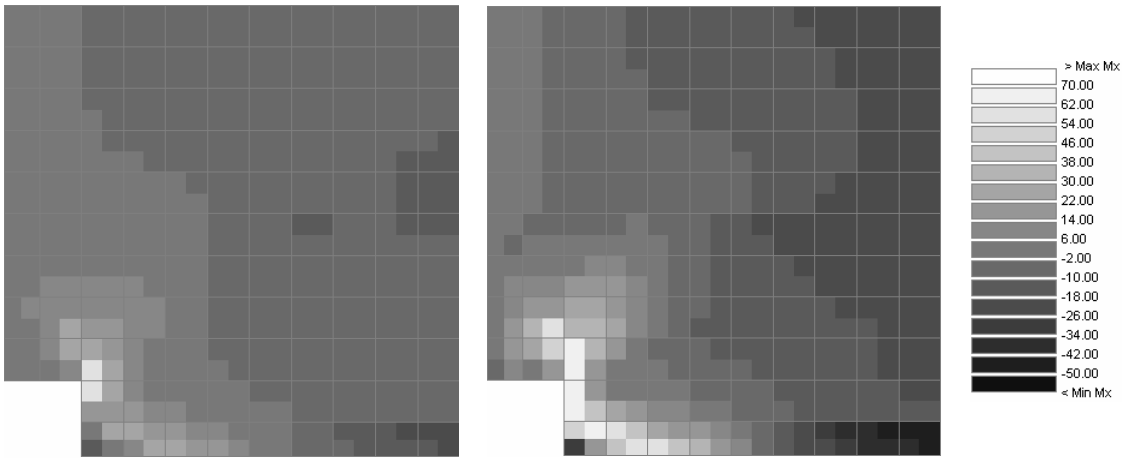

At the load of 6.3 kN/m^2 At the load of 10.4 kN/m^2

Figure 6-15 Distributions of X-direction bending moments in the slab

Because the large magnitude of X-direction bending moments was mainly present in the edge strips of the slab, increasing the flexural stiffness of the edge strips could significantly improve the load carrying capacity of the slab.

6.3.3. X-direction membrane forces in the slab

The distribution of X-direction membrane forces along Section-3 and the average value of the membrane forces in the part of Section-3 are shown in Figure 6-16 (a) and Figure 6-16 (b), respectively. The X-direction average membrane forces along the part of Section-3 do not include the membrane forces in the edge strip and the shell elements adjacent to the edge strip. The X-direction membrane forces were mainly present in the strips of the slab between the columns. The compressive membrane forces were present in the edge strip of the slab, while the tensile membrane forces were present in the shell elements adjacent to the edge strip. The membrane forces in the middle parts of the slab were almost zero.

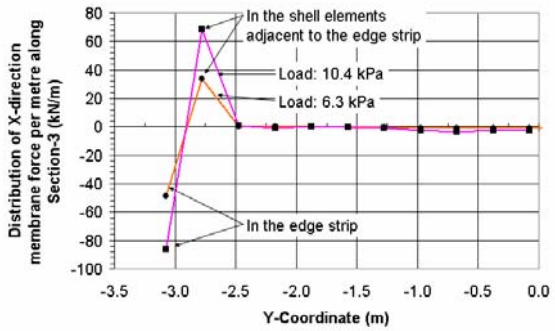

(a) Distribution of X-direction membrane forces along Section-3

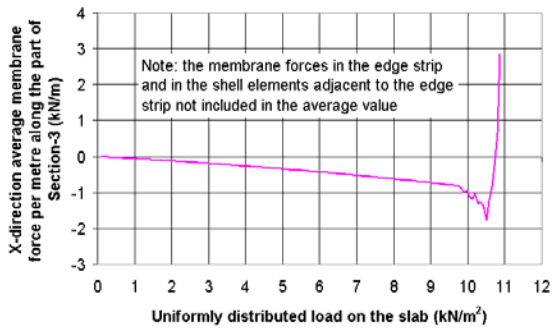

(b) X-direction average membrane forces along the part of Section-3

Figure 6-16 X-direction membrane forces along Section-3

The membrane forces in the edge strip and in the shell elements adjacent to the edge strip of the slab along Section-3 are plotted in Figure 6-17. It shows that the membrane forces in the edge strip of the slab were compressive forces, while they were tensile forces in the shell elements adjacent to the edge strip. The membrane forces increased in direct ratio with the applied loads on the slab before the load of 10.4kN/m^2 (the ultimate load listed earlier in Table 6-2). When the loads exceeded 10.4kN/m^2, the membrane forces dramatically increased and the simulation was stopped when the applied load on the slab reached 10.9kN/m^2.

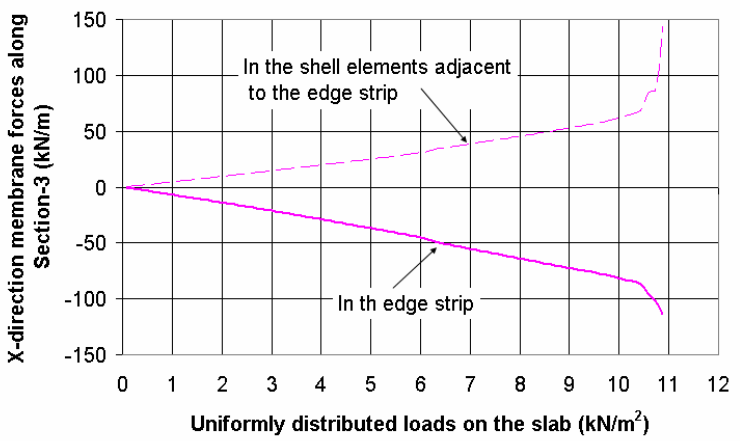

Figure 6-17 Membrane forces in the edge strip and the shell elements adjacent to the edge strip

The distributions of X-direction membrane forces in the slab under the loads of 6.3kN/m^2 and 10.4kN/m^2 are shown in Figure 6-18. It shows that the membrane forces were mainly present in the strips of the slab between the columns and in the central parts of the quarter slab.

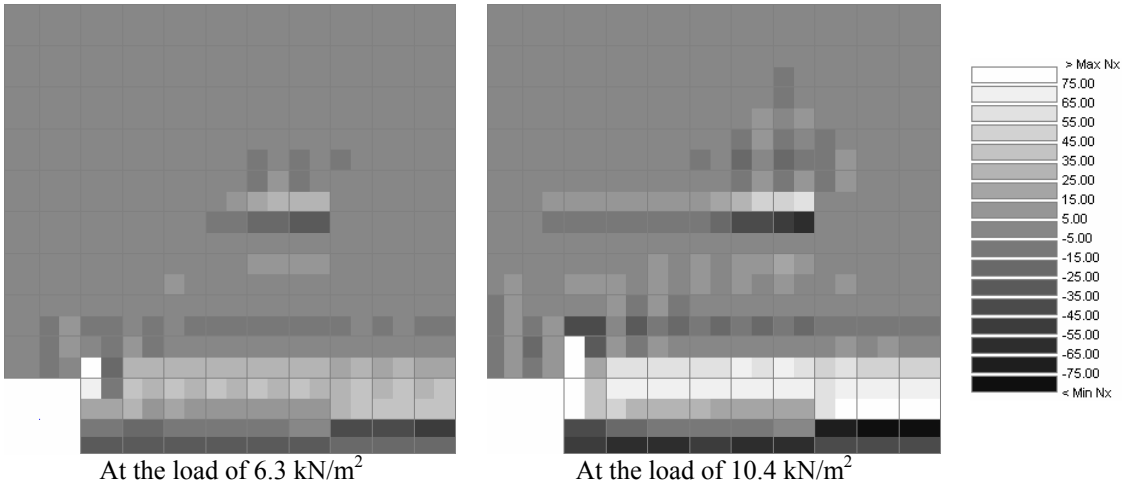

Figure 6-18 Distributions of X-direction membrane forces in the slab

6.3.4. The effect of connection models at ambient conditions

Section 6.2.2 briefly introduced the connection model using the function of the master-slave relations of the nodes among the column, slabs, and the edge strips of the slab. This connection model was used in the analysis of one-bay flat slabs at ambient conditions before and will be used in the analysis of the slabs in fire conditions in the later sections of this chapter. This section investigates the effect of connection models on the results of the modelling by comparing the connection model with a connection model in which the rotation of columns is considered. For simplifying the description, the connection model that takes into consideration of the effect of the rotation of columns on the vertical deflections of the slab is called the ***inclusive connection model***, while the connection model that ignores the effect of the rotation of columns is called the ***exclusive connection model***.

The connection model by considering the effect of the rotation of columns

Figure 6-19 shows the connection model among the column, slabs, and the edge strips of the slab by considering the effect of the rotation of columns on the vertical deflections of the slab (the inclusive connection model). The column is modelled as beam elements, which directly connect with four shell elements at Point-A (node: 57). The shell elements connected to the beam elements have large flexural stiffness of structural members, EI (100 times of the flexural stiffness of the slab at other parts) and they are called ***rigid shell elements***. Therefore, the rotations within the rigid shell elements are very small compared with the other shell elements. The vertical deflections of the slab are affected by the rotation of columns, as shown earlier in Figure 6-8. The other parameters of the structural model are the same as those described earlier in Section 6.1 and Section 6.2.

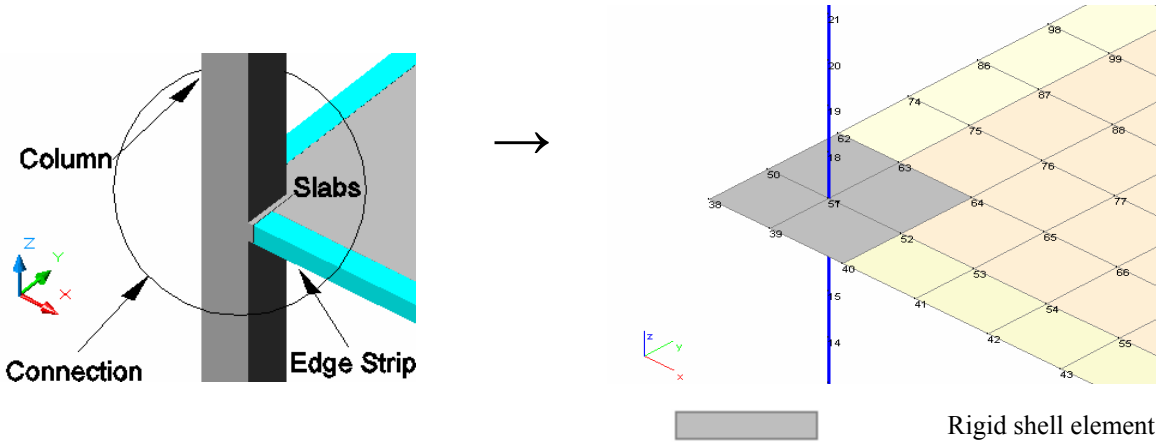

The connection of the structure — The connection of the SAFIR model

Figure 6-19 Modelling of the connection by considering the effect of the rotation of columns

Vertical deflections of the slab

A comparison of the vertical deflections at Point-O between the two connection models is plotted in Figure 6-20. It shows that the vertical deflections using the inclusive connection model were greater than the deflections using the exclusive connection model. When the uniformly distributed loads on the slab reached 9.6kN/m^2, the slab collapsed using the inclusive connection model because the vertical deflection at Point-O reached a dramatically large value. The trend of the increase of vertical deflections was similar when using these two different kinds of connection models.

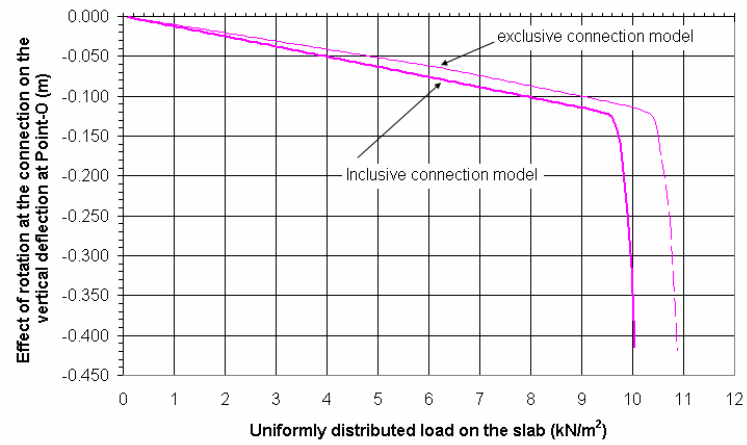

Figure 6-20 Comparison of the vertical deflections at Point-O

Figure 6-21 shows the patterns of the horizontal displacements of the slab at the loads of 6.3kN/m^2 and 9.6kN/m^2 when using the inclusive connection model. The graphs show that the shape of the shell elements at the connection greatly changed when the applied loads on the slab reached 9.6kN/m^2. One of the disadvantages of the inclusive connection model was that the shape of the column did not remain a square throughout the simulation. This means the horizontal displacements of the slab at the connection were overestimated. As a result, the vertical deflections of the slab were overestimated (the value of the vertical deflection was larger than the actual value).

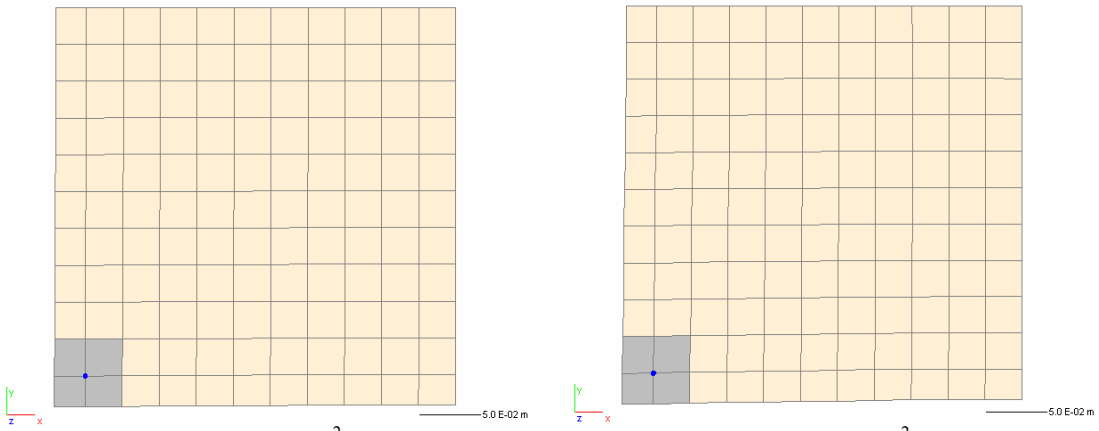

At the load of 6.3 kN/m^2 (scale:10) At the load of 9.6 kN/m^2 (scale:10)

Figure 6-21 Horizontal displacements of the slab by considering the effect of the rotation of columns

Bending moments of the slab

Figure 6-22 shows a comparison of X-direction average bending moments along Section-3 (the midspan of the slab) between the two connection models. The graph shows that the X-direction bending moments in the midspan using the inclusive connection model were larger than that using the exclusive connection model. The trend of the increase of bending moments was similar between the two connection models.

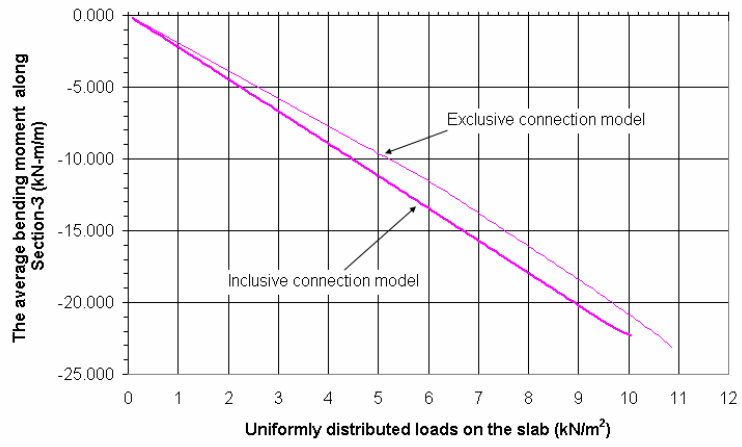

Figure 6-22 Comparison of X-direction average bending moments along Secion-3

Figure 6-23 shows X-direction bending moments along a part of Strip-A. The shaded region in the graph represents the shell elements in the region of the connection. The unbalanced bending moments of the slab in the region of the connection were significantly greater than in the other parts of the slab. The unbalanced bending moments will enlarge the rotation of columns at the connection. The disadvantage of the inclusive connection model was that the

rotation of columns at the connection was overestimated, so the vertical deflections of the slab were overestimated.

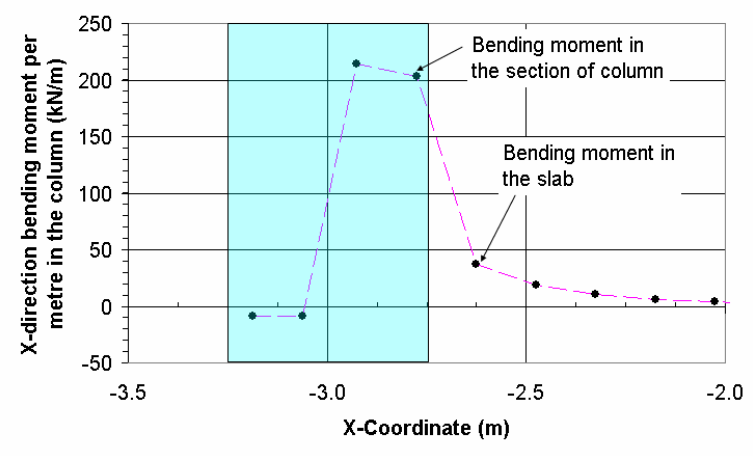

Figure 6-23 Bending moments in the slab at the connection using the inclusive connection model

A comparison of the deflected shape of columns at the connection between the two connection models is shown in Figure 6-24. It is evident that the rotation of columns at the connection using the inclusive connection model was greater than that using the exclusive connection model. In other words, the bending moments and the vertical deflections of the slab were slightly underestimated using the exclusive connection model. When the applied loads on the slab were less than 6.3kN/m^2, the effect of the connection models on bending moments and vertical deflections was small.

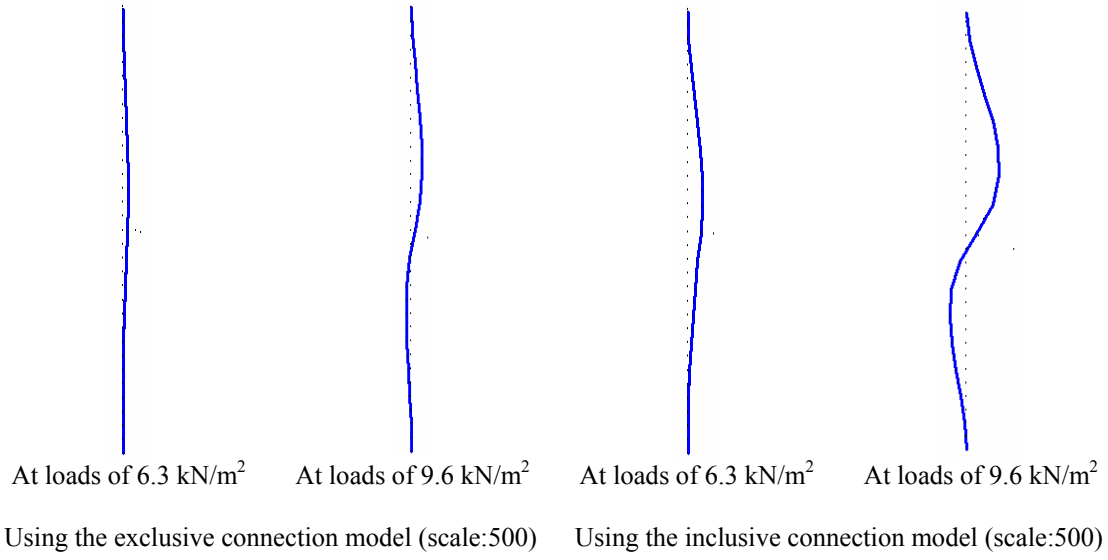

Figure 6-24 Comparison of the deflected shape of columns at the connection

Membrane forces of the slab

Figure 6-25 (a) shows a comparison of the X-direction membrane forces in the edge strip of the slab and the shell elements adjacent to the edge strip between the two connection models. The graph shows that compressive membrane forces were present in the edge strip of the slab and tensile membrane forces were present in the shell elements adjacent to the edge strip. The trend of the increase of membrane forces was similar between the two connection models. Figure 6-25 (b) shows a comparison of the X-direction average membrane forces along the part of Secion-3 between the two connection models. The membrane forces in the edge strip of the slab and the shell elements adjacent to the edge strip were not included in the X-direction average membrane forces. The graph shows that the trend of the increase of the average membrane forces between the two connection models was completely the same when the applied loads on the slab were less than 9.0kN/m^2.

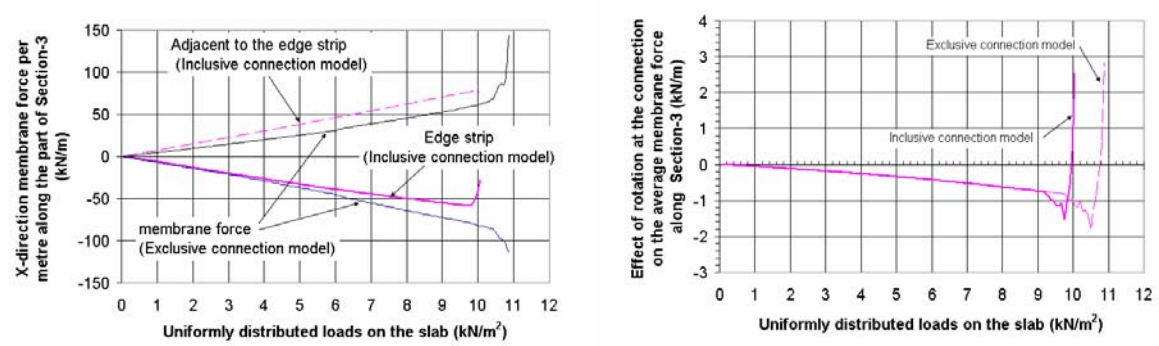

(a) X-direction membrane forces in the edge strip and the shell elements adjacent to the edge strip along Section-3

(b) X-direction average membrane forces along the part of Section-3

Figure 6-25 Comparison of the membrane forces in Section-3

Figure 6-26 shows the distributions of X-direction membrane forces in the slab using the inclusive connection model. Comparing with the graph shown earlier in Figure 6-18, it is evident that the patterns of the distributions of membrane forces were similar between the two connection models. Therefore, the connection models did not significantly affect the distributions of the membrane forces in the slab.

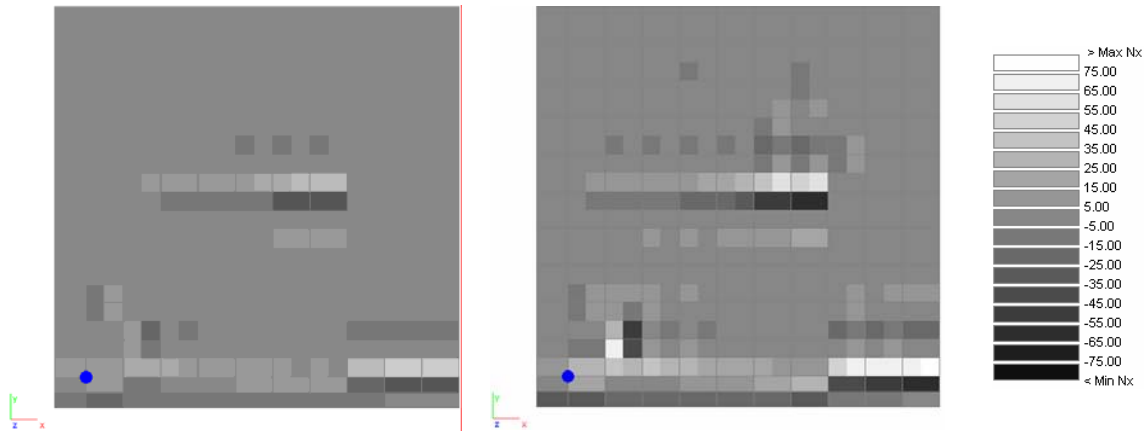

At the load of 6.3 kN/m^2 At the load of 9.6 kN/m^2

Figure 6-26 Distributions of X-direction membrane forces in the slab using the inclusive connection model

6.3.5. Conclusions

The analyses of the one-bay flat slab at ambient temperature conditions have found that:

- SAFIR can predict the ultimate load on flat slabs at ambient conditions using a suitable structural model.
- The membrane forces are mainly present in the strips of the slab between the columns.
- The results of the modelling are sensitive to the connection model. Connection models in SAFIR affect the magnitudes of the displacements, bending moments and membrane forces of the slab.

6.4. Behaviour of the One-Bay Flat Slab in Fire without a Decay phase

This section of the chapter presents the modelling of a one-bay flat slab exposed to an ISO 834 Standard fire without a decay phase beneath. The purpose of the analysis is to investigate the effect of the restraints of columns on the behaviour of flat slabs without edge beams under the fire without a decay phase. The displacements, the bending moments and the membrane forces of the one-bay flat slab are investigated. The effect of the connection model in fire conditions is also discussed.

6.4.1. Displacements of the slab in fire conditions

Figure 6-27 shows the vertical deflections of the slab at Point-O under an ISO 834 Standard fire without a decay phase. The graph shows that the vertical deflection linearly increased from 0.07m at 1 minute to 0.6m at 150 minutes and then dramatically increased to 1.12m at 180 minutes because the yield strength of the bottom reinforcing bars was reduced to a lower value at high temperatures. The temperature of the bottom reinforcing bars was 650^{o}C at 150 minutes and 775^{o}C at 180 minutes, as shown earlier in Figure 6-4 (a). The vertical deflection at Point-O slightly increased to 1.17m at the end of the simulation because the slab deformed to a catenary, which hung on the corner columns. Because the large vertical deflections were present in the slab, the slab experienced failure at 150 minutes, but did not drop to the ground floor due to the effect of the restraints of columns on the strips of the slab between the columns. The temperature of the top reinforcing bars was 80^{o}C at 150 minutes and 136^{o}C at 240 minutes, as shown earlier in Figure 6-4 (b). The yield strength of the top reinforcing bars did not decrease throughout the simulation. The temperature of the top reinforcing bars remained a lower value and this supported the development of the membrane forces in the slab and prevented the collapse of the slab in fire conditions.

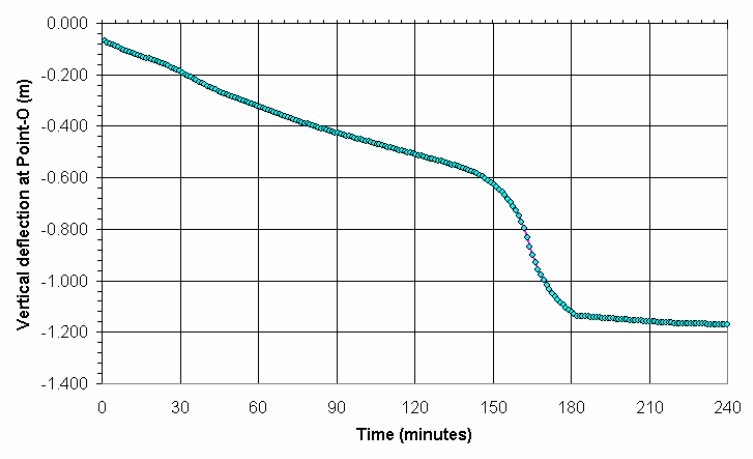

Figure 6-27 Vertical deflections of the slab at Point-O under fire exposure

After four hour's fire exposure the presence of the slab between the two levels of the building prevented the fire spreading to the upper floors. However, the reinforced concrete flat slab was unrepairable due to the large vertical deflection and the reduction of the load capacities.

The patterns of the distributions of vertical deflections at 1, 33, 60, 120, 150, and 180 minutes are shown in Figure 6-28. The white colour in the graphs represents the vertical deflections are greater than 0.2m. The largest value of vertical deflections was in the midpoint of the slab (Point-O) and the smallest value of vertical deflections was around the column.

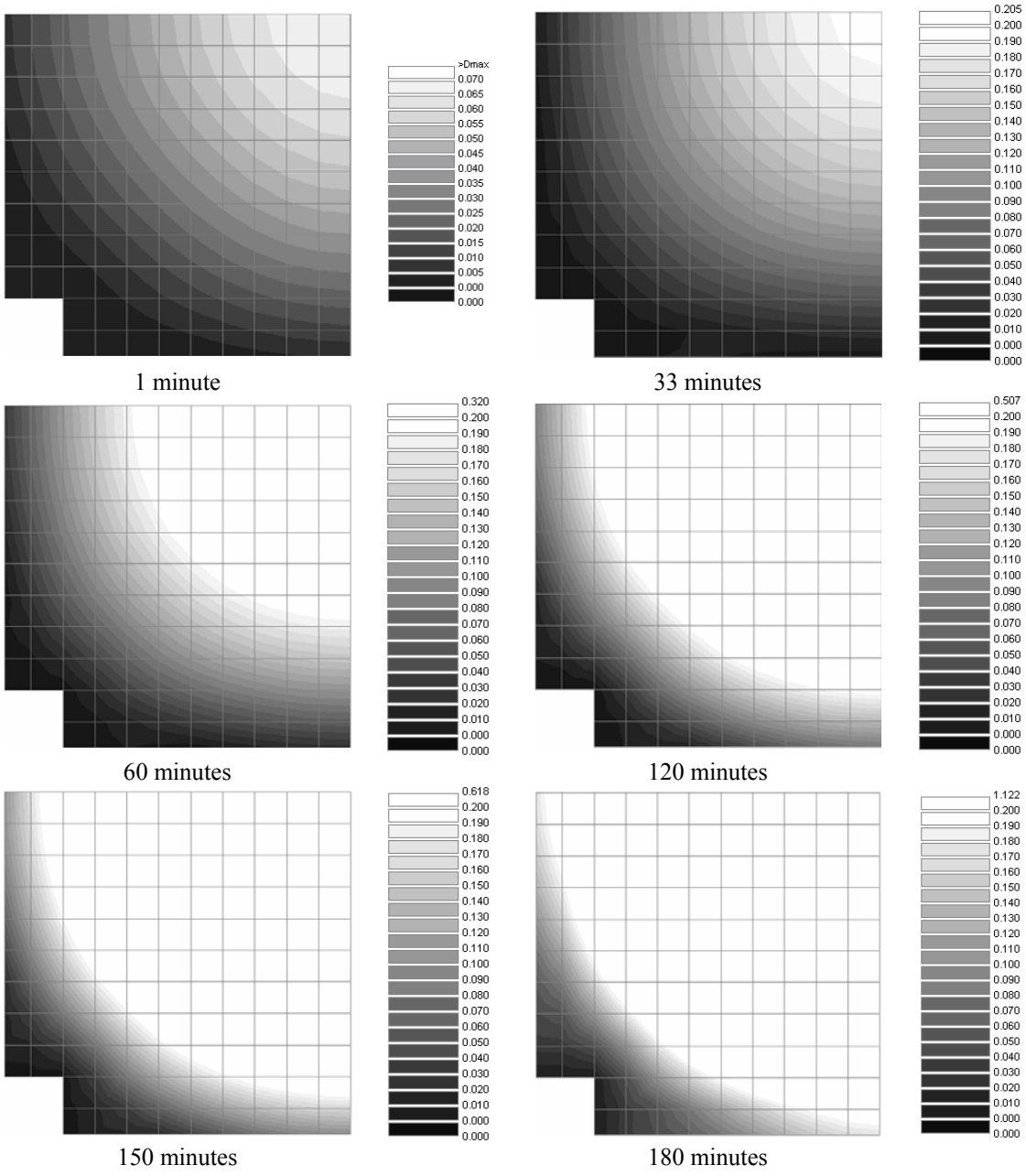

Figure 6-28 Distributions of the vertical deflections of the slab under fire exposure

The vertical deflections of the slab along Strip-A and Strip-C are shown in Figure 6-29 (a) and Figure 6-29 (b), respectively. These graphs show that the larger value of vertical deflections was at the midspan and the smaller value was at the edge of the slab because the restraints of columns reduced the development of vertical deflections along Strip-A.

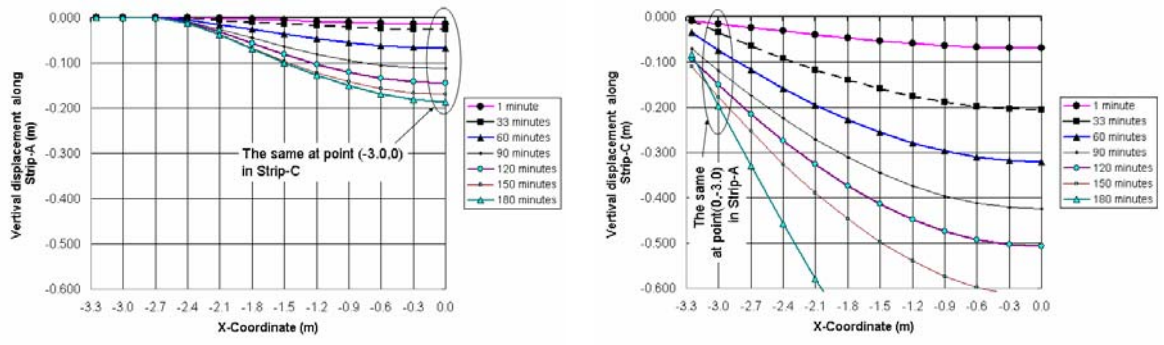

(a) Vertical deflections along Strip-A (b) Vertical deflections along Strip-C

Figure 6-29 Vertical deflections along Strip-A and Strip-C

The horizontal movements of the slab in the Y-direction along the edge of the slab are shown in Figure 6-30. The Y-direction displacement at Point-A equals the displacement at point (-2.7, -3.25) due to the master-slave relations between these points. The negative value in the graph indicates that the column moves away from the slab, and the positive value indicates the opposite. The displacement at Point-A was less than at Point-B due to effect of the restraints of columns on the strips of the slab between the columns. The displacement at Point-A (the centroid of the column) remained negative from 1 minute to 100 minutes and at 33 minutes the maximum negative value of 0.0025m was reached because the thermal expansion of the slab in the strips between the columns pushed the columns away from the slab. After 100 minutes, the Y-direction displacements of the edges of the slab changed to positive values due to the increasing mid-span vertical deflections. The tensile membrane forces in the strips of the slab between the columns pulled the columns towards the slab. At Point-B, the Y-direction displacement of the slab remained positive throughout the simulation because significant membrane forces did not develop in the midspan of the slab.

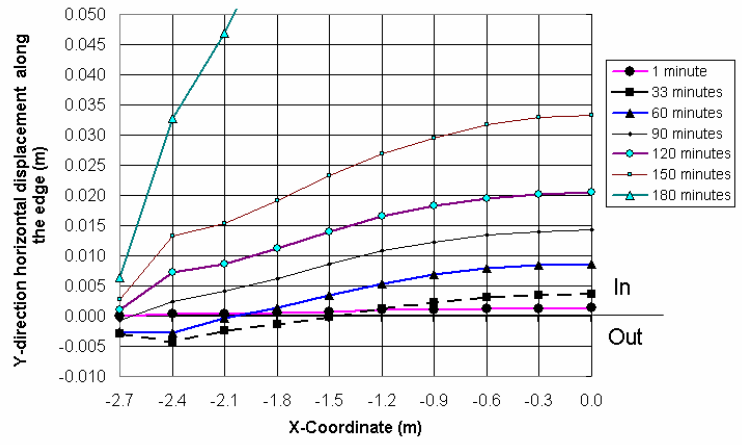

Figure 6-30 Horizontal movements of the slab in the Y-direction along the edge of the slab

Figure 6-31 shows the deflected shapes of columns at 1, 33, 60, 100, 120, and 180 minutes. The graphs show that the rotation of columns at the connection was very small because the flexile stiffness of columns was greater than the stiffness of the slab under fire exposure.

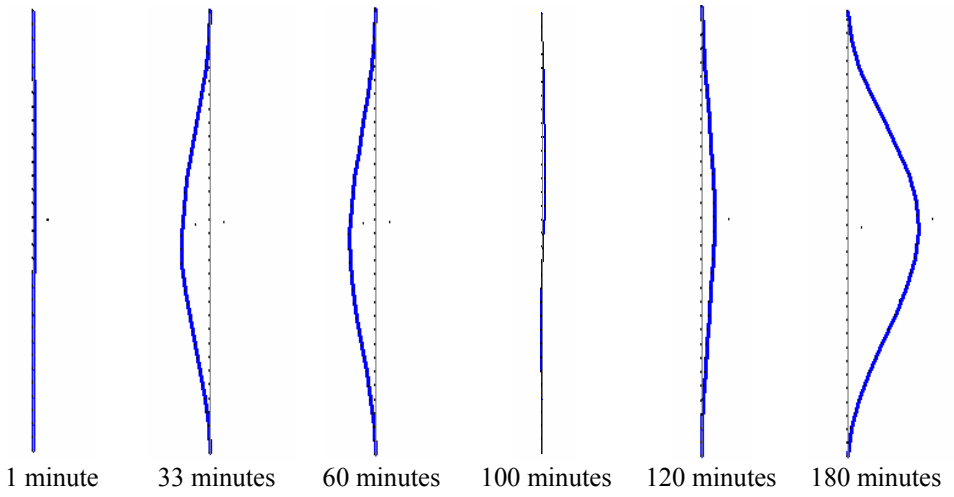

Figure 6-31 Deflected shapes of columns under fire exposure (scale: 250)

6.4.2. Bending moments of the slab in fire conditions

The distribution of X-direction bending moments along Section-3 is shown in Figure 6-32 (a). It shows that the redistribution of bending moments was present in the edge strip of the slab due to the effect of the restraints of columns to the strips of the slab between the columns. The bending moments in the edge strip and in the slab near Point-O against the time are plotted in Figure 6-32 (b). It shows that the bending moments near Point-O were sagging moments, while in the edge strip of the slab the bending moments were changeable. The bending moment near Point-O almost remained a constant value of -13kN-m/m until 150 minutes, and then declined to -6kN-m/m at 180 minutes; after that, it formed a plateau until the end of the simulation. The bending moment in the edge strip of the slab declined to zero at 10 minutes from a negative value of -20kN-m/m at 1 minute, and then increased to a positive value of 30kN-m/m at 33 minutes; after that, it declined to zero again at 150 minutes. From 150 minutes to 180 minutes the bending moment dramatically increased from zero to 24kN-m/m and slightly declined to 20kN-m/m at 240 minutes.

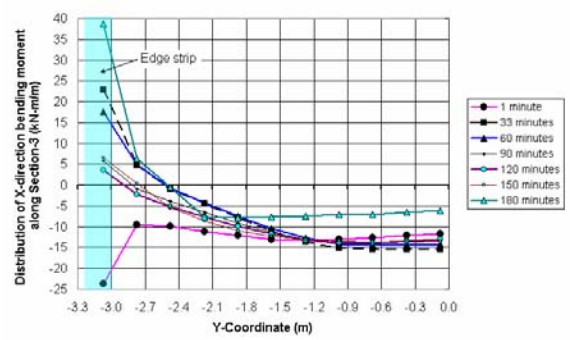

(a) Distribution of X-direction bending moments along Section-3

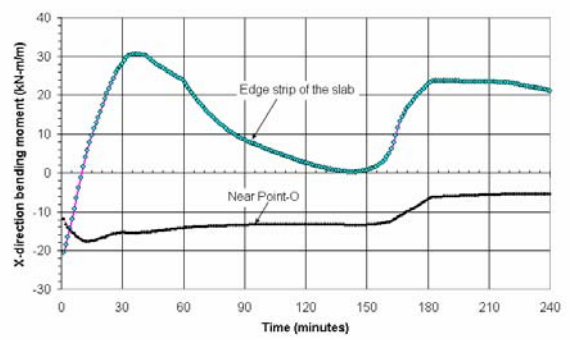

(b) X-direction bending moments near Point-O and in the edge strip of the slab along Section-3

Figure 6-32 Distribution of X-direction bending moments along Section-3

Figure 6-33 shows the X-direction bending moments along Strip-A and Strip-C. The redistribution of bending moments was present along Strip-A. In the first stage of the fire exposure, the thermal expansion on the bottom of the slab was greater than on the top of the slab and this made the curvatures of bending moments move up; as results, the positive bending moments increased and the negative bending moments decreased. When the strengths of concrete and steel decreased at higher temperatures, the bending moment curvatures moved down. The redistribution of bending moments along Strip-C did not obviously occur because of the lack of restraints to the slab in the midspan of the slab.

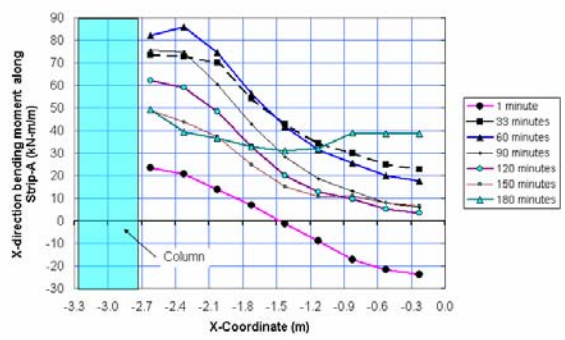

(a) Bending moments along Strip-A

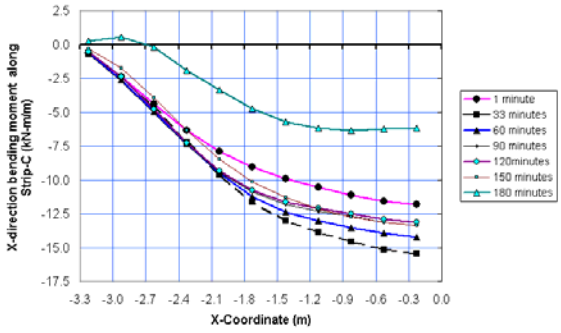

(b) Bending moments along Strip-C

Figure 6-33 X-direction bending moments along Strip-A and Strip-C

The patterns of the distributions of X-direction bending moments at 1, 33, 60, 120, 150, and 180 minutes are shown in Figure 6-34. It shows that the positive bending moments distributed along the edge strip of the slab and along Point-A to Point-O (the diagonal of the flat slab). At 33 minutes the positive bending moments of the slab reached the peak values in the region around the column.

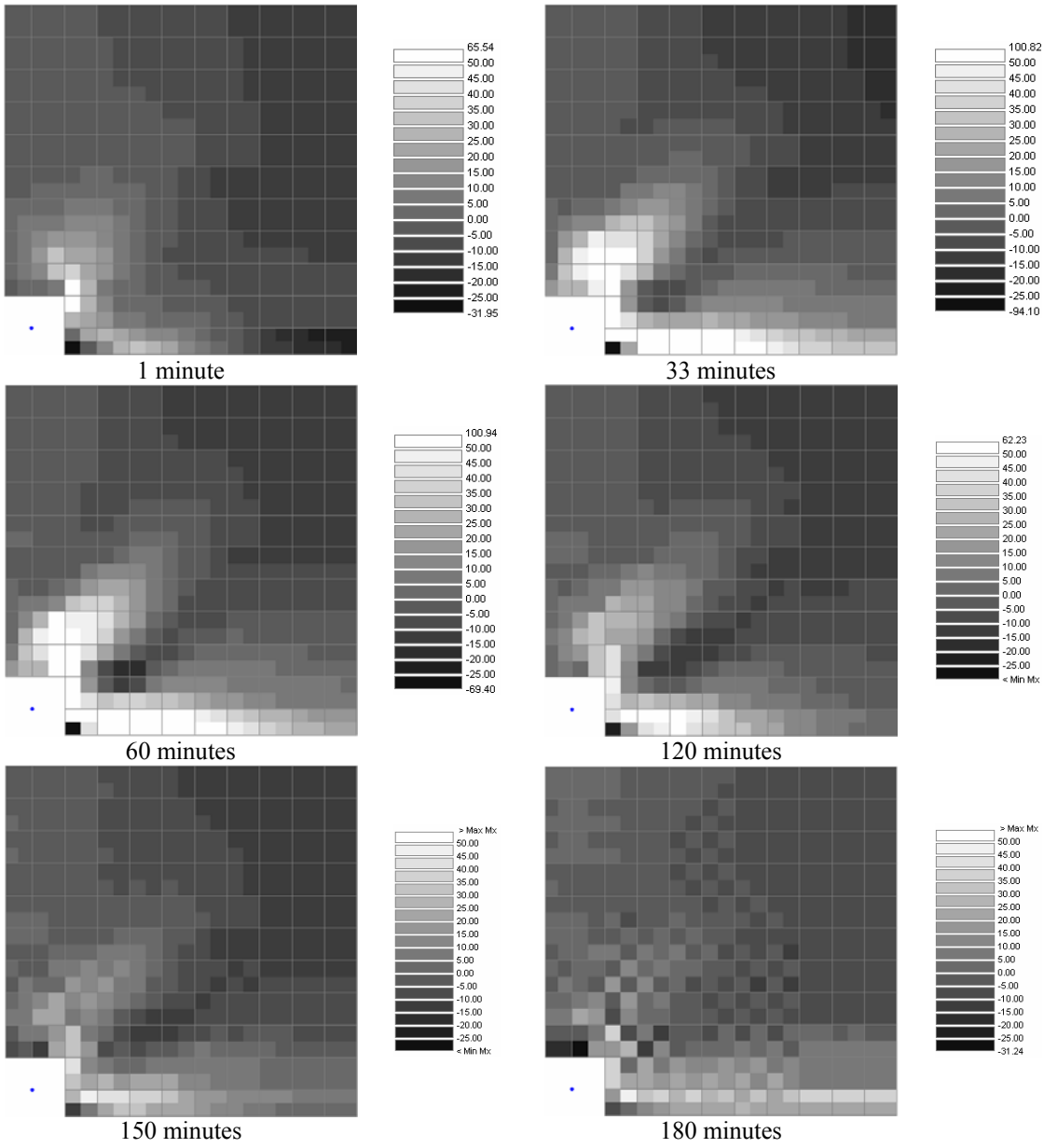

Figure 6-34 Distributions of X-direction bending moments in the slab

The redistribution of bending moments was mainly present in the edge strips of the slab. If the edge strips of the slab are designed to be beams of which flexural stiffness is significantly greater than the slab's, the performance of the slab in fire exposure will be improved. For increasing the fire resistant of slabs, one-bay flat slabs without edge beams are not recommended to be built.

6.4.3. Membrane forces of the slab in fire conditions

The distribution of X-direction membrane forces along Section-3 and the average value of the membrane forces along a part of Section-3 are shown in Figure 6-35 (a) and Figure 6-35 (b), respectively. The average value of the membrane forces along a part of Section-3 did not include the membrane forces in the edge strip and the shell elements adjacent to the edge strip. Figure 6-35 (a) shows that the membrane forces were mainly present in the strips of the slab between the columns. In the middle parts of the slab the membrane forces remained at very small values. Figure 6-35 (b) shows that in the middle parts of the slab the average value of the membrane forces significantly increased from zero at 150 minutes to 15kN/m at 180 minutes and slightly increase to 16kN/m at the end of the simulation.

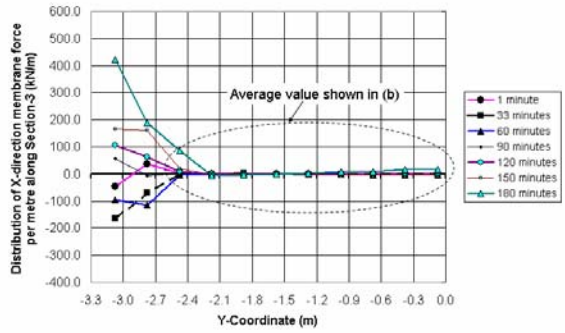

(a) Distribution of X-direction membrane forces along Section-3

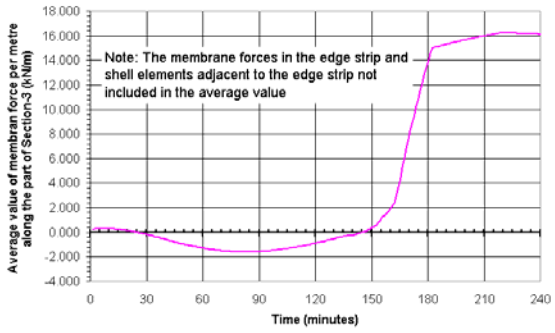

(b) X-direction average membrane forces along a part of Section-3

Figure 6-35 X-direction membrane forces along Section-3

Figure 6-36 shows the X-direction membrane forces in the edge strip of the slab against the time at Section-2 and Section-3. The graph shows that the trends of the development of membrane forces at Section-2 and Section-3 were similar, but the magnitudes of membrane forces were different. At Section-2 in the edge strip, which was close to the column, the compressive membrane forces increased from zero at 1 minute to -300kN/m at 33 minutes, and then declined to zero again at 80 minutes; after that, the tensile membrane forces developed and at 160 minutes they reached 300kN/m. The tensile membrane forces dramatically increased 230kN/m for 20 minutes and reached 530kN/m at 180 minutes. The tensile membrane force almost remained constant from 180 minutes until the end of the simulation. At Section-3 in the edge strip, which was in the midspan of the slab, the compressive membrane forces increased from -40kN/m at 1 minute to -160kN/m at 33 minutes, and then declined to zero at 80 minutes; after that, the tensile membrane forces

developed and at 160 minutes they reached 180kN/m. The tensile membrane forces dramatically increased 270kN/m for 20 minutes and reached 450kN/m at 180 minutes. The tensile membrane force almost remained constant from 180 minutes until the end of the simulation.

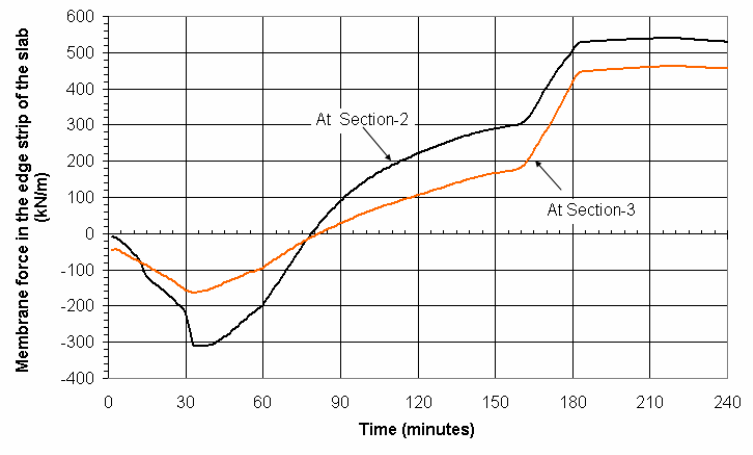

Figure 6-36 X-direction membrane forces in the edge strip of the slab

The patterns of X-direction membrane forces in the slab at 1, 33, 60, 120, 150, and 180 minutes are shown in Figure 6-37. It shows that the membrane forces were mainly present in the strips of the slab between the columns when the slab was exposed to the fire from beneath.

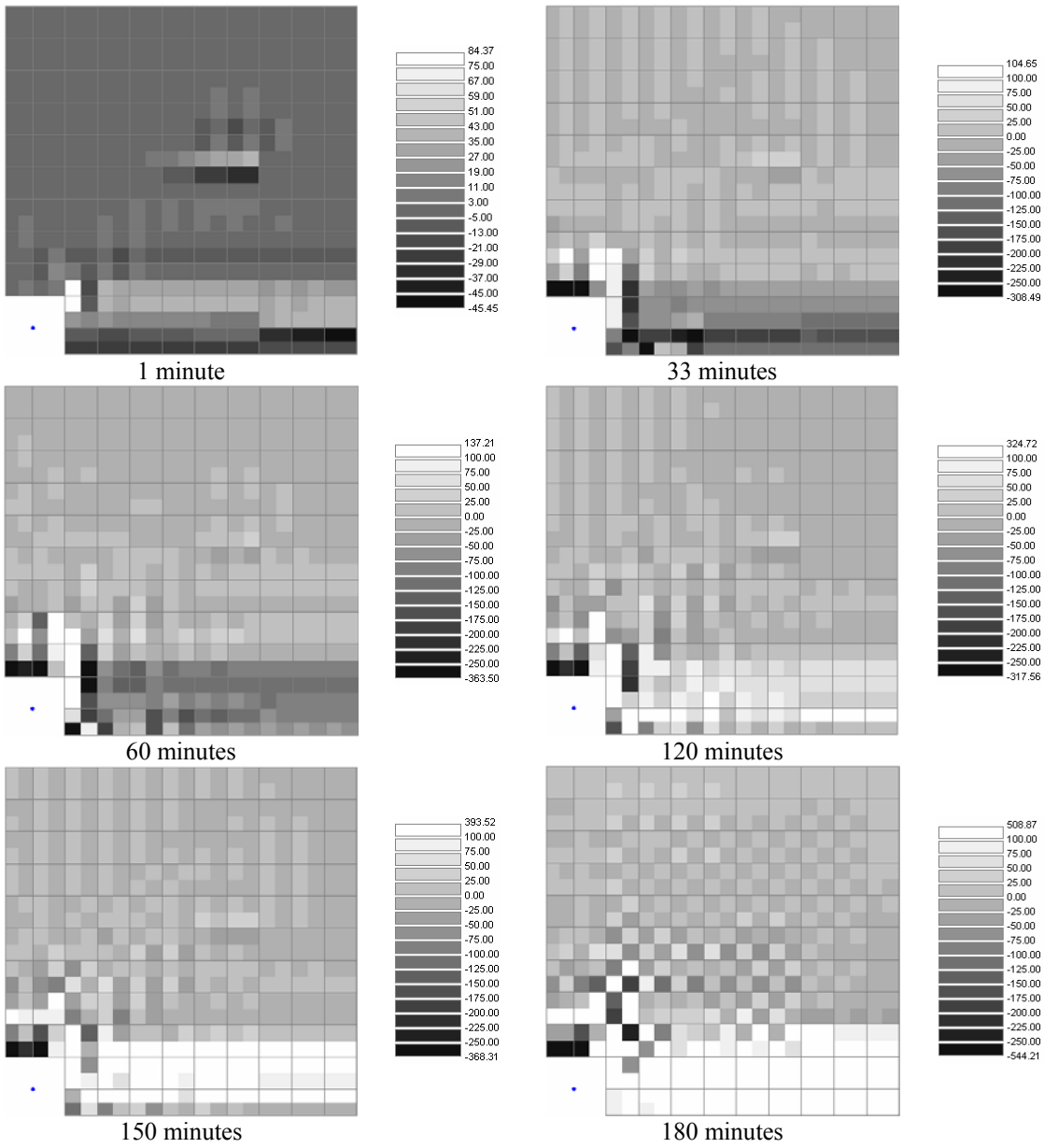

Figure 6-37 Distributions of membrane forces in the slab

When designing a reinforced concrete flat slab without edge beams, special care should be taken in the strips of the slab between the columns. The reinforcing bars on the top and bottom levels of the slab should be continuously arranged in the strips of the slab between the columns and the bars should be anchored in the columns with sufficient lengths. Because of the lack of benefit of continuity and restraint to one-bay flat slabs without edge beams in fire conditions, the performance of one-bay flat slabs in fire exposure is worse than the performance of two-way slabs, which have beams surrounding the edges of the slabs. For simplifying the design of slabs and increasing the fire resistance of slabs, flat slabs should be designed with edge beams.

6.4.4. The effect of the connection model in fire conditions

In this section the effect of the connection model on the results of the analysis of the slab exposed to an ISO 834 Standard fire without a decay phase is discussed. The purpose of this section is to investigate how the connection models in SAFIR affect the behaviour of flat slabs under the fire exposure. The inclusive connection model shown earlier in Figure 6-20 was introduced earlier in Section 6.3.4, while the exclusive connection model shown earlier in Figure 6-7 was described earlier in Section 6.2.2.

Vertical deflections of the slab in fire conditions

A comparison of the vertical deflections at Point-O between the two connection models is shown in Figure 6-20. The vertical deflections when using the inclusive connection model were almost the same before 120 minutes but slightly greater after 120 minutes than the deflections when using the exclusive connection model. At 240 minutes the vertical deflection when using the inclusive and exclusive connection model reached 1.22m and 1.18m, respectively. The trends of the increase of the vertical defections at Point-O were similar between these two different kinds of connection models. The vertical deflection at Point-O was slightly underestimated when using the exclusive connection model and slightly overestimated when using the inclusive connection model after 120 minutes.

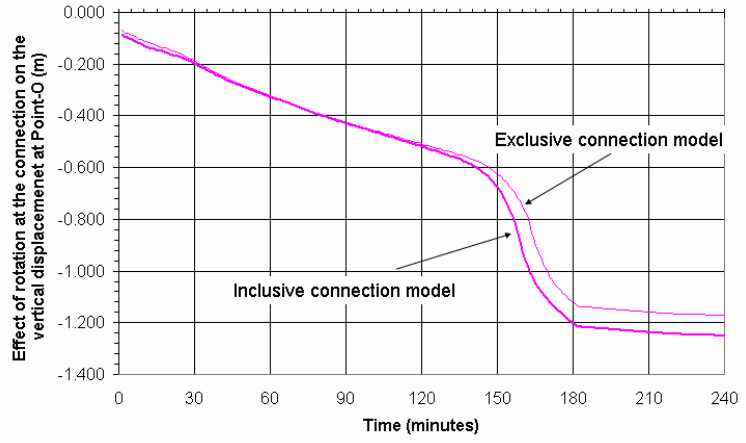

Figure 6-38 Comparison of the vertical deflections at Point-O

Bending moments of the slab in fire conditions

Figure 6-39 shows a comparison of X-direction bending moments along Section-3 near Point-O and in the edge strip of the slab using the two connection models. The bending moments near Point-O were almost the same when using the two connection models due to

the lack of the effect of the membrane forces on the slab in this region. The trends of the development of bending moments in the edge strip of the slab were the same when using the two connection models, but the magnitudes of bending moments were variable when using the two connection models. When using the inclusive connection model, at 180 minutes the bending moment in the edge strip reached 51kN-m/m, which was twice the value of the bending moment when using the exclusive connection model. After 120 minutes the vertical deflections of the slab when using the inclusive connection model were greater those than when using the exclusive connection model. When the vertical deflections of the slab are large, the P-Δ action will be preset in the slab, and as a result, the bending moments in the slab are significantly affected by the P-Δ action.

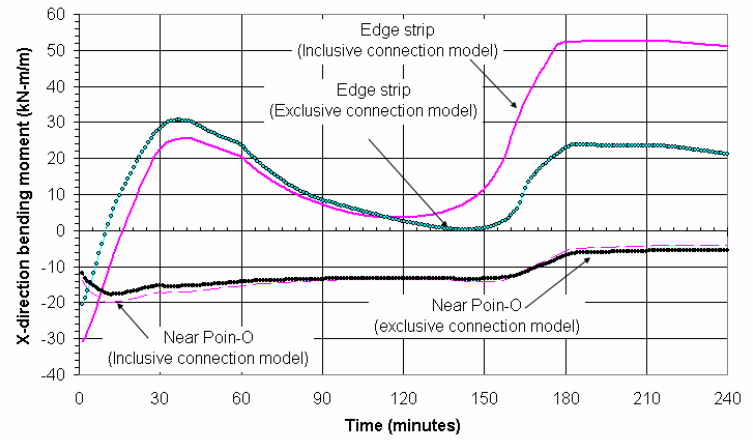

Figure 6-39 Comparison of X-direction bending moments along Section-3 in the edge strip and near Point-O of the slab

Membrane forces of the slab in fire conditions

Figure 6-40 shows a comparison of X-direction membrane forces along Section-3 in the edge strip of the slab using the two connection models. After 110 minutes the tensile membrane forces when using the inclusive connection model were greater than those when using the exclusive connection model. At 180 minutes the tensile membrane forces reached 750kN/m when using the inclusive connection model, while it only reached 450kN/m when using the exclusive connection model. The trends of the development of membrane forces were similar between the two connection models.

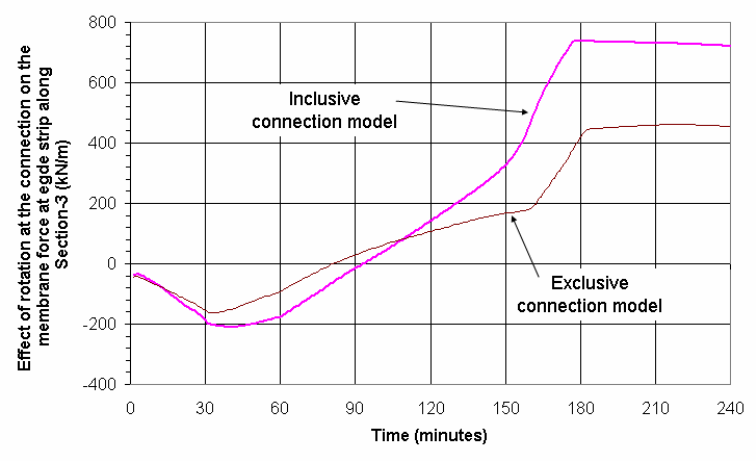

Figure 6-40 Comparison of X-direction membrane forces along Section-3 in the edge strip of the slab

Figure 6-41 shows a comparison of the X-direction average membrane forces along a part of Section-3 between using the two connection models. The membrane forces in the edge strip of the slab and the shell elements adjacent to the edge strip were not taken account of in the average membrane forces. Before 150 minutes the membrane forces were almost the same when using these two connection models. At 180 minutes the membrane force when using the inclusive connection model reached 15kN/m, which was greater then the membrane force of 10kN/m when using the exclusive connection model. The trends of the development of the membrane forces were similar between using the two connection models.

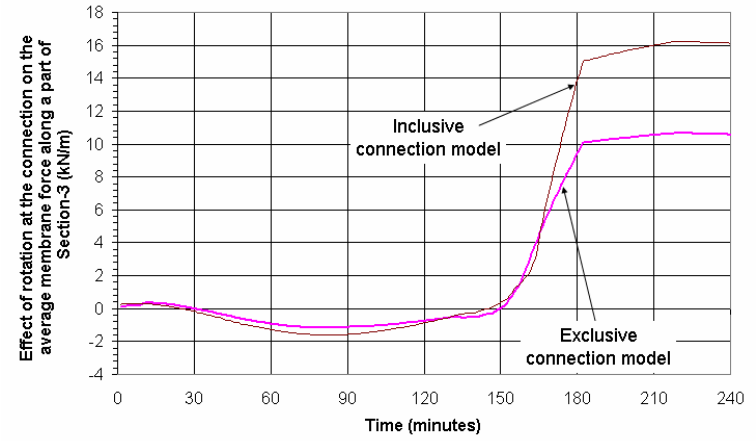

Figure 6-41 Comparison of the X-direction average membrane forces along a part of Section-3

To sum up, the effect of the connection models on the vertical deflections, the bending moments and the membrane forces of the slab mainly occurred after 120 minutes of fire exposure, while the trends of the development of the vertical deflections, the bending

moments and the membrane forces were similar when using both connection models. The results of the analysis of the slab in fire exposure using the exclusive connection model were slightly underestimated at the post stage of the fire (after two hours of fire exposure). Because the results of the modelling was overestimated when using the inclusive connection model and underestimated when using the exclusive connection model, more accurate results of the analysis of the slab in fire exposure lies somewhere between those of the two different connection models.

6.4.5. Conclusion

The analyses of the one-bay flat slabs exposed to an ISO 834 Standard fire without a decay phase have shown that:

- The slab experiences failure at 150 minutes but does not collapse due to the effect of the tensile membrane forces in the strips of the slab between the columns.
- The redistribution of the bending moments and the membrane forces of the slab are mainly present in the edge strip of the slab and along the diagonal of the slab.
- The results of the modelling are sensitive to the connection models. The magnitudes of displacements, bending moments and membrane forces are affected using different kinds of connection models when the duration of the fire exposure is greater than 120 minutes (two hours), but the trends of the developments of displacements bending moments and membrane forces are not affected.
- One-bay flat slabs without edge beams are not recommended to be built because the performance of the slabs in fire exposure is easily improved by adding the edge beams surrounding the slabs.

6.5. Behaviour of the One-Bay Flat Slab in Fire with a Decay Phase

This part of the chapter presents the behaviour of a one-bay flat slab exposed to an ISO 834 Standard fire with a decay phase. The purpose of the analysis is to investigate the effect of the restraint of the columns on the behaviour of the flat slab without edge beams under the fire with a decay phase. The behaviour of the one-bay flat slab from 1 minute to 60 minutes is the same for the slab exposed to an ISO 834 Standard fire with or without a decay phase. Therefore, the behaviour of the flat slab in the decay phase and after the decay phase is mainly discussed in this section.

6.5.1. Vertical deflections of the slab in fire conditions

The vertical deflections of the slab at Point-O in the fire with a decay phase are plotted in Figure 6-42. It shows that the vertical deflection increased from 0.070m at 1 minute to the maximum deflection of 0.372m at 80 minutes and then declined to 0.207m at the end of the simulation. The slab did not collapse throughout the simulation.

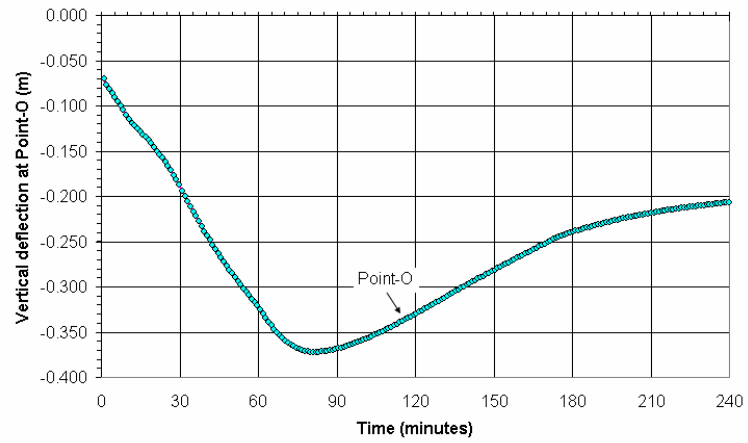

Figure 6-42 Vertical deflections of the slab at Point-O

The patterns of the distributions of vertical deflections at 90, 120, 150, and 180 minutes are shown in Figure 6-43. The white colour in the graphs indicates the vertical deflections were greater than 0.2m. The largest vertical deflection of the slab was in the midpoint of the slab (Point-O) and the smallest values of vertical deflections were around the column. The graphs show that the distribution of the vertical deflection at 240 minutes was significantly different from those at the other times. The pattern of the distribution of the vertical deflection was not

a circular shape around midpoint of the slab (Point-O) at 240 minutes, especially in the region close to the column. The development of vertical deflections is a complicated procedure within the decay phase of the fire and after the exhausting (or extinguishing) of the fire. The behaviour of the slab in the duration of the decay phase and after the exhausting (or extinguishing) of the fire should be taken into account in the performance design of reinforced concrete slabs in fire conditions.

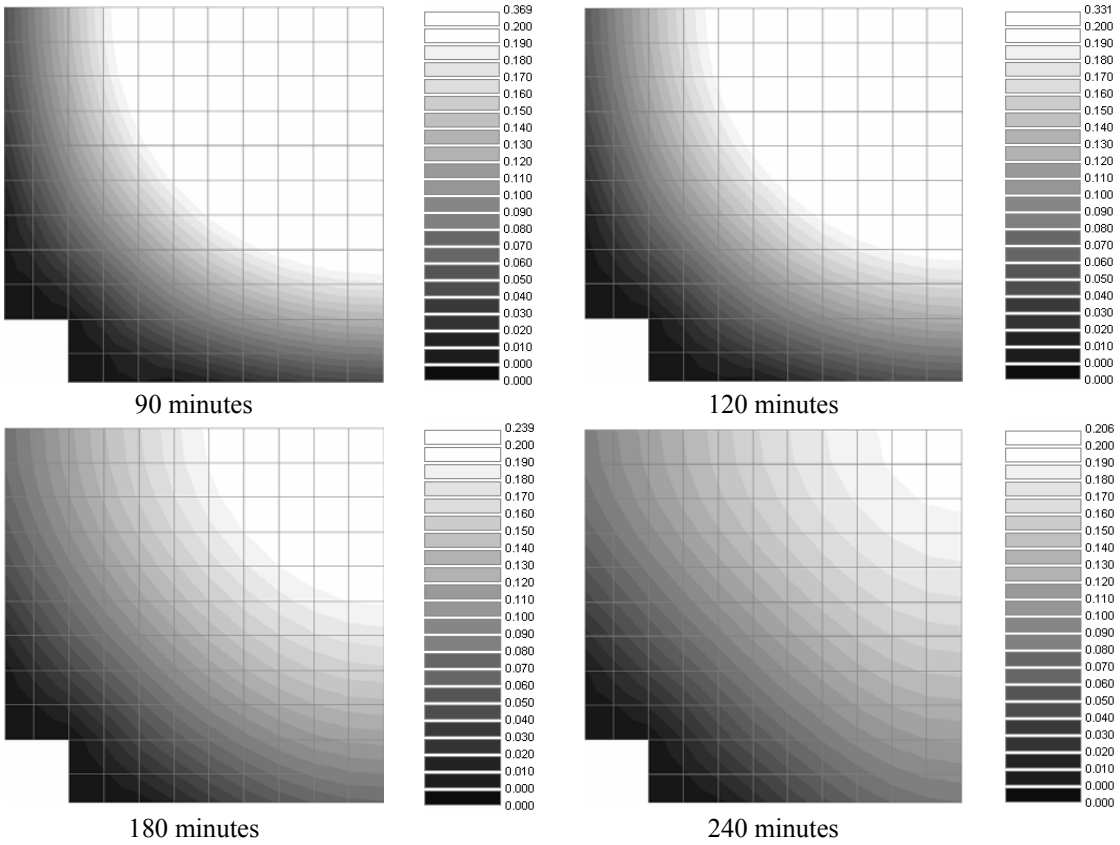

Figure 6-43 Distributions of vertical deflections of the slab in the fire with a decay phase

The vertical deflections of the slab along Strip-A and Strip-C are shown in Figure 6-44 (a) and Figure 6-44 (b), respectively. These graphs show that the vertical deflections had large values at the midspan (Strip-C) and small values at the edge strip of the slab (Strip-A) because the restraint of the columns reduced the development of the vertical deflections along Strip-A. The vertical deflections after 90 minutes remained roughly the same values along Strip-A, while they significantly declined along Strip-C because of the redistribution of bending moments in the slab.

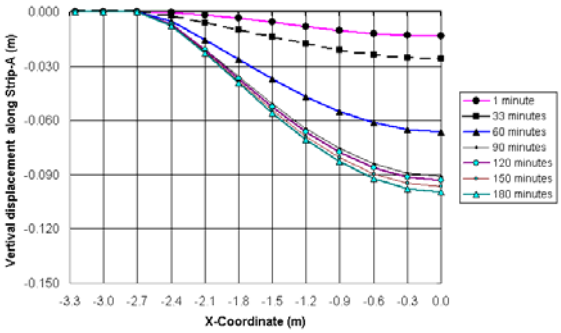

(a) Vertical deflections along Strip-A

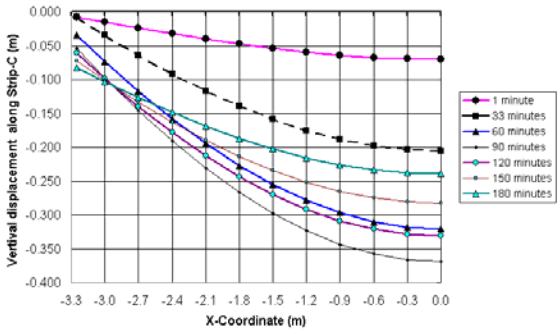

(b) Vertical deflections along Strip-C

Figure 6-44 Vertical deflections along Strip-A and Strip-B in the fire with a decay phase

6.5.2. Bending moments of the slab in fire conditions

The distribution of X-direction bending moments along Section-3 is shown in Figure 6-45 (a). It shows that the redistribution of bending moments was present in the region close to the edge of the slab due to the effect of the restraint of the columns on the strips of the slab between the columns. The bending moments in the edge strip and near Point-O against time are plotted in Figure 6-45 (b). It shows that the bending moments near Point-O were sagging moments, while the bending moments in the edge strip of the slab were variable between sagging and hogging moments. The bending moment near Point-O remained almost a constant value of -13kN-m/m throughout the simulation. The bending moment in the edge strip of the slab declined to zero at 10 minutes from a negative value of -20kN-m/m at 1 minute, and then increased to a positive value of 30kN-m/m at 33 minutes; after that, it declined to zero again at 110 minutes. At 180 minutes the bending moment dramatically increased from zero to -75kN-m/m and continuously increased to -95kN-m/m at 240 minutes. The maximum sagging moment was reached at the end of the simulation.

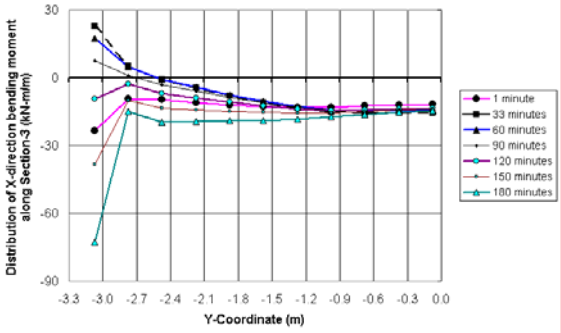

(a) Distribution of X-direction bending moments along Seciton-3

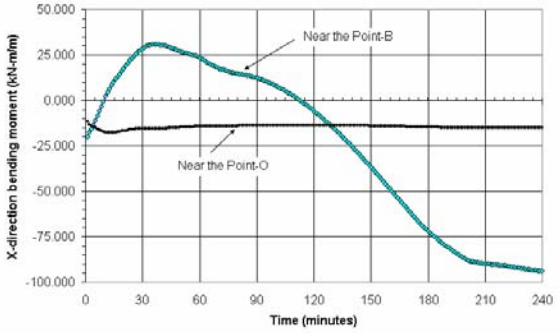

(b) X-direction bending moments near Point-O and in the edge strip along Section-3

Figure 6-45 Distribution of X-direction bending moments along Section-3 in the fire with a decay phase

After the fire exhausted at 170 minutes, the bottom reinforcing bars in the slab dramatically cooled down, but the temperature of the concrete on the top region of the slab still rose due to the wave of heat moving through the slab; as a result, a significant redistribution of bending moments occurred after the exhaustion of the fire.

Figure 6-46 (a) and Figure 6-46 (b) show X-direction bending moments along Strip-A and Strip-C, respectively. The redistribution of bending moments was present along Strip-A. In the first stage of the fire exposure, the thermal expansion on the bottom of the slab was greater than on the top of the slab and this made the curvature of bending moments move up; as a result, the positive bending moments increased and the negative bending moments decreased. In the decay phase of the fire and after the exhaustion of the fire, the concrete and reinforcing bars on the bottom cooled down and shrunk, but on the top region of the slab the thermal expansion was still present due to the rise of the temperatures of the slab on the top region; as a result, the edge strip of the slab bowed up and the bending moments in the midspan of the edge strip of the slab increased. The bending moments along Strip-C almost remained constant in the decay phase of the fire. The redistribution of bending moments was not significant along Strip-C.

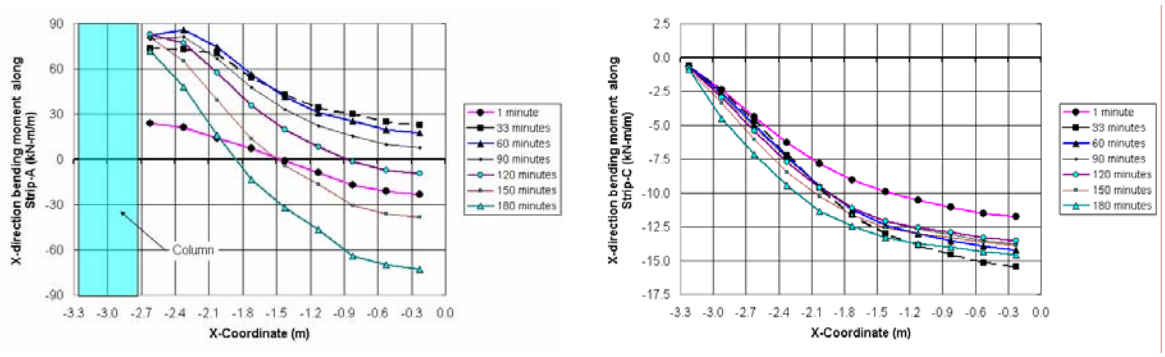

(a) Bending moments along Strip-A (b) Bending moments along Strip-C

Figure 6-46 X-direction bending moments along Strip-A and Strip-C in the fire with a decay phase

The patterns of the distributions of X-direction bending moments are shown in Figure 6-47. It shows that the positive value of bending moments was distributed along the edge strip of the slab and along Point-A to Point-O (the diagonal of the flat slab) before 120 minutes. After 120 minutes the large value of negative bending moments was not only present in the middle part of the edge strip but also present in the region close to the column along Point-A to

Point-O. The significant redistribution of bending moments occurred at the post stage of the fire and after the exhaustion of the fire.

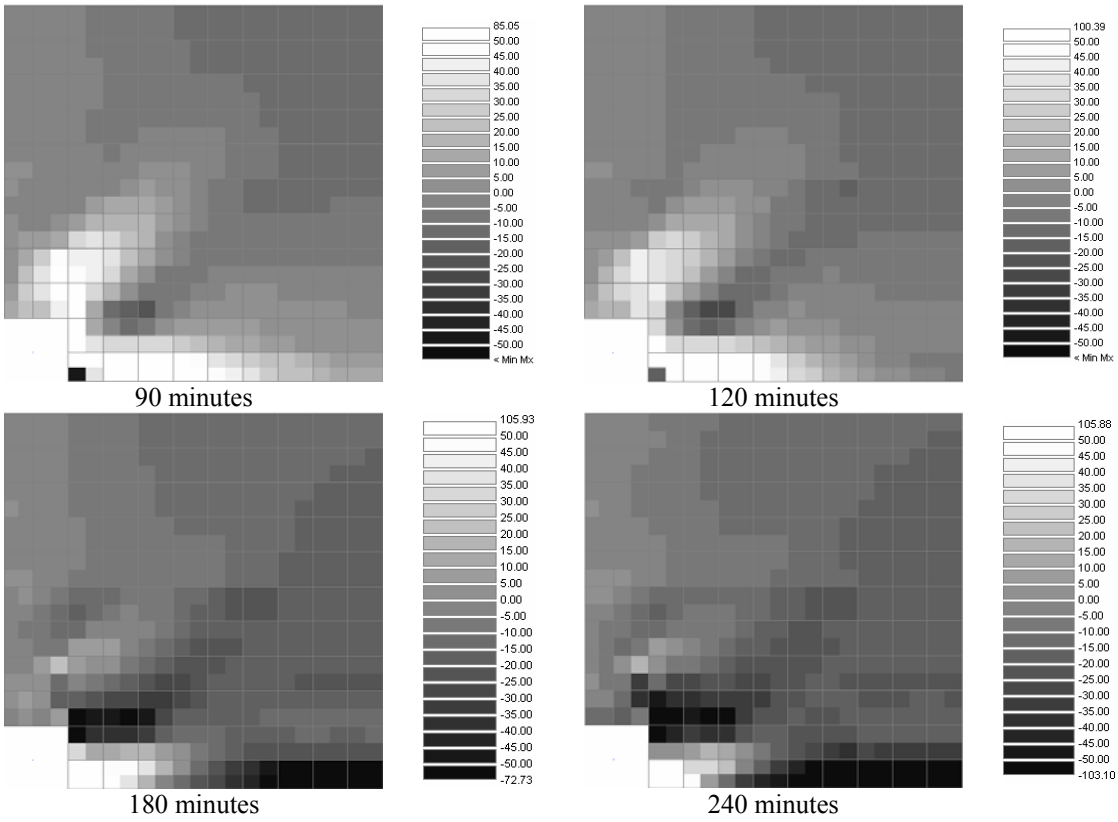

Figure 6-47 Distributions of X-direction bending moments of the slab in the fire with a decay phase

6.5.3. Membrane forces of the slab in fire conditions

X-direction membrane forces along Section-3 and the average value of the membrane forces along a part of Section-3 are shown in Figure 6-48 (a) and Figure 6-48 (b), respectively. The average value of the membrane forces of a part of Section-3 did not included the membrane forces in the edge strip and the shell elements adjacent to the edge strip. Figure 6-48 (a) shows that the membrane forces were mainly present in the strips of the slab between the columns. The membrane forces were almost zero in the middle parts of the slab. Figure 6-48 (b) shows that in the middle parts of the slab the average value of the membrane forces was negative from 25 minutes to 150 minutes, but the magnitude of the membrane forces was very small.

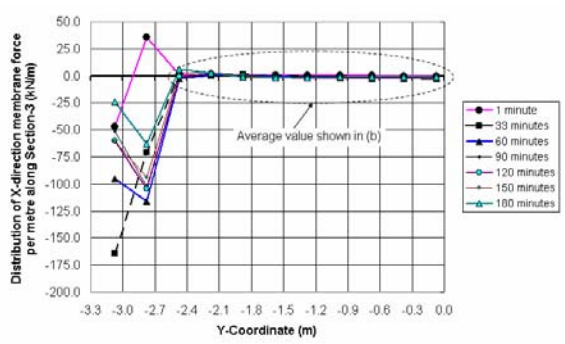

(a) Distribution of X-direction membrane forces along Section-3

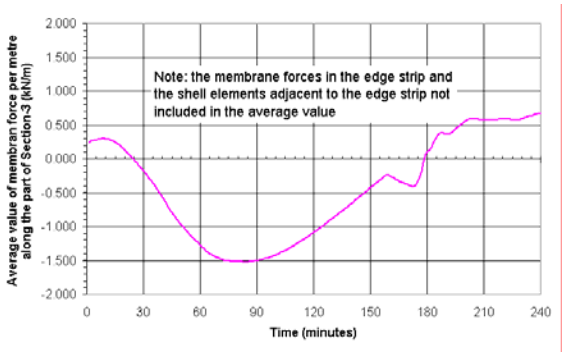

(b) X-direction average membrane forces along the part of Section-3

Figure 6-48 X-direction membrane forces along Section-3 in the fire with a decay phase

Figure 6-49 shows X-direction membrane forces in the edge strip of the slab at Section-2 and Section-3 against the time. The graph shows that compressive membrane forces mainly developed in the edge strip of the slab. The trends of the development of the membrane forces at Section-2 and Section-3 were similar, but the magnitude of the membrane forces was significantly different. At Section-2 in the edge strip, which was close to the column, the compressive membrane force increased from -10kN/m at 1 minute to -300kN/m at 33 minutes, and then declined to -65kN/m at 75 minutes; after that, it slightly increased to -120kN/m at 135 minutes. The compressive membrane force declined to zero at 210 minutes and the tensile membrane force started to develop at Section-2 in the edge strip and at the end of the simulation the tensile membrane force reached 40kN/m. At Section-3 in the edge strip, which was in the midspan of the edge strip, the compressive membrane force developed throughout the simulation. The compressive membrane force increased from -50kN/m at 1 minute to -160kN/m at 33 minutes, and then declined to -40kN/m at 80 minutes; after that, it slightly increased to -60kN/m at 150 minutes, and then started to decline. At the end of the simulation, the compression membrane force declined to -10kN/m at Section-3. The membrane forces in the slab after the exhaustion of the fire were very small compared with the membrane forces in the slab under the fire exposure due to the lack of the restraint to the flat slab without edge beams.

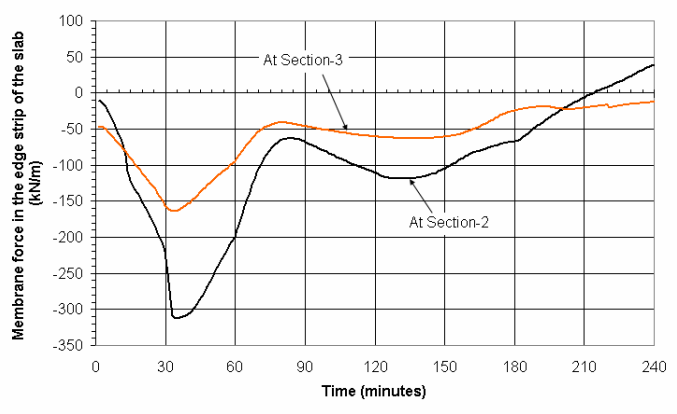

Figure 6-49 Membrane forces in the edge strip of the slab in the fire with a decay phase

The patterns of X-direction membrane forces in the slab are shown in Figure 6-50. It shows that the membrane forces were mainly present in the slab between the columns before 180 minutes.

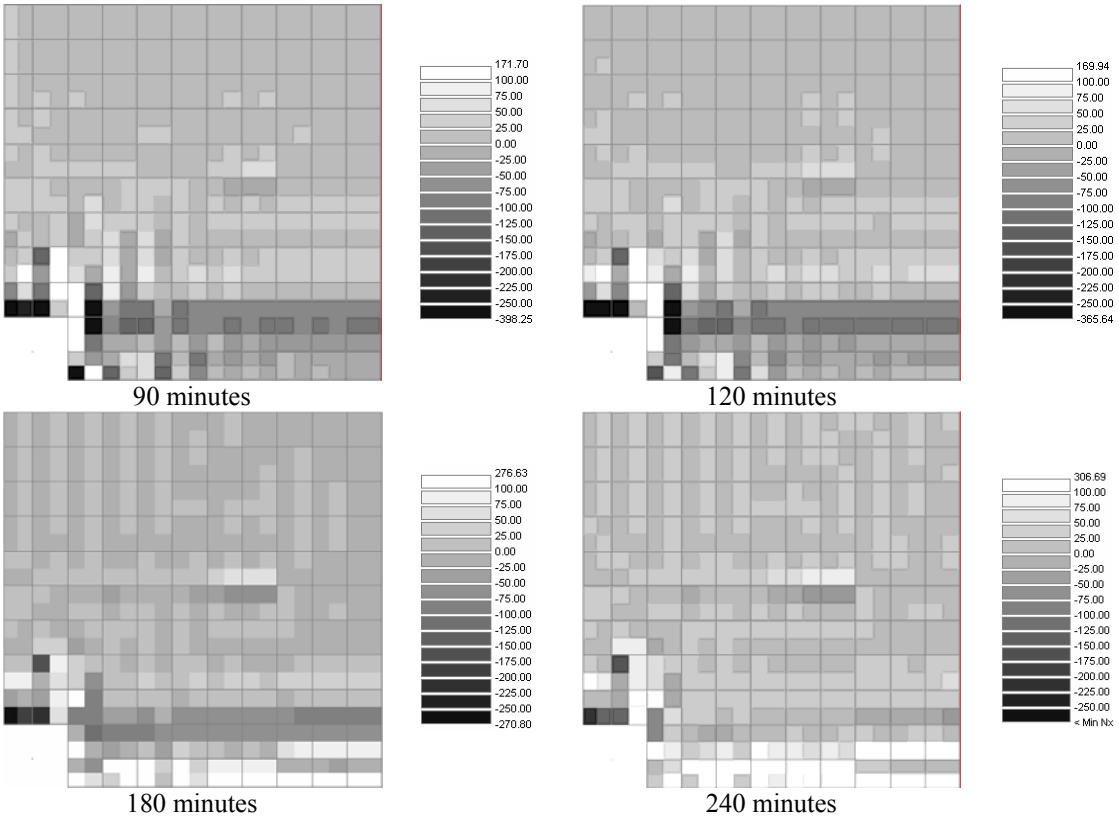

Figure 6-50 Distributions of membrane forces of the slab in the fire with a decay phase

6.5.4. Conclusions

The analysis of a one-bay flat slab without edge beams exposed to an ISO 834 Standard fire with a decay phase has shown that:

- The slab did not fail when it was exposed to a fire with a decay phase.
- The significant redistribution of bending moments is mainly present in the edge strip of the slab in the duration of the decay phase of the fire and after the exhaustion of the fire.
- The membrane forces of the flat slab are mainly present in the strips of the slab between the columns under the fire exposure.

6.6. Conclusions

The main findings of the analyses of the one-bay flat slab at ambient and fire conditions are as follow:

- SAFIR can predict the behaviour of the flat slab at ambient and fire conditions by using a suitable structural model.
- The results of the modelling are sensitive to the connection model for the column, slabs and the edge strips of the slab. The connection model affects the magnitudes of the displacements, the bending moments and the membrane forces of the flat slab, which are slightly underestimated using the inclusive connection model and overestimated using the exclusive connection model.
- The membrane forces are mainly present in the strips of the slab between the columns under the fire exposure.
- The redistribution of bending moments mainly occurs in the edge strips of the slab when the slab is exposed to the fire with or without a decay phase.
- One-bay flat slabs without edge beams are not recommended to be built because the performance of the slabs in fire exposure is easily improved by adding the edge beams surrounding the slabs.

7. THE ANALYSIS OF NINE-BAY FLAT SLABS AT AMBIENT AND FIRE CONDITIONS

This chapter describes the analysis of nine-bay flat slabs at ambient and fire conditions using 3-D shell elements in SAFIR. The purpose of the analysis is to investigate the effects of surrounding thermal conditions of the slab under fire exposure. The slab is exposed to an ISO 834 Standard fire without a decay phase up to 240 minutes (4 hours) or with a decay phase up to 200 minutes (3.3 hours). The location of the fire is varied from beneath all the bays to beneath the middle bay and the middle strip bays of the slab, so the surrounding thermal conditions of the slab will be varied depending on the location of the fire beneath the slab. The displacements, the distributions of the bending moments, and the membrane forces in the slab are investigated. The effects of the location of the fire onto the behaviour of the slab in the fire are discussed.

7.1. Introduction of the Modelled Structure

Figure 7-1 shows a two-level structure having three spans in two directions. The clear height of each level is 3.6m. The floor system of the structure is a reinforced concrete flat slab with surrounding concrete beams (edge beams) which connect corner and edge columns. The fire is assumed to be on the ground floor (beneath the first floor slab); therefore, the behaviour of the first floor slab in fires will be investigated using SAFIR.

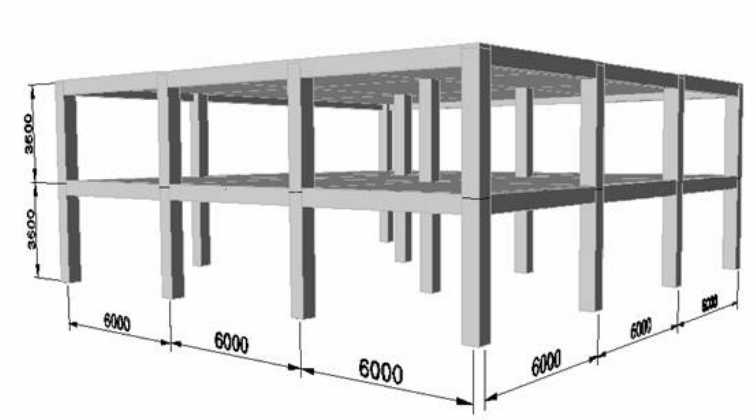

Figure 7-1 Nine-bay flat slabs in a two-level structure

7.1.1. Dimensions and Properties of the structure

The structure comprises three kinds of structural members: reinforced concrete flat slabs (or panels), columns and edge beams. A plan view of the first floor and a profile of the structure

are shown in Figure 7-2 (a) and Figure 7-2 (b), respectively. The first floor slab comprises nine 6m square panels arranged three-by-three. The thickness of the slab is 0.2m. Four edges of the slab are supported by the edge beams (0.25m wide by 0.5m deep) which connect with the corner and edge columns. The cross-section of the columns is a 0.5m square. So, the structure is geometrically symmetrical about two axes, the X-axis and the Y-axis in a coordinate system. If the applied loads and fire exposure beneath the slab are symmetrical about these two axes, the only a quarter of the structure needs to be modelled using SAFIR (shaded portion in Figure 7-2 (a)).

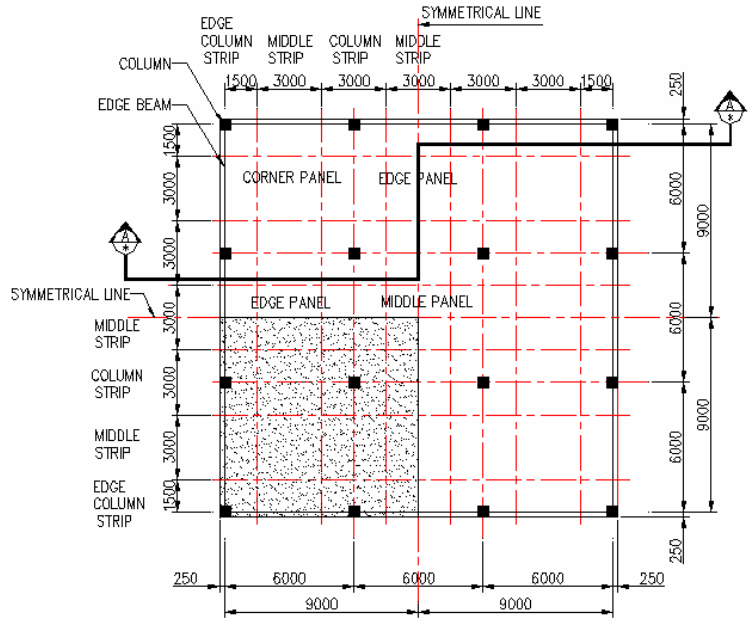

(a) Plan view of the first floor of the structure (units: mm)

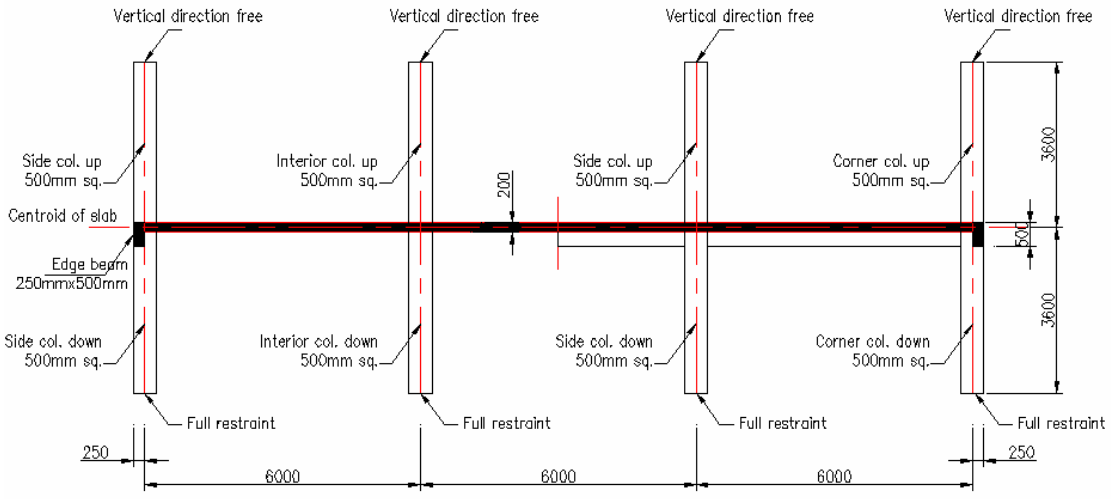

(b) Profile of section A (units: mm)

Figure 7-2 Layout of the first floor and the section view of the structure

The roof of the structure is simplified to vertical loads applied on the top of the columns. The ends of the columns on the ground floor level are fully restrained (six degrees of freedom); whilst on the roof level they are fully restrained in five degrees of freedom with the absence of restraint on the vertical displacement, so the top of the columns can be moved vertically. For the design purpose the slab is classified to three types of strips: column strips, middle strips, and edge column strips.

The properties and parameters of the structure are listed in Table 7-1.

Table 7-1 Properties and parameters of the structure

Flat Slab geometry		
Span (x-direction)	Lx:	6.0m
Span (y-direction)	Ly:	6.0m
Depth or thickness	h:	0.2m
Aspect ratio	L/h:	30
Section of the column		
Cross-section		0.5m x 0.5m
Length	Lc	3.6 m (first and second floor)
Section of the edge beams		
Section		0.25m x 0.5m (width x height)
Concrete properties (columns, beams, and slabs)		
Compressive strength (ambient temperature)	f'_c:	30 MPa
Elastic modulus (ambient temperature)	$E_{c,o}$:	18 GPa
Tensile strength	f'_t:	Zero
Concrete model (thermal and mechanical)		Siliceous aggregate (EC2, 1995)
Concrete cover	c_c:	30mm
Reinforcing Steel properties (columns, beams, and slabs)		
Yield strength (ambient temperature)	$f_{y,o}$:	430 MPa
Elastic modulus (ambient temperature)	$E_{s,o}$:	210 GPa
Steel model (thermal and mechanical)		Hot-rolled steel (EC2, 1995)

7.1.2. Applied load on the structure

The uniformly distributed loads on the flat slab are listed in Table 7-2.

Table 7-2 Uniformly distributed loads on the nine-bay flat slabs

Loads		
Self weight + Superimposed dead load	G	5.3 kN/m^2
Live load	Q	4.0 kN/m^2
Ultimate load (1.2G + 1.6Q)		12.8 kN/m^2
Fire load (1.0G + 0.4Q)		6.9 kN/m^2
Fire Exposure		ISO 834 standard fire without a decay phase (4 hour duration) ISO 834 standard fire with a decay phase (3.3 hour duration)
Initial temperature		20.0 ^{o}C

The applied load on the edge beams is 7.65kN/m (the self-weight of the beams plus the self-weight of the walls and windows upon the beams). In fire conditions the vertical loads applied to the columns are 55.8kN on the corner columns, 125.6kN on the side columns (the edge columns), and 247.0kN on the interior columns.

7.1.3. Reinforcement of the structure

The structural design is based on the ultimate load of 12.8kN/m^2 which was uniformly distributed on the flat slab. The flat slab is designed according to the ***direct design method*** of Section 13.6 in *ACI 318R-89 (Revised 1992)* (ACI, 1992). The arrangement of the top reinforcing bars in the slab is shown in Figure 7-3 (a) where the distribution or temperature bars of Φ8@200 in the two directions are not shown. The layout of the bottom reinforcing bars in the slab is displayed in Figure 7-3 (b). Because the structure is symmetrical in two directions, only a quarter of the layout of the reinforcement in the slab is illustrated in these drawings. X-direction reinforcing bars are placed on the top of Y-direction reinforcing bars of the slab, as shown in Figure 7-3 (e). The reinforcement of all the columns or beams is the same. The longitudinal reinforcing bars with the stirrups in the columns and beams are shown in Figure 7-3 (c) and Figure 7-3 (d), respectively.

In above paragraph only the flexural design of the flat slab was considered. Shear can be critical in the flat slab design. However, shear is generally not critical when slabs carry distributed loads or line loads and are supported by beams or walls (Park et al., 2000). In the design of flat slabs at ambient temperature conditions, the shear stresses can be more critical than the flexural stresses in the region surrounding the columns, so shear may govern the design. For satisfying the requirement of shear design, the thickness of the flat slab and the size of the column or column capital are verified according to *ACI 318R-89 (Revised 1992)* (ACI, 1992). For simplifying the modelling of the structure using the SAFIR shell element model, the effect of column capitals on the flexural behaviour of the flat slab is ignored. The shear failure of flat slabs at ambient or fire conditions are not considered because it can be prevented by changing the size of column capitals and thickness of the slabs.

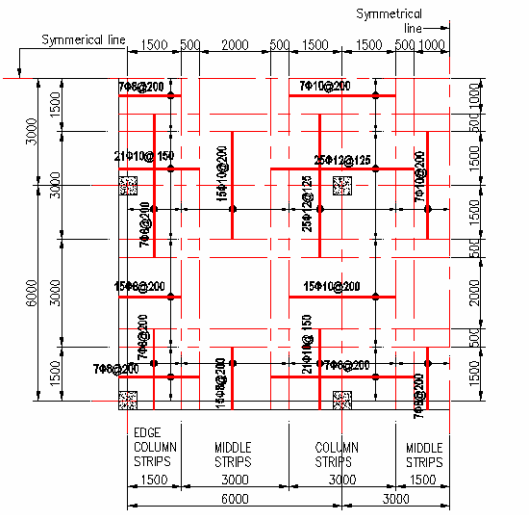

(a) Layout of the top reinforcing bars in the slab

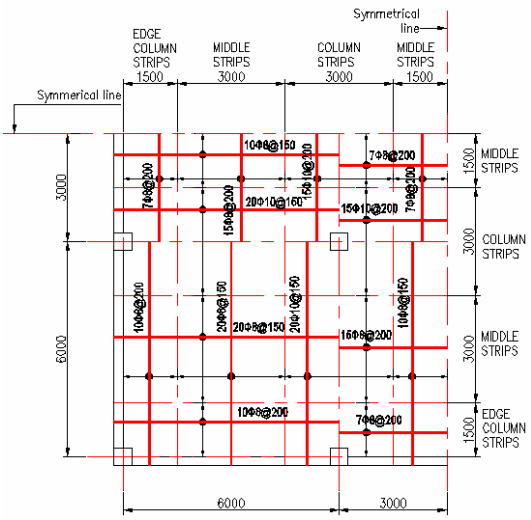

(b) Layout of the bottom reinforcing bars in the slab

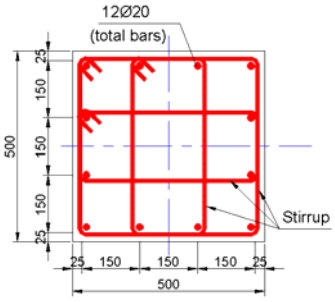

(c) Reinforcement in the column

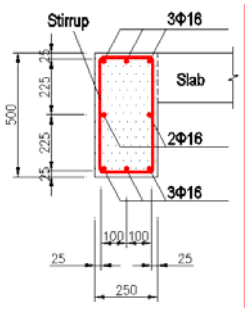

(d) Reinforcement in the edge beams

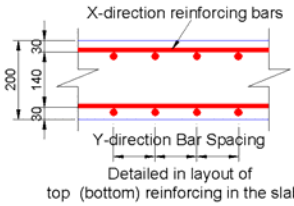

(e) Detail of the reinforcement in the slab

Figure 7-3 Reinforcement of the structural members

7.2. SAFIR Model of the Nine-Bay Flat Slab

This section details the SAFIR structural model of the nine-bay flat slab, which is used in the later sections of this chapter to simulate the slab in different fire conditions.

7.2.1. The thermal model

The thermal analyses of the structural members were presented earlier in Chapter 4 of this thesis. The thermal models of the structural members are briefly summarised below.

The thermal model of the slab was shown earlier in Figure 4-6 with the absence of the reinforcing bars in the slab. It was assumed that the temperatures of the reinforcing bars equalled the temperatures of the concrete at the same horizontal levels in the slab.

The beam thermal model is shown in Figure 7-4 and the distribution of the temperature in the cross-section of the beam at 60 minutes was shown earlier in Figure 4-13 (b), which showed that the beam was exposed to the fire from beneath and a part of the inside surface. The areas of the reinforcing bars in beams were adjusted to match the actual areas of the steel in the input files of the structural model. The concrete on the right side of the distinct line in the graph was modelled as shell elements in the structural analysis, so this part of the concrete in the beams was assumed to be non-load bearing material which did not contribute to the strength and stiffness of the beams in the structural analysis. The torsional stiffness of beams in fire conditions was reduced to 50% of the torsional stiffness at ambient temperature conditions (20^{o}C throughout the simulations). It is assumed that the torsional stiffness of beams did not change throughout the simulation of the slab exposed to the fire.

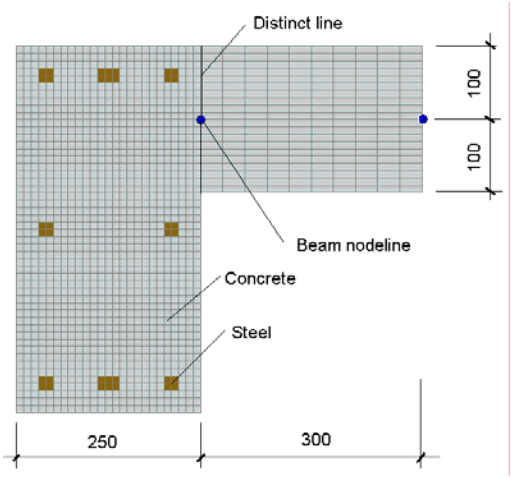

Figure 7-4 Thermal model of the beam

When the edge beams remain at ambient conditions in the simulations of a part of the flat slab exposed to fire, the thermal analysis does not need to be performed for these edge beams.

The columns were at ambient temperature conditions throughout the simulations, so it was not necessary to perform the thermal analysis on them. The cross-section of a column in the SAFIR structural analysis is shown in Figure 7-5. Because the cross-section of the column was symmetrical to the two directions in a coordinate system, only a quarter of the column was modelled. The areas of reinforcing bars were adjusted to be the same with actual areas of the steel in input files of the structural analysis.

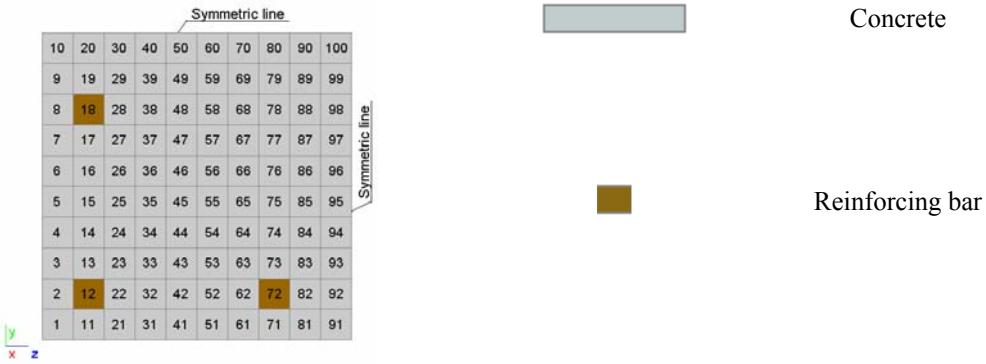

Figure 7-5 Cross-section of a column in SAFIR structural analysis

7.2.2. The structural model

The analyses of the structure exposed to fires are focused on the behaviour of the first floor slabs, so the structure (Figure 7-1) is simplified to a quarter of the structure (Figure 7-6 (a)) that comprises four columns, four edge beams, and a concrete slab supported on the columns and edge beams ((Figure 7-6 (b)). A segment of columns above or below the first floor level is discretized to nine beam elements in SAFIR. The beam members are discretized to a number of 0.3m long beam elements. The concrete slab is modelled as 0.3m square shell elements (total 891 shell elements). In structural analyses, the nodeline should be defined for all the elements. The nodeline is the line where the joint nodes (or joint points) of the beam or shell elements meet each other. The nodeline of the shell elements is at the mid-depth of the slab, while the nodeline of the columns is at the centroid of the cross sections. The nodeline of the beams was shown earlier in Figure 7-4. It showed that the nodeline was perpendicular to the cross section at 0.1m below the top and at the inside surface of the beam. Figure 7-6 (c) shows the SAFIR structural model of a quarter of a nine-bay flat slab with applied boundary

conditions and Figure 7-6 (d) shows the structural model with applied loads on the beams, columns and slabs. A typical top view of the structural model in SAFIR, which is shown in Figure 7-6 (e), will frequently be used in the further discussions of the behaviour of the flat slab to show the distribution of the vertical deflections, the bending moments, and the membrane forces in the slab.

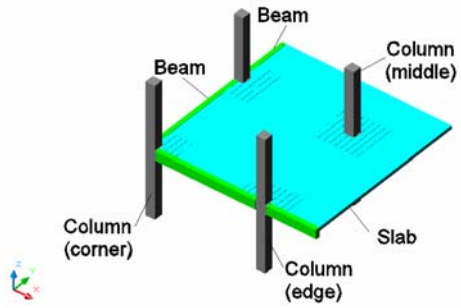

(a) The building is simplified as a quarter of the structure

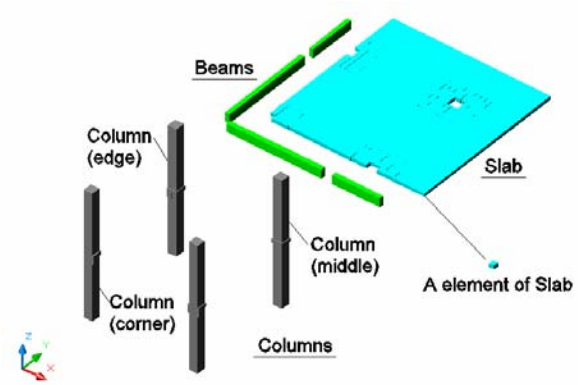

(b) The elements of the structure will be modelled using SAFIR program

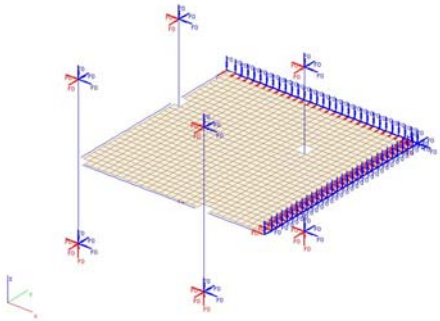

(c) SAFIR structural model of a quarter of the slab with applied boundary conditions

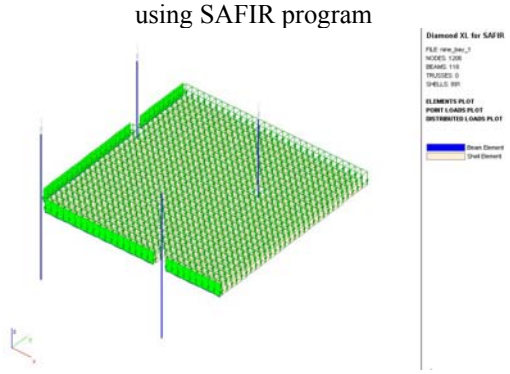

(d) Applied loads on the structure (distribution loads on the shell and beam elements and axial forces on the top of columns)

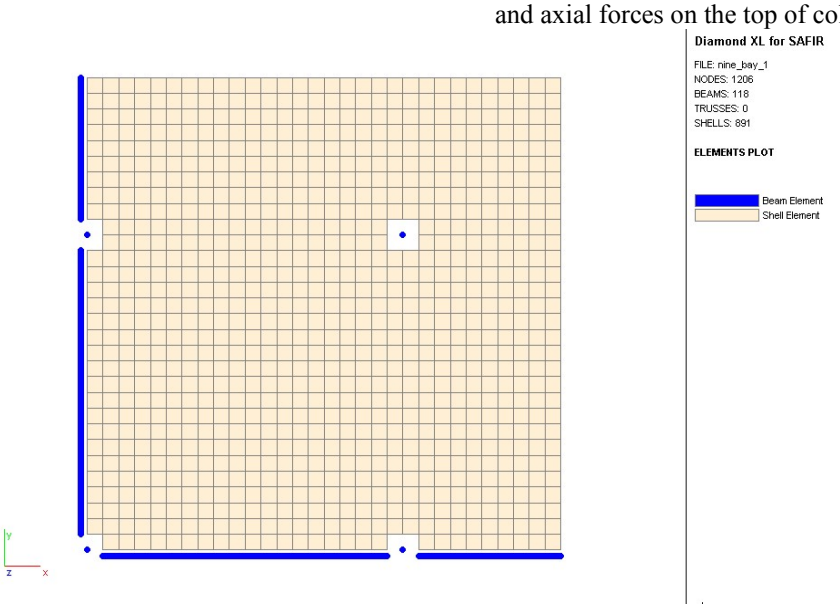

(e) The top view of the SAFIR structural model

Figure 7-6 SAFIR structure model of a nine-bay flab slab

The connections of the beams with the columns, the slabs with the columns, or the slabs with the beams are fulfilled using the function of ***the master-slave relations of displacements*** among the nodes in SAFIR, as shown in Figure 7-7 (a) to (f). Figure 7-7 (a) and Figure 7-7 (b) show the connection of the real building and the SAFIR structural model at the corner column respectively. The nodes of 247, 277 and 278 in the shell elements of the slab, the node of 130 in the beam elements of the column, and the nodes of 1 and 57 in the beam elements of the edge beam members are master-slaved together, as shown in Figure 7-7 (b). The connections at the edge column and at the middle column are shown in Figure 7-7 (c) to (f). The performance of the master-slave relations among the nodes at the connections of the edge column and the middle column are similar to those at the connection of the corner column. The master-slaved nodes have the same movements and rotations throughout the simulations. The effect of the master-slaved nodes on the modelling of structures is discussed earlier in Chapter 6.

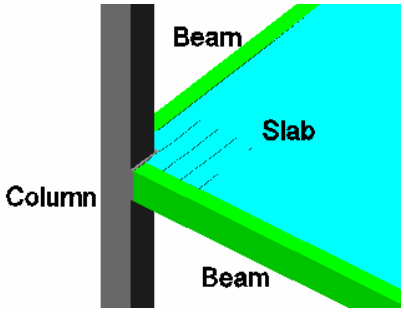

(a) Connection of the real structure at the corner column

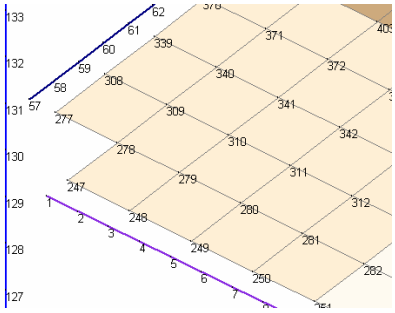

(b) Connection of the SAFIR structural model at the corner column

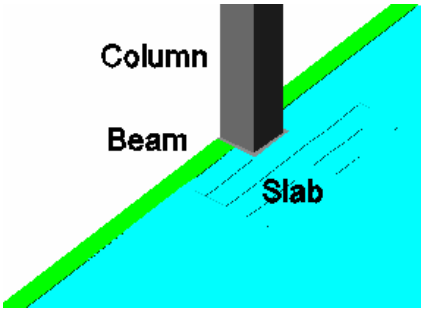

(c) Connection of the real structure at the edge column

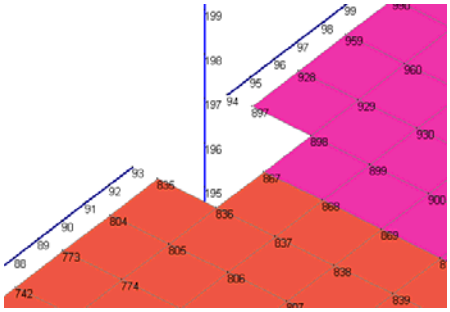

(d) Connection of the SAFIR structural model at the edge column

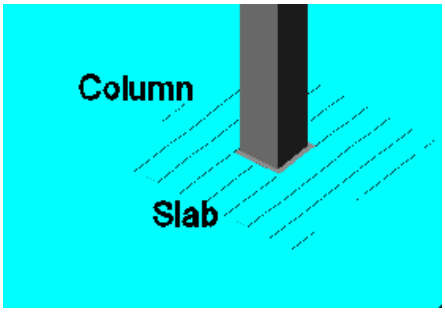

(e) Connection of the real structure at the middle column

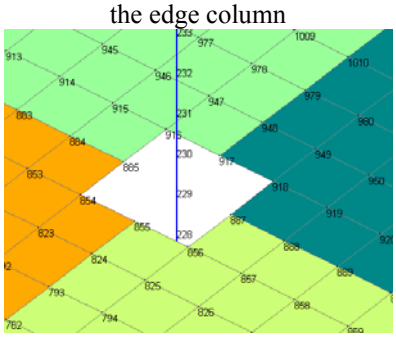

(f) Connection of the SAFIR structural model at the middle column

Figure 7-7 Modelling of the connections among the column, beam, and slab

7.2.3. Assumptions of the analysis

The assumptions of using shell elements and beam elements in SAFIR were detailed earlier in Chapter 3 of this thesis. In addition, some assumptions are also made during the analysis of the reinforced concrete floor system.

- The effects of the capitals or drop panels in the slabs are ignored.

i) The differences of the displacements of the nodes at the connections of the corner, edge, and middle columns are ignored due to the master-slave relations of displacements among these nodes.

- The in-plane flexural stiffness of the slabs is infinite.
- The fire exposure beneath the slab is uniform.
- The shear failure of the slab is not considered in the analysis.
- The torsional stiffness of the beams is not changed throughout the simulations of the slabs exposed to fires.

7.2.4. Conventional signs for the nine-bay flat slab

The top view of a quarter of the nine-bay flat slab is shown in Figure 7-8. For a convenient description of the behaviour of the slab, 16 points, 5 strips and 5 sections are defined. Point-B2, Point-B4, Point-D2, and Point-D4 are at the centroid of the columns, while Point-A1 is the central point of the nine-bay slab. Point-A1 is also the absolute coordinate zero point. The strips along the X-direction are indicated by letters, whilst the sections along the Y-direction are indicated by numbers. Some terms which will be used in further discussions are shown in Figure 7-8 as well (for example: Edge Column-1, Beam-1).

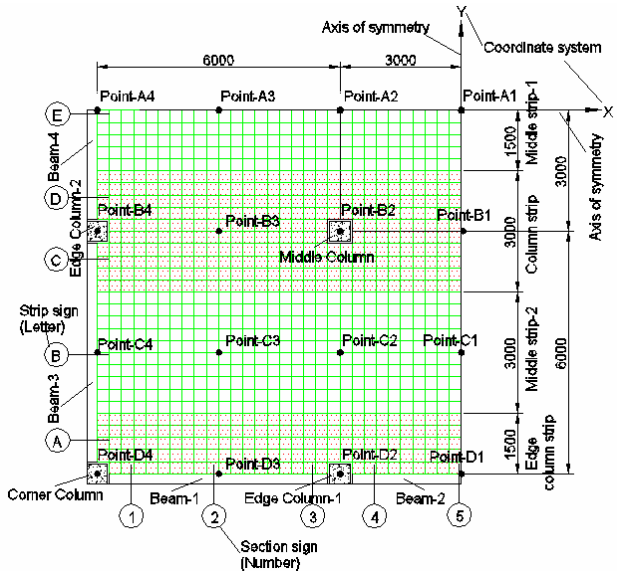

Figure 7-8 Conventional signs of the nine-bay flat slab

The X-coordinate and Y-coordinate of the points are listed in Table 7-3. Any point on the slab can be described as (X-coordinate, Y-coordinate) in the absolute coordinate system.

Table 7-3 X-coordinate and Y-coordinate of the points in Figure 7-8

	Point-A1	Point-A2	Point-A3	Point-A4	Point-B1	Point-B2	Point-B3	Point-B4
X-coordinate	0	-3	-6	-9	0	-3	-6	-9
Y-coordinate	0	0	0	0	-3	-3	-3	-3
	Point-C1	Point-C2	Point-C3	Point-C4	Point-D1	Point-D2	Point-D3	Point-D4
X-coordinate	0	-3	-6	-9	0	-3	-6	-9
Y-coordinate	-6	-6	-6	-6	-9	-9	-9	-9

7.3. Behaviour of the Nine-Bay Flat Slab at Ambient Conditions

This section briefly presents the behaviour of the flat slab at ambient temperature conditions. The aims of this section are to investigate the behaviour of the flat slab at ambient conditions using SAFIR and to set up the initial conditions of the slab under fire exposure. The uniformly distributed load applied to the slab ranges from 5.3kN/m^2 (un-factored self-weight of the slab) to the maximum load which caused the failure of the slab at the end of the simulation. The initial conditions of the flat slab exposed to the fire are coincide with the uniformly distributed loads of 6.9kN/m^2 (the fire load listed in Table 7-2) applied to the slab. It is found that the load capacity of the slab is 22.3kN/m^2, nearly two times the ultimate load of 12.8kN/m^2 listed in Table 7-2.

7.3.1. Vertical deflections of the slab

Figure 7-9 shows the vertical deflections of the slab against the uniformly distributed loads applied to the slab. When the load increased to 22.3kN/m^2 the slab collapsed. This load was nearly two times the ultimate load that was used to design the flat slab at ambient conditions (flexural design of the slab) because of the development of membrane forces in the column strips and middle strips of the slab when the load exceeded the ultimate load of 12.8kN/m^2, as shown later in Figure 7-15. The vertical deflection at Point-D1 was very small because the edge beams were designed to be strong to avoid the beam failure before the slab failure in the simulations. Throughout the simulation, the vertical deflection at Point-C1 was less than at Point-B1, which was closer to the central point of the slab than Point-C1. The maximum vertical deflection of the slab was at Point-A1. When the load reached 22.3kN/m^2, the vertical deflection at Point-A1 reached 0.47m, which was nearly two times the vertical deflection of the load reaching the ultimate load of 12.8kN/m^2, whilst at initial condition of the slab under fire exposure (load of 6.9kN/m^2) it was only 0.056m.

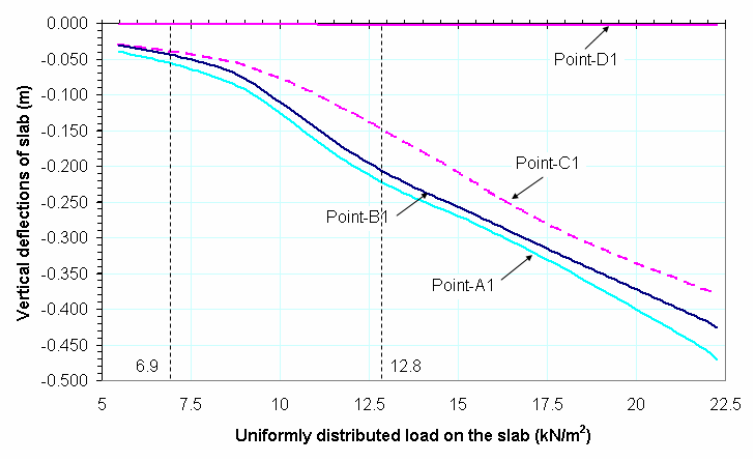

Figure 7-9 Vertical deflections of the slab against applied loads on the slab at ambient conditions

The deflected shapes of the vertical deflections of the slab under the applied loads of 12.8kN/m^2 and 22.3kN/m^2 are shown in Figure 7-10 (a) and Figure 7-10 (b), respectively. These graphs are used to compare the patterns of the vertical deflections of the slab in fire conditions.

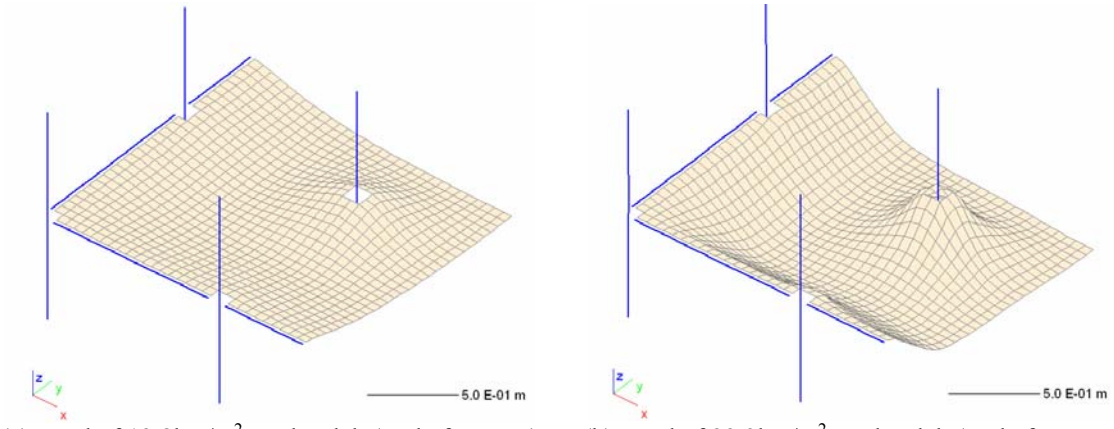

(a) Load of 12.8kN/m^2 on the slab (scale factor: 5) (b) Load of 22.3kN/m^2 on the slab (scale factor: 5)

Figure 7-10 Vertical deflections of the slab under the applied loads of 12.8kN/m^2 and 22.3kN/m^2

7.3.2. Bending moments of the slab

Figure 7-11 shows the distribution of X-direction bending moments along Section-5. The hogging moments are positive and the sagging moments are negative. The graph shows that the negative value of X-direction bending moments non-linearly distributed along Section-5 throughout the simulation due to the development of the membrane forces in the slab.

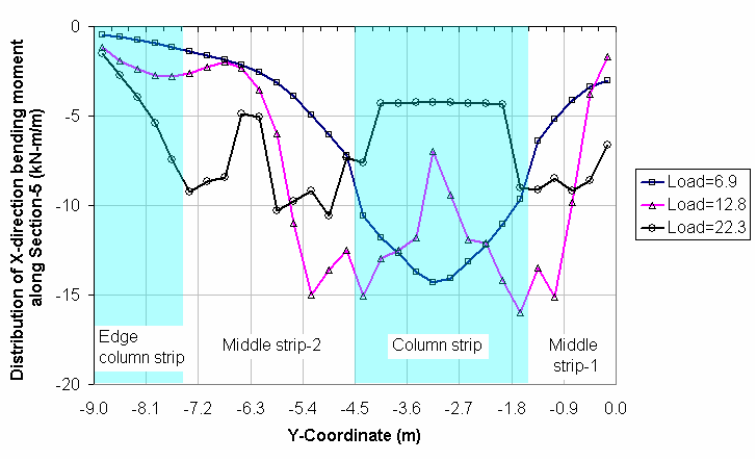

Figure 7-11 Distribution of X-direction bending moments along Section-5 (unit of the loads: kN/m^2)

Figure 7-12 shows the X-direction average bending moments in the strips along section-5. The maximum bending moment of -17kN-m/m was reached in Column strip when the load on the slab increased to 9.3kN/m^2, and then the moment declined to -5kN-m/m under the load of 22.3kN/m^2. In Middle strip-1 and Middle strip-2 the average bending moments almost remained the constant value under the loads from 11.25kN/m^2 to 22.3kN/m^2. The minimum bending moment was in Edge column strip, which was adjacent to the edge beams. The significant redistribution of the bending moment occurred in the slab when the load on the slab reached 9.3kN/m^2 because of the non-linear distribution of bending moments and the development of membrane forces in the slab, which enhanced the flexural capacity of the slab.

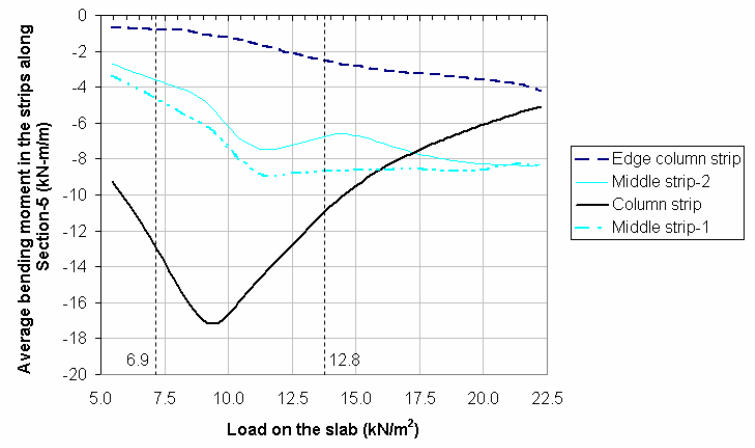

Figure 7-12 X-direction average bending moments in the strips along Section-5

The patterns of the distributions of X-direction bending moments in the slab under the applied loads of 12.8kN/m^2 and 22.3kN/m^2 are shown in Figure 7-13. The patterns can be divided into

four horizontal strips according to the reinforcement in the slab. The graphs show that the distributions of the bending moments were affected by the arrangement of the reinforcing bars, especially by the top reinforcing bars in the slab.

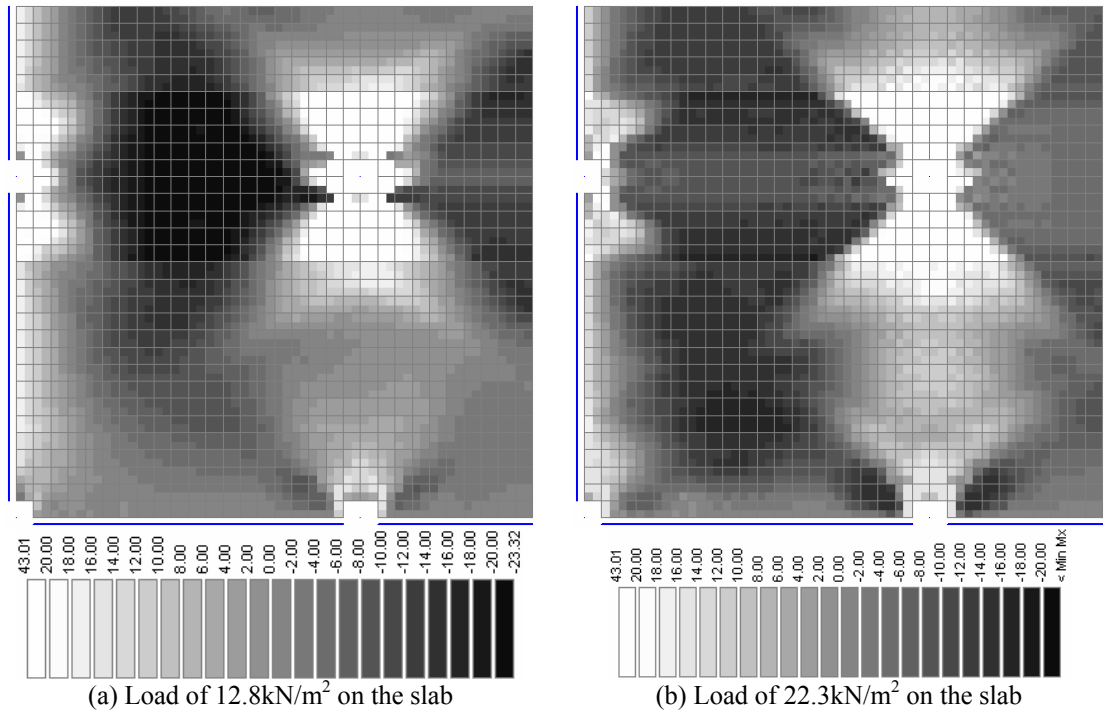

(a) Load of 12.8kN/m^2 on the slab (b) Load of 22.3kN/m^2 on the slab

Figure 7-13 Distributions of X-direction bending moments under loads of 12.8kN/m^2 and 22.3kN/m^2

7.3.3. Membrane forces of the slab

Figure 7-14 shows the distribution of X-direction membrane forces along Section-5. The maximum membrane force was present in the middle part of Column strip. When the load reached 22.3kN/m^2, the membrane forces in Column strip formed a plateau of 280kN/m.

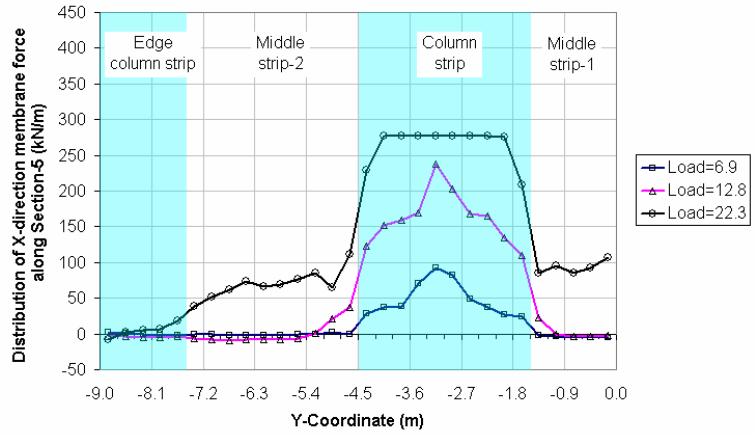

Figure 7-14 Distribution of X-direction membrane forces along Section-5 (unit of the loads: kN/m^2)

Figure 7-15 shows X-direction average membrane forces in the strips along Section-5. The graph shows that tensile membrane forces in Column strip increased constantly from 30kN/m under the load of 5.3kN/m^2 to 260kN/m under the load of 22.3kN/m^2, whilst in Edge column strip the membrane forces were nearly zero. The membrane forces in Middle strip-1 and Middle strip-2 started to develop just after the load on the slab reached the ultimate load of 12.8kN/m^2 when the vertical displacement at Point-A1 exceeded 0.2m (thickness of the slab). The curves of the membrane forces in the strips were increased with the same ratio after the load reached 12.8kN/m^2. The development of the membrane forces in the slab enhanced the ultimate capacity of the slab.

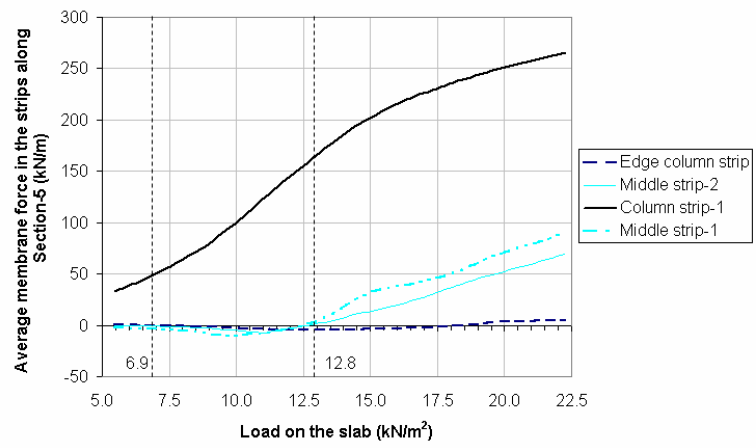

Figure 7-15 X-direction average membrane forces in the strips along Section-5

Figure 7-16 (a) and Figure 7-16 (b) show the distributions of X-direction membrane forces under loads of 12.8kN/m^2 and 22.3kN/m^2, respectively. The graphs illustrate that the patterns of membrane forces can be divided into four horizontal strips coordinated with the arrangement of top reinforcing bars in the slab.

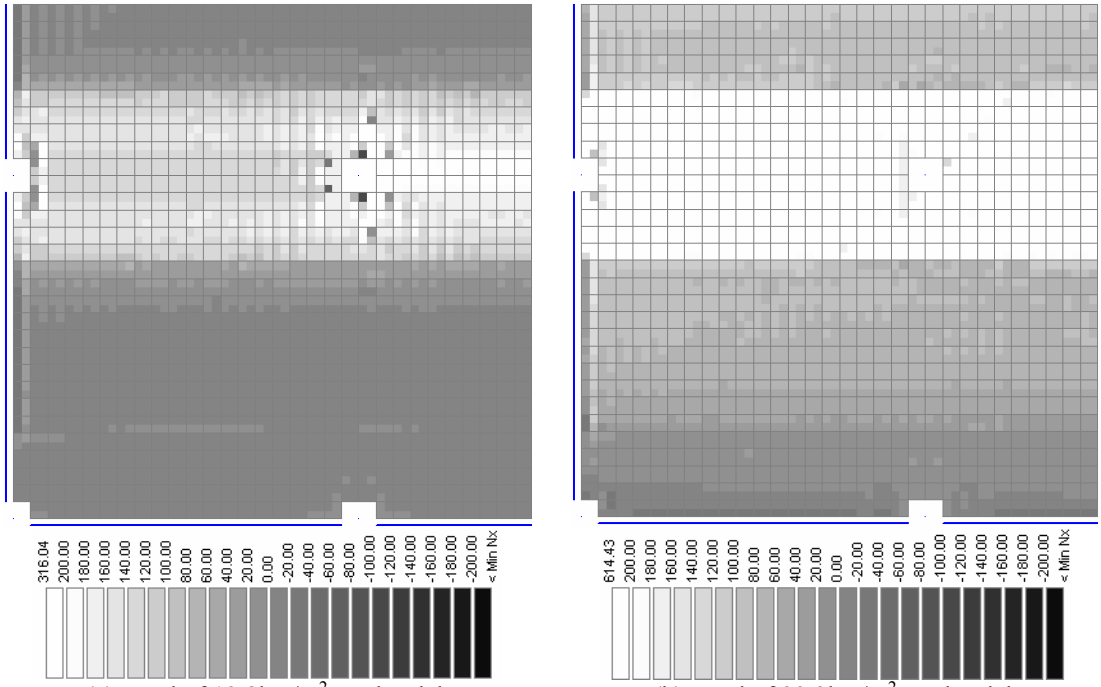

(a) Load of 12.8kN/m^2 on the slab (b) Load of 22.3kN/m^2 on the slab

Figure 7-16 Distribution of X-direction membrane forces under load of 12.8kN/m^2 and 22.3kN/m^2

7.3.4. Initial conditions of the slab exposed to fire

The initial conditions of the flat slab under fire exposure is defined as the conditions of the displacements, the bending moments, and the membrane forces of the slab under applied uniformly distributed load of 6.9kN/m^2 (the fire load) at 20^{o}C. The patterns of the initial distributions of the displacements, the bending moments, and the membrane forces in the slab are shown in Figure 7-17 (a) to (c).

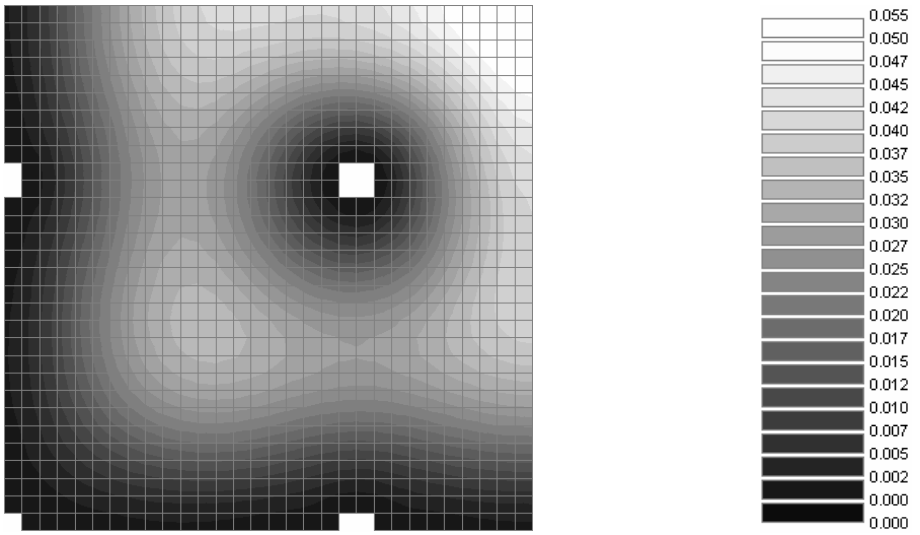

(a) Initial distributions of vertical deflections in the slab

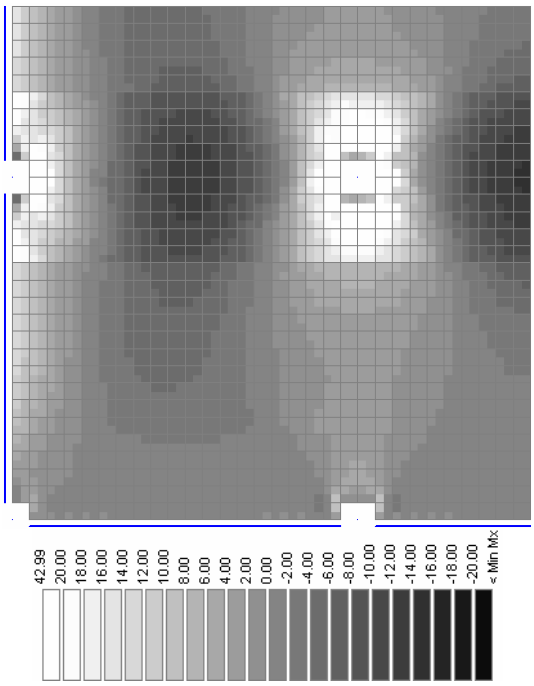

(b) Initial distributions of bending moments in the slab

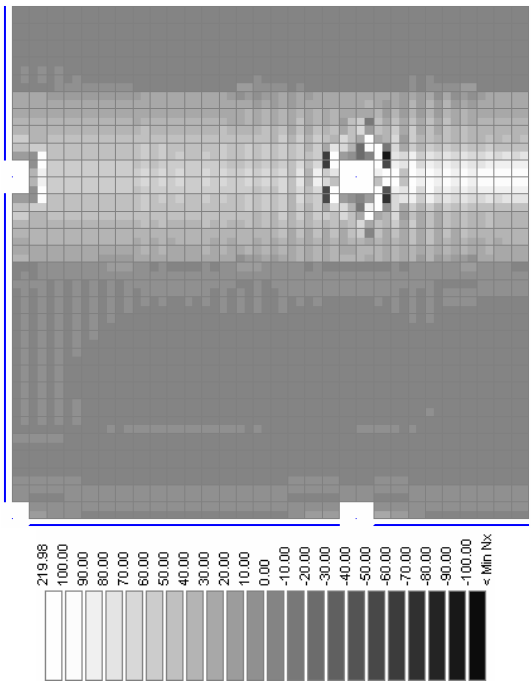

(c) Initial distributions of membrane forces in the slab

Figure 7-17 Initial conditions of the slab exposed to fire (load=6.9kN/m^2, temperature=20^{o}C)

7.3.5. Conclusions

The analysis of the flat slab at ambient temperature conditions shows that:

- The load capacity of the flat slab is 22.3kN/m^2, which is nearly two times the ultimate load of 12.8kN/m^2 because of the effect of the development of membrane forces and redistribution of bending moments in the flat slab.
- The X-direction (or Y-direction) distributions of bending moments and membrane forces can be divided into four strips to analyse depending on the arrangement of reinforcing bars in the slab.

7.4. Fire without a Decay Phase beneath All Bays of the Nine-Bay Flat Slab

This section presents a nine-bay flat slab fully exposed to an ISO 834 Standard fire without a decay phase. The purpose of this section is to investigate the behaviour of the flat slab when all the bays of the slab and all the edge beams are exposed to the fire. The slab is surrounded by edge beams and supported on the edge beams and columns. The edge beams are partially exposed to fires, whilst the columns are at ambient temperature conditions. The displacements of the slab, the distribution of the bending moments, and the distribution of the membrane forces are investigated.

7.4.1. Displacements of the slab in fire conditions

This part of the section investigated the vertical and horizontal displacements of the slab exposed to the fire. It is found that the displacements of the slab are significantly affected by the thermal conditions of the edge beams.

Vertical deflections of the slab

Figure 7-18 shows the vertical deflections of the slab at Point-A1, Point-B1, Point-C1, and Point-D1. The deflection at Point-D1, which is a joint point between the beam element and the shell element, was very small because of the great flexural stiffness of the edge beams that were partially exposed to the fire. Before 33 minutes, the deflection at Point-B1 was larger than at Point-C1, which is a middle point in the middle strip-2, but after 33 minutes the deflection at Point-C1 exceeded the deflection at Point-B1 because of the contribution of the redistribution of bending moments in the slab. The largest deflection of the slab was at Point-A1, the central point of the nine-bay flat slab. The deflection of the slab at Point-A1 considerably increased from the initial deflection of 0.056m to 0.415m at 180 minutes, and then slightly increased to 0.44m at the end of the simulation. There was a crinkle in the deflection curves at 180 minutes when a part of the slab became a catenary.

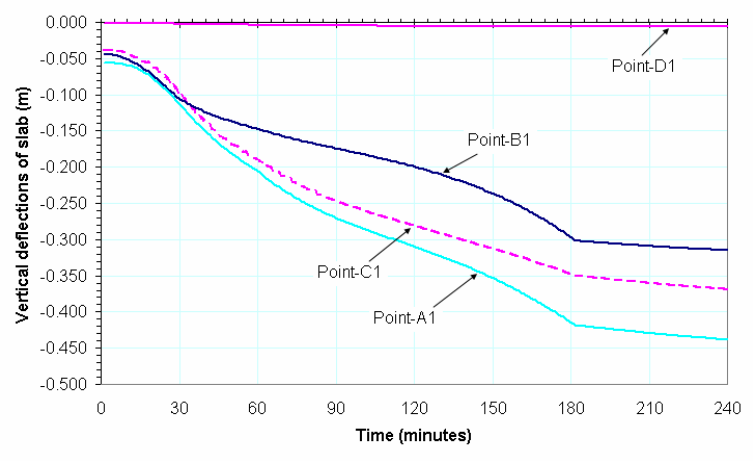

Figure 7-18 Vertical deflections of the slab at Point-A1, -B1, -C1, and –D1

Figure 7-19 (a) and Figure 7-19 (b) shows the distributions of the vertical deflections of the slab at 60 minutes and 180 minutes, respectively. The white colour in the graphs represents the vertical deflections are greater than 0.2m. The maximum vertical deflection at Point-A1 was 0.204m at 60 minutes, as shown in Figure 7-19 (a), but dramatically increased to 0.415m at 180 minutes, as shown in Figure 7-19 (b). The vertical deflections of most parts of the slab at 180 minutes were greater than 0.2m. The illustration of Figure 7-19 (b) indicates that the tensile membrane forces developed completely in the slab at 180 minutes, so the slab deformed into the shape of a catenary hanging on the columns and edge beams.

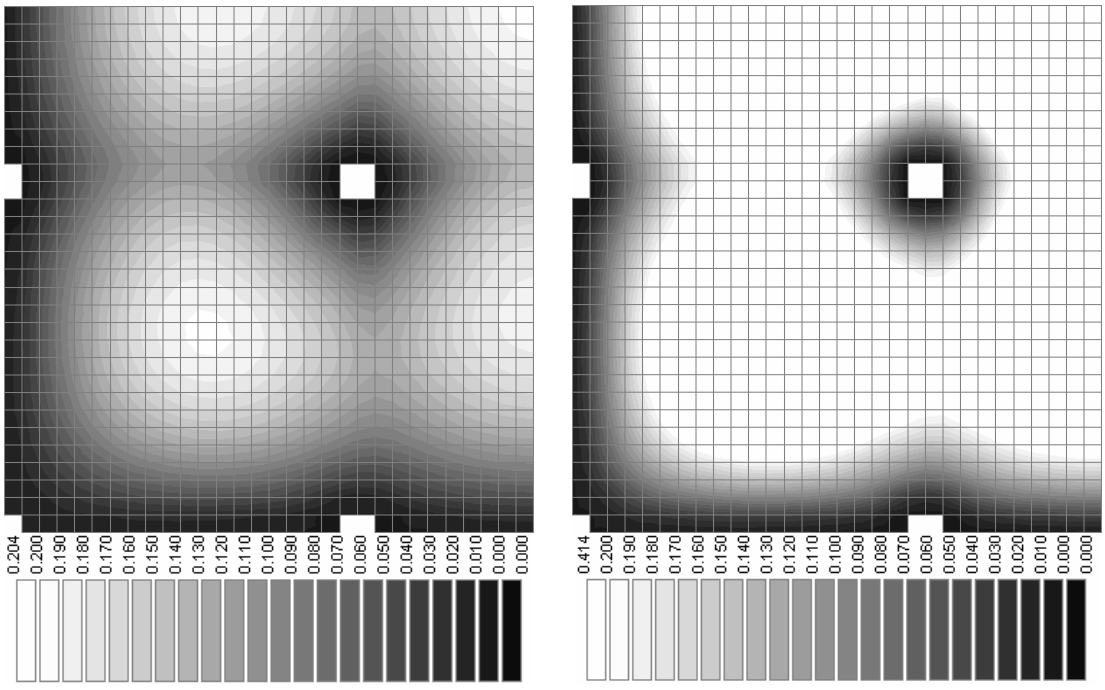

(a) Vertical deflections of the slab at 60 minutes (b) Vertical deflections of the slab at 180 minutes

Figure 7-19 Distributions of vertical defections of the slab at 60 and 180 minutes

Figure 7-20 shows the deflected shape of the slab at 180 minutes. The graph shows that the vertical deflections of the slab between the columns were less than in the central parts of the slab. The slabs were not only hung on the beams and columns, but also were partly supported on the slab acting as a virtual beam between the columns. The slab deformed as a catenary hanging on the columns and the beams, but did not collapse because the top reinforcing bars in the slab anchored in the edge beams and columns. If the top reinforcing bars of the slab fail to anchor into the columns and beams, the slab will collapse. Comparing the displacement patterns in Figure 7-20 and Figure 7-10, it is found that the behaviour of the vertical displacement of the slab in fire conditions was different than at ambient conditions.

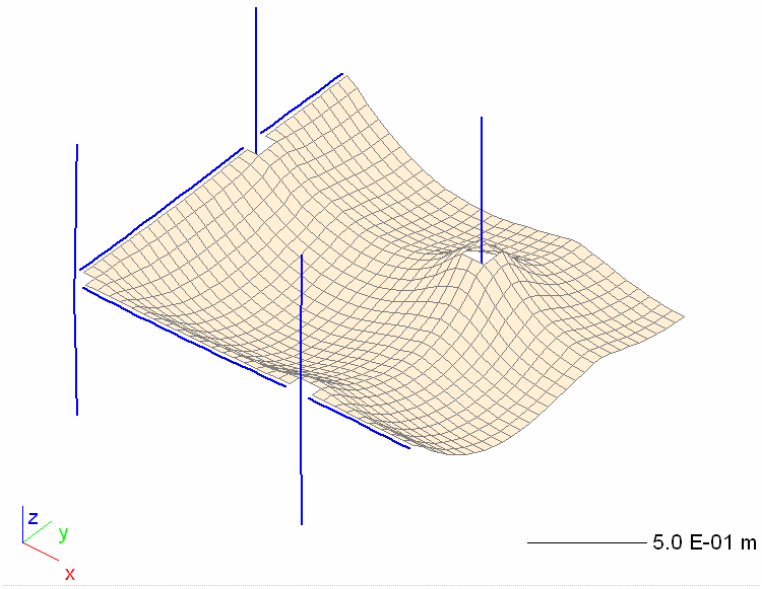

Figure 7-20 Vertical deflected shape of the slab at 180 minutes (scale factor: 5)

Horizontal displacements of the slab

Figure 7-21 shows the distribution of X-direction displacements of the slab from Point-B2 (the centroid of Middle column) to Point-A2. The displacement at Point-B2 equals the displacement at point (-3,-2.7) because of the master-slave relations of these two nodes at the connection of the middle column. The graph shows that the X-direction displacements were positive throughout the fire exposure in Column strip, but they varied from positive to negative in Middle strip-1. The small value of X-direction displacements at Point-B2 was due to the horizontal restraint of the column to the slab. The horizontal displacements affect the development of the compressive membrane forces (or thermal thrust) in the slab significantly, as shown earlier in Figure 5-2 in Chapter 5.

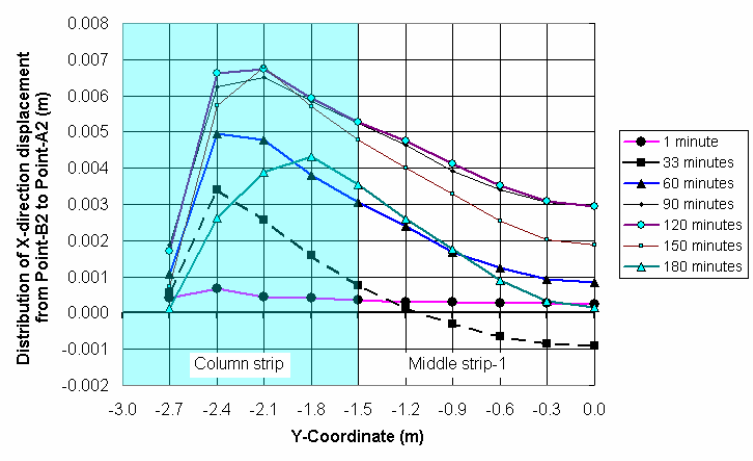

Figure 7-21 Distribution of X-direction displacements from Point-B2 to Point-A2

Figure 7-22 shows the X-direction displacements at Point-B2, Point-B4, Point-D2, and Point-D4. These points were the centroid of the columns (for example, Point-B2 is the centroid of Middle column, as shown in Figure 7-8). The graph shows that the corner column and two edge columns moved away from the slab (the negative value of horizontal displacements), whilst the middle column moved towards the centre of the slab (positive value of horizontal displacements). The horizontal displacements of columns were mainly affected by the thermal expansion of the slab and the edge beams at the first stage of the fire. When the vertical displacements of the slab became larger and larger, the tensile membrane forces in the slab developed very quickly due to the P-Δ action and the thermal bowing action in the slab. The tensile membrane forces in the slab (especially in Column strip) pulled the columns towards the central point of the slab (Point-A1). If there were no edge beams, the horizontal movements of the columns would be towards the central point of the slab. Moving away of the corner column from the slab throughout the simulation of the slab indicates that the horizontal movements of the corner column were dominated by the thermal expansion and horizontal thermal bowing of the edge beams. The vertical thermal bowing of the edge beams were very small due to the fire exposure mainly being on the inside vertical surface of the beams.

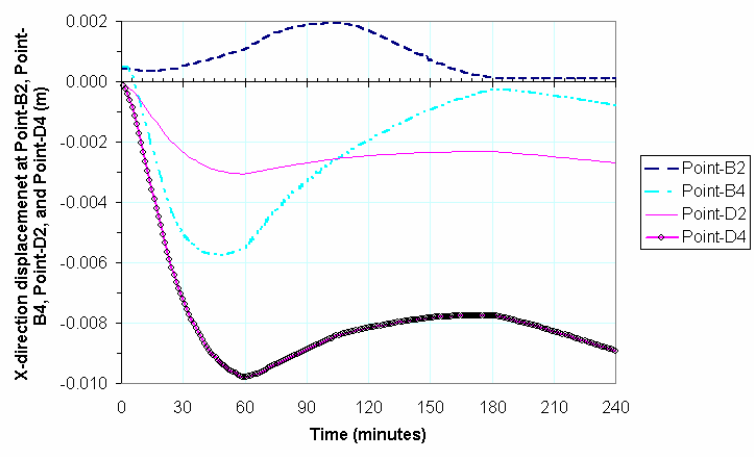

Figure 7-22 X-direction displacements at Point-B2, Point-B4, Point-D2, and Point-D4

At the end of the simulation, the shape of the slab, which was formed by the thermal expansion and horizontal thermal bowing of the edge beams and the tensile membrane forces in the slab, is shown in Figure 7-23. The horizontal movements of the edges of the slab had a tendency to enhance the development of the tensile membrane forces in the slab and reduce the vertical deflections of the slab. The behaviour of the flat slab surrounded by edge beams under fire exposure beneath all bays of the slab is better than the flat slab without the edge beams that had been investigated earlier in Chapter 6.

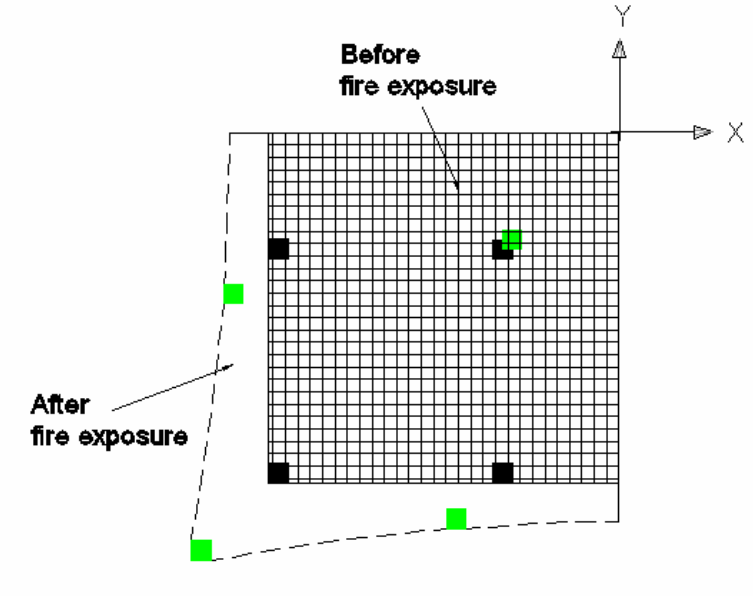

Figure 7-23 Shapes of the slab before and after the simulation

7.4.2. Bending moments of the slab in fire conditions

Because the slab is symmetrical about two axes, only X-direction bending moments are analysed. After analysis of the bending moments in the slab, it is found that the redistribution of bending moments is significantly affected by the arrangement and magnitude of the top reinforcing bars in the slab. The redistribution of bending moments in the slab is one of the main factors affecting the fire endurance and capacity of preventing the collapse of the slab.

Distribution and Redistribution of X-direction bending moments in the slab

Figure 7-24 shows the curvature of X-direction bending moments along Strip-E. The shaded parts in the graph are the column strips, whilst the unshaded parts are the middle strips. At one minute the bending moments were positive (tensile stress in the top reinforcing bars) in the column strips and negative (tensile stress in the bottom reinforcing bars) in the middle strips. When the temperature of the fire rose, the redistribution of bending moments in the slab occurred. The curvature of bending moments non-linearly moved up. At 60 minutes the bending moment in a column strip reached a maximum value of 13.6kN-m/m, which was significantly greater than 2.4kN-m/m at one minute; after that, it declined to 5.3kN-m/m at 180 minutes.

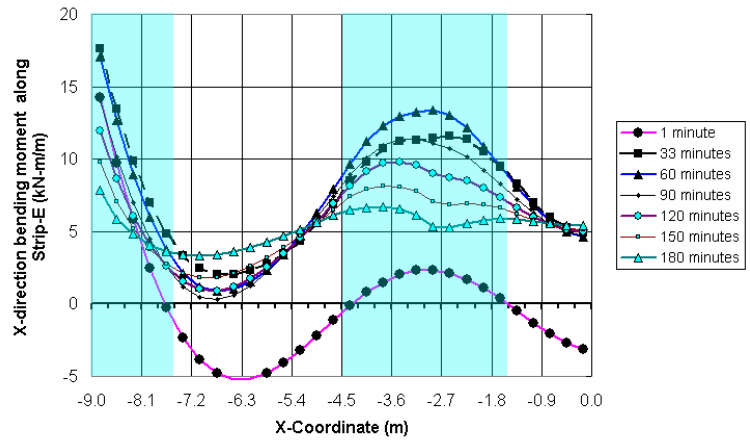

Figure 7-24 X-direction bending moments along Strip-E

The distributions of X-direction bending moments in the slab at 60 minutes and 180 minutes are shown in Figure 7-25. It shows that the trend of the distribution of bending moments could be classified into four regions. These regions are named Edge column strip, Column strip, Middle strip-1, and Middle strip-2, as shown earlier in Figure 7-8. The magnitude of the reinforcing bars in these four strips may be different, according to the structural design of the

slab at ambient conditions using *ACI 318R-89 (Revised 1992)* (ACI, 1992), as shown earlier in Figure 7-3.

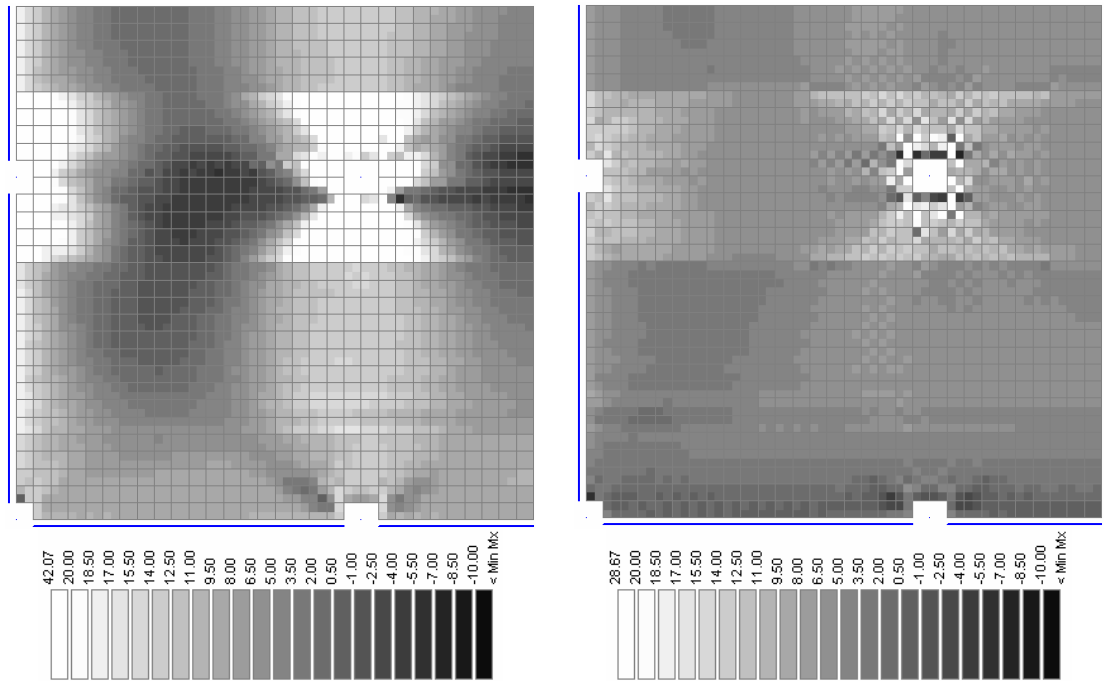

(a) At 60 minutes (b) At 180 minutes

Figure 7-25 Distributions of X-direction bending moments in the slab

Figure 7-26 shows the distribution of X-direction bending moments along Section-1, which is close to the edge of the slab. The graph shows that the bending moments in Middle strip-1 and Middle strip-2 had less variation than in Edge column strip and Column strip. The bending moments in Column strip were greater than in the other strips because the amount of the top reinforcing bars in Column strip was greater than in the other strips; as a result, the flexural capacity of the slab was larger in Column strip than in the other strips. The tendency of the redistribution of bending moments in the slab was that the bending moments were transferred from the region with lower flexural capacity to the region with higher flexural capacity. The arrangement and magnitude of reinforcing bars in the slab significantly affected the redistribution of bending moments in the slab.

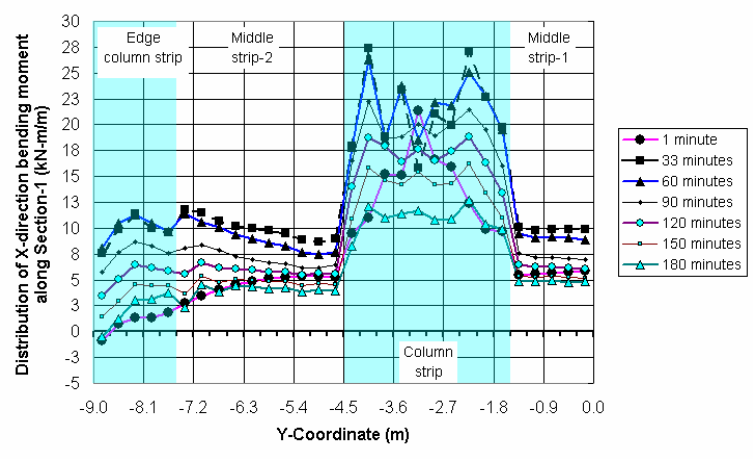

Figure 7-26 Distribution of X-direction bending moments along Section-1

Figure 7-27 shows the distribution of X-direction bending moments along Section-5, which was in the middle of the slab. The graph shows the significant redistribution of bending moments in Middle strip-1 and Middle strip-2 occurred at the first stage of the fire exposure (from 1 minute to 33 minutes). The value of the bending moments continuously increased from negative at 1 minute to positive at 180 minutes in the Column strip, whilst there was no negative bending moments after 33 minutes in the other strips.

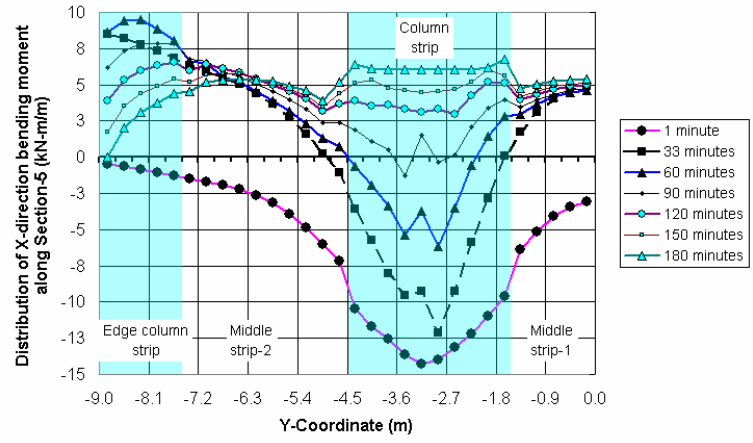

Figure 7-27 Distribution of X-direction bending moments along Section-5

Development of X-direction bending moments in the slab

For comparing the changes of the magnitude of bending moments in the slab against the time of fire exposure, X-direction average bending moments in the strips along Section-1 and Section-5 are plotted in Figure 7-28 (a) and Figure 7-28 (b), respectively.

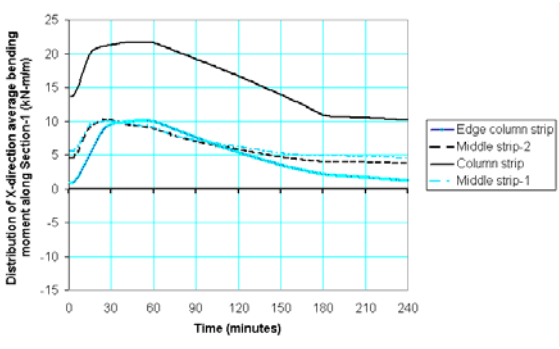

(a) X-direction average bending moments in the strips along Section-1

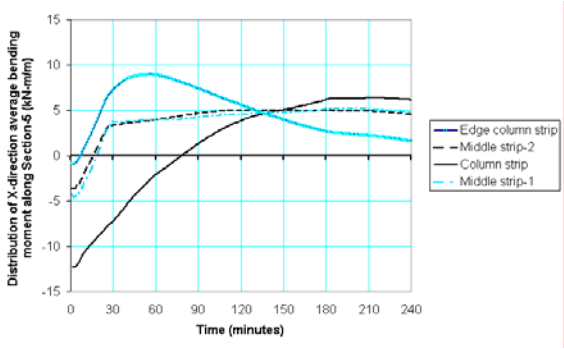

(b) X-direction average bending moments in the strips along Section-5

Figure 7-28 X-direction average bending moments along Section-1 and Section-5

Figure 7-28 (a) shows that the average bending moments in the strips along Section-1 were positive throughout the simulation of the slab in the fire. In Column strip the bending moment increased from 14kN-m/m at 1 minute to 20kN-m/m at 15 minutes and then started to form a plateau until 60 minutes; after that, it linearly declined from 22kN-m/m at 60 minutes to 10kN-m/m at 180 minutes. After 180 minutes, the other plateau of the bending moment was formed in Column strip. There were two crinkles on the bending moment curve in Column strip; one was at 60 minutes and another one was at 180 minutes. The bending moment curves in Edge column strip, Middle strip-1, and Middle strip-2 had a similar trend to the curve in Column strip, but the magnitude of bending moments was smaller than in Column strip.

Figure 7-28 (b) shows that the average bending moment in Column strip along Section-5 continuously increased from -12.4kN-m/m at 1 minute to 6kN-m/m at 180 minutes and then almost remained a constant value until the end of the simulation. There was a crinkle on the bending moment curve in Column strip at 180 minutes. The trend and magnitude of bending moments in Edge column strip was the same in Middle strip-2. The curves of bending moments in these two strips rose from 1 minute to 30 minutes and then started to form a huge bending moment plateau until the end of the simulation. The curve of Middle strip-1 fluctuated from 1 minute to 180 minutes and linearly declined until 240 minutes. There were two crinkles on the curves in Edge column strip and Middle strip-2: one was at 30 minutes and another was at 180 minutes.

The development of the redistribution of bending moments is a complicated procedure in the flat slab exposed to fire. The significant redistribution of bending moments occurred at the first stage of fire exposure. The main trend of the redistribution of bending moments in the

slab was from the negative bending moments (the tensile forces in the bottom reinforcing bars) to the positive bending moments (the tensile forces in the top reinforcing bars) because the temperatures of the reinforcing bars in the bottom of the slab rose more quickly than in the top of the slab. The negative flexural capacity of the slab significantly declined when the temperatures of the bottom reinforcing bars exceeded 300^{o}C because the yield strength of the hot-rolled steel started to decrease at 300^{o}C, as shown earlier in Figure 2-18.

7.4.3. Membrane forces of the slab in fire conditions

The X-direction membrane forces of the slab are analysed in this part of the section. It is found that the arrangement of reinforcing bars affects the distribution of membrane forces; the tensile membrane forces lag occurs in the middle strips of the flat slab exposed to fires.

Distribution of X-direction membrane forces in the slab

Figure 7-29 (a) and Figure 7-29 (b) show the distributions of X-direction membrane forces in the flat slab at 60 minutes and 180 minutes, respectively. The graphs show that the patterns of the membrane forces were similar to the patterns of the bending moments shown earlier in Figure 7-25. The trend of the distribution of the membrane forces in the slab can be classified into four regions that were relative to the arrangement of the reinforcing bars in the slab. The four regions, whose notations were the same as the regions in the bending moment of the slab, were Edge column strip, Column strip, Middle strip-1, and Middle strip-2 (Figure 7-8).

Figure 7-29 (a) shows that the membrane forces were tensile forces in Column strip and compressive forces in the other strips at 60 minutes. Figure 7-29 (b) shows that the membrane forces were tensile forces at 180 minute in all the strips.

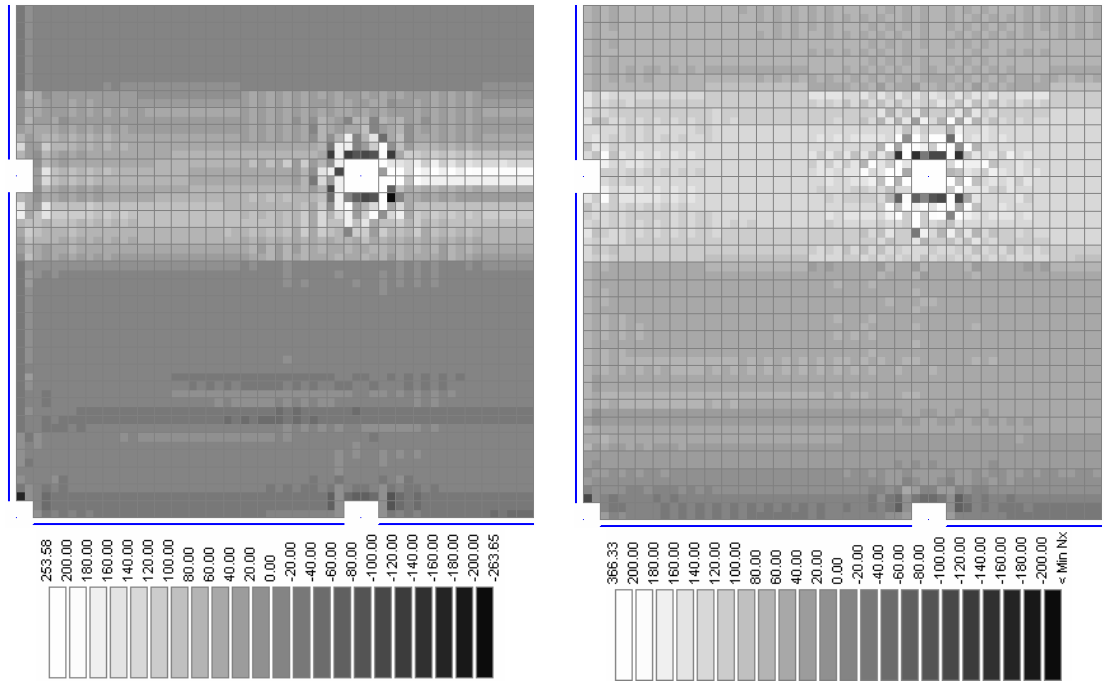

(a) 60 minutes (b) 180 minutes

Figure 7-29 Distributions of X-direction membrane forces in the slab at 60 minutes and 180 minutes

Figure 7-30 shows the distribution of X-direction membrane forces along Section-1. The graph shows that the distribution of membrane forces in Column strip and Edge column strip was like a seesaw along Section-1 because of the effect of the restraint of the columns on the slab. The distribution of membrane forces in Middle strip-1 and Middle strip-2 was much smoother than in Edge column strip and Column strip. The tensile membrane forces were present throughout the simulation in Column strip and after 60 minutes in the other strips. The compressive membrane forces were present in Edge column strip, Middle strip-1, and Middle strip-2 before 60 minutes.

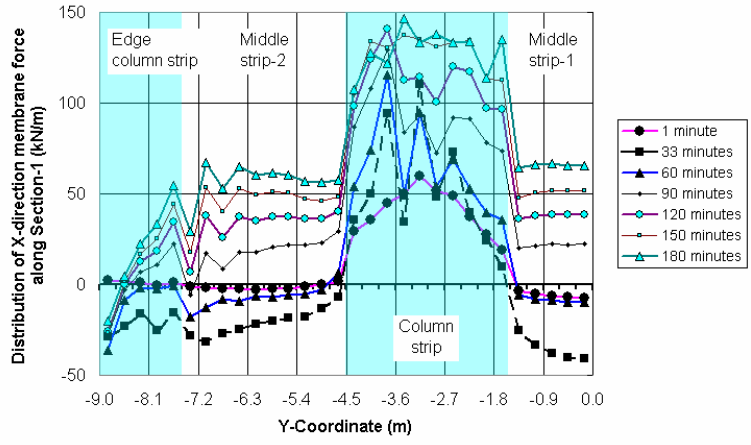

Figure 7-30 Distribution of X-direction membrane forces along Section-1

The distribution of X-direction membrane forces along Section-5 was similar to along Section-1, as shown in Figure 7-31. It shows that the distribution of membrane forces in Edge column strip along Section-5 had less fluctuation than along Section-1 because the effect of the restraint of the columns on the slab was less in Edge column strip.

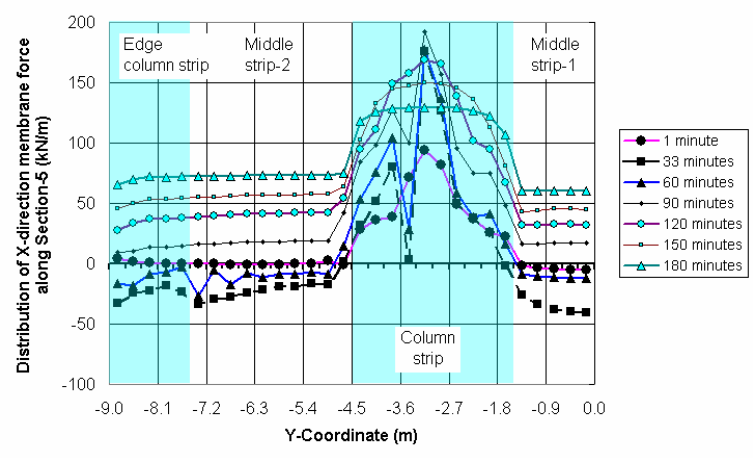

Figure 7-31 Distribution of X-direction membrane forces along Section-5

Development of X-direction membrane forces in the slab

Figure 7-32 shows the average membrane forces along Section-1 and Section-5 in Edge column strip, Column strip, Middle strip-1, and Middle strip-2. In Column strip the trend of the average membrane forces along Section-1 was similar with along Section-5. The tensile membrane forces in Column strip slightly declined at the first stage of fire exposure, and then constantly increased to 130kN/m at about 150 minutes. After that, it slightly declined to 120kN/m at the end of the simulation. In Middle strip-1 and Middle strip-2, the compressive membrane forces developed until about 60 minutes and at 30 minutes the maximum compressive membrane force was reached. After 60 minutes, the membrane forces became tensile forces in these strips and increased to about 70kN/m at 180 minutes, and then slightly decrease until 240 minutes, when the simulation was stopped. The phenomenon of the tensile membrane force lag was present in Middle strip-1 and Middle strip-2 because of the effect of the restraint of the columns and edge beams on the slab. Therefore, the reinforcing bars, especially the top reinforcing bars, arranged continuously in the column strips can enhance the capacity of preventing the collapse of the slab.

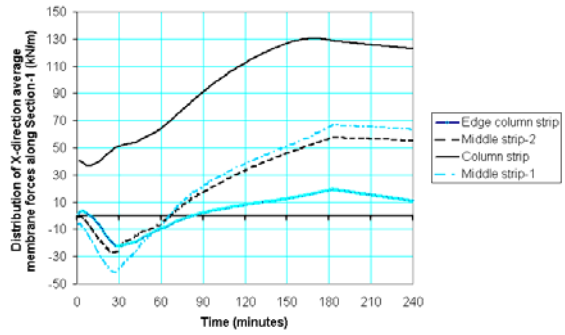

(a) X-direction membrane forces in the strips along Section-1

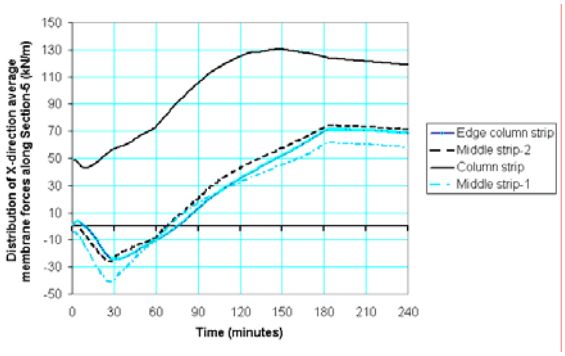

(b) X-direction membrane forces in the strips along Section-5

Figure 7-32 X-direction average membrane forces in the strips along Section-1 and Section-5

7.4.4. Conclusions

The analysis of the nine-bay flat slab with all bays exposed to an ISO 834 Standard fire without a decay phase has found that:

- The thermal conditions of the edge beams significantly affect the vertical and horizontal displacements of the slab.
- The redistribution of bending moments in the slab is drastically affected by the arrangement and quantity of reinforcing bars in the slab.
- The arrangement of reinforcing bars affects the distribution of the membrane forces in the slab.
- The tensile membrane force lag is present in the middle strip of the flat slab exposed to fires because of the effect of the restraint of the columns and edge beams on the slab.
- The arrangement and quantity of the top reinforcing bars in the column strip are important for improving the fire endurance and preventing the collapse of the slab in fire conditions.

7.5. Fire with a Decay Phase beneath All Bays of the Nine-Bay Flat Slab

This section presents a nine-bay flat slab fully exposed to an ISO 834 Standard fire with a decay phase. The purpose of this section is to investigate the behaviour of the slab when all the bays and all the edge beams are exposed to the fire with a decay phase. The slab is surrounded by edge beams and supported on the edge beams and columns. The edge beams are partially exposed to the fire and the columns are at ambient temperature conditions throughout the simulation. The fire exhausts at 170 minutes, but the simulation is extended up to 200 minutes. Typically, the decay phase of the fire is not considered in the fire endurance tests of slabs. However, some concrete buildings have collapsed after the fires have been controlled in some actual incidents of fires, as reviewed in Chapter 2.

7.5.1. Displacements of the slab in fire conditions

This part of the section investigates the vertical and horizontal displacements of the slab exposed to the fire with a decay phase. It is found that the thermal conditions and axial stiffness of the edge beams significantly affect the vertical and horizontal displacement of the slab in the fire.

Vertical deflections of the slab

Figure 7-33 shows the vertical deflections of the slab exposed to the fire with a decay phase at Point-A1, Point-B1, Point-C1, and Point-D1; the vertical deflections of the slab exposed to the fire without a decay phase at Point-A1 are also plotted in this graph for comparisons. The vertical deflection at Point-A1 was nearly a constant of 0.230m from 75 minutes to 140 minutes and constantly dropped to 0.260m at 170 minutes. The maximum vertical deflection at Point-A1 was 0.260m at 170 minutes when the fire exhausted and then slightly declined to 0.255 until the end of the simulation. The vertical deflections at Point-B1 and Point-C1 had a similar trend to that at Point-A1, while the vertical deflection at Point-D1 was very small due to the effect of the edge beams which have a large flexural stiffness of the cross-section. At the end of the simulation, the diversity of the vertical deflections between at Point-A1 and Point-B1 was 0.079m. There were no crinkles in the deflection curves. It is evident that the slab did not collapse and did not deform to a catenary at the end of the simulation. The slab did not collapse because of the redistribution of bending moments, the development of membrane forces in the slab, and the effect of the restraint of the edge beams on the slab. The

increase of the vertical deflections of the flat slab in the decay phase of the fire was small compared to those in the fire without a decay phase because of the redistribution of bending moments and the development of membrane forces in the slab.

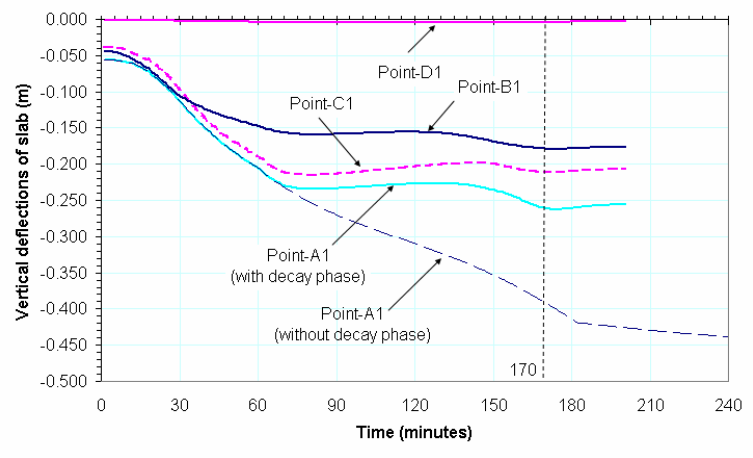

Figure 7-33 Vertical deflections of the slab at Point-A1, -B1, -C1, and –D1 in the fire with a decay phase

Figure 7-34 shows the distributions of the vertical deflections of the slab at 180 minutes under the fire with a decay phase. The vertical deflections of most parts of the slab were less than 0.2m. The regions where the vertical deflections were greater than 0.2m were in the middle parts of the plates.

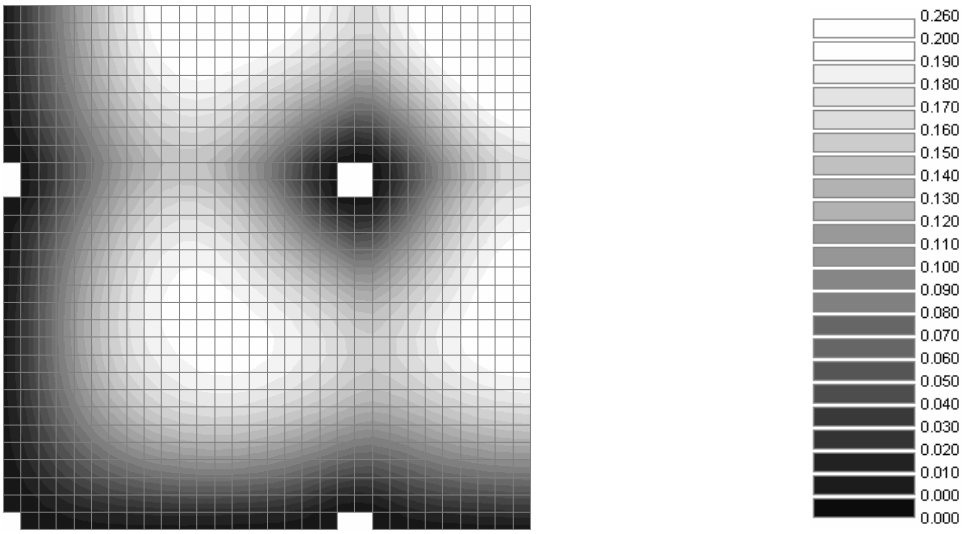

Figure 7-34 Vertical deflections of the slab at 180 minutes in the fire with a decay phase

Figure 7-35 shows the deflected shape of the slab exposed to the fire with a decay phase at 180 minutes. The pattern was similar to the pattern present earlier in Figure 7-20, but the value of the vertical deflections was significantly smaller than the value in Figure 7-20.

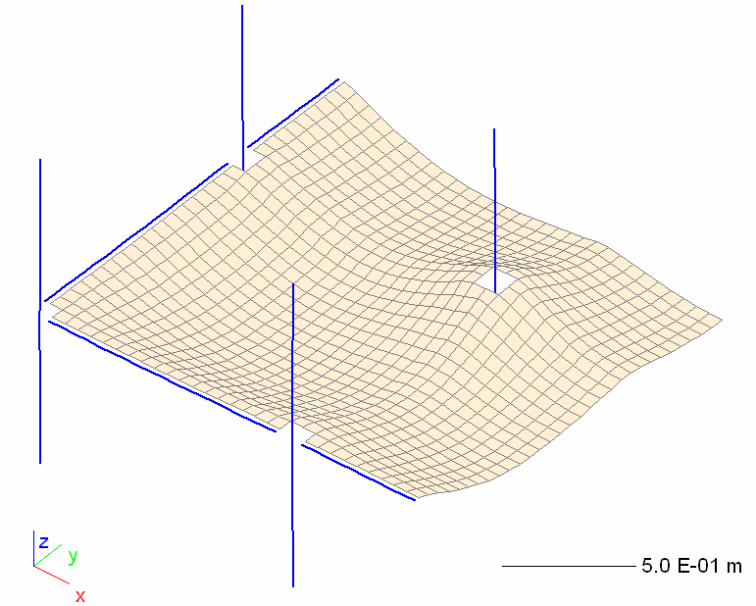

Figure 7-35 Vertical deflected shape of the slab at 180 minutes in the fire with a decay phase (scale factor: 5)

Horizontal displacements of the slab

Figure 7-36 shows the distribution of X-direction displacements from Point-B2 to Point-A2 in the slab exposed to the fire with a decay phase. The maximum X-direction displacement was in Column strip. The movements of the slab were towards the central part of the slab after 60 minutes. The horizontal movements of the slab were affected by the horizontal bowing action of the edge beams, the development of membrane forces in the slab, and the restraint of the columns to the slab.

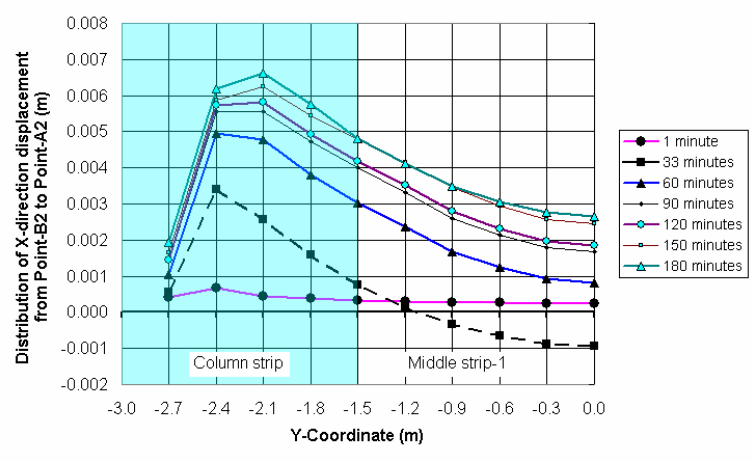

Figure 7-36 Distribution of X-direction displacements from Point-B2 to Point-A2 in the fire with a decay phase

Figure 7-37 shows a comparison of X-direction displacements at Point-A2 of the slab exposed to the fire with or without a decay phase. In the decay phase of the fire, The X-direction displacement at Point-A2 increased from 0.0018m at 75 minutes to 0.0029m at 160 minutes because the thermal expansion of the edge beams could not develop when the edge beams cooled down and the columns pushed the edge beams towards the centre of the slab. The tensile membrane forces developed in the slab when it cooled down due to the restraint of the edge beams and columns to the slab.

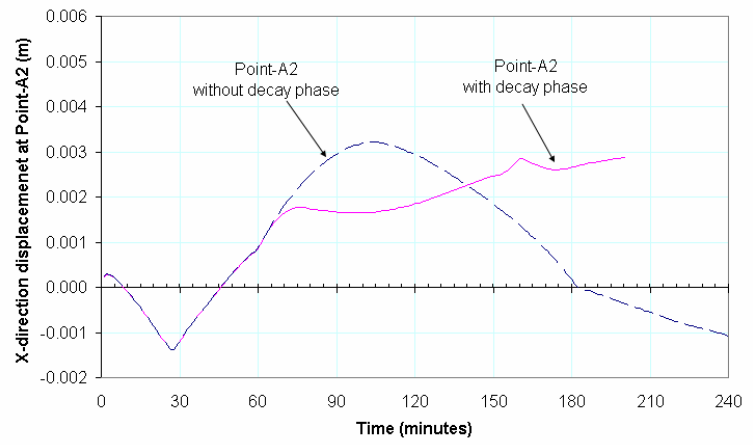

Figure 7-37 Comparison of X-direction displacements at Point-B2 of the slab in the fire with or without a decay phase

Figure 7-38 shows the X-direction displacements at Point-B2, Point-B4, Point-D2, and Point-D4 (cetroids of the columns) when the slab was exposed to the fire with a decay phase. X-direction displacement at Point-B4 was more variable than at Point-D2. The edge beams were

arranged along the X-direction at Point-D2 and significantly affected the X-direction displacements, whilst the edge beams were arranged along the Y-direction at Point-B4 and did not affect the X-direction displacements too much because the axial stiffness of the beams was much greater than the lateral stiffness of the beams. The X-direction displacement at Point-D4 of the slab exposed to the fire without a decay phase is also illustrated in Figure 7-38. Comparing the curves of X-direction displacements at Point-D4 for the slab in the fire with and without the decay phase, it is evident that the thermal conditions of the edge beams greatly affected the horizontal movements of the slab.

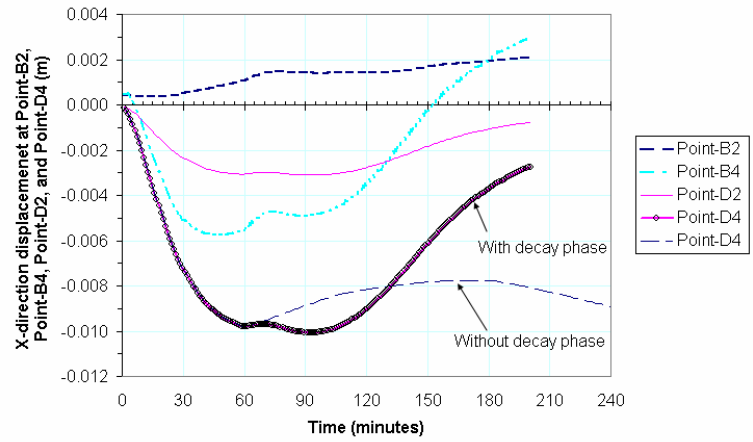

Figure 7-38 X-direction displacements at Point-B2, -B4, -D2, and -D4 in the fire with a decay phase

7.5.2. Bending moments of the slab in fire conditions

In this part of the section, the bending moments of the slab exposed to an ISO 834 Standard fire with a decay phase are discussed. A significant redistribution of bending moments in the decay phase of the fire is to be found and thermal bowing action of the slab in the decay phase contributes to the formation of the pattern of the vertical deflections of the slab.

Redistribution of X-direction bending moments in the slab

Figure 7-39 shows the curvatures of X-direction bending moments along Strip-A, Strip-B, Strip-D, and Strip-E. In the decay phase the redistribution of bending moments in the slab was significant than those before the decay phase of the fire. At 180 minutes the bending moments in all the strips became negative. The maximum bending moment of -20kN-m/m was reached at 180 minutes in Strip-D, which was in Column strip of the slab; this peak value was two times the value of the bending moment at ambient temperature conditions.

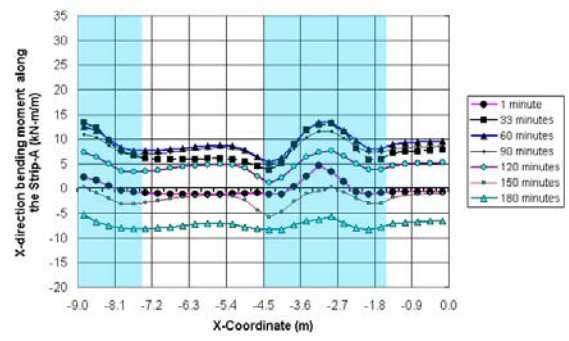

(a) X-direction bending moments along Strip-A

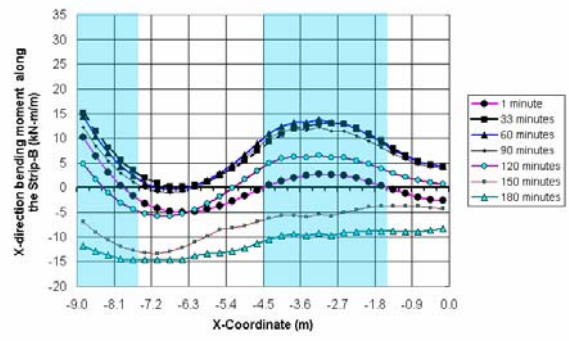

(b) X-direction bending moments along Strip-B

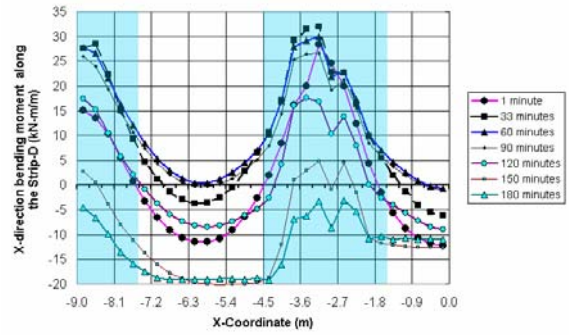

(c) X-direction bending moments along Strip-D

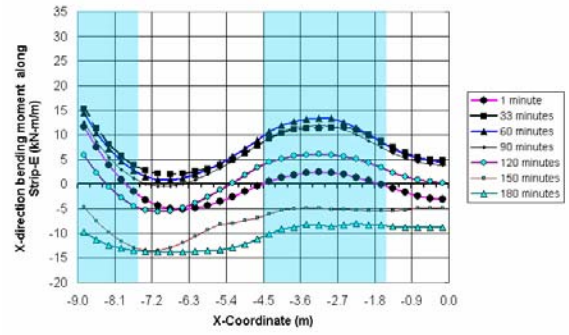

(d) X-direction bending moments along Strip-E

Figure 7-39 X-direction bending moments along Strip-A, Strip-B, Strip-D, and Strip-E in the fire with a decay phase

Distribution of X-direction bending moments in the slab

The distributions of X-direction bending moments in the slab exposed to the fire with a decay phase at 75 minutes and 180 minutes are shown in Figure 7-40 (a) and Figure 7-40 (b), respectively. At 75 minutes the values of the bending moments for most parts of the slab were positive values, but at 180 minutes the values of the bending moments became negative values. The larger negative bending moments were present in the midspan of the slab along Column strip.

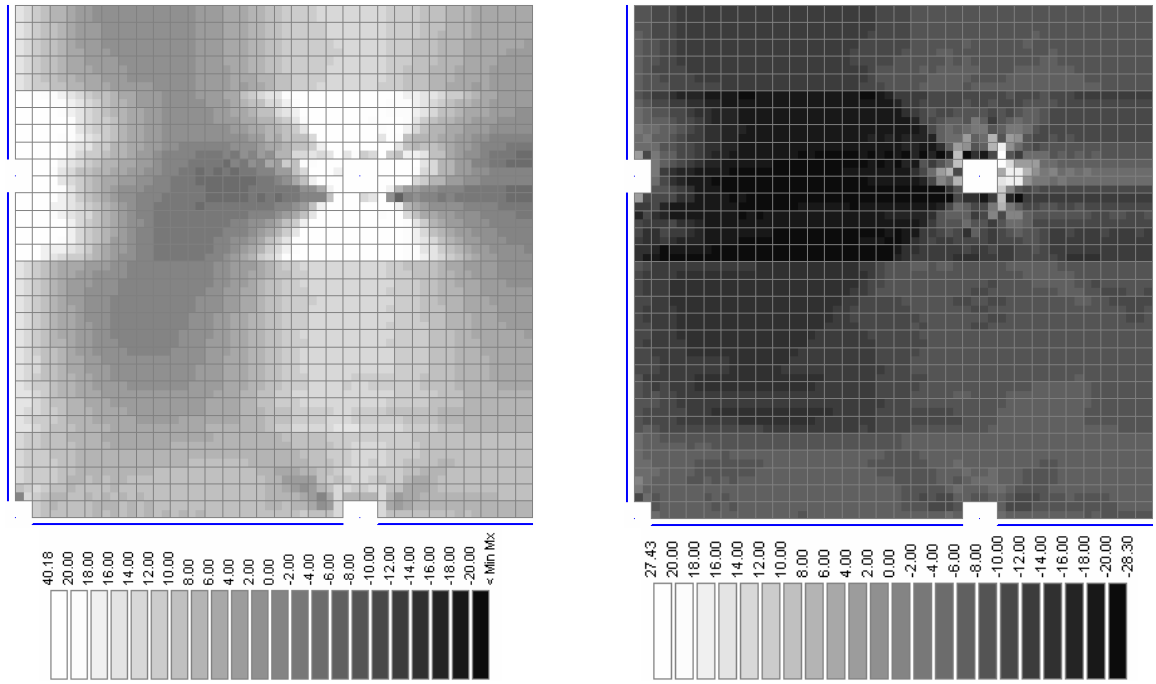

(a) At 75 minutes (b) At 180 minutes

Figure 7-40 Distributions of X-direction bending moments at 75 minutes and 180 minutes in the fire with a decay phase

The distribution of X-direction bending moments along Section-1 is shown in Figure 7-41. It shows that the X-direction bending moments in Column strip were more unstable, while in the other strips they were smoother than in Column strip, especially in Middle strip-1, where the bending moments were almost constantly distributed along Section-1.

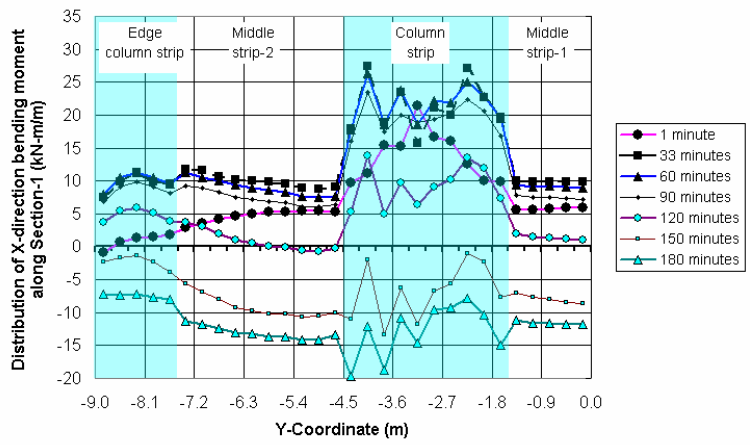

Figure 7-41 Distribution of X-direction bending moments along Section-1 in the fire with a decay phase

The distribution of X-direction bending moments along Section-5 is shown in Figure 7-42. The deviation of the bending moments in Column strip was slighter than in Section-1 because the effect of the restraints of the columns to the slab was reduced in Section-5.

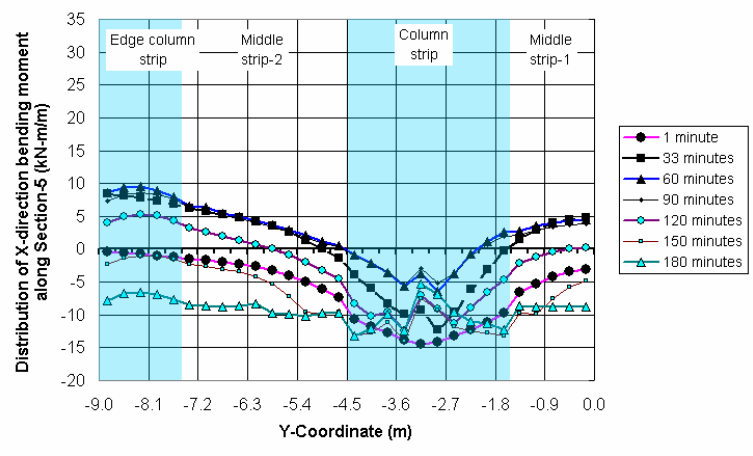

Figure 7-42 Distribution of X-direction bending moments along Section-5 in the fire with decay phase

Development of X-direction bending moments in the slab

The average bending moments in the strips along Section-1 and Section-5 are shown in Figure 7-43 and Figure 7-44, respectively. Figure 7-43 shows that the significant changes of the bending moments in the decay phase of the fire occurred in Column strip where the bending moments dropped from 20kN-m/m at 75 minutes to zero at 135 minutes and reached -13kN m/m at 170 minutes because the bottom reinforcing bars cooled down and the length of the reinforcing bars became shorter; meanwhile, the temperatures of the top concrete continuously rose; as a result, the compressive membrane forces developed on the top concrete.

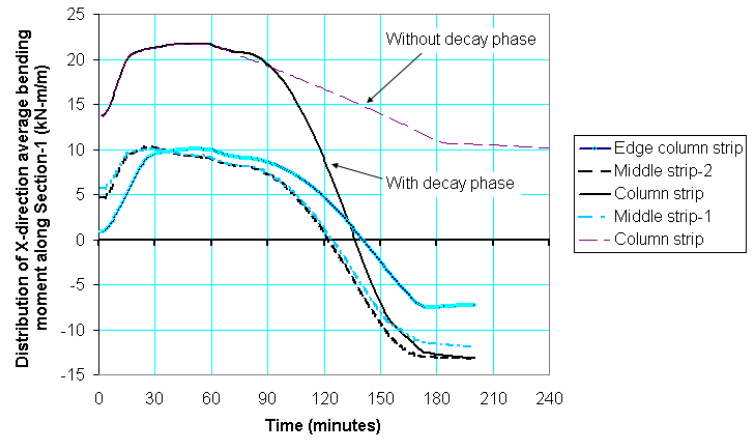

Figure 7-43 X-direction average bending moments in the strips along Section-1

Figure 7-44 shows that the X-direction average bending moment in Column strip declined from -12.5kN-m/m at 1 minute to -1.0kN-m/m at 75 minutes, and then increased to -12.0kN m/m at 135 minutes; after that, it slightly declined to -10.0kN-m/m at the end of the simulation. The trend and magnitude of the bending moments of the slab in the fire with and without a decay phase were completely different after 75 minutes. The decay phase of the fire significantly affected the distribution and redistribution of bending moments in the slab.

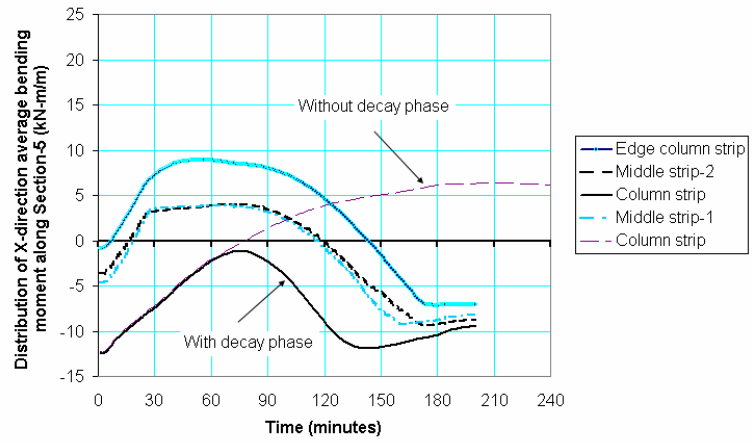

Figure 7-44 X-direction average bending moments in the strips along Section-5

7.5.3. Membrane forces of the slab in fire conditions

This part of the section presents the X-direction membrane forces in the slab when the slab was exposed to the fire with a decay phase. It is found that the distribution of the membrane forces is affected by the arrangement of the reinforcing bars in the slab and the magnitude of the tensile membrane forces dramatically increase in the decay phase of the fire.

Distribution of X-direction membrane forces in the slab

Figure 7-45 (a) and Figure 7-45 (b) show the distributions of X-direction membrane forces in the slab exposed to the fire with a decay phase at 75 minutes and 180 minutes, respectively. The trend of the distribution of the membrane forces in the slab can be divided into four regions that depended on the arrangement of the reinforcing bars in the slab. The notations of the four regions were Edge column strip, Column strip, Middle strip-1, and Middle strip-2, as shown earlier in Figure 7-8. The tensile membrane forces developed in Column strip throughout the simulation, while the compressive and tensile membrane forces were present

in the other strips. The tensile membrane forces mainly developed in the strips of the slab within and after the decay phase of the fire due to the reduction of the temperatures of the bottom reinforcing bars in the slab.

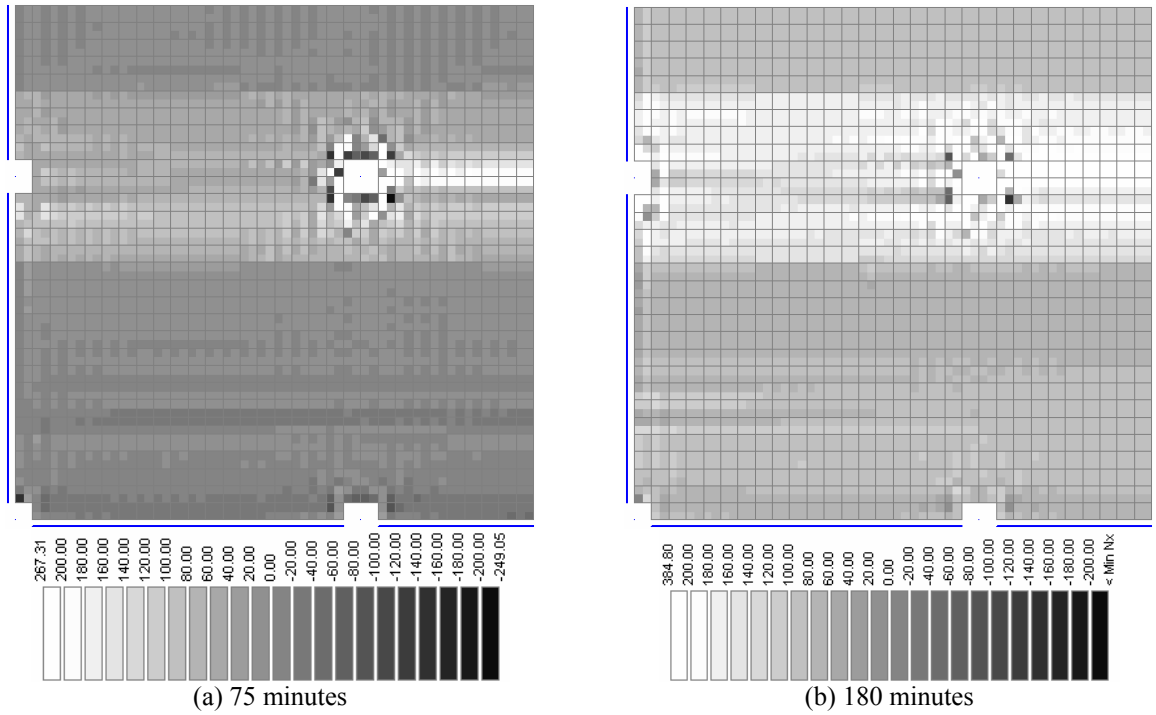

(a) 75 minutes (b) 180 minutes

Figure 7-45 Distributions of X-direction membrane forces in the slab at 75 minutes and 180 minutes in the fire with a decay phase

Figure 7-46 shows the distribution of X-direction membrane forces along Section-1 when the slab was exposed to the fire with a decay phase. The graph shows that the distribution of the membrane forces in Edge column strip, Middle strip-2, and Column strip was variable along Section-1 within and after the decay phase of the fire because of the effects of the restraint of the columns and the decrease of temperatures of the edge beams within and after the decay phase of the fire. The distribution of the membrane forces in Middle strip-1 along Section-1 was much smoother than in the other strips.

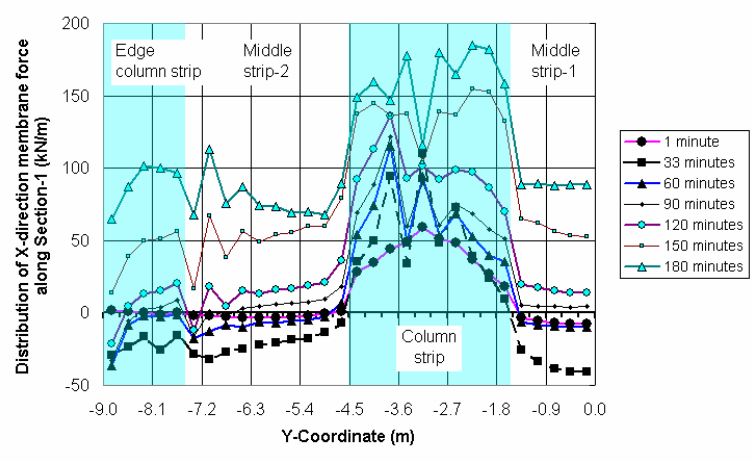

Figure 7-46 Distribution of X-direction membrane forces along Section-1 in the fire with a decay phase

Figure 7-47 shows the distribution of X-direction membrane forces along Section-5 when the slab was exposed to the fire with a decay phase. The graph shows that the distribution of membrane forces in the Column strip was variable along Section-5, while the distribution of membrane forces in Edge column strip and Middle strip-1 along Section-5 within and after the decay phase of the fire had less fluctuation than along Section-1.

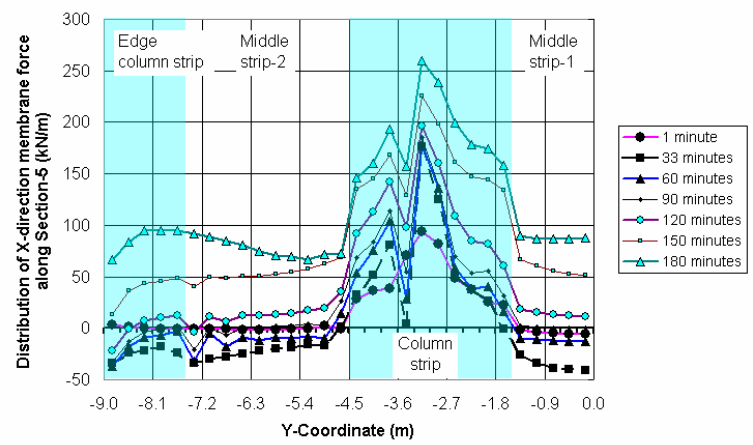

Figure 7-47 Distribution of X-direction membrane forces along Section-5 in the fire with a decay phase

Development of X-direction membrane forces in the slab

Figure 7-48 (a) and Figure 7-48 (b) show the average membrane forces along Section-1 and Section-5 in the strips when the slab was exposed to the fire with a decay phase, respectively. The average membrane forces along Section-1 and Section-5 in Column strip when the slab was exposed to the fire without a decay phase are also plotted in these figures. The development of membrane forces was the same between the slabs exposed to the fire with and

without a decay phase before 75 minutes; after 75 minutes the trend and magnitude of the membrane forces were totally different between the slabs exposed to the fire with and without a decay phase. Along Section-1, the membrane forces increased from 73kN/m at 75 minutes to 170kN/m at the end of the simulation when the slab was exposed to the fire with a decay phase. Along Section-5, the membrane forces dramatically increased from 85kN/m at 75 minutes to 200kN/m at the end of the simulation when the slab was exposed to the fire with a decay phase. The trend and magnitude of the membrane forces were almost the same within Middle strip-1, Middle strip-2 and Edge column strip along Section-1 and Section-5. The tensile membrane force lag was present in Middle strip-1, Middle strip-2, and Edge column strip along Section-1 and Section-5 because the compressive membrane forces developed in these strips.

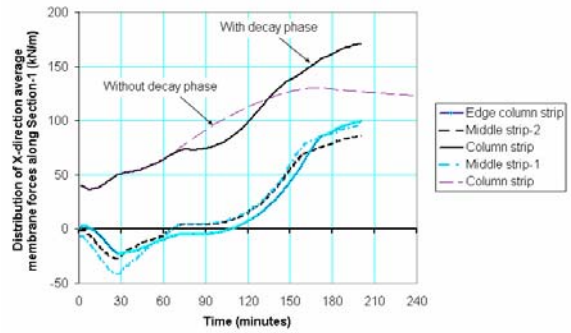

(a) X-direction average membrane forces in the strips along Section-1

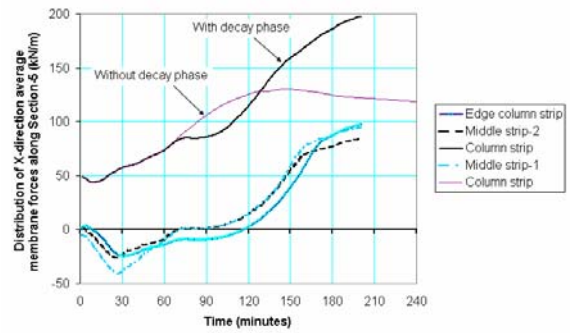

(a) X-direction average membrane forces in the strips along Section-5

Figure 7-48 X-direction average membrane forces in the strips along Section-1 and Section-5

7.5.4. Conclusions

The analysis of the nine-bay flat slab with all bays exposed to an ISO 834 Standard fire with a decay phase has found that:

- The thermal conditions of the edge beams significantly affect the vertical and horizontal displacements of the slab.
- The distribution and redistribution of bending moments significantly change within and after the decay phase of the fire.
- The tensile membrane forces dramatically increase within and after the decay phase of the fire.
- The tensile membrane force lag is present in the flat slab.
- The arrangement of reinforcing bars affects the distribution of membrane forces in the slab.
- The collapse of the slab could occur within or after the decay phase of the fire depending on the development of membrane forces and bending moments in the slab.
- It is recommended that further research of reinforced concrete slabs in fire conditions should focus on the behaviour of reinforced concrete slabs in fires with a decay phase.

7.6. Fire without a Decay Phase beneath the Middle Bay of the Nine-Bay Flat Slab

This section of the thesis investigates the behaviour of the nine-bay flat slab when its single middle bay is exposed to an ISO 834 Standard fire without a decay phase beneath, as shown in Figure 7-49. The purpose of this section is to investigate the behaviour of the slab when only one bay is exposed to the fire and all the edge beams are at ambient temperature conditions. The surrounding walls are in the centroid line of the columns. The breadth of the walls is 0.1m and it is assumed that the walls do not affect the development of vertical deflections of the slab. The boundary thermal conditions of the slab were detailed earlier in Chapter 4, as shown earlier in Figure 4-10 (b). A quarter of the flat slab (the Modelling region in Figure 7-49) is modelled using SAFIR. The edge beams and the columns are at ambient conditions throughout the simulation. The displacement of the slab and the membrane forces in the slab are discussed, while the bending moments in the slab are demonstrated in this section.

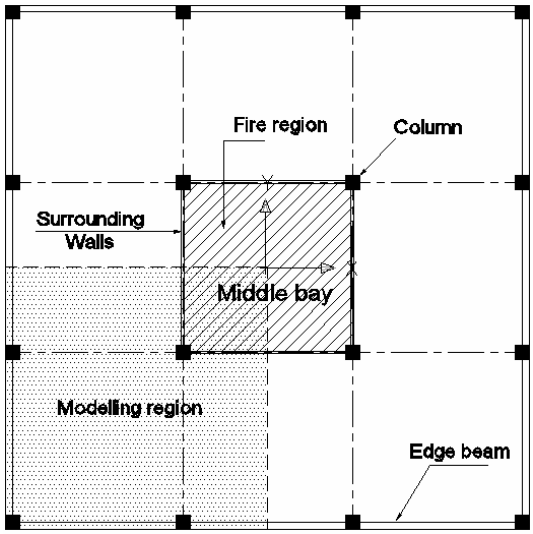

Figure 7-49 Plan view of the flat slab (the middle bay exposed to the fire)

7.6.1. Displacements of the slab

This part of the section investigates the vertical and horizontal displacements of the slab when its middle bay was exposed to the fire. It is found that the behaviour of the slab when the middle bay is exposed to the fire is better than the behaviour of the slab when all the bays are exposed to the fire. At the end of the simulation the slab does not deform to a catenary due to

the restraint of the surrounding structural members, which are at ambient temperature conditions, to the middle bay of the slab, which was in fire conditions.

Vertical deflections of the slab

Figure 7-50 shows the vertical deflections of the slab at Point-A1, Point-B1, Point-C1 and Point-D1 when the middle bay of the slab was exposed to the fire. The vertical deflection at Point-A1 when all the bays are exposed to the fire is also illustrated in the figure. The slab at Point-C1 and Point-D1 was at ambient temperature conditions (20^{o}C). The vertical deflection at Point-C1 slightly increased from 0.04m at 1 minute to 0.05m at the end of the simulation, while at Point-B1, which is at the fire distinct line, it smoothly increased from 0.045m at 1 minute to 0.15m at 240 minutes. The slab at Point-A1 was in the fire conditions throughout the simulation. The vertical deflection at Point-A1 dramatically increased from 0.06m at 1 minute to 0.38m at 240 minutes, but the slab did not deform to a catenary because a sufficient redistribution of bending moments developed in Column strip and the surrounding structural members of the middle bay were at ambient temperature conditions, which reduced the increase of the vertical deflections of the slab. The largest differential of the vertical deflections between at Point-B1 and Point-A1 was 0.23m at 240 minutes.

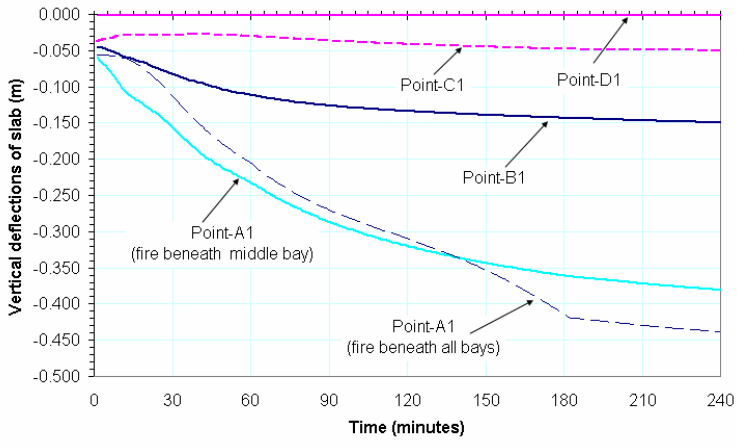

Figure 7-50 Vertical deflections of the slab at Point-A1, -B1, -C1, and –D1 (the middle bay in fire conditions)

Figure 7-51 shows the vertical deflections of the slab at 60 minutes and 180 minutes. The white colour in the graphs represents the vertical deflections are greater than 0.2m. The graphs show the corner panel of the slab was slightly affected by the fire because of the existence of the middle column, which restricted the increase of the vertical deflections of the

slab in the corner panel, while the column strips in the edge panel were significantly affected by the fire because of the large vertical deflections of the slab in the middle bay and the development of membrane forces in the slab.

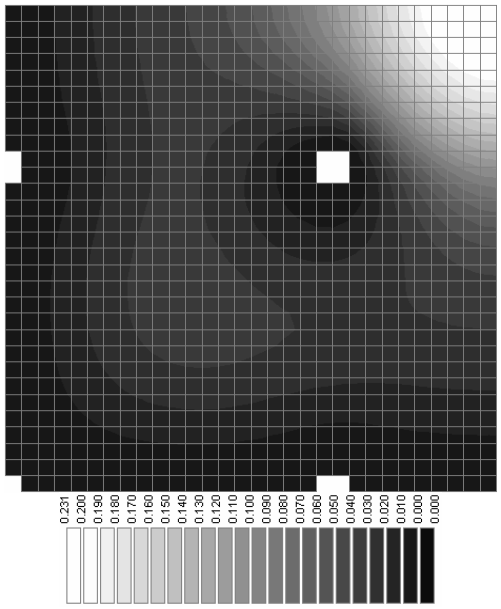

(a) Vertical deflections of the slab at 60 minutes

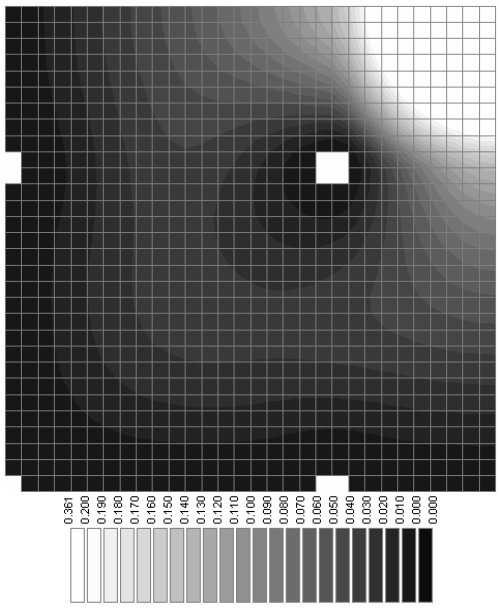

(b) Vertical deflections of the slab at 180 minutes

Figure 7-51 Vertical deflections of the slab at 60 and 180 minutes (the middle bay in fire conditions)

Figure 7-52 shows the deflected shape of the slab at 180 minutes. The slab in the fire room did not collapse due to the proper anchorage of the reinforcing bars in the slab to the surrounding slabs and columns, which were at ambient temperature conditions. The slab in the middle bay suffered the large deflection, which can be compared with the real fire scenario shown earlier in Figure 2.13 (a) and Figure 2.13 (b).

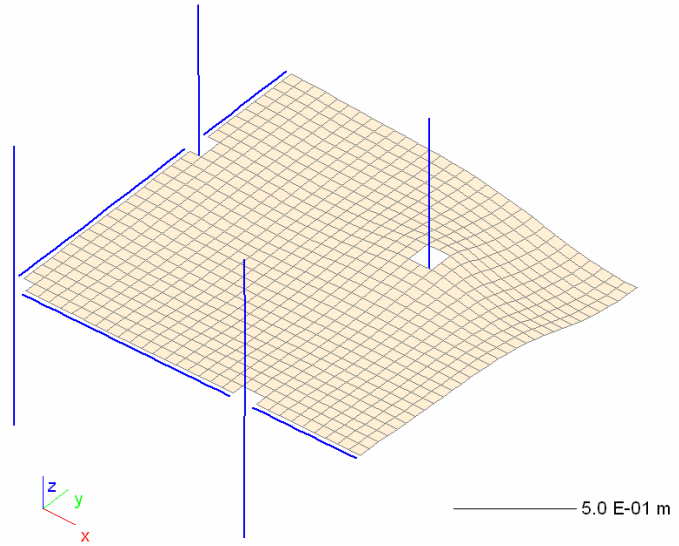

Figure 7-52 Vertical deflected shape of the slab at 180 minutes (scale factor: 5; the middle bay in fire conditions)

Horizontal displacements of the slab

Figure 7-53 shows the distribution of X-direction displacements of the slab from Point-B2 to Point-A2 when the middle bay of the slab was exposed to the fire. The variation of displacements when the middle by of the slab was exposed to the fire was smaller than that when all the bays were exposed to the fire mainly because the edge beams were at ambient temperature conditions. At the first stage of the fire the thermal thrust of the slab (or the compressive membrane force) developed in Middle strip, which increased the fire endurance of the slab.

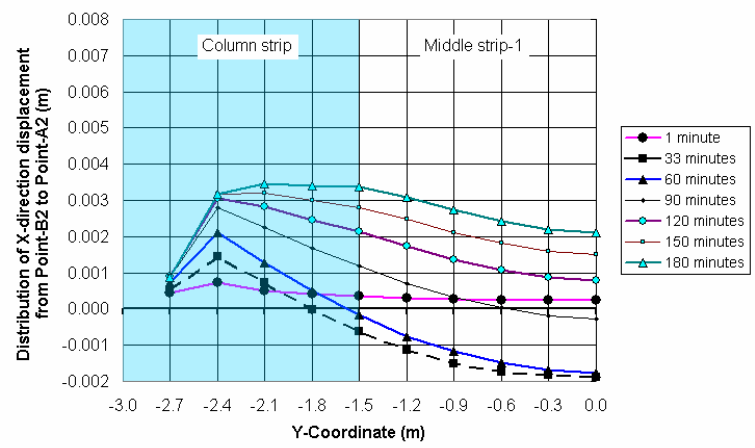

Figure 7-53 Distribution of X-direction displacements from Point-B2 to Point-A2 (the middle bay in fire conditions)

Figure 7-54 shows a comparison of X-direction displacements of the slab at Point-A2 exposed to the fire beneath the middle bay and beneath all the bays. At Point-A2, the value of the X-direction displacement at 95 minutes changed to a positive value when the fire was beneath the middle bay, while at 45 minutes it changed to a positive value when the fire was beneath all the bays. The negative value of X-direction displacements indicates that the compressive membrane forces had developed in the slab.

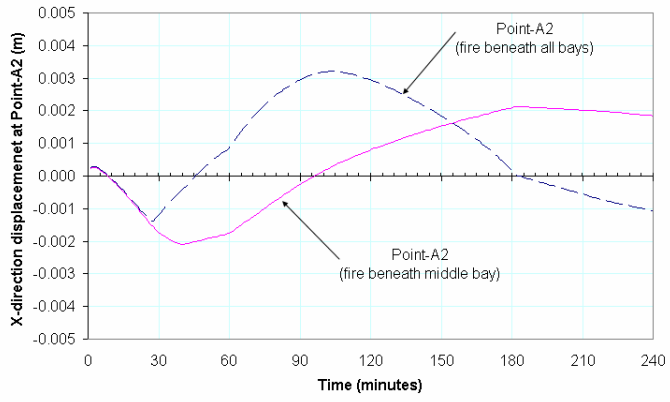

Figure 7-54 Comparison of X-direction displacements of the slab at Point-A2

7.6.2. Bending moments of the slab

Figure 7-55 shows the distributions of X-direction bending moments in the slab at 60 minutes and 180 minutes when the middle bay of the slab was exposed to the fire. The graphs show that redistributions of X-direction bending moments were mainly present in the middle bay (middle panel).

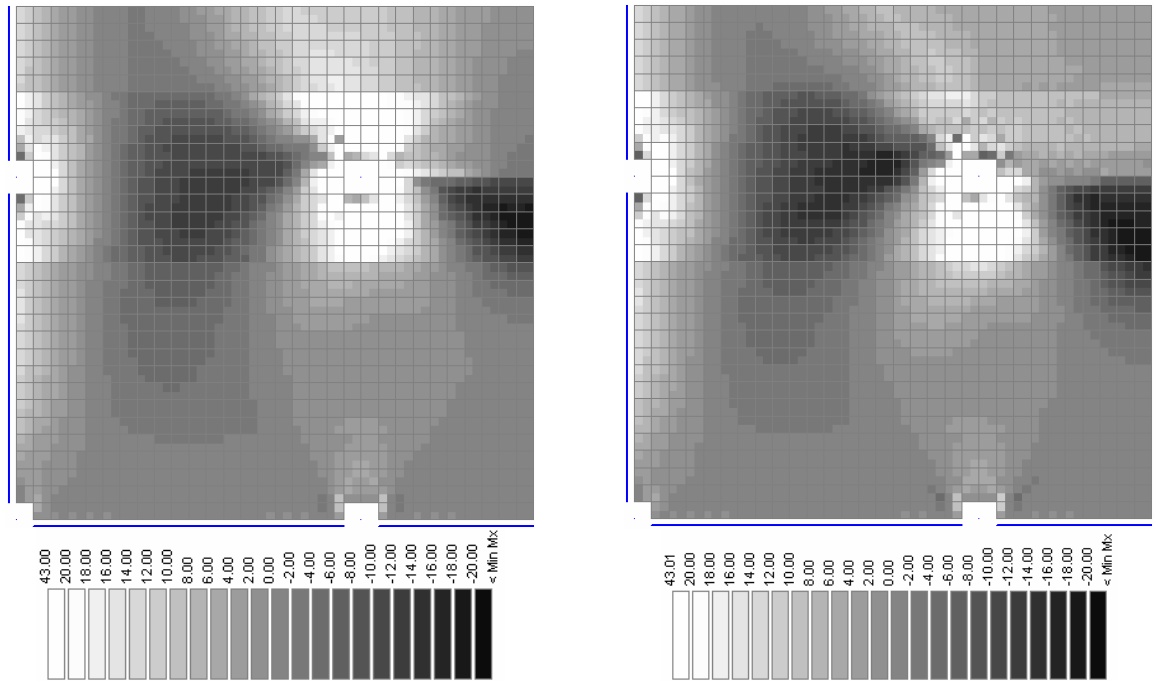

(a) At 60 minutes (b) At 180 minutes

Figure 7-55 Distributions of X-direction bending moments in the slab (the middle bay in fire conditions)

7.6.3. Membrane forces of the slab

The distribution of X-direction membrane forces in the slab along Section-5 is shown in Figure 7-56. It shows that the membrane forces in Edge column strip and Middle strip-2 were very small. The distribution of membrane forces in Column strip can be divided into two regions from the distinct line of the fire; one region was in the slab under fire exposure and another region was in the slab at ambient temperature conditions (20^{o}C). In Column strip the tensile membrane forces developed throughout the simulation. In the non-fire region of Column strip close to the distinct line of the fire, the tensile membrane forces sharply increased because the large strain, which was greatly affected by the large vertical deflection, developed in the reinforcing bars at ambient temperatures. The membrane forces in Middle

strip-1 linearly developed through Section-5. Before 90 minutes the membrane forces were compressive forces in Middle strip-1.

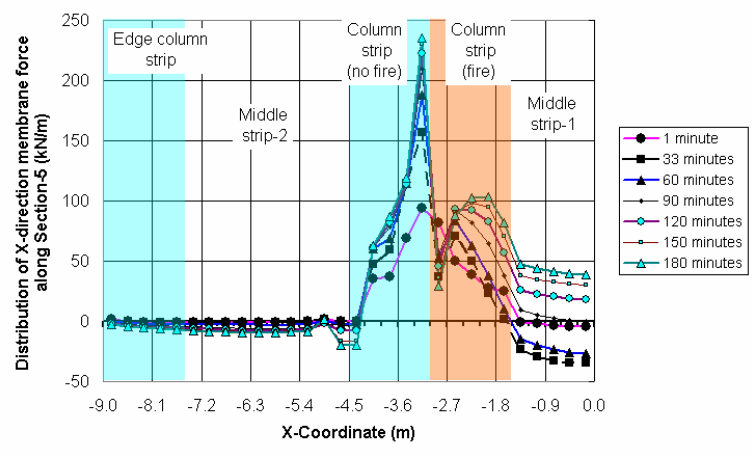

Figure 7-56 Distribution of X-direction membrane forces in the slab along Section-5 (the middle bay in fire conditions)

Figure 7-57 shows the X-direction average membrane forces in the strips along Section-5 when the middle bay of the slab was exposed to the fire. The membrane forces in the non-fire part of Column strip were greater than those in the fire part of Column strip. The membrane forces in the non-fire part of Column strip increased from 50kN/m at 1 minute to 100kN/m at the end of the simulation. The membrane forces were compressive forces in Middle strip-1 before 90 minutes; after that, the tensile membrane forces increased to 45kN/m at 180 minutes and remained a constant value of 45kN/m until the end of the simulation. The tensile membrane force lag presented in Middle strip-1 due to the development of compressive membrane forces in the slab before 90 minutes.

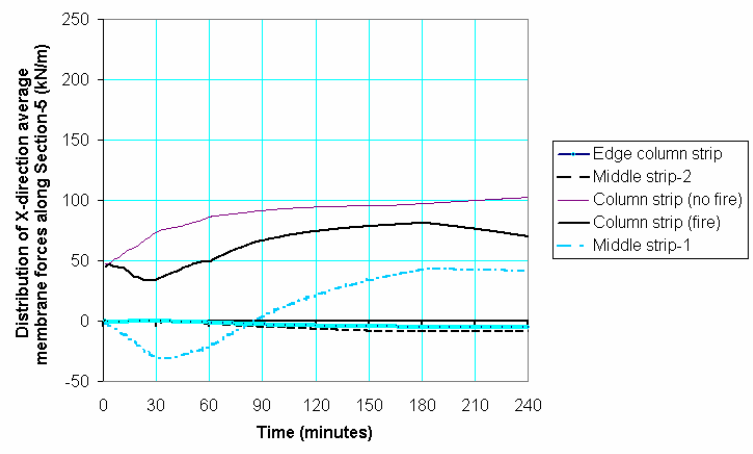

Figure 7-57 X-direction average membrane forces in the strips along Section-5 (the middle bay in fire conditions)

Figure 7-58 shows the distributions of X-direction membrane forces in the slab at 60 minutes and 180 minutes when the middle bay of the slab was exposed to the fire. The membrane forces along the strips were almost constant except in Column strip where the membrane forces around the fire distinct line were variable.

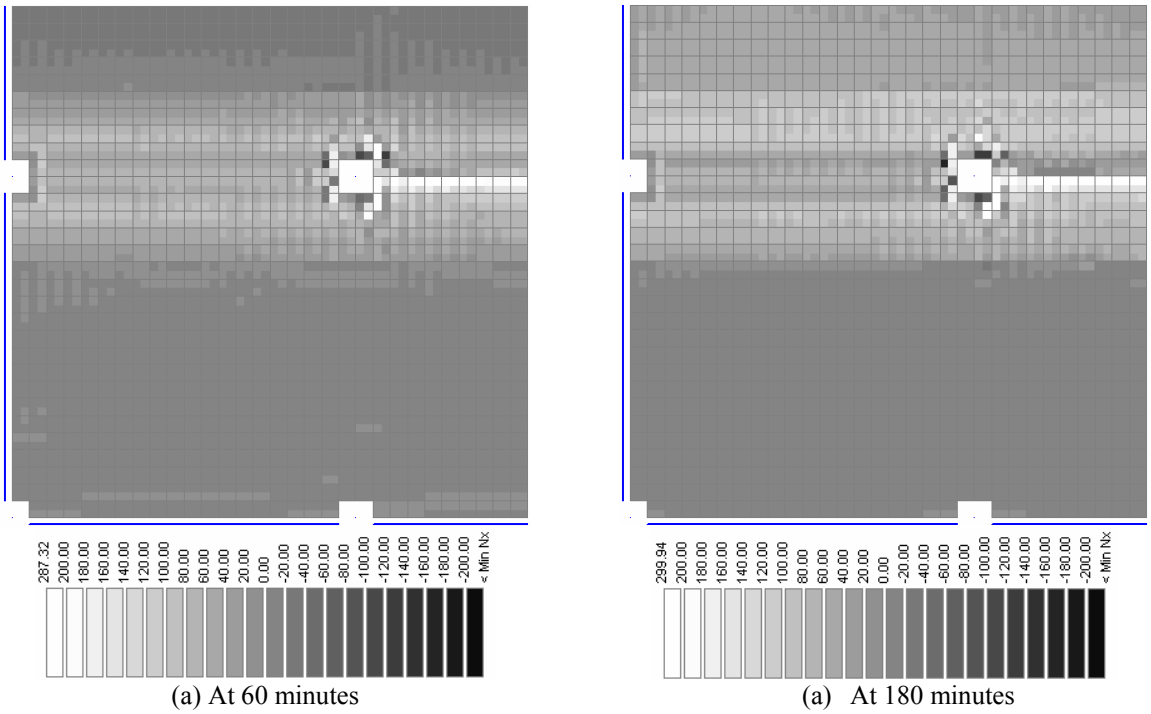

(a) At 60 minutes (a) At 180 minutes

Figure 7-58 Distributions of X-direction membrane force in the slab at 60 minutes and 180 minutes (the middle bay in fire conditions)

7.6.4. Conclusions

The analysis of the nine-bay flat slab when the single middle bay (the middle panel) was exposed to the fire has shown that:

- The slab does not deform to a catenary after four hours' fire exposure due to the restraint of the surrounding structural members, which are at ambient temperature conditions.
- The distribution of membrane forces in the column strip is different in the fire region and non-fire region; the magnitude of membrane forces in the non-fire region is greater than in the fire region.
- The tensile membrane force lag is present in Middle strip-1 due to the development of compressive membrane forces in Middle strip-1.
- The fire in the middle panel slightly affects the behaviour of the slab in the corner panel, but greatly affects the behaviour of the slab in the edge panels.

7.7. Fire without a Decay Phase beneath the Middle Strip Bays of the Nine-Bay Flat Slab

This section of the chapter investigates the behaviour of the middle strip bays of the slab which is exposed to an ISO 834 Standard fire without a decay phase. The plan view of the flat slab is shown in Figure 7-59. The purpose of this section is to investigate the behaviour of the slab when more bays (thee bays) are exposed to the fire. The surrounding walls of 0.1m thick are placed at the centroid lines of the columns on the slab. It is assumed that the surrounding walls do not affect the development of vertical deflections of the slab. Beam-4, as shown earlier in Figure 7-8, is under fire exposure, while the other beams and all the columns are at ambient temperature conditions throughout the simulation. A quarter of the flat slab is modelled using SAFIR due to the symmetry of the structure and the fire exposure to the two axes, the X-axis and the Y-axis. The thermal boundary conditions of the flat slab were detailed earlier in Chapter 4 of this thesis. The displacements of the slab and the membrane forces in the two directions, the X-direction and Y-direction, are discussed, while the bending moments in the two directions are demonstrated in this section.

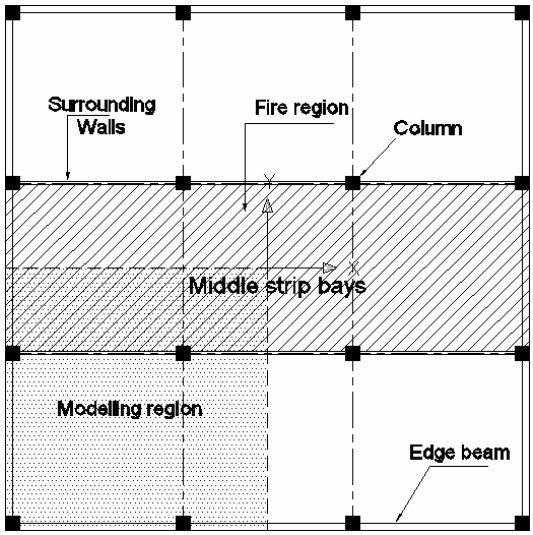

Figure 7-59 Plan view of the flat slab (middle strip bays exposed to the fire)

7.7.1. Displacements of the slab

Vertical deflections of the slab

Figure 7-60 shows the vertical deflections of the slab at Point-A1, Point-B1, Point-C1, Point-D1, Point-A2 and Point A3 when the middle strip bays of the slab were exposed to the

fire. The vertical deflections of all the bays of the slab exposed to the fire are also plotted in Figure 7-60 for comparing. Point-A1, Point-A2 and Point-A3 were in fire conditions throughout the simulation, whilst Point-C1 and Point-D1 were at ambient conditions. Point-B1 is at the distinct line of the fire. The vertical deflection at Point-A1 dropped quickly from 0.06m at 1 minute to 0.13m at 13 minutes because the development of Y-direction compressive membrane forces in Y-direction Middle strip-1 enhanced the thermal bowing of the slab. Meanwhile, the vertical deflection at Point-C1 slightly decreased from 0.04m to 0.03m. After that, the vertical deflection at Point-A1 continuously increased to 0.40m at 240 minutes, as at Point-B1, the vertical deflection slightly increased to 0.05m at 240 minutes due to the effect of the redistribution of bending moments in the slab. The vertical deflection at Point-B1 constantly increased from 0.04m at 1 minute to 0.17m at the end of the simulation. The differential of the vertical deflections between at Point-A1 and Point-B1 at 240 minutes was 0.23m. Before 150 minutes the vertical deflection at Point-A1 when the middle strip bays were exposed to the fire was greater than that when all the bays were exposed to fire because the vertical deflections in the first stage of the fire (1 minute to 17 minutes) when the middle strip bays were exposed to the fire were larger than that when all the bays were exposed to fire. The vertical deflection at Point-A3 had a similar trend to at Point-A1, but the magnitude of the deflection was smaller than at Point-A1. The vertical deflection at Point-A2 dramatically increased from 0.04m at 1 minute to 0.12m at 13 minutes, but after 13 minutes the increase of the deflection was slower than at Point-A1 and at 240 the deflection at Point-A2 increased to 0.27m. The differential of the vertical deflections between at Point-A1 and Point-A2 was 0.13m at 240 minutes, which was less than the differential between at Point-A1 and Point-B1.

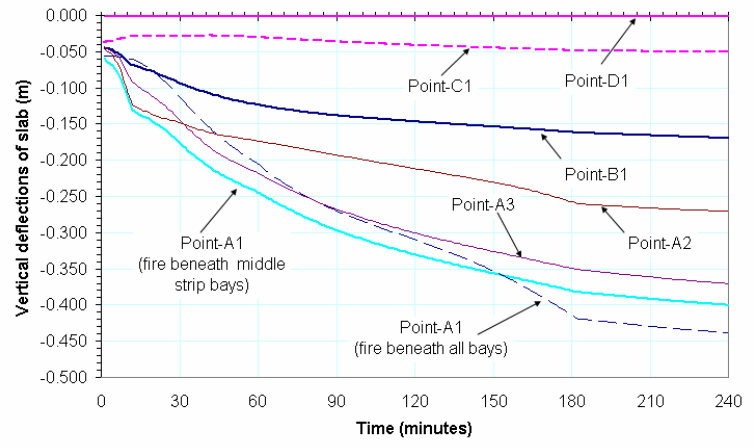

Figure 7-60 Vertical deflections of the slab at Point-A1, -B1, -C1, –D1, A2, and A3 (the middle strip bays in fire conditions)

The distributions of the vertical deflections of the slab at 60 minutes and 180 minutes when the middle strip bays were exposed to the fire is shown in Figure 7-61. The white colour in the graphs represents the vertical deflections are greater than 0.2m. Figure 7-61 (b) shows that the vertical deflections in most parts of the middle strip bays were greater than 0.2m because the large vertical deflections of the slab were affected not only by the thermal bowing action at the rise of the temperatures in the slab but also by the other factors, such as the redistribution of bending moments in the slab, the declined flexile stiffness of the slab, and P-Δ action at large vertical deflections. The development of vertical deflections of the slab under fire exposure is a complicated procedure, which can not be predicted only using simple calculated methods.

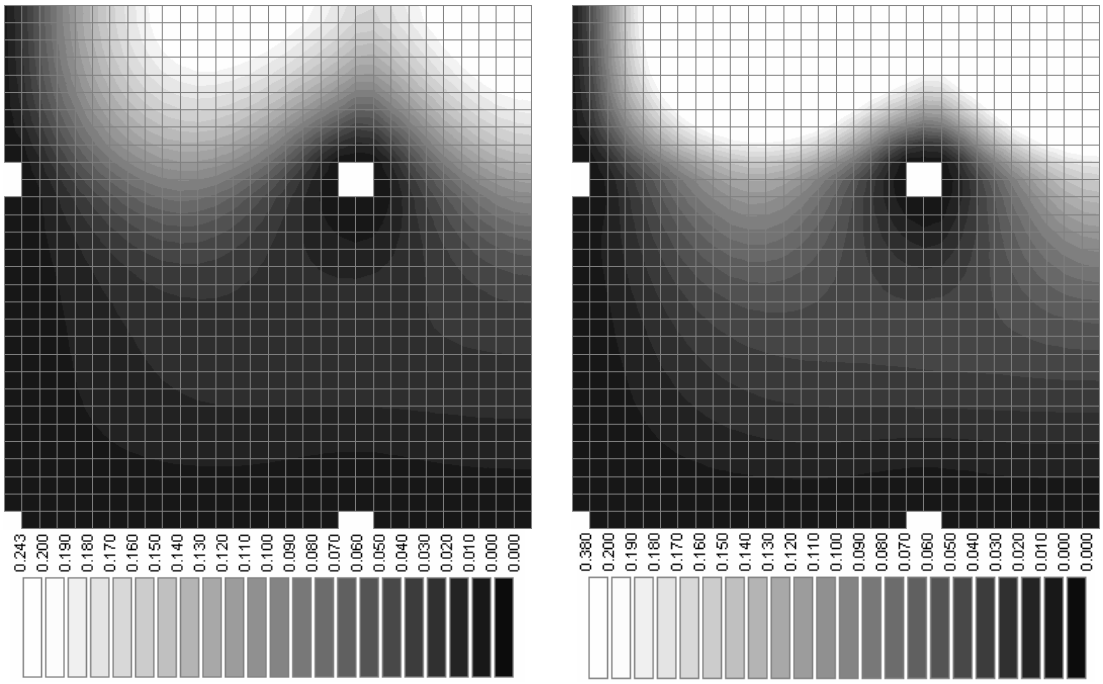

(a) Vertical deflections of the slab at 60 minutes (b) Vertical deflections of the slab at 180 minutes

Figure 7-61 Vertical deflections of the slab at 60 and 180 minutes (the middle strip bays in fire conditions)

Figure 7-62 shows the deflected pattern of the slab at 180 minutes when the middle strip bays were exposed to the fire beneath. The middle strip bays of the slab hung on the edge beams and the cold parts of the slab acting as a virtual beam between the columns.

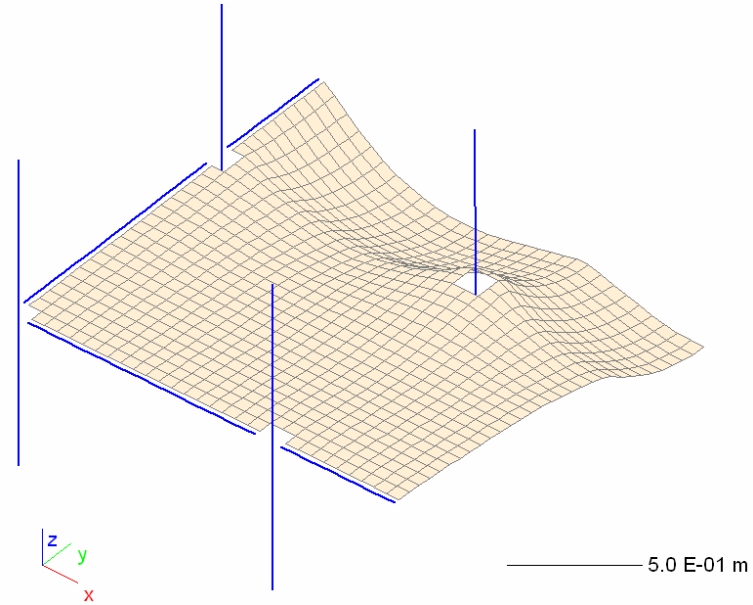

Figure 7-62 Vertical deflected shape of the slab at 180 minutes (Scale factor: 5; the middle strip bays in fire conditions)

X-direction displacements of the slab

Figure 7-63 shows the distribution of X-direction displacements from Point-B2 to Point-A2 when the middle strip bays were exposed to the fire. The X-direction movements of the slab were mainly towards the central part of the flat slab (the positive value of X-direction movements in the graph).

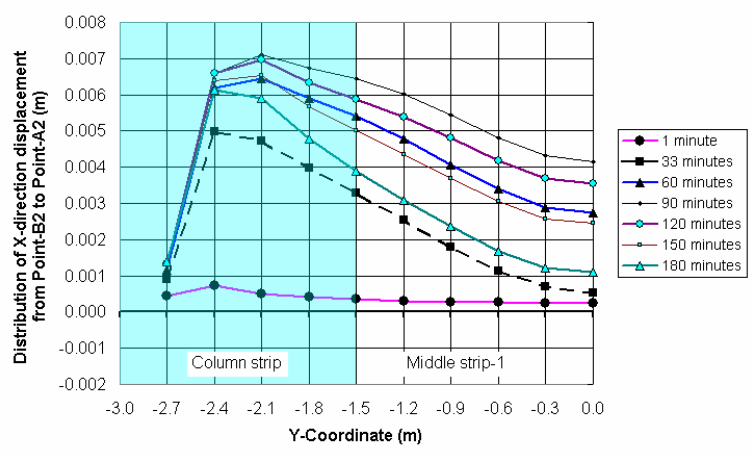

Figure 7-63 Distribution of X-direction displacements from Point-B2 to Point-A2 (the middle strip bays in fire conditions)

A comparison of X-direction displacements at Point-A2 between the fire beneath the middle strip bays and beneath all the bays is shown in Figure 7-64. It shows that when the fire was

beneath the middle strip bays the displacements at Point-A2 were greater than those when all the bays were exposed to fire.

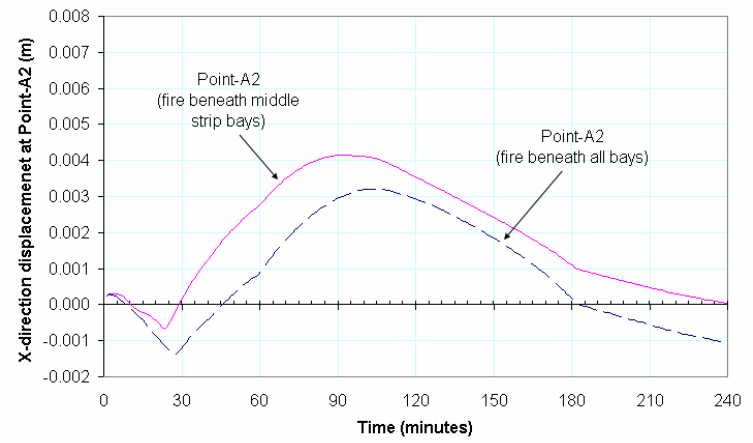

Figure 7-64 Comparison of X-direction displacements at Point-A2

Y-direction displacements of the slab

Figure 7-65 shows the distribution of Y-direction displacements from Point-B2 to Point-B1. The Y-direction displacement at Point-B2 was the same as at the point (-2.7, 3.0) because of the master-slave relations between Point-B2 and the point (-2.7, 3.0). Y-direction displacements in the Y-direction middle strip-1 were negative after 90 minutes due to the effect of thermal condition of Edge beam-4, which was partially exposed to the fire.

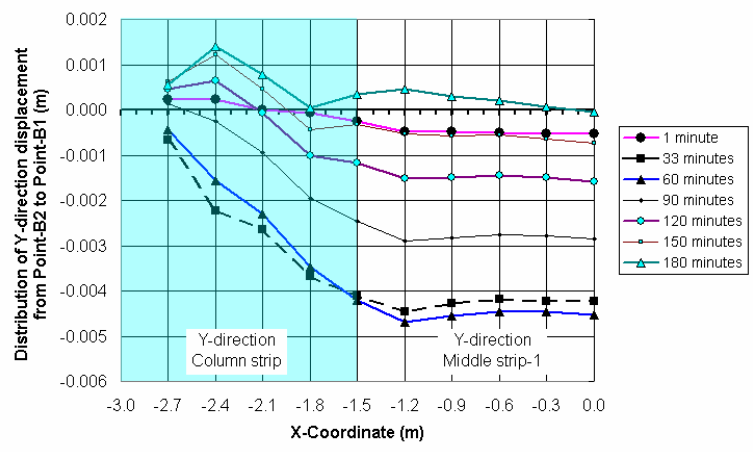

Figure 7-65 Distribution of Y-direction displacements from Point-B2 to Point-B1 (the middle strip bays in fire conditions)

A comparison of Y-direction displacements at Point-B1 between the fire beneath the middle strip bays and beneath all the bays is shown in Figure 7-66. It shows that when the fire was beneath the middle strip bays, the Y-direction displacements were negative throughout the simulation. The Y-direction movement at Point-B1 dramatically increased from -0.0005m at 1 minute to -0.004m at 13 minutes because the thermal thrust of the slab pushed the surrounding structural members at the first stage of fire exposure when the vertical deflection was small and Y-direction membrane forces were compressive forces in the most part of the slab. The Y-direction movement reached -0.0047m at 60 minutes, and then the direction of the movements changed to towards the central part of the slab due to the development of Y-direction tensile membrane forces in the Y-direction middle strip. The thermal expansion of the edge beam (Edge beam-4) enhanced the Y-direction movement of the slab away from the central part of the slab and reduced the movement towards the central part of the slab. Therefore, the thermal expansion of Edge beam-4 affected the development of membrane forces in the slab.

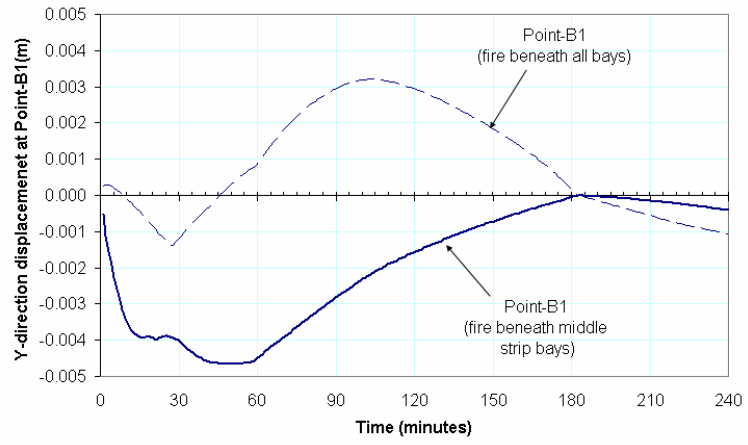

Figure 7-66 Comparison of Y-direction displacements at Point-B1

Y-direction movements of the columns are shown in Figure 7-67, which is labelled *Y-direction movement at Point-B2, Point-B4, Point-D2 and Point-D4* because these points were the centroids of the columns. Point-B4, which had the maximum value of the Y-direction movements within these points, was connected with Edge beam-4 which was under fire exposure. The movement at Point-B2 increased to -0.003m at 60 minutes due to the thermal expansion of the beams and the lack of the development of tensile membrane forces in the slab; after 60 minutes, the movement constantly declined to -0.0018m at 180 minutes due to the development of tensile membrane forces in the slab. At 180 minutes, the Y-direction movement at Point-B2 stopped decreasing and then began increasing until the end of the

simulation because the middle strip bays of the slab deformed to a catenary in Y-direction and thermal expansion continuously developed in Edge beam-4.

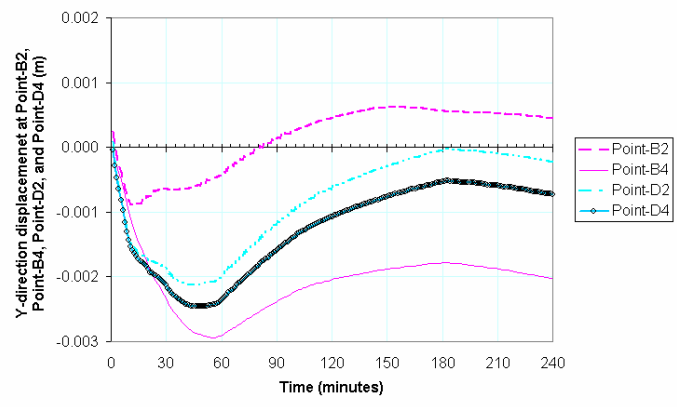

Figure 7-67 Y-direction movements at Point-B2, Point-B4, Point-D2 and Point-D4

7.7.2. Bending moments of the slab

Figure 7-68 shows the distributions of X-direction bending moments in the slab at 60 minutes and 180 minutes when the middle strip bays of the slab were exposed to the fire. The graphs show that the redistribution of X-direction bending moments was mainly present in the fire region of the slab. In the non-fire region of the slab, the value of X-direction bending moments remained almost the same value throughout the simulation.

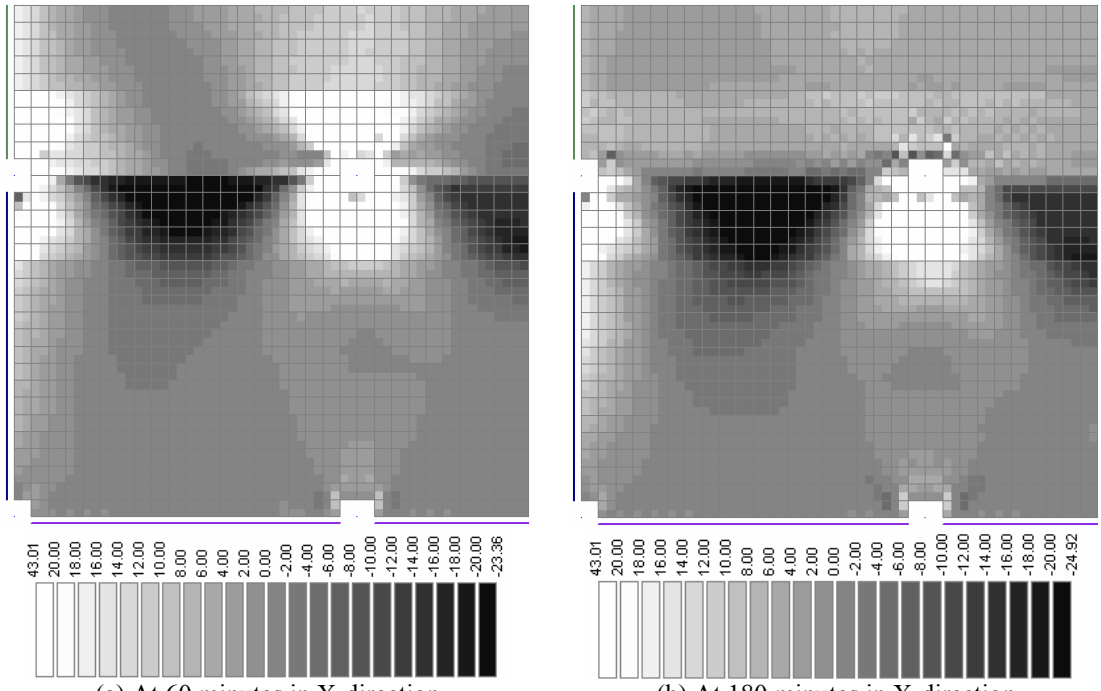

(a) At 60 minutes in X-direction (b) At 180 minutes in X-direction

Figure 7-68 Distributions of X-direction bending moments in the slab at 60 minutes and 180 minutes (the middle strip bays in fire conditions)

Figure 7-69 shows the distributions of Y-direction bending moments in the slab at 60 minutes and 180 minutes when the middle strip bays of the slab were exposed to the fire. The graphs show that the redistribution of Y-direction bending moments was mainly present in Middle strip-1 and Column strip of the slab; however, a part of Column strip was at ambient temperature conditions. In Edge column strip, which was at ambient temperature conditions, the distribution of Y-direction bending moments was slightly affected by the fire because the bending moment curves in the fire region of the slab moved up and down, which slightly affected the bending moment curves in the remote part of the slab in the non-fire region of the slab.

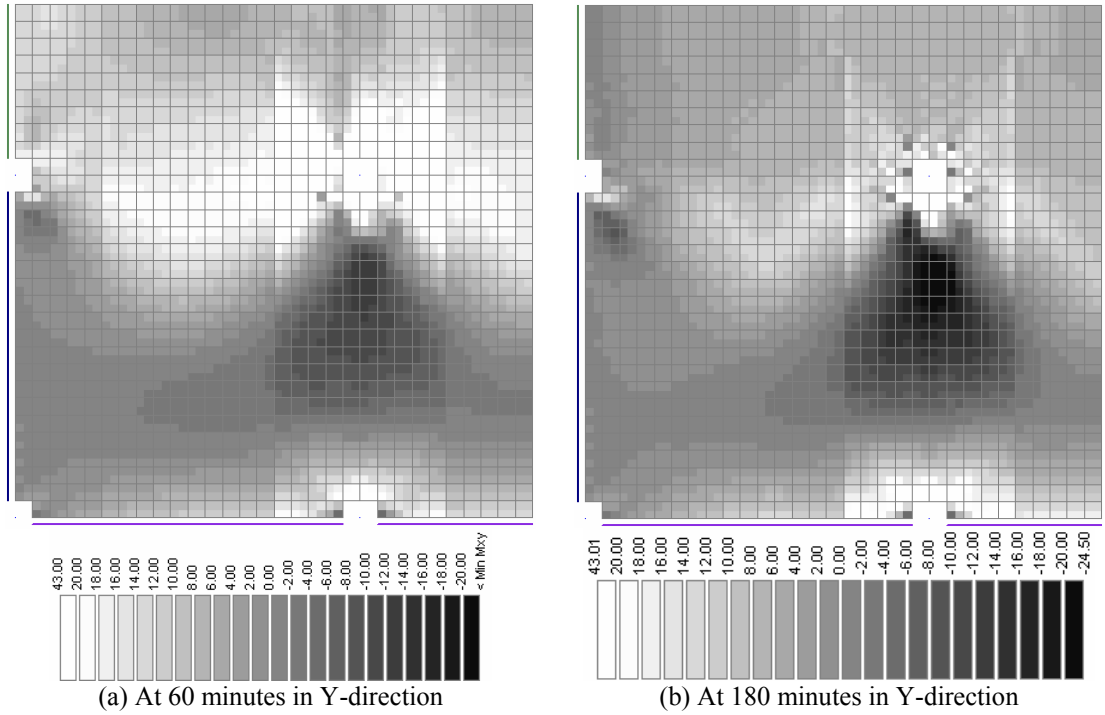

(a) At 60 minutes in Y-direction (b) At 180 minutes in Y-direction

Figure 7-69 Distributions of Y-direction bending moments in the slab at 60 minutes and 180 minutes (the middle strip bays in fire conditions)

7.7.3. Membrane forces of the slab

X-direction membrane forces in the slab

The distribution of X-direction membrane forces in the slab along Section-5 is shown in Figure 7-70. It shows that the magnitude of the membrane forces in Edge column strip and Middle strip-2 was very small. The distribution of the membrane forces in Column strip can be divided into two regions from the distinct line of the fire; one region was in the slab under fire exposure and another region was in the slab at ambient temperature conditions. The

tensile membrane forces were present in Column strip throughout the simulation. In non-fire region of Column strip close to the distinct line of the fire, the tensile membrane forces increased sharply because of the large strain of cold reinforcing bars in the slab, which was greatly affected by the large vertical deflections. The membrane forces in Middle strip-1 linearly developed through Section-5. Before 90 minutes the membrane forces were compressive forces in Middle strip-1.

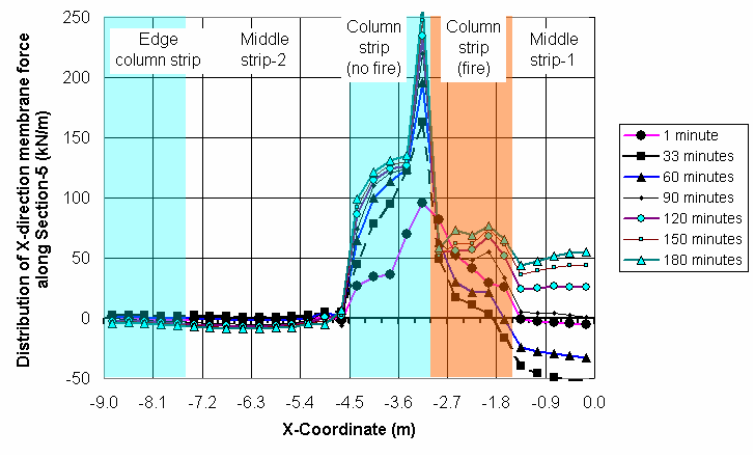

Figure 7-70 Distribution of X-direction membrane forces along Section-5 (the middle strip bays in fire conditions)

Figure 7-71 shows the X-direction average membrane forces in the strips along Section-5 when the middle strip bays of the slab were exposed to the fire. The membrane forces in the non-fire region of Column strip were different in trend and magnitude to those in the fire region of Column strip. The membrane forces in the non-fire region of Column strip increased from 50kN/m at 1 minute to 155kN/m at the end of the simulation. The membrane forces in the fire region of Column strip dropped from 50kN/m at 1 minute to 10kN/m at 30 minutes and then increased to 70kN/m at 180 minutes; after that, they slightly declined to 55kN/m at 240 minutes when the slab deformed to a catenary in the Y-direction. The membrane forces were compressive forces in Middle strip-1 before 90 minutes; at 30 minutes, the maximum value of -50kN/m was reached. After 90 minutes, the tensile membrane forces developed in Middle strip-1; at 180 minutes the maximum tensile membrane force of 50kN/m was reached. A tensile membrane force plateau was formed from 180 minutes to the end of the simulation in Middle strip-1. The tensile membrane force lag was present in Middle strip-1 due to the development of compressive membrane forces in the slab before 90 minutes.

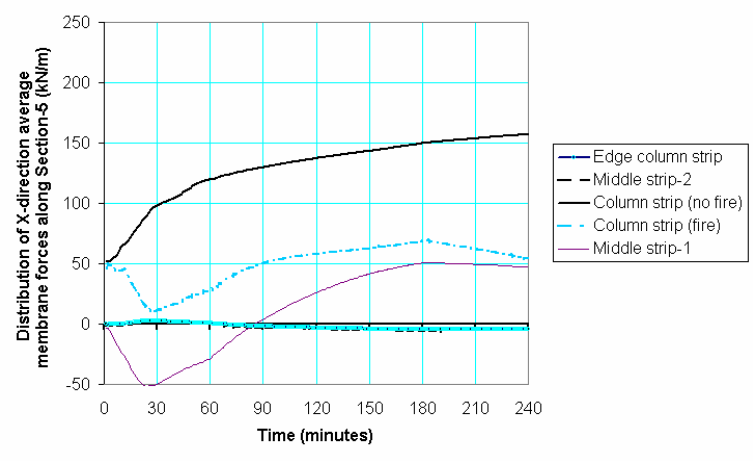

Figure 7-71 Distribution of X-direction average membrane forces along Section-5 (the middle strip bays in fire conditions)

Figure 7-72 shows the distributions of X-direction membrane forces in the slab at 60 minutes and 180 minutes when the middle strip bays of the slab were exposed to the fire. The membrane forces along the strips were almost constant except in Column strip. In non-fire region of Column strip the tensile membrane forces were greater than those in the fire region of Column strip.

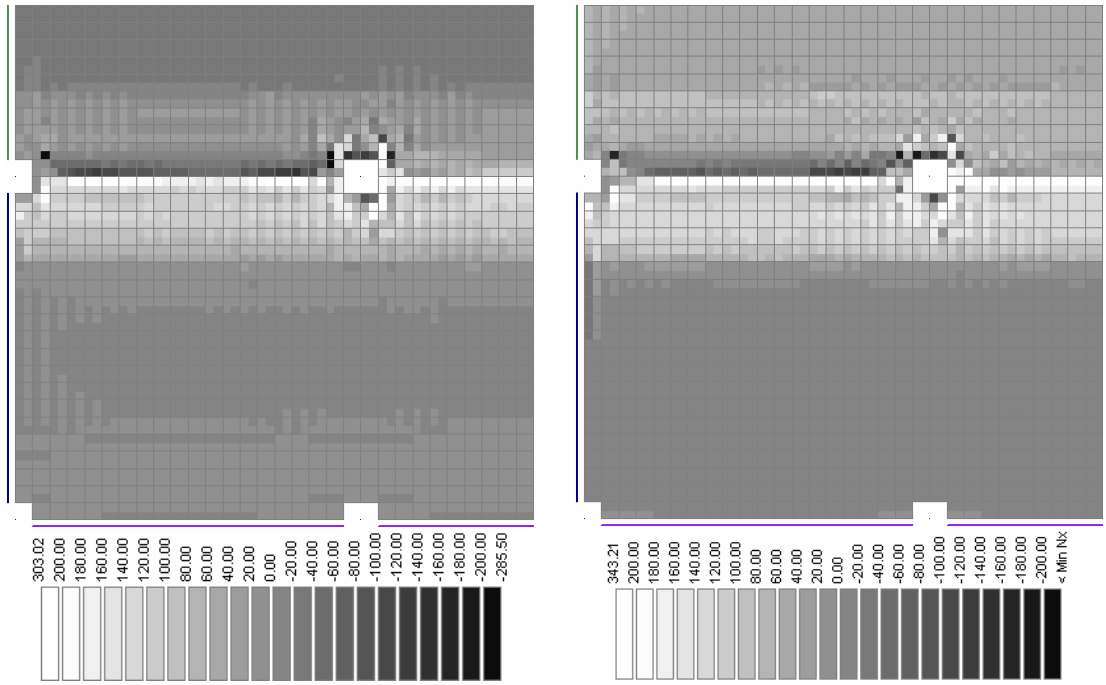

(a)At 60 minutes in X-direction (b) At 180 minutes in X-direction

Figure 7-72 Distributions of X-direction membrane forces at 60 minutes and 180 minutes (the middle strip bays in fire conditions)

Y-direction membrane forces in the slab

The distribution of Y-direction membrane forces in the slab along Strip-E is shown in Figure 7-73. It shows that the membrane forces can be divided into four regions: Y-direction Edge column strip, Y-direction Middle strip-2, Y-direction Column strip, and Y-direction Middle strip-1. The tensile membrane forces developed in Y-direction Column strip and compressive membrane forces developed in Y-direction Edge column strip due to the restraint of the columns and edge beams to the slab. In Y-direction Middle strip-1 and Y-direction Middle strip-2, the membrane forces varied from the compressive forces to the tensile forces. Comparing Figure 7-73 with Figure 7-70, it is evident that the distribution of the membrane forces in the Y-direction and X-direction were totally different. The location of the fire in the building significantly affected the distribution of membrane forces in the slab.

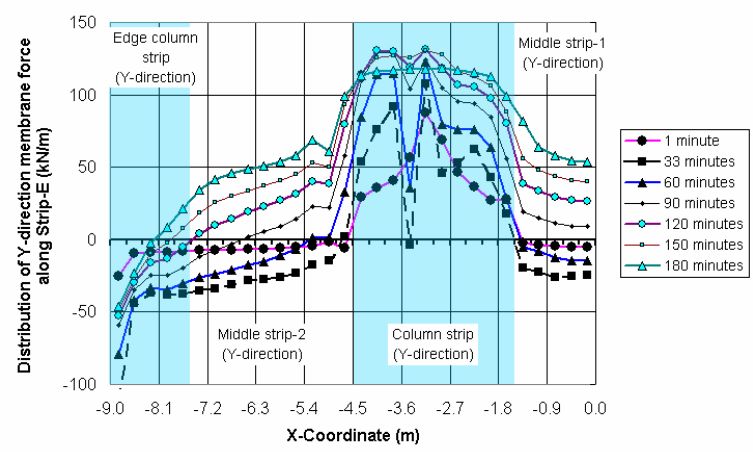

Figure 7-73 Distribution of Y-direction membrane forces along Strip-E (the middle strip bays in fire conditions)

Figure 7-74 shows the Y-direction average membrane forces in the Y-direction strips along Strip-E when middle strip bays of the slab were exposed to the fire. In Y-direction Column strip, the membrane forces decreased from 50kN/m at 1 minute to 22kN/m at 13 minutes and then increased to 122kN/m at 150 minutes; after that, they slightly decreased to 115kN/m at 180 minutes. In Y-direction Edge column strip, the membrane forces were compressive forces throughout the simulation and the maximum compressive membrane force of -65kN/m was reached at 13 minutes; after that, the membrane forces decreased to -5kN/m at 180 minutes. The trend and magnitude of membrane forces in Y-direction Middle strip-1 and Y-direction Middle strip-2 were the same. The compressive membrane forces in Y-direction Middle

strip-1 and Y-direction Middle strip-2 increased from zero at 1 minute to -37kN/m at 13 minutes and then linearly declined to zero again at 75 minutes; after that, the tensile membrane forces started to develop and at 180 minutes reached a peak value of 55kN/m. The plateaus were formed in the duration from 180 minutes to 240 minutes in all the Y-direction strips due to the slab deforming to a catenary in the Y-direction. The tensile membrane force lag was present in Y-direction Middle strip-1 and Y-direction Middle strip-2 due to the effects of the restraints of the columns, edge beams and the non-fire region of the slab on the fire region of the slab.

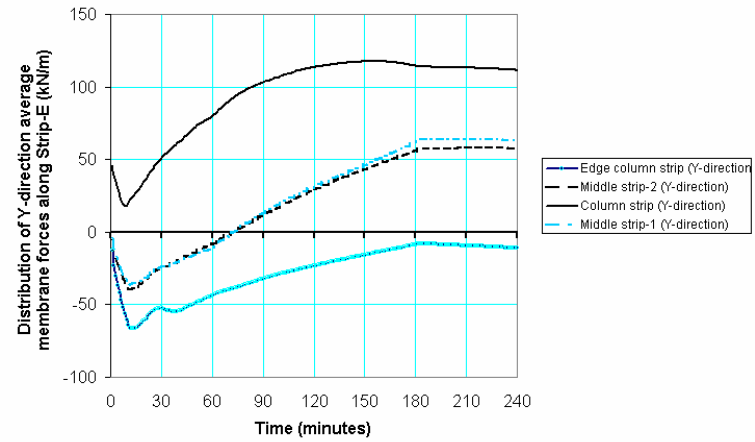

Figure 7-74 Distribution of Y-direction average membrane forces along Strip-E (the middle strip bays in fire conditions)

Figure 7-75 shows the distributions of Y-direction membrane forces in the slab at 60 minutes and 180 minutes when the middle strip bays of the slab were exposed to the fire. The membrane forces along the Y-direction strips were almost constant, especially in the non-fire region of the slab.

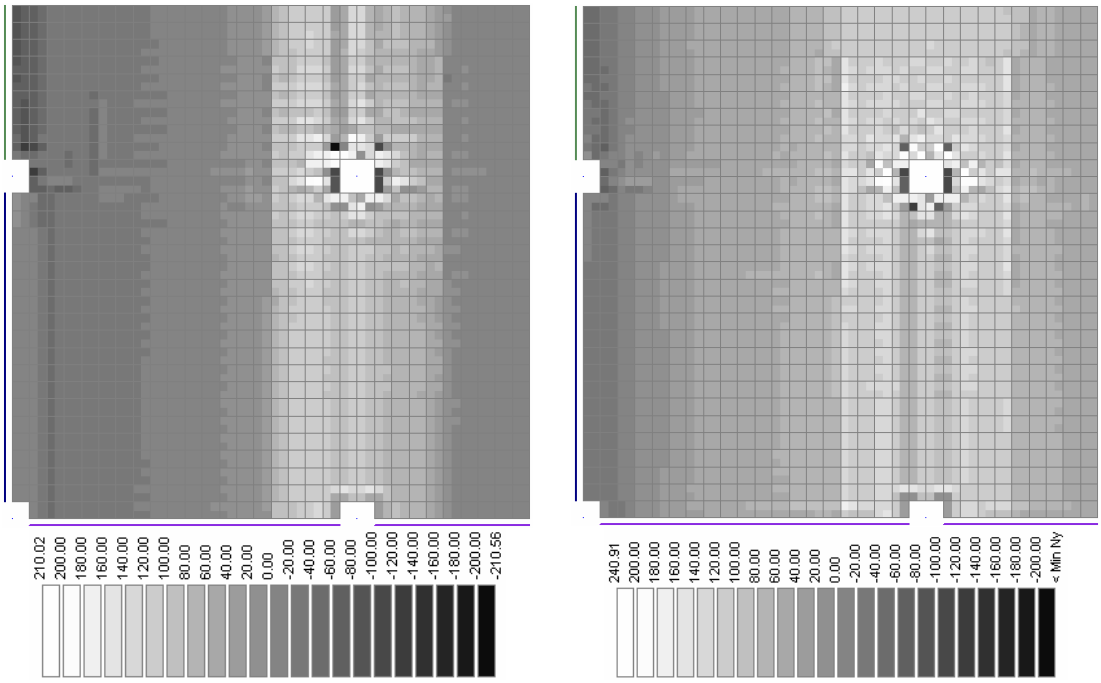

(a) At 60 minutes in Y-direction (b) At 180 minutes in Y-direction

Figure 7-75 Distributions of Y-direction membrane forces at 60 minutes and 180 minutes (the middle strip bays in fire conditions)

7.7.4. Conclusions

The analysis of the nine-bay flat slab when the middle strip bays (three panels) were exposed to the fire has shown that:

- The slab deforms as a catenary in the Y-direction after three hours' fire exposure.
- The distribution of X-direction and Y-direction membrane forces are completely different; the X-direction membrane forces in Edge column strip and Middle strip-2 are almost zero, while the Y-direction membrane forces in Y-direction Edge column and Y-direction Middle strip-2 develop throughout the simulation.
- The distributions of X-direction membrane forces in the column strip are varied in the fire region and non-fire region; the magnitude of the membrane forces in the non-fire region is greater than in the fire region.
- The tensile membrane force lag is present in X-direction Middle strip-1, Y-direction Middle strip-1 and Y-direction Middle strip-2 due to the earlier development of compressive membrane forces in these strips.
- The distribution of X-direction bending moments in X-direction Middle strip-2 and Edge column strip are slightly affected by the fire.

7.8. Conclusions

The main findings of the research on the nine-bay flat slabs are follows:

- The location of the fire beneath the flat slab significantly affects the distribution of bending moments and membrane forces in the slab; the more bays of the flat slab exposed to the fire, the worse conditions occur.
- The reinforcement in the slab affects the distribution of bending moments and membrane forces in the slab.
- The edge beams play important roles in the prevention of the collapse of the slab in fire conditions.
- The tensile membrane force lag is present in the slab due to the earlier development of the compressive membrane forces in the middle strip.
- The fire with a decay phase can have a more severe impact on the slab than the ISO 834 Standard fire.

8. CONCLUSIONS AND RECOMMENDATIONS

8.1. Introduction

This research task was conducted to study the behaviour of reinforced concrete flat slabs in fire conditions. The main objective of this research was to investigate the influence of the membrane action and the redistribution of bending moments on the behaviour of reinforced concrete flat slabs subjected to fires. The study of the membrane action and the redistribution of bending moments was performed with 3-D finite element analyses using SAFIR on one-way slabs, one-bay flat slabs and nine-bay flat slabs.

8.2. One-Way Slabs in Fire Conditions Using 3-D Shell Element Models

The research has been carried out into the behaviour of one-way reinforced concrete slabs exposed to an ISO 834 Standard fire with or without a decay phase using 3-D shell element models. The restraint conditions at the supports and the widths of the slabs were varied, but all slabs were free to rotate at the supports.

8.2.1. Main conclusions

The main conclusions of the research on one-way slabs using 3-D shell element models are as follow:

i) Y-direction bowing actions, bending moments and displacements in the region close to the supports are significantly affected by Z-direction restraints (vertical restraints at the supports).

ii) Y-direction restraints (perpendicular to the slab) at the supports do not obviously affect the behaviour of the slab in the X-direction (parallel to the span).

iii) The bending moments are non-linearly distributed along the cross-sections of the slab in the region close to the supports. The distribution of bending moments along the cross-section is more non-linear in the wider slab than in the narrower slab.

iv) The tensile membrane force lag (defined on page 98) is present in the slab due to the earlier development of compressive membrane forces in the region close to the edge. The tensile membrane force lag is greater in the wider slab than in the narrower slab.

v) The top reinforcing bars in the slab are the key to preventing the collapse of the slab when it is restrained in the X-direction at the supports.

vi) The worst scenario of one-way slabs with horizontal restraints at the supports could be when the slabs are exposed to the fire with a decay phase.

8.2.2. The slab in fire conditions with vertical restraints at supports

The analysis of the slab with full restraints in the Z-direction at supports when the slab was exposed to an ISO 834 Standard fire has shown that:

i) The Y-direction bowing action, the bending moments, and the displacements of the slab are significantly affected by Z-direction restraints within 0.5m from the supports.

ii) The bending moments are non-linearly distributed along the cross-section in the region close to the supports, while they are linearly distributed along the cross-section in the region close to the midspan; the bending moments in the midspan can be predicted using the principles of structural mechanics.

iii) X-direction membrane forces are present in the cross-section of the slab as self-balanced forces along the cross-section.

8.2.3. The slab in fire conditions with X- and Z-direction restraints

The analyses of the Pin-Pin supported slabs with full X-direction and Z-direction restraints when the slabs were exposed to an ISO 834 Standard fire have shown that:

i) Y-direction restraints at the supports do not obviously affect the behaviour of the slab in the X-direction.

ii) The tensile membrane force lag is present in the slab and it is greater in the wider slab than in the narrower slab.

iii) The top reinforcing bars are the key in preventing the collapse of the slab.

iv) The bending moments are non-linearly distributed along the cross-section close to the supports and it is more non-linear in the wider slab than in the narrower slab.

v) The Y-direction bowing of the slab is slightly reduced by X-direction restraints at the supports in the initial stage of the fire (1 minute to 33 minutes).

vi) The tendency of the bowing radius (defined on page 78) is the same in the slabs with different widths.

vii) The wider slab has the larger vertical deflection in the midpoint of the slab.

viii) Both the 2-D beam element model and the 3-D shell element model can precisely predict the failure of the slab, but the process of the development of the vertical deflections and membrane forces is completely different.

8.2.4. The slab in the fire with a decay phase

The analysis of the Pin-Pin supported slab with full X-direction and Z-direction restraints when the slab was exposed to an ISO 834 Standard fire with a decay phase has shown that:

i) The vertical deflection at the middle point (Point-O) declines within and after the decay phase of the fire.

ii) The bending moments dramatically increase within the decay phase of the fire until the plastic hinges are formed in the slab.

iii) The compressive membrane forces dramatically increase within and after the decay phase of the fire.

iv) The plastic hinges are formed in the slab at 150 minutes due to the increase of the compressive membrane forces and the bending moments in the slab.

v) The worst scenario of one-way slabs in fire conditions could be when the slabs are exposed to the fire with a decay phase.

8.2.5. Recommendations for the design of one-way slabs

i) One-way slabs have excellent fire behaviour if they are designed to have axial restraints at the supports.

ii) One-way slabs with axial restraints should have continuous top reinforcing bars to resist the tensile membrane forces which are produced in fire conditions; these bars should be well anchored in the supports.

iii) The top and bottom reinforcing bars in precast concrete slabs should be enhanced in the region close to the free edges if the width of the slab is greater than 1.0m.

iv) Precast concrete slabs should have reinforcing bars perpendicular to the span on the top and bottom levels of the slab.

8.3. One-Bay Flat Slabs without Edge Beams

The research has been carried out into the analyses of one-bay reinforced concrete flat slabs without edge beams at ambient and fire conditions using 3-D finite element models. Because the one-bay flat slabs without edge beams are not recommended for construction in most building codes, there are no recommendations for design. Shear failure of the slab was not considered in the analysis.

8.3.1. Main conclusions

The main conclusions of the analyses of the one-bay flat slab at ambient and fire conditions are as follow:

i) SAFIR can predict the behaviour of the flat slab at ambient and fire conditions by using a suitable structural model.

ii) The results of the modelling are sensitive to the connection model for the column, slabs and the edge strips of the slab. The connection model affects the magnitudes of the displacements, bending moments and membrane forces of the flat slab, which are slightly underestimated using the inclusive connection model (defined on page 134) and overestimated using the exclusive connection model (defined on page 134).

iii) The membrane forces are mainly present in the strips of the slab between the columns under the fire exposure.

iv) The redistribution of bending moments mainly occurs in the edge strips of the slab when the slab is exposed to the fire with or without a decay phase.

v) One-bay flat slabs without edge beams are not recommended to be built because the performance of the slabs in fire exposure is easily improved by adding the edge beams surrounding the slabs.

8.3.2. One-bay flat slabs at ambient conditions

The analyses of one-bay flat slabs at ambient conditions have found that:

i) SAFIR can predict the behaviour of flat slabs at ambient temperatures using a suitable structural model.

ii) The membrane forces are mainly present in the strips of the slab between the columns.

iii) The results of the modelling are sensitive to the connection model. The connection model in SAFIR affects the magnitudes of the displacements, bending moments and membrane forces of the flat slab.

8.3.3. One-Bay flat slabs in fire without a decay phase

The analyses of the flat slabs exposed to an ISO 834 Standard fire without a decay phase have shown that:

i) The slab experiences failure at 150 minutes but does not collapse due to the restraint provided by the columns and the tensile membrane behaviour developing in the slabs.

ii) The redistribution of the bending moments and the membrane forces of the slab are mainly present in the edge strip of the slab and along the diagonal of the slab.

iii) The results of the modelling are sensitive to the connection models. The magnitudes of displacements, bending moments and membrane forces are affected using different kinds of connection models when the duration of the fire exposure is greater than 120 minutes (two hours), but the trends of the developments of displacements bending moments and membrane forces are not affected.

8.3.4. Behaviour of one-bay flat slabs in fire with a decay phase

The analysis of the one-bay flat slab without edge beams exposed to an ISO 834 Standard fire with a decay phase has shown that:

i) The slab did not fail when it was exposed to a fire with a decay phase.

ii) The significant redistribution of bending moments is mainly present in the edge strip of the slab in the duration of the decay phase of the fire and after the exhaustion of the fire.

iii) The membrane forces of the flat slab are mainly present in the strips of the slab between the columns under the fire exposure.

8.4. Nine-bay Flat Slabs at Ambient and Fire Conditions

The research has been carried out into the analyses of nine-bay reinforced concrete flat slabs at ambient and fire conditions using finite element models. The location of the fire is varied from beneath all the bays to beneath the single middle bay and the middle strip bays of the slab. Shear failure of the slab was not considered in the analysis.

8.4.1. Main conclusions

The main findings of the research on the nine-bay flat slabs are as follows:

i) The location of the fire beneath the flat slab significantly affects the distribution of bending moments and membrane forces in the slab; the more bays of the flat slab exposed to the fire, the worse conditions occur.

ii) The reinforcement in the slab affects the distribution of bending moments and membrane forces in the slab.

iii) The edge beams play important roles in the prevention of the collapse of flat slabs in fire conditions.

iv) The tensile membrane force lag is present in the slab due to the earlier development of the compressive membrane forces in the middle strip.

v) The fire with a decay phase can have a more severe impact on the slab than the ISO 834 Standard fire.

8.4.2. Nine-bay flat slabs at ambient conditions

The analysis of the flat slab at ambient conditions shows that:

i) The load capacity of the flat slab is 22.3kN/m^2, which is nearly two times the calculated ultimate load of 12.8kN/m^2 because of the development of membrane behaviour and the redistribution of bending moments in the flat slab.

ii) The X-direction (or Y-direction) distributions of bending moments and membrane forces can be divided into four strips to analyse depending on the arrangement of reinforcing bars in the slab.

8.4.3. Fire without a decay phase beneath all the bays of nine-bay flat slabs

The analysis of the nine-bay flat slab with all bays exposed to an ISO 834 Standard fire without a decay phase has found that:

i) The thermal conditions of the edge beams significantly affect the vertical and horizontal displacements of the slab.

ii) The redistribution of bending moments in the slab is drastically affected by the arrangement and quantity of reinforcing bars in the slab.

iii) The arrangement of reinforcing bars affects the distribution of the membrane forces in the slab.

iv) The tensile membrane force lag is present in the middle strip of the flat slab exposed to fires because of the effect of the restraint of columns and edge beams on the flat slab.

v) The arrangement and quantity of the top reinforcing bars in the column strip are important for improving the fire endurance and preventing the collapse of the flat slab in fire conditions.

8.4.4. Fire with a decay phase beneath all the bays of nine-bay flat slabs

The analysis of the nine-bay flat slab with all bays exposed to an ISO 834 Standard fire with a decay phase has found that:

i) The thermal conditions of the edge beams significantly affect the vertical and horizontal displacements of the slab.

ii) The distribution and redistribution of bending moments significantly change within and after the decay phase of the fire.

iii) The tensile membrane forces dramatically increase within and after the decay phase of the fire.

iv) The tensile membrane force lag is present in the flat slab.

v) The arrangement of reinforcing bars affects the distribution of membrane forces in the slab.

vi) The collapse of the slab could occur within or after the decay phase of the fire depending on the development of membrane forces and bending moments in the slab.

vii) It is recommended that further research of reinforced concrete slabs in fire conditions should focus on the behaviour of reinforced concrete slabs in fires with a decay phase.

8.4.5. Fire without a decay phase beneath the middle bay of nine-bay flat slabs

The analysis of the flat slab when the single middle bay (the middle panel) was exposed to the fire has shown that:

i) The slab does not deform to a catenary after four hours' fire exposure due to the restraint of the surrounding structural members, which are at ambient temperature conditions.

ii) The distribution of membrane forces in the column strip is different in the fire region and non-fire region; the magnitude of membrane forces in the non-fire region is greater than in the fire region.

iii) The tensile membrane force lag is present in the Middle strip-1 due to the earlier development of compressive membrane forces in the Middle strip-1.

iv) The fire in the middle panel slightly affects the behaviour of the slab in the corner panel, but greatly affects the behaviour of the slab in the edge panels.

8.4.6. Fire without a decay phase beneath the middle strip bays of nine-bay flat slabs

The analysis of the flat slab when the middle strip bays (three panels) were exposed to the fire has shown that:

i) The slab deforms as a catenary in the Y-direction after three hours' fire exposure.

ii) The distribution of X-direction and Y-direction membrane forces are completely different; the X-direction membrane forces in the Edge column strip and the Middle strip-2 are almost zero, while the Y-direction membrane forces in the Y-direction Edge column and the Y-direction Middle strip-2 develop throughout the simulation.

iii) The distribution of X-direction membrane forces in the column strip is different in the fire region and non-fire region; the magnitude of the membrane forces in the non-fire region is greater than in the fire region.

iv) The tensile membrane force lag is present in the X-direction Middle strip-1, Y-direction Middle strip-1 and Y-direction Middle strip-2 due to the earlier development of compressive membrane forces in these strips.

v) The distribution of X-direction bending moments in the X-direction Middle strip-2 and Edge column strip are slightly affected by the fire exposure.

8.4.7. Recommendations for the design of multi-bay flat slabs

i) Multi-bay flat slabs have excellent fire behaviour if they are designed with edge beams.

ii) The reinforced concrete edge beams should have sufficient flexural stiffness under fire exposure.

iii) When edge beams are designed to be steel beams, they should be thermally protected.

iv) The top reinforcing bars in the column strips of flat slabs should be well anchored in the columns and edge beams.

v) The strips of the slab between the columns should be designed to be virtual beams with stirrups which have good integrity in fire conditions.

8.5. Recommendations for future research

It is recommended that the future research into the fire performance of reinforced concrete slabs should focus on the following areas:

i) The behaviour of reinforced concrete slabs exposed to an ISO Standard fire with a decay phase, varying the decay rates and the duration of the fire exposure.

ii) The behaviour of reinforced concrete slabs after the fire is exhausted or extinguished.

iii) The fire behaviour of reinforced concrete one-way slabs should be investigated by varying the position of the line of the thrust at the supports using 3-D shell element models.

iv) The fire behaviour of reinforced concrete flat slabs should be investigated by varying the flexural stiffness and thermal conditions of edge beams.

v) Finite element modelling techniques for whole reinforced concrete buildings exposed to fires.

REFERENCES

Abrams, M. S. & Gustaferro, A. H. (1969), 'Fire Endurance of Two-Course Floors and Roofs', Journal of the American Concrete Institute, vol. 66, no. 2, pp. 92-102.

ACI (1992), Building code requirements for reinforced concrete (ACI 318) (revised 1992) and commentary (ACI 318R-89) (revised 1992), [rev. 1992]. edn, American Concrete Institute, Detroit, Mich.

Anderberg, Y. (1983), Properties of Materials at High Temperatures- Steel, RILEM Report, University of Lund, Sweden.

Anderberg, Y. & Forsen, N. E. (1982), Fire Resistance of Concrete Structures, Division of Structural Mechanics and Concrete Construction, Lund Institute of Technology, Lund, Sweden.

Anderberg, Y. & Thelandersson, S. (1976), Stress and Deformation Characteristics of Concrete, 2- Experimental Investigation and Material Behaviour Model, Bulletin 54, University of Lund, Sweden.

ASTM (1999), ASTM fire test standards, 5th edn, Astm, West Conshohocken, PA.

Bailey, C. G. (2001), 'Membrane action of unrestrained lightly reinforced concrete slabs at large displacements', Engineering Structures, vol. 23, no. 5, pp. 470-483.

Bailey, C. G., Lennon, T. & Moore, D. B. (1999), 'The behaviour of full-scale steel-framed buildings subjected to compartment fires', The Structrual Engineer, vol. 77, no. 8, pp. 15-21.

Bailey, C. G. & Moore, D. B. (2000a), 'The structural behaviour of steel frames with composite floorslabs subject to fire: Part 1: Theory', The Structrual Engineer, vol. 78, no. 11, pp. 19-27.

Bailey, C. G. & Moore, D. B. (2000b), 'The structural behaviour of steel frames with composite floorslabs subject to fire: Part 2: Design', The Structrual Engineer, vol. 78, no. 11, pp. 28-33.

Bailey, C. G., White, D. S. & Moore, D. B. (2000), 'The tensile membrane action of unrestrained composite slabs simulated under fire conditions', Engineering Structures, vol. 22, no. 11, pp. 1583-1595.

Bazant, Z. P. & Kaplan, M. F. (1996), Concrete at high temperatures: material properties and mathematical models, Longman, Harlow.

Beitel, J. & Iwankiw, N. (2002), Analysis of Needs and Existing Capabilities for Full-Scale Fire Resistance Testing, National Technical Information Service (NTIS), Technology Administration. http://www.ntis.gov

BIA (1992), New Zealand Building Code and Approved Documents, New Zealand Building Industry Authority, Wellington, New Zealand.

Buchanan, A. H. (2001), Structural design for fire safety, Wiley, Chichester, England ; New York.

Cembureau & FIP (1979), Concrete for fire resistant construction, Cement and Concrete Association, Wexham Springs, Slough. U.K.

EC2 (2002), Eurocode 2: Design of concrete structures. ENV 1992: Part1-2: General rules-Structrue fire design, European committee for Standardization, Brussels, Belgium.

EC3 (1995), Eurocode 3: Design of steel structures. ENV 1993 Part 1-2: General rules-Structural fire design, European Committee for Standardization, Brussels, Belgium.

Enochsson, O. & Dufvenberg, P. (2001), Concrete slabs designed with finite element methods: modelling parameters, crack analyses and reinforcement design, Lulea University of Technology. http://epubl.luth.se/1402-1617/2001/328/index-en.html

Feasey, R. & Buchanan, A. H. (2002), 'Post-flashover fires for structural design', Fire Safety Journal, vol. 37, no. 1, pp. 83-105.

Fleischmann, C. & Buchanan, A. H. (2002), 'Analytical methods for determining fire resistance of concrete members', in The SFPE Handbook of Fire Protection Engineering, Third Edition, ed. DiNenno, P. J., National Fire Protection Association, Massachusetts, pp. 4-239 to 4-256.

Franssen, J. M., Kodur, V. K. R. & Mason, J. (2002a), User's manual for SAFIR2001 free: A computer program for analysis of structures at elevated temperature conditions, University of Liege, Departement Structures de Genie Civil, Service Ponts et Charpentes, Belgium.

Franssen, J. M., Kodur, V. K. R. & Mason, J. (2002b), Elements of theory for SAFIR2001 free: A computer program for analysis of structures at elevated temperature conditions, University of Liege, Department Structures de Genie Civil, Service Ponts et Charpentes, Belgium.

Griffiths, J. M. (1936), Thermal expansion of typical American rocks, Bulletin No. 128, Iowa Engineering Experiment Station, Iowa State College.

Gustaferro, A. H., CRSI. Engineering Practice Committee. & CRSI. Committee on Fire Ratings. (1980), Reinforced concrete fire resistance, 1st edn, Concrete Reinforcing Steel Institute, Chicago.

Gustaferro, A. H., Martin, L. D. & Prestressed Concrete Institute. (1989), Design for fire resistance of precast prestressed concrete, 2nd edn, Prestressed Concrete Institute, Chicago.

Harmathy, T. Z. (1993), Fire safety design and concrete, Longman Scientific & Technical; Wiley, Harlow, Essex, England, New York, NY.

Hayes, B. (1968), 'Allowing for membrane action in the plastic analysis of rectangular reinforced concrete slabs', Magazine of Concrete Research, vol. 20, no. 65, pp. 205-212.

ISO (1975), Fire resistance tests - elements of building construction. ISO 834-1975, International Organization for Standardization.

Issen, L. A., Gustaferro, A. H. & Carlson, C. C. (1970), 'Fire tests of concrete members; An improved method for estimating thermal restraint forces', Fire Test Performance, pp.153-185.

Kirby, B. R. & Preston, R. R. (1988), 'High temperature properties of hot-rolled structural steels for use in fire engineering design studies', Fire Safety Journal, vol. 13, pp. 27-37.

Lie, T. T. (1972), Fire and buildings, Applied Science Publishers, London.

Lie, T. T. (1995), 'Fire temperature-time relatoins', in SFPE Handbook of fire protectin engineering, Society of Fire Protection Engineers, USA.

Lim, L. C. S. (2003), Membrane action in fire exposed concrete floor systems: a thesis submitted in partial fulfilment of the requirements for the degree of Doctor of Philosophy, Department of Civil Engineering, University of Canterbury, Christchurch, New Zealand.

Malhotra, H. L. (1982), Design of fire-resisting structures, Surrey University Press; distributed in the U.S. by Chapman and Hall, Glasgow, New York.

Newman, G. M., Robinson, J. T. & Bailey, C. G. (2000), Fire Safe Design: A New Approach to Multi-Story Steel-Framed Buildings, The Steel Construction Institute, Berkshire, U.K.

Olenick, S. M. & Carpenter, D. J. (2003), 'An updated international survey of computer models for fire and smoke', Journal of Fire Protection Engineering, vol. 13, no. 2, pp. 87-110.

Park, R. (1964), 'Tensile membrane behaviour of uniformly loaded rectangular reinforced concrete slabs with fully restrained edges', Magazine of Concrete Research, vol. 16, no. 46, pp.39-44.

Park, R. & Gamble, W. L. (2000), Reinforced concrete slabs, 2nd edn, Wiley, New York.

Pettersson, O., Magnusson, S. E. & Thor, J. (1976), Fire engineering design of steel structures, Division of Structural Mechanics and Concrete Construction Lund Institute of Technology; Swedish Institute of Steel Construction, Lund, Sweden; Stockholm, Sweden.

Purkiss, J. A. (1996), Fire safety engineering design of structures, Butterworth-Heinemann, Oxford; Boston.

Routley, G. J., Jennings, C. & Chubb, M. (1991), High-rise Office Building Fire, One Meridian Plaza, Philadelphia, Pennsylvannia, Report 049, Emergency Management Agency, National Fire Data Centre, Marylan, U.S.A.

Sawczuk, A. & Winnicki, L. (1965), 'Plastic behaviour of simply supported reinforced concrete plates at moderately large deflections', International Journal of Solids and Structures, vol. 1, pp. 97-111.

Schneider, U. (1985), Behaviour of Concrete at High Temperatures, RILEM Committee 44-PHT.

Schneider, U. (1988), 'Concrete at high temperatures - a general review', Fire Safety Journal, vol. 13, pp. 55-68.

Selvaggio, S. L. & Carlson, C. C. (1963), Effect of restraint on fire resistance of prestressed concrete, American Society for Testing and Materials, STP 344.

SNZ (1995), The Design of Concrete Structures, NZS 3101: Part1:1995 edn, Standard New Zealand, Wellington, New Zealand.

Sozen, M. A. & Siess, C. P. (1980), Reinforced concrete floor slabs: research and design, American Society of Civil Engineers, New York.

Taylor, R. (1965), 'A note on a possible basis for a new method of ultimate load design of reinforced concrete slabs', Magazine of Concrete Research, vol. 17, no. 53, pp. 183-186.

Vecchio, F. J. & Collins, M. P. (1990), 'Investigating the collapse of a warehouse', Concrete International, vol. 12, no. 3, pp. 72-78.

Wade, C. A. (1991), 'Fire engineering design of reinforced and prestressed concrete elements', in BRANZ Study Report No.33, Building Research Association of New Zealand.

Wood, R. H. (1961), Plastic and elastic design of slabs and plates with particular reference to reinforced concrete floor slabs, Thames and Hudson, London.

APPENDIX A – TYPICAL INPUT FILES FOR THE THERMAL ANALYSIS

The appendix details two input files of thermal analyses using SAFIR: a typical input file for concrete slabs and a typical input file for reinforced concrete edge beams.

Input file for the thermal model of concrete slabs

This file is for the thermal analysis of a 0.2m thick concrete slab exposed to an ISO 834 Standard fire from beneath. The width of the slab is 0.2m. The effect of reinforcing bars in the slab is not considered. The mane of the file is *shell_200.IN*.

```
    NPTTOT      1843
     NNODE    82
      NDIM     2
 NDIMMATER     1
   NDDLMAX     1
      FROM     1   TO    82 STEP     1 NDDL     1
  END_NDDL
  TEMPERAT
      TETA       0.9
  TINITIAL      20.0
  MAKE.TSH
 LARGEUR11    190000
 LARGEUR12       100
   NORENUM
slab200.tsh
      NMAT     1
  ELEMENTS
     SOLID    40
        NG     2
     NVOID     0
  END_ELEM
     NODES
      NODE     1     -0.100     -0.100
     GNODE    41      0.100     -0.100
      NODE    42     -0.100      0.100
     GNODE    82      0.100      0.100
 FIXATIONS
   END_FIX
NODOFSOLID
      ELEM     1     1   42   43     2     1         0.
     GELEM    40    40   81   82    81     1         0.     1
  FRONTIER
         F         1       FISO         NO         NO         NO
         F        40         NO         NO        F20         NO
 END_FRONT
  SYMMETRY
   END_SYM
 PRECISION    1.0E-3
 MATERIALS
SILCONCEC2
       92.       25.         9.       0.56
      TIME
                 1.0       30.0
                30.0    14400.0
   ENDTIME
IMPRESSION
 TIMEPRINT      30.0
```

Input file for the thermal model for reinforcing concrete beams

This file is for the thermal analysis of a 0.25mX0.50m concrete beam with 0.3m wide concrete slab on one side exposed to an ISO 834 Standard fire from beneath and inside surfaces. The thickness of the slab is 0.2m. The effect of reinforcing bars in the slab is not considered, while the effect of reinforcing bars in the beams is considered. The name of the file is *beam_250_500.IN*.

```
    NPTTOT      5001
     NNODE 1536
      NDIM    2
 NDIMMATER    1
   NDDLMAX    1
      FROM    1   TO 1570 STEP    1 NDDL    1
  END_NDDL
  TEMPERAT
      TETA       0.9
  TINITIAL      20.0
  MAKE.TEM
 LARGEUR11    190000
 LARGEUR12       100
   NORENUM
beam_250_500.TEM
      NMAT    2
  ELEMENTS
     SOLID 1450
        NG    2
     NVOID    0
  END_ELEM
     NODES
      NODE    1     -0.25  -0.125
     GNODE   51      0.25  -0.125
    REPEAT   51         0   0.010   25
      NODE 1327      0.05   0.155
     GNODE 1347      0.25   0.155
    REPEAT   21         0   0.030    9
  NODELINE       0.2     0.125
     YC_ZC       0.0       0.0
 FIXATIONS
   END_FIX
NODOFSOLID
      ELEM    1    1   52   53    2    1    0
     GELEM   50   50  101  102   51    1    0    1
    REPEAT   50   51                             24
      ELEM 1251 1306 1327 1328 1307    1    0
     GELEM 1270 1325 1346 1347 1326    1    0    1
    REPEAT   20   21                              9
   NEW_MAT  154    2
   NEW_MAT  155    2
   NEW_MAT  204    2
   NEW_MAT  205    2
   NEW_MAT 1004    2
   NEW_MAT 1005    2
   NEW_MAT 1054    2
   NEW_MAT 1055    2
   NEW_MAT  604    2
   NEW_MAT  605    2
   NEW_MAT  654    2
   NEW_MAT  655    2
   NEW_MAT  554    2
   NEW_MAT  555    2
```

```
   NEW_MAT 1025     2
   NEW_MAT 1026     2
   NEW_MAT 1075     2
   NEW_MAT 1076     2
   NEW_MAT  196     2
   NEW_MAT  197     2
   NEW_MAT  246     2
   NEW_MAT  247     2
   NEW_MAT  646     2
   NEW_MAT  647     2
   NEW_MAT  696     2
   NEW_MAT  697     2
   NEW_MAT  596     2
   NEW_MAT  597     2
   NEW_MAT 1046     2
   NEW_MAT 1047     2
   NEW_MAT 1096     2
   NEW_MAT 1097     2
   NEW_MAT  175     2
   NEW_MAT  176     2
   NEW_MAT  225     2
   NEW_MAT  226     2
  FRONTIER
         F          1      FISO        NO        NO       F20
         F          2        NO        NO        NO       F20
        GF         49        NO        NO        NO       F20     1
         F         51      FISO        NO        NO        NO
        GF       1151      FISO        NO        NO        NO    50
         F       1201      FISO      FISO        NO        NO
         F       1202        NO      FISO        NO        NO
        GF       1230        NO      FISO        NO        NO     1
         F       1251      FISO        NO        NO        NO
        GF       1431      FISO        NO        NO        NO    20
         F         50        NO        NO       F20       F20
         F        100        NO        NO       F20        NO
        GF       1250        NO        NO       F20        NO    50
         F       1270        NO        NO       F20        NO
        GF       1450        NO        NO       F20        NO    20
 END_FRONT
  SYMMETRY
   END_SYM
 PRECISION    1.0E-3
 MATERIALS
SILCONCEC2
        92.       25.        9.      0.56
  STEELEC2
        25         9       0.5
      TIME
                  1.0      15.0
                 15.0    3600.0
                 30.0   14400.0
  END_TIME
IMPRESSION
 TIMEPRINT      60.0
```

APPENDIX B – TYPICAL INPUT FILES FOR THE STRUCTURAL ANALYSIS

The appendix collects three typical input files for 3-D structural analyses using SAFIR. These input files are for structural analysis of one-way slabs, one-bay flat slabs, and nine-bay flat slabs exposed to an ISO 834 Standard fire.

Input file for the 3-D structural model of one-way slabs

This file is for the 3-D structural analysis of a one-way slab exposed to an ISO 834 Standard fire. The thickness of the slab is 0.2m; the span of the slab is 5.0m and the width of the slab is 1.0m. The supports of the slab are Pin-Pin with full X-direction restraints. A quarter of the slab is modelled using SAFIR.

```
    NPTTOT       3840
     NNODE  105
      NDIM    3
 NDIMMATER    2
   NDDLMAX    6
EVERY_NODE    6
      FROM    1   TO  105 STEP    1 NDDL    6
  END_NDDL
    STATIC
     NLOAD    1
   OBLIQUE    0
  COMEBACK    0.0001
NARCLENGTH     0.005
 LARGEUR11     40360
 LARGEUR12        80
   NORENUM
      NMAT    3
  ELEMENTS
     SHELL   80    2
   NGTHICK    8
    NGAREA    2
   NREBARS    4
  END_ELEM
     NODES
      NODE    1     -2.50     -0.50      0.00
     GNODE   21      0.00     -0.50      0.00    1
    REPEAT   21      0.00     0.125      0.00    4
 FIXATIONS
```

```
   BLOCK    1          F0       NO       F0       NO       NO       F0
   BLOCK   22          F0       NO       F0       NO       NO       F0
   BLOCK   43          F0       NO       F0       NO       NO       F0
   BLOCK   64          F0       NO       F0       NO       NO       F0
   BLOCK   85          F0       F0       F0       F0       NO       F0
   BLOCK   21          F0       NO       NO       NO       F0       F0
   BLOCK   42          F0       NO       NO       NO       F0       F0
   BLOCK   63          F0       NO       NO       NO       F0       F0
   BLOCK   84          F0       NO       NO       NO       F0       F0
   BLOCK  105          F0       F0       NO       F0       F0       F0
   BLOCK    2          NO       NO       NO       NO       NO       F0
   BLOCK   86          NO       F0       NO       F0       NO       F0

    SAME    3     2    NO    NO    NO    NO    NO   YES
    SAME    4     2    NO    NO    NO    NO    NO   YES
    SAME    5     2    NO    NO    NO    NO    NO   YES
    SAME    6     2    NO    NO    NO    NO    NO   YES
    SAME    7     2    NO    NO    NO    NO    NO   YES
    SAME    8     2    NO    NO    NO    NO    NO   YES
    SAME    9     2    NO    NO    NO    NO    NO   YES
    SAME   10     2    NO    NO    NO    NO    NO   YES
    SAME   11     2    NO    NO    NO    NO    NO   YES
    SAME   12     2    NO    NO    NO    NO    NO   YES

    SAME   12     2    NO    NO    NO    NO    NO   YES
    SAME   13     2    NO    NO    NO    NO    NO   YES
    SAME   14     2    NO    NO    NO    NO    NO   YES
    SAME   15     2    NO    NO    NO    NO    NO   YES
    SAME   16     2    NO    NO    NO    NO    NO   YES
    SAME   17     2    NO    NO    NO    NO    NO   YES
    SAME   18     2    NO    NO    NO    NO    NO   YES
    SAME   19     2    NO    NO    NO    NO    NO   YES
    SAME   20     2    NO    NO    NO    NO    NO   YES

    SAME   87    86    NO   YES    NO   YES    NO   YES
    SAME   88    86    NO   YES    NO   YES    NO   YES
    SAME   89    86    NO   YES    NO   YES    NO   YES
    SAME   90    86    NO   YES    NO   YES    NO   YES
    SAME   91    86    NO   YES    NO   YES    NO   YES
    SAME   92    86    NO   YES    NO   YES    NO   YES
    SAME   93    86    NO   YES    NO   YES    NO   YES
    SAME   94    86    NO   YES    NO   YES    NO   YES
    SAME   95    86    NO   YES    NO   YES    NO   YES
    SAME   96    86    NO   YES    NO   YES    NO   YES
    SAME   97    86    NO   YES    NO   YES    NO   YES
    SAME   98    86    NO   YES    NO   YES    NO   YES
    SAME   99    86    NO   YES    NO   YES    NO   YES
    SAME  100    86    NO   YES    NO   YES    NO   YES
    SAME  101    86    NO   YES    NO   YES    NO   YES
    SAME  102    86    NO   YES    NO   YES    NO   YES
    SAME  103    86    NO   YES    NO   YES    NO   YES
    SAME  104    86    NO   YES    NO   YES    NO   YES
END_FIX
```

```
NODOFSHELL
SHELL200_0_1.TSH
 TRANSLATE    1    1
 TRANSLATE    2    2
 END_TRANS
SHELL200_0_2.TSH
 TRANSLATE    1    1
 TRANSLATE    2    2
 END_TRANS
      ELEM    1    1    2   23   22    1
     GELEM    6    6    7   28   27    1    1
      ELEM    7    7    8   29   28    2
     GELEM   20   20   21   42   41    2    1
    REPEAT   20   21                        3
 PRECISION    1.0e-6
     LOADS
  FUNCTION     FLOAD
   DISTRSH         1       0.0       0.0   -6900.0
  GDISTRSH        80       0.0       0.0   -6900.0    1
  END_LOAD
 MATERIALS
SILCONCEC2
       0.2   30.0E+6    0.0E+6                          1
  STEELEC2
210000.E+6       0.3  430.0E+6
 SILCONC2D
       0.2   30.0E+6    0.0E+6                          1
      TIME
               0.05       5.0
                 1.      20.0
                 4.      32.0
                 8.    1800.0
                 8.   14400.0
  END_TIME
LARGEDISPL
     EPSTH
IMPRESSION
 TIMEPRINT       64
 PRINTDEPL
PRNNXSHELL
PRNMXSHELL
```

Input file for the 3-D structural model of one-bay slabs

This file is for the 3-D structural analysis of a one-bay flat slab exposed to an ISO 834 Standard fire. The thickness of the slab is 0.2m; the spans of the flat slab in two directions are 6.0m. The flat slab is supported on four columns with cross section of 0.5mX0.5m. There are no edge beams surrounded the flat slab. A quarter of the flat slab is modelled using SAFIR.

```
    NPTTOT     18416
     NNODE  181
      NDIM    3
 NDIMMATER    2
   NDDLMAX    7
EVERY_NODE    6
      FROM    1   TO   33 STEP    2 NDDL    7
      FROM    2   TO   32 STEP    2 NDDL    1
      FROM   34   TO   37 STEP    1 NDDL    0
      FROM   38   TO   39 STEP    1 NDDL    0
      FROM   40   TO   40 STEP    1 NDDL    7
      FROM   62   TO   64 STEP    1 NDDL    7
      FROM   50   TO   51 STEP    1 NDDL    0
      FROM   52   TO   52 STEP    1 NDDL    7
  END_NDDL
    STATIC
     NLOAD    1
   OBLIQUE    0
  COMEBACK    0.0001
NARCLENGTH     0.005
 LARGEUR11     43252
 LARGEUR12       100
   NORENUM
      NMAT    3
  ELEMENTS
      BEAM   16    1
        NG    2
    NFIBER  400
     SHELL  117   12
   NGTHICK    8
    NGAREA    2
   NREBARS    4
  END_ELEM
     NODES
      NODE    1    -3.000    -3.000      -3.6
     GNODE   33    -3.000    -3.000       3.6    1
      NODE   34    -3.500    -3.500       0.0
     GNODE   37    -3.500    -3.500       3.6    1
      NODE   38    -3.250    -3.250       0.0
      NODE   39    -3.000    -3.250       0.0
      NODE   40    -2.700    -3.250       0.0
     GNODE   49     0.000    -3.250       0.0    1
    REPEAT   12       0.0      0.25       0.0    1
    REPEAT   12       0.0      0.30       0.0   10
 FIXATIONS
     BLOCK    1        F0     F0     F0     F0     F0     F0     F0
     BLOCK   33        F0     F0     NO     F0     F0     F0     F0
     BLOCK   17        NO     NO     NO     NO     NO     F0     F0
```

BLOCK	49	F0	NO	NO	NO	F0	F0
BLOCK	61	F0	NO	NO	NO	F0	F0
BLOCK	73	F0	NO	NO	NO	F0	F0
BLOCK	85	F0	NO	NO	NO	F0	F0
BLOCK	97	F0	NO	NO	NO	F0	F0
BLOCK	109	F0	NO	NO	NO	F0	F0
BLOCK	121	F0	NO	NO	NO	F0	F0
BLOCK	133	F0	NO	NO	NO	F0	F0
BLOCK	145	F0	NO	NO	NO	F0	F0
BLOCK	157	F0	NO	NO	NO	F0	F0
BLOCK	169	F0	NO	NO	NO	F0	F0
BLOCK	181	F0	F0	NO	F0	F0	F0
BLOCK	170	NO	F0	NO	F0	NO	F0
BLOCK	171	NO	F0	NO	F0	NO	F0
BLOCK	172	NO	F0	NO	F0	NO	F0
BLOCK	173	NO	F0	NO	F0	NO	F0
BLOCK	174	NO	F0	NO	F0	NO	F0
BLOCK	175	NO	F0	NO	F0	NO	F0
BLOCK	176	NO	F0	NO	F0	NO	F0
BLOCK	177	NO	F0	NO	F0	NO	F0
BLOCK	178	NO	F0	NO	F0	NO	F0
BLOCK	179	NO	F0	NO	F0	NO	F0
BLOCK	180	NO	F0	NO	F0	NO	F0
BLOCK	41	NO	NO	NO	NO	NO	F0

SAME	40	17	YES	YES	YES	YES	YES	YES	YES
SAME	52	17	YES	YES	YES	YES	YES	YES	YES
SAME	62	17	YES	YES	YES	YES	YES	YES	YES
SAME	63	17	YES	YES	YES	YES	YES	YES	YES
SAME	64	17	YES	YES	YES	YES	YES	YES	YES

```
   END_FIX
 NODOFBEAM
column500.TEM
 TRANSLATE    1    1
 TRANSLATE    2    2
 END_TRANS
      ELEM    1    1    2    3   63    1
     GELEM   16   31   32   33   63    1    2
NODOFSHELL
SLAB200_1.tsh
 TRANSLATE    1    1
 TRANSLATE    2    2
 END_TRANS
SLAB200_2.tsh
 TRANSLATE    1    1
 TRANSLATE    2    2
 END_TRANS
SLAB200_3.tsh
 TRANSLATE    1    1
 TRANSLATE    2    2
 END_TRANS
SLAB200_4.tsh
 TRANSLATE    1    1
 TRANSLATE    2    2
 END_TRANS
SLAB200_5.tsh
 TRANSLATE    1    1
 TRANSLATE    2    2
 END_TRANS
SLAB200_6.tsh
 TRANSLATE    1    1
 TRANSLATE    2    2
 END_TRANS
SLAB200_7.tsh
 TRANSLATE    1    1
 TRANSLATE    2    2
 END_TRANS
SLAB200_8.tsh
 TRANSLATE    1    1
 TRANSLATE    2    2
 END_TRANS
SLAB200_9.tsh
 TRANSLATE    1    1
 TRANSLATE    2    2
 END_TRANS
SLAB200_10.tsh

 TRANSLATE    1    1
 TRANSLATE    2    2
 END_TRANS
SLAB200_11.tsh

 TRANSLATE    1    1
 TRANSLATE    2    2
 END_TRANS
SLAB200_12.tsh
 TRANSLATE    1    1
 TRANSLATE    2    2
 END_TRANS
```

```
      ELEM    1   40   41   53   52    7
     GELEM    4   43   44   56   55    7    1
      ELEM    5   44   45   57   56    8
     GELEM    6   45   46   58   57    8    1
      ELEM    7   46   47   59   58    9
     GELEM    9   48   49   61   60    9    1
      ELEM   10   52   53   65   64    1
     GELEM   13   55   56   68   67    1    1
      ELEM   14   56   57   69   68    2
     GELEM   15   57   58   70   69    2    1
      ELEM   16   58   59   71   70    3
     GELEM   18   60   61   73   72    3    1
      ELEM   19   62   63   75   74   10
      ELEM   20   63   64   76   75    1
     GELEM   24   67   68   80   79    1    1
      ELEM   25   68   69   81   80    2
     GELEM   26   69   70   82   81    2    1
      ELEM   27   70   71   83   82    3
     GELEM   29   72   73   85   84    3    1
    REPEAT   11   12                             3
      ELEM   63  110  111  123  122   11
      ELEM   64  111  112  124  123    4
     GELEM   68  115  116  128  127    4    1
      ELEM   69  116  117  129  128    5
     GELEM   70  117  118  130  129    5    1
      ELEM   71  118  119  131  130    5
     GELEM   73  120  121  133  132    5    1
    REPEAT   11   12                             1
      ELEM   85  134  135  147  146   12
      ELEM   86  135  136  148  147    6
     GELEM   90  139  140  152  151    6    1
      ELEM   91  140  141  153  152    5
     GELEM   92  141  142  154  153    5    1
      ELEM   93  142  143  155  154    5
     GELEM   95  144  145  157  156    5    1
    REPEAT   11   12                             2
 PRECISION    1.0e-6
     LOADS

  FUNCTION     FLOAD
   DISTRSH         1    0.0    0.0  -6300.0
  GDISTRSH       117    0.0    0.0  -6300.0   1
  NODELOAD        33    0.0    0.0 -55790.0   0.0   0.0   0.0
  END_LOAD
 MATERIALS
SILCONCEC2
       0.2   36.0E+6    0.0E+6                            1
  STEELEC2
210000.E+6       0.3  565.0E+6
SILCONCEC2
       0.2    0.0E+6    0.0E+6                            1
      TIME
              0.025       5.0
                 1.      20.0
                 4.      32.0
                 8.    1800.0
                 8.   14400.0
  END_TIME
LARGEDISPL
     EPSTH
IMPRESSION
 TIMEPRINT     64.0
 PRINTDEPL
   PRINTMN
PRNNXSHELL
PRNMXSHELL
```

Input file for the 3-D structural model of nine-bay slabs

This file is for the 3-D structural analysis of a nine-bay flat slab exposed to an ISO 834 Standard fire. The thickness of the slab is 0.2m; the flat slab comprises nine 6m square panels arrange three-by-three. The flat slab is supported on 16 columns with cross-section of 0.5mX0.5m. There are edge beams surrounded the flat slab. A quarter of the flat slab is modelled using SAFIR.

```
    NPTTOT    251000
     NNODE 1206
      NDIM    3
 NDIMMATER    2
   NDDLMAX    7
EVERY_NODE    6
      FROM    1   TO   37 STEP    2 NDDL    7
      FROM    2   TO   36 STEP    2 NDDL    1
      FROM   38   TO   56 STEP    2 NDDL    7
      FROM   39   TO   55 STEP    2 NDDL    1
      FROM   57   TO   93 STEP    2 NDDL    7
      FROM   58   TO   92 STEP    2 NDDL    1
      FROM   94   TO  112 STEP    2 NDDL    7
      FROM   95   TO  111 STEP    2 NDDL    1
      FROM  114   TO  146 STEP    2 NDDL    7
      FROM  115   TO  145 STEP    2 NDDL    1
      FROM  147   TO  179 STEP    2 NDDL    7
      FROM  148   TO  178 STEP    2 NDDL    1
      FROM  180   TO  212 STEP    2 NDDL    7
      FROM  181   TO  211 STEP    2 NDDL    1
      FROM  213   TO  245 STEP    2 NDDL    7
      FROM  214   TO  244 STEP    2 NDDL    1
      FROM  246   TO  246 STEP    1 NDDL    0
      FROM  266   TO  266 STEP    1 NDDL    0
      FROM  866   TO  866 STEP    1 NDDL    0
      FROM  886   TO  886 STEP    1 NDDL    0
      FROM  247   TO  265 STEP    1 NDDL    7
      FROM  267   TO  276 STEP    1 NDDL    7
      FROM  277   TO  835 STEP   31 NDDL    7
      FROM  897   TO 1176 STEP   31 NDDL    7
      FROM  278   TO  278 STEP    1 NDDL    7
      FROM  296   TO  298 STEP    1 NDDL    7
      FROM  897   TO 1176 STEP   31 NDDL    7
      FROM  836   TO  898 STEP   31 NDDL    7
      FROM  854   TO  856 STEP    1 NDDL    7
      FROM  885   TO  887 STEP    2 NDDL    7
      FROM  916   TO  918 STEP    1 NDDL    7
END_NDDL
    STATIC
     NLOAD    1
   OBLIQUE    0
  COMEBACK    0.0001
NARCLENGTH     0.005
 LARGEUR11   1943991
 LARGEUR12       400
   NORENUM
      NMAT    3
  ELEMENTS
      BEAM  118    3
        NG    2
    NFIBER 1536
     SHELL  891   37
   NGTHICK    8
    NGAREA    2
   NREBARS    4
  END_ELEM
```

```
    NODES
     NODE    1    -8.700    -9.125       0.0
    GNODE   37    -3.300    -9.125       0.0    1
     NODE   38    -2.700    -9.125       0.0
    GNODE   56     0.000    -9.125       0.0    1
     NODE   57    -9.125    -8.700       0.0
    GNODE   93    -9.125    -3.300       0.0    1
     NODE   94    -9.125    -2.700       0.0
    GNODE  112    -9.125     0.000       0.0    1
     NODE  113    -9.125    -9.125       3.0
     NODE  114    -9.000    -9.000      -3.6
    GNODE  146    -9.000    -9.000       3.6    1
     NODE  147    -3.000    -9.000      -3.6
    GNODE  179    -3.000    -9.000       3.6    1
     NODE  180    -9.000    -3.000      -3.6
    GNODE  212    -9.000    -3.000       3.6    1
     NODE  213    -3.000    -3.000      -3.6
    GNODE  245    -3.000    -3.000       3.6    1
     NODE  246    -9.000    -9.000       0.0
    GNODE  276     0.000    -9.000       0.0    1
   REPEAT   31       0.0       0.30       0.0   30
FIXATIONS

    BLOCK  114        F0     F0     F0     F0     F0     F0     F0
    BLOCK  147        F0     F0     F0     F0     F0     F0     F0
    BLOCK  180        F0     F0     F0     F0     F0     F0     F0
    BLOCK  213        F0     F0     F0     F0     F0     F0     F0
    BLOCK  146        F0     F0     NO     F0     F0     F0     F0
    BLOCK  179        F0     F0     NO     F0     F0     F0     F0
    BLOCK  212        F0     F0     NO     F0     F0     F0     F0
    BLOCK  245        F0     F0     NO     F0     F0     F0     F0
    BLOCK  130        NO     NO     NO     NO     NO     F0     F0
    BLOCK  163        NO     NO     NO     NO     NO     F0     F0
    BLOCK  196        NO     NO     NO     NO     NO     F0     F0
    BLOCK  229        NO     NO     NO     NO     NO     F0     F0

    BLOCK  307        F0     NO     NO     NO     F0     F0
    BLOCK  338        F0     NO     NO     NO     F0     F0
    BLOCK  369        F0     NO     NO     NO     F0     F0
    BLOCK  400        F0     NO     NO     NO     F0     F0
    BLOCK  431        F0     NO     NO     NO     F0     F0
    BLOCK  462        F0     NO     NO     NO     F0     F0
    BLOCK  493        F0     NO     NO     NO     F0     F0
    BLOCK  524        F0     NO     NO     NO     F0     F0
    BLOCK  555        F0     NO     NO     NO     F0     F0
    BLOCK  586        F0     NO     NO     NO     F0     F0
    BLOCK  617        F0     NO     NO     NO     F0     F0
    BLOCK  648        F0     NO     NO     NO     F0     F0
    BLOCK  679        F0     NO     NO     NO     F0     F0
    BLOCK  710        F0     NO     NO     NO     F0     F0
    BLOCK  741        F0     NO     NO     NO     F0     F0
    BLOCK  772        F0     NO     NO     NO     F0     F0
    BLOCK  803        F0     NO     NO     NO     F0     F0
    BLOCK  834        F0     NO     NO     NO     F0     F0
    BLOCK  865        F0     NO     NO     NO     F0     F0
    BLOCK  896        F0     NO     NO     NO     F0     F0
    BLOCK  927        F0     NO     NO     NO     F0     F0
    BLOCK  958        F0     NO     NO     NO     F0     F0
    BLOCK  989        F0     NO     NO     NO     F0     F0
    BLOCK 1020        F0     NO     NO     NO     F0     F0
    BLOCK 1051        F0     NO     NO     NO     F0     F0
    BLOCK 1082        F0     NO     NO     NO     F0     F0
    BLOCK 1113        F0     NO     NO     NO     F0     F0
    BLOCK 1144        F0     NO     NO     NO     F0     F0
    BLOCK 1175        F0     NO     NO     NO     F0     F0
    BLOCK 1206        F0     F0     NO     F0     F0     F0
    BLOCK 1177        NO     F0     NO     F0     NO     F0
```

BLOCK 1178	NO	F0	NO	F0	NO	F0
BLOCK 1179	NO	F0	NO	F0	NO	F0
BLOCK 1180	NO	F0	NO	F0	NO	F0
BLOCK 1181	NO	F0	NO	F0	NO	F0
BLOCK 1182	NO	F0	NO	F0	NO	F0
BLOCK 1183	NO	F0	NO	F0	NO	F0
BLOCK 1184	NO	F0	NO	F0	NO	F0
BLOCK 1185	NO	F0	NO	F0	NO	F0
BLOCK 1186	NO	F0	NO	F0	NO	F0
BLOCK 1187	NO	F0	NO	F0	NO	F0
BLOCK 1188	NO	F0	NO	F0	NO	F0
BLOCK 1189	NO	F0	NO	F0	NO	F0
BLOCK 1190	NO	F0	NO	F0	NO	F0
BLOCK 1191	NO	F0	NO	F0	NO	F0
BLOCK 1192	NO	F0	NO	F0	NO	F0
BLOCK 1193	NO	F0	NO	F0	NO	F0
BLOCK 1194	NO	F0	NO	F0	NO	F0
BLOCK 1195	NO	F0	NO	F0	NO	F0
BLOCK 1196	NO	F0	NO	F0	NO	F0
BLOCK 1197	NO	F0	NO	F0	NO	F0
BLOCK 1198	NO	F0	NO	F0	NO	F0
BLOCK 1199	NO	F0	NO	F0	NO	F0
BLOCK 1200	NO	F0	NO	F0	NO	F0
BLOCK 1201	NO	F0	NO	F0	NO	F0
BLOCK 1202	NO	F0	NO	F0	NO	F0
BLOCK 1203	NO	F0	NO	F0	NO	F0
BLOCK 1204	NO	F0	NO	F0	NO	F0
BLOCK 1205	NO	F0	NO	F0	NO	F0

BLOCK 56	F0	NO	NO	NO	F0	F0	F0
BLOCK 112	NO	F0	NO	F0	NO	F0	F0
BLOCK 3	NO	NO	NO	NO	NO	F0	F0
BLOCK 5	NO	NO	NO	NO	NO	F0	F0
BLOCK 7	NO	NO	NO	NO	NO	F0	F0
BLOCK 9	NO	NO	NO	NO	NO	F0	F0
BLOCK 11	NO	NO	NO	NO	NO	F0	F0
BLOCK 13	NO	NO	NO	NO	NO	F0	F0
BLOCK 15	NO	NO	NO	NO	NO	F0	F0
BLOCK 17	NO	NO	NO	NO	NO	F0	F0
BLOCK 19	NO	NO	NO	NO	NO	F0	F0
BLOCK 21	NO	NO	NO	NO	NO	F0	F0
BLOCK 23	NO	NO	NO	NO	NO	F0	F0
BLOCK 25	NO	NO	NO	NO	NO	F0	F0
BLOCK 27	NO	NO	NO	NO	NO	F0	F0
BLOCK 29	NO	NO	NO	NO	NO	F0	F0
BLOCK 31	NO	NO	NO	NO	NO	F0	F0
BLOCK 33	NO	NO	NO	NO	NO	F0	F0
BLOCK 35	NO	NO	NO	NO	NO	F0	F0
BLOCK 40	NO	NO	NO	NO	NO	F0	F0
BLOCK 42	NO	NO	NO	NO	NO	F0	F0
BLOCK 44	NO	NO	NO	NO	NO	F0	F0
BLOCK 46	NO	NO	NO	NO	NO	F0	F0
BLOCK 48	NO	NO	NO	NO	NO	F0	F0
BLOCK 50	NO	NO	NO	NO	NO	F0	F0
BLOCK 52	NO	NO	NO	NO	NO	F0	F0
BLOCK 54	NO	NO	NO	NO	NO	F0	F0
BLOCK 59	NO	NO	NO	NO	NO	F0	F0
BLOCK 61	NO	NO	NO	NO	NO	F0	F0
BLOCK 63	NO	NO	NO	NO	NO	F0	F0
BLOCK 65	NO	NO	NO	NO	NO	F0	F0
BLOCK 67	NO	NO	NO	NO	NO	F0	F0
BLOCK 69	NO	NO	NO	NO	NO	F0	F0
BLOCK 71	NO	NO	NO	NO	NO	F0	F0
BLOCK 73	NO	NO	NO	NO	NO	F0	F0
BLOCK 75	NO	NO	NO	NO	NO	F0	F0
BLOCK 77	NO	NO	NO	NO	NO	F0	F0
BLOCK 79	NO	NO	NO	NO	NO	F0	F0

BLOCK	81	NO	NO	NO	NO	NO	F0	F0
BLOCK	83	NO	NO	NO	NO	NO	F0	F0
BLOCK	85	NO	NO	NO	NO	NO	F0	F0
BLOCK	87	NO	NO	NO	NO	NO	F0	F0
BLOCK	89	NO	NO	NO	NO	NO	F0	F0
BLOCK	91	NO	NO	NO	NO	NO	F0	F0
BLOCK	96	NO	NO	NO	NO	NO	F0	F0
BLOCK	98	NO	NO	NO	NO	NO	F0	F0
BLOCK	100	NO	NO	NO	NO	NO	F0	F0
BLOCK	102	NO	NO	NO	NO	NO	F0	F0
BLOCK	104	NO	NO	NO	NO	NO	F0	F0
BLOCK	106	NO	NO	NO	NO	NO	F0	F0
BLOCK	108	NO	NO	NO	NO	NO	F0	F0
BLOCK	110	NO	NO	NO	NO	NO	F0	F0
BLOCK	279	NO	NO	NO	NO	NO	F0	

SAME	1	130	YES	YES	YES	YES	YES	YES	YES
SAME	57	130	YES	YES	YES	YES	YES	YES	YES
SAME	37	163	YES	YES	YES	YES	YES	YES	YES
SAME	38	163	YES	YES	YES	YES	YES	YES	YES
SAME	93	196	YES	YES	YES	YES	YES	YES	YES
SAME	94	196	YES	YES	YES	YES	YES	YES	YES
SAME	247	130	YES	YES	YES	YES	YES	YES	YES
SAME	277	130	YES	YES	YES	YES	YES	YES	YES
SAME	278	130	YES	YES	YES	YES	YES	YES	YES
SAME	265	163	YES	YES	YES	YES	YES	YES	YES
SAME	267	163	YES	YES	YES	YES	YES	YES	YES
SAME	835	196	YES	YES	YES	YES	YES	YES	YES
SAME	897	196	YES	YES	YES	YES	YES	YES	YES
SAME	854	229	YES	YES	YES	YES	YES	YES	YES
SAME	855	229	YES	YES	YES	YES	YES	YES	YES
SAME	856	229	YES	YES	YES	YES	YES	YES	YES
SAME	885	229	YES	YES	YES	YES	YES	YES	YES
SAME	887	229	YES	YES	YES	YES	YES	YES	YES
SAME	916	229	YES	YES	YES	YES	YES	YES	YES
SAME	917	229	YES	YES	YES	YES	YES	YES	YES
SAME	918	229	YES	YES	YES	YES	YES	YES	YES
SAME	248	3	YES	YES	YES	YES	YES	YES	YES
SAME	249	5	YES	YES	YES	YES	YES	YES	YES
SAME	250	7	YES	YES	YES	YES	YES	YES	YES
SAME	251	9	YES	YES	YES	YES	YES	YES	YES
SAME	252	11	YES	YES	YES	YES	YES	YES	YES
SAME	253	13	YES	YES	YES	YES	YES	YES	YES
SAME	254	15	YES	YES	YES	YES	YES	YES	YES
SAME	255	17	YES	YES	YES	YES	YES	YES	YES
SAME	256	19	YES	YES	YES	YES	YES	YES	YES
SAME	257	21	YES	YES	YES	YES	YES	YES	YES
SAME	258	23	YES	YES	YES	YES	YES	YES	YES
SAME	259	25	YES	YES	YES	YES	YES	YES	YES
SAME	260	27	YES	YES	YES	YES	YES	YES	YES
SAME	261	29	YES	YES	YES	YES	YES	YES	YES
SAME	262	31	YES	YES	YES	YES	YES	YES	YES
SAME	263	33	YES	YES	YES	YES	YES	YES	YES
SAME	264	35	YES	YES	YES	YES	YES	YES	YES
SAME	268	40	YES	YES	YES	YES	YES	YES	YES
SAME	269	42	YES	YES	YES	YES	YES	YES	YES
SAME	270	44	YES	YES	YES	YES	YES	YES	YES
SAME	271	46	YES	YES	YES	YES	YES	YES	YES
SAME	272	48	YES	YES	YES	YES	YES	YES	YES
SAME	273	50	YES	YES	YES	YES	YES	YES	YES
SAME	274	52	YES	YES	YES	YES	YES	YES	YES
SAME	275	54	YES	YES	YES	YES	YES	YES	YES
SAME	276	56	YES	YES	YES	YES	YES	YES	YES
SAME	308	59	YES	YES	YES	YES	YES	YES	YES

SAME	339	61	YES	YES	YES	YES	YES	YES	YES
SAME	370	63	YES	YES	YES	YES	YES	YES	YES
SAME	401	65	YES	YES	YES	YES	YES	YES	YES
SAME	432	67	YES	YES	YES	YES	YES	YES	YES
SAME	463	69	YES	YES	YES	YES	YES	YES	YES

```
      SAME  494   71  YES  YES  YES  YES  YES  YES  YES
      SAME  525   73  YES  YES  YES  YES  YES  YES  YES
      SAME  556   75  YES  YES  YES  YES  YES  YES  YES
      SAME  587   77  YES  YES  YES  YES  YES  YES  YES
      SAME  618   79  YES  YES  YES  YES  YES  YES  YES
      SAME  649   81  YES  YES  YES  YES  YES  YES  YES
      SAME  680   83  YES  YES  YES  YES  YES  YES  YES
      SAME  711   85  YES  YES  YES  YES  YES  YES  YES
      SAME  742   87  YES  YES  YES  YES  YES  YES  YES
      SAME  773   89  YES  YES  YES  YES  YES  YES  YES
      SAME  804   91  YES  YES  YES  YES  YES  YES  YES
      SAME  928   96  YES  YES  YES  YES  YES  YES  YES
      SAME  959   98  YES  YES  YES  YES  YES  YES  YES
      SAME  990  100  YES  YES  YES  YES  YES  YES  YES
      SAME 1021  102  YES  YES  YES  YES  YES  YES  YES
      SAME 1052  104  YES  YES  YES  YES  YES  YES  YES
      SAME 1083  106  YES  YES  YES  YES  YES  YES  YES
      SAME 1114  108  YES  YES  YES  YES  YES  YES  YES
      SAME 1145  110  YES  YES  YES  YES  YES  YES  YES
      SAME 1176  112  YES  YES  YES  YES  YES  YES  YES
      SAME  296  163  YES  YES  YES  YES  YES  YES  YES
      SAME  297  163  YES  YES  YES  YES  YES  YES  YES
      SAME  298  163  YES  YES  YES  YES  YES  YES  YES
      SAME  836  196  YES  YES  YES  YES  YES  YES  YES
      SAME  867  196  YES  YES  YES  YES  YES  YES  YES
      SAME  898  196  YES  YES  YES  YES  YES  YES  YES

   END_FIX
 NODOFBEAM
column500.TEM
 TRANSLATE    1    1
 TRANSLATE    2    2
 END_TRANS
BEAM_250_500X.TEM
 TRANSLATE    1    1
 TRANSLATE    2    2
 TRANSLATE    3    3
 END_TRANS
BEAM_250_500.TEM
 TRANSLATE    1    1
 TRANSLATE    2    2
 TRANSLATE    3    3
 END_TRANS
      ELEM    1    1    2    3  113    2
     GELEM   18   35   36   37  113    2    2
      ELEM   19   38   39   40  113    2
     GELEM   27   54   55   56  113    2    2
      ELEM   28   57   58   59  113    3
     GELEM   45   91   92   93  113    3    2
      ELEM   46   94   95   96  113    3
     GELEM   54  110  111  112  113    3    2
      ELEM   55  114  115  116  196    1
     GELEM   70  144  145  146  196    1    2
      ELEM   71  147  148  149  229    1
     GELEM   86  177  178  179  229    1    2
      ELEM   87  180  181  182  130    1
     GELEM  102  210  211  212  130    1    2
      ELEM  103  213  214  215  163    1
     GELEM  118  243  244  245  163    1    2
NODOFSHELL

SLAB200_1.tsh
 TRANSLATE    1    1
 TRANSLATE    2    2
 END_TRANS
SLAB200_2.tsh
 TRANSLATE    1    1
 TRANSLATE    2    2
 END_TRANS
```

```
SLAB200_3.tsh
 TRANSLATE    1    1
 TRANSLATE    2    2
 END_TRANS
SLAB200_4.tsh
 TRANSLATE    1    1
 TRANSLATE    2    2
 END_TRANS
SLAB200_5.tsh
 TRANSLATE    1    1
 TRANSLATE    2    2
 END_TRANS
SLAB200_6.tsh
 TRANSLATE    1    1
 TRANSLATE    2    2
 END_TRANS
SLAB200_7.tsh
 TRANSLATE    1    1
 TRANSLATE    2    2
 END_TRANS
SLAB200_8.tsh
 TRANSLATE    1    1
 TRANSLATE    2    2
 END_TRANS
SLAB200_9.tsh
 TRANSLATE    1    1
 TRANSLATE    2    2
 END_TRANS
SLAB200_10.tsh
 TRANSLATE    1    1
 TRANSLATE    2    2
 END_TRANS
SLAB200_11.tsh
 TRANSLATE    1    1
 TRANSLATE    2    2
 END_TRANS
SLAB200_12.tsh
 TRANSLATE    1    1
 TRANSLATE    2    2
 END_TRANS
SLAB200_13.tsh
 TRANSLATE    1    1
 TRANSLATE    2    2
 END_TRANS
SLAB200_14.tsh
 TRANSLATE    1    1
 TRANSLATE    2    2
 END_TRANS
SLAB200_15.tsh
 TRANSLATE    1    1
 TRANSLATE    2    2
 END_TRANS
SLAB200_16.tsh
 TRANSLATE    1    1
 TRANSLATE    2    2
 END_TRANS
SLAB200_17.tsh
 TRANSLATE    1    1
 TRANSLATE    2    2
 END_TRANS
SLAB200_18.tsh
 TRANSLATE    1    1
 TRANSLATE    2    2
 END_TRANS
SLAB200_19.tsh
 TRANSLATE    1    1
 TRANSLATE    2    2
 END_TRANS
```

```
SLAB200_20.tsh
 TRANSLATE    1    1
 TRANSLATE    2    2
 END_TRANS
SLAB200_21.tsh
 TRANSLATE    1    1
 TRANSLATE    2    2
 END_TRANS
SLAB200_22.tsh
 TRANSLATE    1    1
 TRANSLATE    2    2
 END_TRANS
SLAB200_23.tsh
 TRANSLATE    1    1
 TRANSLATE    2    2
 END_TRANS
SLAB200_24.tsh
 TRANSLATE    1    1
 TRANSLATE    2    2
 END_TRANS
SLAB200_25.tsh
 TRANSLATE    1    1
 TRANSLATE    2    2
 END_TRANS
SLAB200_26.tsh
 TRANSLATE    1    1
 TRANSLATE    2    2
 END_TRANS
SLAB200_27.tsh
 TRANSLATE    1    1
 TRANSLATE    2    2
 END_TRANS
SLAB200_28.tsh
 TRANSLATE    1    1
 TRANSLATE    2    2
 END_TRANS
SLAB200_29.tsh
 TRANSLATE    1    1
 TRANSLATE    2    2
 END_TRANS
SLAB200_30.tsh
 TRANSLATE    1    1
 TRANSLATE    2    2
 END_TRANS
SLAB200_31.tsh
 TRANSLATE    1    1
 TRANSLATE    2    2
 END_TRANS
SLAB200_32.tsh
 TRANSLATE    1    1
 TRANSLATE    2    2
 END_TRANS
SLAB200_33.tsh
 TRANSLATE    1    1
 TRANSLATE    2    2
 END_TRANS
SLAB200_34.tsh
 TRANSLATE    1    1
 TRANSLATE    2    2
 END_TRANS
SLAB200_35.tsh
 TRANSLATE    1    1
 TRANSLATE    2    2
 END_TRANS
SLAB200_36.tsh
 TRANSLATE    1    1
 TRANSLATE    2    2
 END_TRANS
```

```
SLAB200_37.tsh
 TRANSLATE    1    1
 TRANSLATE    2    2
 END_TRANS

      ELEM    1  247  248  279  278    1
     GELEM    4  250  251  282  281    1    1
      ELEM    5  251  252  283  282    2
     GELEM   14  260  261  292  291    2    1
      ELEM   15  261  262  293  292    3
     GELEM   18  264  265  296  295    3    1
      ELEM   19  267  268  299  298    4
     GELEM   22  270  271  302  301    4    1
      ELEM   23  271  272  303  302    5
     GELEM   27  275  276  307  306    5    1
      ELEM   28  277  278  309  308    1
     GELEM   32  281  282  313  312    1    1
      ELEM   33  282  283  314  313    2
     GELEM   42  291  292  323  322    2    1
      ELEM   43  292  293  324  323    3
     GELEM   47  296  297  328  327    3    1
      ELEM   48  297  298  329  328    4
     GELEM   52  301  302  333  332    4    1
      ELEM   53  302  303  334  333    5
     GELEM   57  306  307  338  337    5    1
    REPEAT   30   31                             3
      ELEM  148  401  402  433  432    6
     GELEM  152  405  406  437  436    6    1
      ELEM  153  406  407  438  437    7
     GELEM  162  415  416  447  446    7    1
      ELEM  163  416  417  448  447    8
     GELEM  167  420  421  452  451    8    1
      ELEM  168  421  422  453  452    9
     GELEM  172  425  426  457  456    9    1
      ELEM  173  426  427  458  457   10
     GELEM  177  430  431  462  461   10    1
    REPEAT   30   31                             1
      ELEM  208  463  464  495  494    6
     GELEM  212  467  468  499  498    6    1
      ELEM  213  468  469  500  499    7
     GELEM  222  477  478  509  508    7    1
      ELEM  223  478  479  510  509   11
     GELEM  227  482  483  514  513   11    1
      ELEM  228  483  484  515  514   12
     GELEM  232  487  488  519  518   12    1
      ELEM  233  488  489  520  519   10
     GELEM  237  492  493  524  523   10    1
    REPEAT   30   31                             5

      ELEM  388  649  650  681  680    6
     GELEM  392  653  654  685  684    6    1
      ELEM  393  654  655  686  685    7
     GELEM  402  663  664  695  694    7    1
      ELEM  403  664  665  696  695   13
     GELEM  407  668  669  700  699   13    1
      ELEM  408  669  670  701  700   14
     GELEM  412  673  674  705  704   14    1
      ELEM  413  674  675  706  705   10
     GELEM  417  678  679  710  709   10    1
    REPEAT   30   31                             1

      ELEM  448  711  712  743  742   15
     GELEM  452  715  716  747  746   15    1
      ELEM  453  716  717  748  747   16
     GELEM  454  717  718  749  748   16    1
      ELEM  455  718  719  750  749   17
     GELEM  460  723  724  755  754   17    1
      ELEM  461  724  725  756  755   18
     GELEM  462  725  726  757  756   18    1
      ELEM  463  726  727  758  757   19
     GELEM  467  730  731  762  761   19    1
```

```
  ELEM  468  731  732  763  762   20
 GELEM  472  735  736  767  766   20    1
  ELEM  473  736  737  768  767   21
 GELEM  474  737  738  769  768   21    1
  ELEM  475  738  739  770  769   22
 GELEM  477  740  741  772  771   22    1
REPEAT   30   31                        3
  ELEM  568  836  837  868  867   15
 GELEM  571  839  840  871  870   15    1
  ELEM  572  840  841  872  871   16
 GELEM  573  841  842  873  872   16    1
  ELEM  574  842  843  874  873   17
 GELEM  579  847  848  879  878   17    1
  ELEM  580  848  849  880  879   18
 GELEM  581  849  850  881  880   18    1
  ELEM  582  850  851  882  881   19
 GELEM  585  853  854  885  884   19    1
  ELEM  586  856  857  888  887   20
 GELEM  589  859  860  891  890   20    1
  ELEM  590  860  861  892  891   21
 GELEM  591  861  862  893  892   21    1
  ELEM  592  862  863  894  893   22
 GELEM  594  864  865  896  895   22    1
  ELEM  595  867  868  899  898   23
 GELEM  598  870  871  902  901   23    1
  ELEM  599  871  872  903  902   24
 GELEM  600  872  873  904  903   24    1
  ELEM  601  873  874  905  904   25
 GELEM  606  878  879  910  909   25    1
  ELEM  607  879  880  911  910   26
 GELEM  608  880  881  912  911   26    1
  ELEM  609  881  882  913  912   27
 GELEM  612  884  885  916  915   27    1
  ELEM  613  887  888  919  918   28
 GELEM  616  890  891  922  921   28    1
  ELEM  617  891  892  923  922   29
 GELEM  618  892  893  924  923   29    1
  ELEM  619  893  894  925  924   30
 GELEM  621  895  896  927  926   30    1
  ELEM  622  897  898  929  928   23
 GELEM  626  901  902  933  932   23    1
  ELEM  627  902  903  934  933   24
 GELEM  628  903  904  935  934   24    1
  ELEM  629  904  905  936  935   25
 GELEM  634  909  910  941  940   25    1
  ELEM  635  910  911  942  941   26
 GELEM  636  911  912  943  942   26    1
  ELEM  637  912  913  944  943   27
 GELEM  641  916  917  948  947   27    1
  ELEM  642  917  918  949  948   28
 GELEM  646  921  922  953  952   28    1
  ELEM  647  922  923  954  953   29
 GELEM  648  923  924  955  954   29    1
  ELEM  649  924  925  956  955   30
 GELEM  651  926  927  958  957   30    1
REPEAT   30   31                        3
  ELEM  742 1021 1022 1053 1052   31
 GELEM  746 1025 1026 1057 1056   31    1
  ELEM  747 1026 1027 1058 1057   32
 GELEM  756 1035 1036 1067 1066   32    1
  ELEM  757 1036 1037 1068 1067   33
 GELEM  761 1040 1041 1072 1071   33    1
  ELEM  762 1041 1042 1073 1072   34
 GELEM  766 1045 1046 1077 1076   34    1
  ELEM  767 1046 1047 1078 1077   35
 GELEM  771 1050 1051 1082 1081   35    1
REPEAT   30   31                        1
```

```
      ELEM  802 1083 1084 1115 1114   31
     GELEM  806 1087 1088 1119 1118   31    1
      ELEM  807 1088 1089 1120 1119   32
     GELEM  816 1097 1098 1129 1128   32    1
      ELEM  817 1098 1099 1130 1129   36
     GELEM  821 1102 1103 1134 1133   36    1
      ELEM  822 1103 1104 1135 1134   37
     GELEM  826 1107 1108 1139 1138   37    1
      ELEM  827 1108 1109 1140 1139   35
     GELEM  831 1112 1113 1144 1143   35    1
    REPEAT   30   31                        2
 PRECISION    1.0e-6
     LOADS
  FUNCTION     FLOAD
   DISTRSH         1   0.0   0.0   -6900.0
  GDISTRSH       891   0.0   0.0   -6900.0   1
  NODELOAD       146   0.0   0.0  -55790.0   0.0   0.0   0.0
  NODELOAD       179   0.0   0.0 -125600.0   0.0   0.0   0.0
  NODELOAD       212   0.0   0.0 -125600.0   0.0   0.0   0.0
  NODELOAD       245   0.0   0.0 -247000.0   0.0   0.0   0.0
 DISTRBEAM         1   0.0   0.0   -7650.0
GDISTRBEAM        54   0.0   0.0   -7650.0   1
  END_LOAD
 MATERIALS
SILCONCEC2
       0.2   30.0E+6    0.0E+6                          1
  STEELEC2
210000.E+6       0.3  430.0E+6
SILCONCEC2
       0.2    0.0E+6    0.0E+6                          1
      TIME
               0.025       5.0
                  1.      20.0
                  4.      32.0
                  8.    1800.0
                  8.   14400.0
  END_TIME
LARGEDISPL
     EPSTH
IMPRESSION
 TIMEPRINT     64.0
 PRINTDEPL
   PRINTMN
PRNNXSHELL
PRNMXSHELL
```